

# UNCLASSIFIED

AD NUMBER
AD466390
NEW LIMITATION CHANGE
TO Approved for public release, distribution unlimited
FROM Distribution authorized to U.S. Gov't. agencies and their contractors; Administrative/Operational use; May 1965. Other requests shall be referred to Air Force Aero Propulsion Lab, Wright-Patterson AFB OH 45433-0000.
AUTHORITY
AFAPL ltr, 21 Jul 1971

THIS PAGE IS UNCLASSIFIED

AFAPL-TR-65-45

Part I

20

466390

# ROTOR-BEARING DYNAMICS DESIGN TECHNOLOGY

## Part I : State-of-the-Art

N. F. Rieger

Mechanical Technology Incorporated

TECHNICAL REPORT AFAPL-TR-65-45, PART I

May 1965

Air Force Aero-Propulsion Laboratory  
Research and Technology Division  
Air Force Systems Command  
Wright-Patterson Air Force Base, Ohio

RECEIVED  
JUN 1 1965  
JISIA E

DDG FILE COPY

### NOTICES

When U.S. Government drawings, specifications, or other data are used for any purpose other than a definitely related Government procurement operation, the Government thereby incurs no responsibility nor any obligation whatsoever, and the fact that the government may have formulated, furnished, or in any way supplied the said drawings, specifications, or other data, is not to be regarded by implication or otherwise, or in any manner licensing the holder or any other person or corporation, or conveying any rights or permission to manufacture, use, or sell any patent invention that may in any way be related thereto.

Qualified users may obtain copies of this report from the Defense Documentation Center.

Defense Documentation Center release to the Clearinghouse for Federal Scientific and Technical Information (formerly OTS) is not authorized. Foreign announcement and dissemination by the Defense Documentation Center is not authorized. Release to foreign nationals is not authorized.

DDC release to OTS is not authorized in order to prevent foreign announcement and distribution of this report. The distribution of this report is limited because it contains technology identifiable with items on the strategic embargo lists excluded from export or re-exports under U. S. Export Control Act of 1949 (63 Stat. 7); as amended (50 U.S.O. App. 2020, 2031), as implemented by AFR 400-10.

Copies of this report should not be returned to the Research and Technology Division unless return is required by security considerations, contractual obligations or notice on a specific document.

**NOTICE:** When government or other drawings, specifications or other data are used for any purpose other than in connection with a definitely related government procurement operation, the U. S. Government thereby incurs no responsibility, nor any obligation whatsoever; and the fact that the Government may have formulated, furnished, or in any way supplied the said drawings, specifications, or other data is not to be regarded by implication or otherwise as in any manner licensing the holder or any other person or corporation, or conveying any rights or permission to manufacture, use or sell any patented invention that may in any way be related thereto.

18 19  
APL TR-65-45-PT. 1

⑥ ROTOR-BEARING DYNAMICS DESIGN TECHNOLOGY.  
Part I : State-of-the-Art.

(upper case)

⑩ by N. F. Rieger.

⑤ Mechanical Technology, Inc., Latham, N. Y.

TECHNICAL REPORT AFAPL-TR-65-45, PART I

⑪ May 1965,

⑨ Final rept. 1 apr 64 - 1 apr 65,

Air Force Aero Propulsion Laboratory  
Research and Technology Division  
Air Force Systems Command  
Wright-Patterson Air Force Base, Ohio

# FOREWORD

This report was prepared by Mechanical Technology Incorporated, 968 Albany-<sup>New</sup> Shaker Road, Latham, New York 12110 under USAF Contract No. AF 33(615)-1895. The contract was initiated under Project No. 3145, "Dynamic Energy Conversion Technology," Task No. 314511, "Nuclear Mechanical Power Units." The work was administered under the direction of the Air Force Aero Propulsion Laboratory, Research and Technology Division, with Mr. John L. Morris (APFL) acting as project engineer.

This report covers work conducted from 1 April 1964 to 1 April 1965.

This report was submitted by the author for review on 15 April 1965. It is Part I of final documentation issued in multiple parts and is also identified by the contractor's designation MTI-65TR18.

This technical report has been reviewed and is approved.

*Arthur V. Churchill*  
ARTHUR V. CHURCHILL, Chief  
Fuels and Lubricants Branch  
Technical Support Division  
Air Force Aero Propulsion Laboratory

# ABSTRACT

The basic aspects of rotor-bearing dynamics have been collated and are here presented in systematic fashion. The rotor-bearing system and its forces are first discussed. The properties of rotor whirl, critical speed and system stability are discussed in detail. Effects arising from running a rotor through its critical speed are reviewed. Balancing of rigid and flexible rotors is considered with regard to balancing machines, computed calculation of unbalance, and acceptable levels of unbalance. Axial and torsional effects on machine systems are included. Throughout, the important literature relating to each topic is specified, discussed and set in perspective.

# TABLE OF CONTENTS

<u>NOMENCLATURE</u>	<u>Page</u>
.....	vii
<b>SECTION I - INTRODUCTION</b> .....	1
Purpose and Need .....	1
Dynamical Problems of Rotating Machinery .....	1
Scope of the Present Volume .....	3
Sources of Text Material .....	5
Rotor Bearing System Analysis .....	6
The Remaining Problems of Rotor Bearing Dynamics .....	7
State-of-the-Art .....	9
<b>SECTION II - ANALYTICAL REPRESENTATION OF THE ROTOR BEARING SYSTEM</b> .....	10
Dynamical System of the Machine .....	10
The Rotor .....	11
Dynamical Representation of the Rotor .....	12
Torsional Systems .....	15
The Bearings .....	16
Dynamical Representation of the Bearings .....	20
The Machine Structure .....	21
Forces Acting in a Rotor Bearing System .....	22
<b>SECTION III - DYNAMIC RESPONSE OF UNBALANCED FLEXIBLE ROTORS</b> .....	41
Introductory Remarks on the Influence of Unbalance .....	41
Nature of Whirl Motions .....	42
Whirling of a Simple Undamped Rotor .....	44
Critical Whirling of a Simple Undamped Rotor .....	47
Influence of Viscous Frictions on Rotor Motion .....	48
Force Transmitted from an Unbalanced Rotor with Viscous Damping .....	51
Influence of Internal Friction on Rotor Whirl Motion .....	53
Rotor Dynamic Characteristics with Viscous and Hysteretic Damping .....	56
Influence of Unsymmetrical Bearing Stiffness on Rotor Motions .....	58
Whirling of a Rotor Having Unsymmetrical Stiffness .....	60
Sub-Harmonic Whirling .....	65
Operation of Rotors in Fluid-Film Bearings .....	67
Single Disk Elastic Rotor in Fluid-Film Bearings .....	68
Two-Mass Rotor in Damped Flexible Bearings .....	73
Uniform Elastic Rotor in Damped Flexible Bearings .....	75
Development of Rotor Bearing Dynamics .....	77
<b>SECTION IV - CRITICAL SPEED</b> .....	113
Calculation of Critical Speed .....	113
Whirling Modes of Elastic Systems .....	113
Influence of Rotor Bearing Properties on Critical Speed .....	114
Exact Methods .....	119
Discrete Mass Systems .....	120
Methods of Solution .....	122
Continuous Systems .....	125
Approximate Methods .....	129

TABLE OF CONTENTS  
(cont)

	<u>Page</u>
Rayleigh's Method .....	130
Ritz's Method .....	138
Iterative Methods .....	140
Southwell's Method .....	143
Dunkerley's Method .....	145
Effect of Disk Gyroscopic Action on Critical Speed .....	146
 SECTION V - STABILITY .....	 162
The Nature of Whirl Motions .....	162
Stability of a Simple Rotor .....	165
Stability of a Damped Rotor in Rigid Bearings .....	166
Influence of Internal Friction on Rotor Stability .....	167
Whirling of a Shaft with Unsymmetrical Stiffness .....	171
Hydrodynamic Instability .....	175
Mechanics of Hydrodynamic Instability .....	176
Rigid Rotor in Fluid-Film Bearings .....	177
Synchronous Whirl .....	184
Hydrostatic Bearings .....	195
Whirling of a Flexible Rotor in Fluid-Film Bearings .....	197
General Theory of Stability of Small Amplitude Motions .....	201
Stability of Two-Mass Rotor with Unbalance .....	207
 SECTION VI - TRANSITION OF A ROTOR THROUGH A CRITICAL SPEED .....	 236
Introduction .....	238
Flexible Undamped Rotor in Rigid Bearings .....	238
Influence of External Friction on Rotor Motion .....	240
Amplitude Buildup .....	242
Effect of Flexible Bearings on Transition Phenomena .....	243
Experimental Observation of Transition Phenomena .....	245
 SECTION VII - BALANCE OF ROTATING MACHINERY .....	 254
Need for Balancing .....	254
Concept of Unbalance .....	255
Rigid Rotor Balancing .....	255
Flexible Rotor Balancing .....	256
Practical Rotor Balancing .....	257
Field Balancing .....	257
Balancing Machines .....	258
Determination of Required Correction Weights .....	259
Influence Coefficient Method .....	262
Acceptable Level of Unbalance .....	265
 SECTION VIII - TORSIONAL AND AXIAL EFFECTS .....	 275
Nature of Influence on System .....	276
Sources of Torsional Excitation .....	277
Critical Speeds of Torsional Systems .....	278
Methods of Suppressing Torsional Vibrations .....	279

TABLE OF CONTENTS  
(cont)

	<u>Page</u>
Sources of Axial Vibration .....	281
Critical Speeds of Axial Vibration .....	282
Suppression of Axial Vibrations .....	283
Axial Vibrations of a Hydrostatic Thrust Bearing .....	283
Effect of Axial Force and Drive Torque on Bending Motions .....	287

APPENDICES

A - FUNDAMENTALS OF HYDRODYNAMIC LUBRICATION THEORY .....	306
B - TRANSFORMATION FORMULAE FOR STATIONARY AND ROTATING COORDINATES .....	316
C - REFERENCES .....	319

NOMENCLATURE

Principal nomenclature is listed below. In certain cases the same symbol has been re-used to denote another variable, in two separate places in the text. In these instances, symbols are specifically defined within the text.

The nomenclature used in the cited literature is not uniform, and in presenting certain parameters from the literature as curves herein, and in analysis, it has not always been possible to present a wholly uniform set of notation. Where exceptions occur, these are either re-defined within the text, or, in the case of a curve figure, the figure source is specified for direct referral.

A	Cross sectional area
A, B	Integration constants
a	Eccentricity of mass center
a, b	Shaft semi-lengths
C	Bearing radial clearance
C	Torsional rigidity of cross-section
$C_{xx}, C_{xy}, C_{yx}, C_{yy}$	Bearing velocity damping coefficients
c	Viscous damping coefficient of velocity
$c_c$	Critical velocity damping coefficient $2 \sqrt{mK}$
d	Diameter
E	Modulus of elasticity
E	Hysteresis energy loss per cycle
e	Radial displacement of journal
F	Force
g	Gravitational acceleration
h	Fluid film thickness
I	Moment of inertia of disk
$I_p$	Polar moment of inertia
$I_T$	Transverse moment of inertia
i	$\sqrt{-1}$
$\hat{i}, \hat{j}$	Unit vectors in $\eta$ directions
$K_{xx}, K_{xy}, K_{yx}, K_{yy}$	Bearing spring coefficients
k	Shaft flexibility
$k_{ij}$	Stiffness influence coefficients
L	Length

L	Length ratio ( $L_2/L_1$ )
$l_1, l_2$	Shaft semi-lengths
$z$	Unbalance position ratio
M	Bending moment
M	Bearing gas mass
$M_D$	Bearing restoring moment
m	Mass
N	Speed, rpm
$N_c$	Critical speed
P	End force
$P_c$	Euler critical load ( $\pi^2 EI/L^2$ )
P	Pressure
$P_a$	Ambient pressure
$P_o$	Recess pressure
$p, q$	Whirl ellipse major and minor radii
Q	Small tangential force
q	Damped critical speed
q	Torsional shaft stiffness
q	Generalized displacement coordinate
q	Generalized velocity coordinate
$q_1, q_2$	Coefficients
R	Journal radius
R	Gas constant
r	Radius whirl orbit in x, y coordinates
$r, \theta$	Polar coordinates of position
$\hat{r}, \hat{s}$	Unit vectors in $\eta$ directions
S	Sommerfeld number
S	Whirl threshold speed ratio ( $\omega/\omega_1$ )
T	Temperature
T	Torque
T	Kinetic energy
t	Time
t	Thickness

U	Tangential velocity
u	Unbalance, $W_a$ oz. in
v	Potential energy
V	Linear velocity
V	Journal radial velocity
W	Work per shaft revolution
W	Work
W	Bearing load
$\frac{W}{W}$	Weight ratio ( $uL/w$ )
w	Specific weight
w	Gas flow rate
x	Journal velocity in x-direction
x,y	Stationary Cartesian coordinates of position
y	Journal velocity in y-direction
z	Bearing length coordinate
z	Shaft length coordinate
$\alpha$	Transient phase angle
$\alpha$	Angular acceleration
$\dot{\alpha}$	Synchronous angular whirl velocity
$\alpha_i$	Discrete-effect eigenvalues
$\alpha_{ij}$	Influence coefficients
$\alpha_{11}$	Influence coefficient
$\beta$	Steady-state phase angle
$\beta, \gamma$	Instantaneous small angles of inclination
$\gamma$	Dimensionless damping coefficient (Lewis)
$\gamma$	Constant
$\delta$	Deflection
$\epsilon$	Bearing eccentricity ratio $\left(\frac{e}{c}\right)$
$\epsilon$	Strain
$\epsilon$	Eccentricity ratio
$\epsilon'$	$\partial\epsilon/\partial t$
$\epsilon_i$	Phase angle
$\epsilon$	Error perturbation

$\zeta$	Damping ratio ( $c/c_c$ )
$\xi$	Whirl orbit radius in $\xi, \eta$ coordinates
$\eta$	Bearing operation eccentricity
$\textcircled{B}$	Dimensionless shaft stiffness ratio
$\theta$	Bearing angular coordinate
$\theta, \phi$	Angles
$\kappa$	Speed-dependent shaft stiffness
$\Lambda$	Compressibility number $\left[ 6\mu\omega/p_s \right] \left( \frac{R}{c} \right)^2$
$\Lambda$	Complex eigenvalue
$\Lambda$	Transient vibration frequency with coulomb damping
$\Lambda^*$	$= \Lambda \left[ 1 - (2\dot{\alpha}/\omega) \right]$
$\lambda^4$	Natural frequency parameter ( $W\omega^2/gEI$ )
$\mu$	Viscosity
$\nu$	Poisson's ratio
$\nu$	Stiffness ratio (shaft:bearing)
$\nu$	Rotor whirl frequency
$\xi$	Mode shape coefficient
$\xi$	Span ratio for mass location
$\xi, \eta$	Rotating Cartesian coordinates of position
$\pi$	3.141592....
$\sigma$	Stress
$\tau$	Dimensionless time $\omega_c t$
$\phi$	Attitude angle
$\phi$	Angle of shaft twist per unit length
$\phi_1(z)$	Displacement function
$\Omega$	Dimensionless speed ratio ( $\omega/\omega_c$ )
$\omega$	Circular frequency of rotation
$\omega_c$	Critical speed, radian/sec.

## INTRODUCTION

### Purpose and Need

Rotor-bearing dynamics has recently emerged as a specialized technology in machine design, due to the growing demand for reliable rotating machinery capable of stable operation at higher and higher speeds. As machine operating speeds have increased, so has the presence of dynamic effects in the motion become more significant. The design and development of high-speed rotating machinery has thus become increasingly dependent upon a knowledge of the dynamic characteristics of the rotor in its bearings.

The purpose of this volume is to present the existing knowledge in the major areas of rotor-bearing dynamics in a single volume. As such it constitutes for each area a comprehensive and definitive introduction to the mechanics of rotors in bearings, and also a fully-documented reference to the subject literature, in which the contributions are collated, evaluated and set in perspective. This information is of value to designers of rotating machinery as a sourcebook of rotordynamic effects and of experience obtained by many investigators with many different machine types. It may be used by analysts seeking data on the basic mechanics of whirl motions, stability, run-up or run-down rotor characteristics, or any type of system critical speed calculation; and on the formulation of the equations of motion in each of these instances. Despite the very extensive subject literature in both rotordynamics and bearing technology, there exists no specific text devoted to the problems of rotors in bearings, nor is any critical compilation of the subject literature available. Therefore, this volume meets both these needs.

### Dynamical Problems of Rotating Machinery

The dynamic aspects of high-speed rotating machinery design are directed towards achieving stable motions of minimum amplitude at all operating speeds. At low speeds, less than the first system critical speed, the overall problem may be dealt with by careful balancing. But at high speeds, above the first system critical speed, the most refined multiplane balancing cannot avert the stability problems of hysteretic whirling, dissimilar rotor lateral stiffness, and resonant whipping. Other methods involving rotor construction and system viscous damping

are effective in overcoming these problems - the existence of which may be predicted at the design stage using the data contained herein.

The design problems of rotating machinery may be classified as follows:

1. Function capability and operational safety.
2. Static stress levels: The influence of centrifugal, thermal, and bending effects; creep and fatigue of disks, shafts, bearings, and stator casing under environmental conditions.
3. Dynamic stress levels: bending, torsional, and axial stresses in the rotor.
4. Clearance maintenance; rotor-stator, journal-bearing, no touching.
5. Erosion, corrosion of working surfaces.
6. Transmitted structural vibrations and noise level.

The problems of rotor-bearing dynamics must be solved within this total framework. Specific dynamical problem areas of the machine design are as follows:

1. Critical speed amplitude buildup.
2. Multiplane balancing.
3. Rotor dynamic stress levels. Bending, axial, torsional.
4. Shrink-fit or elastic hysteresis whirl stability.
5. Stability with differing lateral stiffnesses.
6. Bearing stability. Resonant whipping. Half-frequency whirl. Pneumatic hammer.

7. Subharmonic whirl amplitude buildup.
8. Transmitted bearing force. Structural vibration.
9. Noise generation.

A knowledge of the manner in which each separate effect influences the rotor behavior is needed for the design of both rotor and bearings. Analytically, the complete interrelationship of all factors cannot be known explicitly -- even for the most simple rotor type. However, it is usually sufficient to investigate each effect separately, and in instances where contrary tendencies exist, the combined effect may be considered. This is the approach used in the following sections.

#### Scope of the Present Volume

Before analysing the motion of a rotor in bearings, it is first necessary to specify what is intended by the terms "rotor" and "bearing". This is done in Section 2. The constructional make-up of a rotor is reviewed together with the manner in which the physical proportions contribute to the dynamic rotor properties. The various types of bearing are discussed; gas, liquid; hydrostatic, hydrodynamic, hybrid; laminar, turbulent; and the features which contribute to the motion of the rotor are identified and classified in terms of relative importance for each of the above cases. Forces which arise in the motion are also reviewed in this Section. These are classified in terms of their origin and action on the rotor-bearing system.

Section 3 is a discussion of the effects produced by a number of specific influences on the rotor in its bearings. In particular these are: rotor unbalance; viscous friction arising from bearings, process fluid or environment; internal friction due to shrink-fit slippage or elastic hysteresis; dissimilar lateral stiffness of the shaft; flexible bearings; subharmonic whirling fluid-film bearings; attenuation of transmitted rotor force by the bearing fluid-film. In most cases, it is only necessary to consider the performance of a simple, single-disk rotor to gain sufficient understanding of the principles associated with each effect. These results cover the fundamental system critical speed. Where

information is needed on higher critical speeds, the rotor profile must possess as many masses as there are critical speeds involved.

Each rotor-bearing system possesses a number of critical speeds, but the most suitable method for calculating a given case varies according to complexity and the accuracy to which the required result must be attained. Section 4 consists of a discussion, with examples, of the most commonly-used exact and approximate methods for the calculation of critical speeds. The influence of system damping, shear, rotatory inertia and gyroscopic effects are considered.

The stability of rotors in bearings is considered in Section 5. Following an introductory statement on the nature of whirl motions and their basic mechanics, the stability properties of elastic rotor-bearing systems is examined. This is extended to the case of an elastic rotor in flexible bearings subjected to both viscous and hysteretic friction. The stability criterion used varies from case to case. In simple instances, it is sufficient to check the rotor whirl amplitude equations for instability indicated by positive, real time exponents. Others may require the stability condition be obtained using the Routh-Hurwitz criterion. Hydrodynamic instability is introduced by a discussion of the mechanics of fluid-film whirl. From this, the method of stability analysis of rotors in bearings is developed and applied in turn to liquid bearings, gas bearings, rigid rotors, and elastic rotors. Results for several bearing types are included, extending through the two-mass rotor in damped, flexible supports.

All high-speed rotors pass through at least one system critical speed during each cycle of operation. The dynamics of this transition are discussed in Section 6 for the cases of a simple rotor in rigid bearings, damped rigid bearing rotor, and for flexible bearings. The rotor motion includes the influence of the transients induced during start-up, and the interaction between the transient and the critical speed amplitude buildup may determine the performance of the machine.

Balancing of flexible rotors is discussed in Section 7. This subject is the least tangible aspect of rotordynamics, and at present it may not be reduced to an identical routine even between rotors of the same size and shape — much less eliminated by standard design practice. The need and technique for balancing a rigid rotor statically and dynamically are stated, and the distinction between

this and flexible rotor balancing is discussed. Practical aspects of machine balancing and field balancing are considered, followed by a discussion of the principles of balancing machines, and the determination of the required correction weights. The influence-coefficient method is then discussed in detail as applied to the balancing of high-speed flexible rotors. The example of a small high-speed rotor is used to demonstrate and compare the effectiveness of multi-plane balancing by the influence-coefficient method with rigid-rotor two-plane static-dynamic balancing. Finally, the levels of residual unbalance which will be acceptable in operation is discussed.

Section 8, the final section, deals with additional effects such as the axial and torsional motions which occur most commonly in high-speed machinery. Sources, critical speed calculations, and methods of suppression for both torsional and axial vibrations are considered. Axial vibrations of a fluid-film thrust bearing are discussed in detail. These effects are drawn together by considering the influence of torsion and axial motion on the bending motions during whirling for a rotor with distributed mass-elastic properties.

Considerable specialized knowledge in disciplines other than rotor-bearing dynamics is drawn on in the text and, where possible, the required analytical procedure has been given in some detail to make the particular subject self-contained. Hydrodynamic lubrication is a subject in itself. The basic steps from Reynolds' equation of three-dimensional viscous lubricant flow to pressure distribution load capacity, friction, and damping and elastic properties of the fluid-film are outlined in Appendix A. Appendix B presents the derivation on various equations of the rotating coordinates; complex plane, vectorially,  $\xi$ ,  $\eta$  coordinates,  $r$ ,  $\theta$  coordinates. Appendix C is the bibliographical listing of the published references cited in the main text.

#### Sources of Text Material

The references listed in Appendix C are the major source from which the material of this book has been drawn. As this volume is unique in its field, no other texts were available for comparison - with the exception of Dimentberg (Ref. 1). This work is concerned with the mathematical analysis of rotor motions for amplitude and stability, an objective which it accomplishes with elegance and thoroughness.<sup>1</sup>

- 
1. On translation from Russian to English, inadequate proof-reading has permitted the inclusion of a great number of algebraic and textual errors.

Dimentberg deals with elastic rotor-bearing systems, but omits all reference to fluid-film bearings and their effect on rotor motions. The only guidance provided in this direction concerns a relatively simple use of a simple, unbalanced, elastic rotor which operates in bearings having identical coordinate stiffnesses, that are damped in one direction. The emphasis throughout is on obtaining analytical, closed-form solutions to the problems considered, often in the face of extremely complex and tedious algebra. No use is made of the digital computer. Bearing in mind that the first satisfactory solutions to the lubrication problem were obtained after adapting the basic equations to digital computation, it is obvious that the rotor in fluid-film bearings was beyond the scope of Dimentberg's book. Pinkus and Sternlicht (Ref. 2) contains basic hydrodynamic theory, plus a chapter on hydrodynamic instability that includes an analysis of the balanced rotor in fluid-film bearings. This work is the only reference which discusses bearing stability theory in its modern analytical aspect. The numerical results included for many bearing types make this work a valuable design text. Most of the techniques and applications for bearing stability cited in the present volume have been developed since the publication of the above reference.

#### Rotor-Bearing System Analysis

Throughout this work, the objective of all analyses is to obtain a knowledge of the dynamic performance of the entire machine. This is implied by the term "rotor-bearing system", in which the basic components involved in the total motion are coupled analytically as occurs physically in the machine. Dynamic considerations associated with rotor, bearings, and foundation are discussed in Section 2. This analytical representation is possible on the condition that the motions of all components are small allowing the system equations to be linearized. The dynamic properties of the rotor and its bearing supports may then be determined individually and linked together through the boundary conditions. This approach applied to liquid and gas bearing systems has been very successful in determining the threshold of stability since the stable, balanced state from which instability is approached consists of small motions which satisfy the analytical assumptions. However, the true dynamic response of a fluid-film bearing is highly non-linear, and so relatively little work has been done on the analysis of systems with large amplitude motions. This is due to the analytical complexity involved in solving the non-linear response equations. Apart from certain exploratory studies, the

practical need for a total solution has not been pressing, particularly as it means that a separate rotor-bearing response analysis is required for each bearing type. Practical considerations, therefore, compel the investigator to separate the rotor and the bearing and to represent the fluid-film forces by linear gradients, harmonic motions, and small displacements. This method is quite general in application, and is well-suited to the preparation of a general computer program in which the rotor becomes a discrete-mass-elastic system. The effect of any type of bearing may then be examined for which the dynamic coefficients are available.

#### The Remaining Problems of Rotor-Bearing Dynamics

Remaining problems are concerned with: (1) obtaining a better understanding of the mechanics of certain system processes, such as hysteretic damping and resonant whipping, and (2) with obtaining data on various configurations which inherently possess a high threshold of stability, or induce small-amplitude whirl motions through damping. An itemized listing of the most significant of these problems is as follows:

##### Rotor

1. Stiffness characteristics for built-up rotors.  
At present, experience is used to assign practical stiffness values where force is transmitted between components across a friction interface, such as a shrunk-on sleeve. A problem exists in deciding the effective contact area and variation in constant pressure.
2. Stiffness characteristics for rotor with abrupt section change.  
These changes do not allow the full stiffness of the section to be utilized because of St. Venant end effects. A meaningful general evaluation is needed for guidance.
3. Refined balancing technique.  
Faster, larger, more flexible rotors operate between higher critical speeds and must have smaller unbalance levels. Further information on the influence of typical unbalance on the rotor-bearing system is needed for more refined balancing, including dynamic pedestal effects, the influence of thermal distortions of the rotor and techniques for overcoming or compensating, and the effect of gravity.
4. Rotor representation as a simple system.  
Where a simple rotor model gives adequate dynamic data, the problem of accurate representation of mass-elastic data from a complex rotor, with several disks and a shaft, exists. Better guidance data on rotor model specification is required.

5. Effective mass of a submerged rotor.  
Pump rotors for many fluids including liquid metals entrain the surrounding medium in which the inertia properties contribute to the system mass and, hence, dynamic characteristics.
6. Vertical rotor precession and nutation.  
Ultracentrifuge and spin-test rotors involve these effects. Data on safe working practice and gyroscopic stability boundaries is needed.

#### Bearing

1. Non-linear bearing effects on rotor motion.  
The subharmonic and superharmonic properties arising from large amplitude rotor motions are little known. A convenient method of calculation is needed which is also suitable for stability analyses. At present, stability calculations are based on small displacement stability from the steady-state position. The stability of the whirl orbit itself is unknown.
2. Acceleration of gas-bearing rotor through critical speeds.  
These systems have small clearances and low damping and the possibility of touching is greater during transition. An examination of the simple rotor in a damped elastic gas bearing is needed to determine amplitude buildup.
3. Resonant whipping.  
An examination of the conditions under which a rotor may be driven through the resonant whipping condition, is required for ultra-high speed rotors and to permit less stringent bearing stability design requirements.
4. Shock, impact, and random vibration response.  
The performance of gas and fluid-film bearings under shock and impact conditions is lacking, although recent experiments indicate touch can be survived quite readily, and that the bearing may not be the limiting component. Harmonic load component performance has been documented and offers an introduction. Random vibration studies of gas bearings are needed to establish design criteria for non-steady environments.

#### Rotor-bearing system.

1. Shock, impact and random vibration response.  
An extension of bearing requirement No. 4 to a system study is needed, beginning with a simple rotor in fluid-film bearings.
2. Bending, axial, and torsional mode coupling.  
Simultaneous existence of several modes of vibration can result in coupling. Bending-torsional system studies have been initiated for geared systems. The influence on the mode shape and the critical speed due to the coupling gears contact forces may be significant, and variable.

3. Built-in dampers.  
Possible attenuation improvement in rotor and pedestal motions by built-in dampers and tuners designed to suit the system may be achieved. The damper attenuation studies are required.
4. System response to external excitation.  
The effect on the system of a resonating component would be valuable in determining the dynamic response of the system to turbine blade vibrations, disk axial vibrations, or to externally impressed high-frequency forces.

State-of-the-Art.

The small-amplitude motions of the system are understood with sufficient accuracy for immediate practical purposes. The analytical tools have been developed to deal with these problems. More data is now required on many practical aspects of dynamic response and on how these influence the system and its motions.

## II

### ANALYTICAL REPRESENTATION OF THE ROTOR-BEARING SYSTEM

#### Dynamical System of the Machine

As a first step in the dynamical analysis of any machine it is necessary to establish from the proposed machine layout those components which will act together to constitute the dynamical system of the machine. In most instances, the rigidity of the bearing housings and their supports reduces motions of these components to a minimum. The rotating components are, in general, much more able to respond to rotor dynamic forces, and so the dynamical system of any machine is centered around the rotor itself. In a complex system the dynamical constitution of the rotor may be different for different types of motion; for example, in the geared system shown in Figure 2.01, bending motions of each shaft are unlikely to be transmitted to any significant degree through the gear meshes, whereas torsional motions will be both transmitted and influenced by the gear ratio. If the shafts shown in this system are very flexible, the total motion may contain both bending and torsional component motions. But if the shafts are designed to transmit power and to resist bending deflection, the system motions are unlikely to be coupled, and the equations describing both types of motion are thereby greatly simplified. The most commonly-occurring motions in any machine system are:

1. Rigid body motions
2. Bending motions of shafts
3. Torsional motions
4. Axial motions
5. Plate-mode motions of impellers, disks and gear wheels

Both translatory and conical rigid-body intermodal coupling, and rigid-body-bending coupling are common in rotordynamic systems; torsional motions with some bending motion due to shaft and bearing displacement are encountered in high-speed gearboxes and other transmission systems. The influence of torsion on bending modes has been considered by Johnson (Ref. 3). Axial-torsional coupling may occur with long transmission- and propeller-shaft systems, where the thrust bearing flexibility allows the system to move axially, and bending-axial motions due to axial thrust in turbomachinery are well known. Where the shaft

is short and light-weight, it may participate in the high-frequency plate mode vibrations of the disks or gears which it carries. Each of these types of motion is shown diagrammatically in Figure 2.02.

Generally speaking, the possibility of coupling will be indicated if a calculated natural frequency of any of the above simple, uncoupled, types of motion lies close to the natural frequency of any other simple uncoupled motion. Where this occurs, an analysis of the coupled motions is necessary to obtain the true natural frequencies and mode shapes.

The motions with which this report is mainly concerned are the rigid-body modes and the bending modes of a flexible rotor in flexible supports. Analysis of these particular motions is an important part of the design of all rotating machinery. The other types of motion listed above also occur in these systems, but their effect is generally speaking more straightforward, and adequate treatments are available in the subject literature, except insofar as coupling, particularly bending coupling, is concerned. Section 8 deals more specifically with the influence of axial and torsional effects on the system.

In order to establish the dynamic system it is necessary to anticipate the extent to which each individual mechanical component is likely to enter into the system motions. The rotor, the bearings, and the foundation are three basic component groupings. The following sections review the make-up, interaction, and participation of these items.

### The Rotor

Mechanically, a rotor consists of a number of components which are rigidly attached, forming a shaft which rotates and performs useful work. Many rotors consist of a basic shaft upon which are mounted components such as bladed turbine wheels, impellers, drive couplings, electrical armature laminations and coil windings, gear wheels, and so on, Figure 2.03. The shaft serves to locate the working components centrally along the elastic axis of the rotor. They may also be attached elsewhere, perhaps by disk-to-disk bolting, in which case the rotor is made stiffer. A drum-type rotor may also be used to reduce rotor deflections where the bearing span is large, Figure 2.04. This type of construction is common in turbine practice, and

is also used for high-speed guide rolls on paper-making machines, newsprint machines, etc. Other rotor types are short in length, as in the case of helicopter rotors. One end of the shaft is connected through a gearbox, clutch, flywheel and universal joints to a prime mover, which itself has either a crank-shaft or a rotor. The other end of the shaft carries a propeller consisting of several long flexible blades, Figure 2.05. The ventilation fan unit of Figure 2.06 has a similar overall construction. In each of these cases, the designer wishes to know: How will the stiffness of each rotor component influence the overall motion of the rotor in its supports? How will the mass and inertia properties of each rotor component influence this motion?

### Dynamical Representation of Rotor

Dynamically, a rotor is the aggregate of the effective mass-elastic properties of its constituent mechanical components. It responds as such in proportion to the variety of harmonic impulses which it receives. Frequently, rotor motions may be analyzed directly using known formulae, due to the simplicity and symmetry of the mechanical system which they represent. Such calculations are often possible where the information required concerns only the first few critical speeds. As the speed range of many simple machines contains only one or, at the most, two critical speeds, these machines may often be calculated quickly and conveniently. The rotor elasticity is represented by a simple equivalent shaft, and the rotor mass is concentrated at as many mass-stations as there are modes to be calculated. The mass arrangement is determined by the actual machine layout. Both bending and torsional oscillations of one-, two-, and three-span machines may be calculated with good accuracy with such a representation. Very frequently, the shaft mass is relatively small compared with the mass of the gears, impellers, and so on, carried by the shaft, and the mass-elastic layout is established directly. Figure 2.07 shows the analytical representation of several mechanical rotor systems.

More complex rotor systems cannot be evaluated through any simple method, and an adequate mass-elastic representation often requires a large number of masses, joined by shafts of differing stiffnesses. Where the actual rotor is a stepped shaft, the calculation of an equivalent shaft in bending is tedious, and the inconvenience of hand calculations may warrant the use of a computer in

this instance. The equivalent torsional shaft may be calculated directly. Where symmetry is absent between the stiffnesses, or between the masses, computer calculation usually becomes an essential time-saver.

Large rotating disks have considerable gyroscopic and rotatory inertia. At moderately-high speeds, especially where large amplitude of critical motions occur, the inclusion of the forces arising from gyroscopic and rotatory effects in the equations of motion is usually necessary, or the accuracy of the result will be impaired. The mass and the stiffness of both systems shown in Figure 2.08 are equal; the critical speeds and mode shapes are not equal, because the end inertias are dissimilar. Where these effects must be included, critical speed calculations become more complicated by the addition of another degree of freedom in the rotor system for each mass-station. These effects are discussed more fully in Section 4.

Computer analysis of the dynamic performance of a rotor in its bearings allows all simplifying assumptions to be dispensed with, and the rotor geometry may then be faithfully represented in the calculation input data. The rotor profile becomes increasingly complex as the operational demands of the machine in which it operates become more stringent. Smaller size, greater speed, minimum thermal distortion, and volume, machine- and function-optimization all tend toward rotors which have abrupt profile changes, minimum-weight sections, dissimilar materials acting in composite sections, all require an optimized distribution of mass-elastic properties to achieve the required dynamic performance characteristics. In these cases, the only way to obtain meaningful design data is by a computerized analysis. In this, the rotor is first divided into an appropriate number of sections so that its mass-elastic properties may be represented with reasonable accuracy by the system shown in Figure 2.09. Within each prescribed section of the rotor, the section mass  $\frac{W}{g} \left[ d_o^2 - d_i^2 \right] L$  is concentrated at its c.g., and is considered to act at this c.g. throughout the motion being analyzed. These concentrated masses are further assumed to be linked by massless elastic members which represent the transverse flexural beam stiffness over the distance between the rotor masses. This is the basic mass-elastic representation. More refined programs also take into account the rotatory inertia of each concentrated mass, and the gyroscopic effect arising from

rotation of the deflected rotor shape. Shear effects may also be included with bending if needed, but this effect is generally quite minor.

In preparing program input, the rotor mass values are readily obtained from the proposed layout. Greater difficulty is experienced in selecting stiffness values between shaft portions of different sections, or in tapering sections of shaft. One method of overcoming the first problem is to place a 'dummy' station of zero mass at the junction between the shaft sections. The stiffness of each length of uniform shaft is then calculated, overcoming the need for determining the equivalent second moment of area for the stepped section. Where the shaft is tapered, it may be replaced by a number of stepped sections. These are then incorporated using the above method. These effects are shown in Figure 2.10.

In many instances, the shaft sections are made tubular to minimize weight or heat transfer and rotor thermal expansion, for example, between a turbine disk and a gas bearing. The flexural stiffness of a short thin tube may be calculated approximately using beam theory, but the actual deflections are governed by the cylindrical shell equations and the particular boundary conditions of the application. No actual design data is available for this condition which will clarify the extent to which the beam theory is valid.

The reinforcing effect of shrunk-on disks or sleeves is also incompletely understood at present. A turbine disk shrunk-on to the center of a thin flexible shaft will provide little additional stiffness, whereas an outer coating applied to a roll may stiffen the roll considerably, even though the stiffness is transmitted by contact friction between the surfaces. In estimating both these cases the experience of the analyst is at present needed to allow for the stiffening. It is customary to assume that the effect of the shrunk-on section is effective over the length of the disk or sleeve, and that it may be represented by a certain increase in diameter of the basic shaft. Similar problems occur in the representation of bolted joints. Here, the true stiffness involves the bolt tension, the effectiveness of the joint, clearance of the studs in their holes, and the support provided by other mating or guide surfaces of the joint. This complexity is usually avoided in analysis by assuming a rigid joint which has the stiffness of the built-up portion of the rotor, as shown in Figure 2.11.

The above remarks on analysis of complex rotor profiles may be summarized by saying that when the desired mass distribution of the rotor has been decided with reference to complexity and the number of anticipated bending critical speeds within the speed range to be investigated, the calculation of stiffness properties of the rotor between the various stations is then undertaken. Complications arise where changes of section occur, either abruptly or by taper. Usually tapered sections may be adequately represented by a relatively few stepped sections. The use of dummy mass stations then allows uniform beam analysis to be applied, through the computer calculation itself. The stiffening effect of shrunk-on disks and sleeves is allowed for by providing a suitable diameter increase for the basic shaft or rotor section, based on experience. Bolted joints are assumed rigid for small amplitude motions. The required rotor input data for the computer program is then:

For each mass station:	mass $m_i$ ;
	polar and transverse moments of inertia
	$I_{pi}, I_{ti}$ .
Between each mass station:	cross section area $A_i$ ;
	second moment of area $I_i$ ;
	shaft section length $L_i$ ;
	modulus of elasticity $E$ .
Speed range requirement:	Speed range and increments.

### Torsional Systems

As moment of inertia is proportional to  $D^4$ , the inertia properties of torsional systems are usually concentrated in the large disks such as turbine disks, impellers, and gears. Where the shaft inertia is important, it may usually be included as a single additional mass located at the center of each shaft length. A more difficult problem is posed in determining the torsional stiffness of the shafts and other mechanical elements between the gears. In any torsional system experience indicates that accurate results may be obtained only if the total torsional system is considered, including the flexibility of all gear teeth, shafts of varying section, splines, keys, couplings, bolted connections, stiffening sleeves, clutch and drive mechanisms. Data on these effects is given by Nestorides (Ref. 4) and by Ker Wilson (Ref. 5). The predominant effects in the analytical system emerge when the total system is prepared.

The analysis of complex torsional systems is readily performed on a digital computer. This approach again allows the real problem to be investigated; complexity is no longer a barrier often requiring unacceptable simplification. This is particularly important where branched and looped torsional systems are concerned.

The end result of a torsional vibration analysis is the natural frequencies of the system, and the associated mode shapes. The torsional damping which arises from elastic hysteresis and bearing and gear lubrication is usually extremely small, and unless the system carries a fan or a propeller, the amplitudes of vibration at a system natural frequency may be very large. In this case a torsional vibration damper, such as a viscous shear damper, a pumping-chamber damper, or a Coulomb friction damper may be required. The mode shape then allows the most suitable position for this damper to be selected. In general, the introduction of even a small amount of damping reduces vibration amplitudes manyfold. Optimum damper design will usually make the torsional vibrations of a machine quite negligible.

#### The Bearings

Bearings support and constrain the rotor. As mechanical components, they serve a variety of functions, ranging from providing a means of low-friction static load support, to the attenuation of rotor amplitude, transmitted force, and structure-borne noise in high-speed rotating machinery. Because of their flexibility, bearings influence the dynamic performance of the rotor which they support, by determining the position of the system critical speeds, along with the flexibility of the rotor itself. For this reason, unless the bearing stiffness is high compared with the rotor stiffness, calculated values of rigid-bearing critical speeds may differ considerably from the real values. Linn and Prohl (Ref. 6) have considered the influence of bearing flexibility on critical speed calculations, and recent investigations have also included the influence of bearing damping. There exists a wide variety of bearing types, and the particular choice for a given application is based on the range of performance requirements which must be fulfilled. For example, where high load capacity is the predominant requirement, an externally-pressurized (hydrostatic) bearing may be needed; and if low bearing power loss or minimal temperature rise is also required, the hydrostatic bearing may have to be gas lubricated. In cases where rotor stability is the limiting factor, cylindrical

self-acting (hydrodynamic) bearings are known to have a low stability threshold speed, whereas hydrodynamic tilting-pad journal bearings are highly stable. An extensive comparative listing of bearing types with advantages and disadvantages could be prepared.

Bearings may be classified in the following ways:

- |                |                 |             |             |
|----------------|-----------------|-------------|-------------|
| 1. Directional | Journal         | Thrust      | Combination |
| 2. Type        | Rolling Element | Fluid-film. |             |

Fluid-film bearings may be further classified:

- |                               |                |              |        |
|-------------------------------|----------------|--------------|--------|
| 3. Mechanism of Load Support: | Hydrodynamic   | Hydrostatic  | Hybrid |
| 4. Lubricant type:            | Incompressible | Compressible |        |
| 5. Lubricant                  | Laminar        | Turbulent    |        |

Most machines require both journal and thrust bearings. The choice between rolling element bearings and fluid-film bearings depends upon many factors such as load, speed, temperature, reliability, stability, durability, support equipment, radioactive environment, corrosion, and other factors. In general, where moderate operating conditions apply throughout, the low cost and overall convenience of rolling element bearings offer great advantages in a design. But where any single factor becomes overriding in the design, such as extreme load, ultra-high speed, extremes of temperature, or either a radioactive or corrosive environment, some form or type of fluid-film bearing exists which is well-suited to the overriding factor, and this type of bearing is then selected in preference.

Hydrodynamic bearings operate by creating a convergent wedge of fluid between the bearing surfaces through their relative motion. The resultant pressures generated by the motion of the fluid are sufficient to support the bearing load. A number of hydrodynamic bearing types are shown in Figure 2.12. This type of bearing has the advantage of simplicity of operation with a minimum of supporting apparatus. Load capacity may be moderately high, and bearing stiffness may be made fairly high by design. As there is little associated apparatus, dynamically stable hydrodynamic bearings are obtained by selection of a geometric form which has inherent stability, or a high threshold, if high speeds of rotation are involved, or the impressed cyclic loading of the machine occurs at submultiples of the speed of rotation.

As stated above, plain cylindrical bearings have a low stability threshold; four-axial groove, elliptical, segmented arc, and partial-arc bearings have inherently much higher instability threshold speeds; and tilting-pad bearings are inherently stable up to pad flutter speeds, i.e., as long as the pads tend to "follow" the shaft motions. The dynamic stiffness and damping characteristics of most important hydrodynamic bearing types have been obtained for use in rotor dynamic calculations. The influence of these bearing properties on the performance of a rotor are discussed in Sections 3 and 5.

Hydrostatic bearings operate by supporting the applied journal load upon a film of lubricant which is fed into the bearing under pressure from some external source, such as a pump. This principle is shown in Figure 2.13 for a hydrostatic journal bearing. The flow of the lubricant is restricted (a) by restrictions within the bearing, and (b) by the narrow clearance space. Better control over bearing performance is obtained by adequate restrictor design. External restrictors may be either inlet nozzles feeding into the clearance space, or capillary feeders. Some bearings have been designed so that the area surrounding the lubricant inlet holes act as a restrictor. These bearings are said to be inherently compensated. Some form of flow restrictor is required for all hydrostatic bearings. The critical design area for all types of hydrostatic bearings is the area surrounding the inlet restrictor or nozzle, the diffuser or pressure chamber, and the zone where the lubricant flow enters the clearance space. This area controls the pressure drop, bearing flow and dynamic performance of the bearing. A particular problem associated with hydrostatic bearings is pneumatic hammer, in which pressure surges cause heavy vibrations in the supply lines and of the journal within the housing. Pneumatic hammer is closely associated with the depth of the pressure chamber. Deep chambers increase the likelihood of this effect. This is less important with a multi-inlet bearing using diffusers to avoid inherent compensation. Pneumatic hammer may lead to lock-up of a journal against its bearing in certain cases. Dynamic stiffness and damping properties have been obtained by Lund (Ref. 7) and others for the more common types of hydrostatic bearings. Hydrostatic bearings are important where either high load capacity, high axial or radial stiffness, or accurate control of position or concentricity are required.

Where an externally pressurized bearing is used in a high speed application, the pressures generated by the rotation influence the regular hydrostatic pressure distribution. This type is known as a hybrid bearing, and the bearing load capacity, stiffness and dynamic response are different from the purely hydrostatic bearing. Analyses have been made to determine the extent of these effects, see Lund (Ref. 7).

Each of the bearing types discussed above have been operated on both incompressible and compressible lubricants. Incompressible lubricants include: oil, water, kerosene, mercury; liquid butane, nitrogen, and other liquified process gases; liquid metals such as sodium, potassium, NaK. Compressible lubricants include: air, hydrogen, helium, nitrogen, oxygen, and the inert gases; butane and other organic vapors; ammonia, freon, and other refrigerant gases; and steam, wet and superheated. Where the lubricant is incompressible, the major property governing the performance of the bearing, and hence the system, is the viscosity. This is principally determined by the operating temperature of the bearing, which depends upon the bearing friction; it is also governed to a lesser extent by the operating pressures of the fluid. Density is not a factor in incompressible lubrication, except in deterring mass flow. Mass flow may be important where the lubricant acts as a bearing coolant, in which the heat transfer coefficient of the lubricant will also be important. Thrust bearing designs often require consideration of the heat transfer characteristics. Heavily loaded designs may be water cooled through the pedestals.

For compressible lubricants the variation of density with pressure is of importance in determining bearing performance, in addition to viscosity. For conventional circumstances, the flow of gas through the bearing is isothermal and so the thermal characteristics of these bearings are usually unimportant. Both compressibility and viscosity appear in the compressible Reynolds' equation, as indicated in Appendix A. The load capacity conferred by a compressible lubricant is considerably less than that of an incompressible lubricant, and the dynamic stiffness and damping characteristics are likewise much lower. An exception exists in the case of an externally pressurized gas bearing, where the bearing stiffness properties may be made comparable with those for an incompressible lubricant.

Conventional bearing operation involves laminar flow of the lubricant, but applications exist where the flow is turbulent. High speed operation with low viscosity, high density lubricants promotes turbulent lubrication. Closed cycle space power plants may operate with liquid mercury or liquid metals as the lubricant. Water lubricated bearings in a high speed pump may lead to turbulent operation. Studies in turbulent lubrication were initiated by Taylor (Ref. 8), Wilcock (Ref. 9) and Smith and Fuller (Ref. 10). Constantinescu (Ref. 11) developed a theoretical analysis based on Prandtl's mixing length-hypothesis. The basic equations were computerized by Arvas, Sternlicht and Wernick (Ref. 12). Results were compared for several geometries with the experimental results of Smith and Fuller (Ref. 10) and others. The unsatisfactory comparison led to the development of a new approach based on the Boussinesq-Reichard-Elirod 'eddy-viscosity' concept by Ng (Ref. 13), extended to finite length bearings by Ng and Pan (Ref. 14). The predictions of the eddy-viscosity theory have since been verified for a variety of bearing types by Orcutt (Refs. 15 and 16) for both static and dynamic bearing properties.

#### Dynamic Representation of the Bearings

With fluid-film bearings, rotor response is influenced by the bearing stiffness, and by the fluid-film damping properties. These properties are determined by the bearing geometry and by the conditions of operation, and their derivation is briefly summarized in Appendix A. For a journal operating with eccentricity ratio  $\epsilon$  within the clearance, any additional load  $F'$  applied as shown gives rise to a displacement  $x$  in the direction of the load, plus an additional displacement  $y$  at right angles to this displacement. In addition, if the displacements are applied dynamically, additional resistances arise due to the velocity of load application, in both  $x$  and  $y$  directions. The bearing forces resulting from a general  $x, y$  displacement of the journal in the  $x$ - and  $y$ - directions are therefore

$$F_x = K_{xx}x + K_{xy}y + C_{xx}\dot{x} + C_{xy}\dot{y} \quad (2.01)$$

$$F_y = K_{yx}x + K_{yy}y + C_{yx}\dot{x} + C_{yy}\dot{y}$$

The coefficients  $K_{xx}$   $K_{xy}$   $K_{yx}$   $K_{yy}$  are referred to as the bearing stiffness coefficients, and the coefficients  $C_{xx}$   $C_{xy}$   $C_{yx}$   $C_{yy}$  are the bearing damping coefficients. These coefficients depend on bearing operating eccentricity  $\epsilon$  which for any given bearing type is a function of Sommerfeld number  $S = \left(\frac{\mu NLD}{W}\right) \left(\frac{R}{C}\right)^2$ . Values of the bearing stiffness and damping coefficients are listed in Table 2.01

for the plain cylindrical bearing, the four axial-groove bearing, and for the tilting-pad bearing, for incompressible lubricants.

Equations 2.01 are the analytical representation of the bearing in terms of its dynamic properties. The motions of a rigid rotor operating in fluid-film bearings may be investigated using these expressions. The fluid-film damping is the major source of damping in such systems, and its incorporation into the system equations allows the rotor amplitude and transmitted force to be calculated at the critical speeds. When the rotor is displaced from its equilibrium operating position, the dynamic forces generated by the fluid-film act upon its mass and tend to restore it. If the motions are induced by rotating unbalance, the resulting whirl motions involve the unbalance force, the rotor mass, and the dynamic bearing forces. This problem may thus be formulated for analysis using these expressions. Unbalance response of a rotor in fluid-film bearings is discussed in Section 3, and the stability of rotor motion is considered in Section 5.

#### The Machine Structure

Some form of supporting structure is required to carry the rotor-bearing system. In small machines such as motors this usually takes the form of a casing, whereas in a larger machine such as a steam turbine, the rotor-bearing system may be supported on pedestals which are attached directly to the foundations of the building. In most cases these supports are elastic to some discernible degree, and thereby participate in the overall motion of the system.

Vibrations of motor casings as rings are discussed by Den Hartog (Ref. 17). At certain frequencies within the machine operating speed range, residual unbalance in the rotor has been known to excite ring modes of the casing. These vibrations give rise to noticeable noise (casing hum) which must be eliminated by design changes, or by the inclusion of additional damping in the casing. Oscillations of turbine platforms are discussed by Stodola (Ref. 18) and by Geiger (Ref. 19) both of whom indicated that the foundation sway flexibility lowers the fundamental bending critical speed of the turbine set. In small compressors, the bearing housings are often attached to the casing, and may possess considerable flexibility. Figure 2.14 shows a design where

each bearing support is a thin diaphragm to provide maximum angular flexibility for the bearings to follow the free-free bending mode of the rotor without sacrifice of radial support stiffness.

In most instances it is quite adequate to incorporate the stiffness and damping properties of a bearing housing or pedestal by the addition of a further spring and dashpot connected to the housing mass as shown in Figure 2.09. These effects may be readily incorporated into a general computer program which calculated dynamic response, or critical speed, for the multi-mass rotor discussed previously. Pedestal flexibility may significantly affect the dynamic performance of a machine by lowering the fundamental bending critical speed, if the pedestal spring and damping properties are comparable in value to bearing or rotor properties, particularly if the pedestal mass is large and capable of joining the system oscillations, possibly as a separate pedestal mode in which the rotor stands still. Certain bearing supports have been proposed based on this principle to minimize rotor vibrations. The arrangement, consists of a spring and a dashpot of some type which is connected to the rotor, backed up with a second spring, as shown in Figure 2.15. The back-up spring is considerably stiffer than the other spring. When the rotor speeds are low, dynamic transmitted forces are small, and the back-up spring is effectively rigid. The soft spring restrains the amplitudes somewhat, but the motions are sufficient to cause the dashpot to operate and dissipate vibrational energy. At high speeds, transmitted forces are much higher, and the stiff spring then provides attenuation not available with a rigid foundation. The dashpot is considerably stiffer, in the same order as the back-up spring, as its resistance forces  $ck$  depend upon the velocity of motion. The soft spring here has negligible effect, and the system stiffness is thus shared between the dashpot and the back-up spring. Between low and high speeds there is a gradual transition between these two conditions. The overall effect is a support with effectively constant increase in stiffness and damping. Any type of linear dashpot will give this effect, such as an orifice- or piston-dashpot.

#### Forces Acting in a Rotor-Bearing System

In order to determine the motion of the rotor mass it is necessary first to determine the nature and magnitude of the forces to which it is subjected. Knowing the forces involved allows the equation of motion to be formulated and integrated to give the required rotor dynamic properties.

Forces arise from the environment in which the rotor-bearing system operates, and from the nature of the system itself. A useful classification of forces in mechanical systems has been given by Ziegler (Ref. 20), Table 2.02. From the classification given it is possible to infer the dynamic characteristics of particular system types.

Table 2.03 classifies the forces acting on a rotor-bearing system in terms of the nature of their application, together with examples of systems where these forces occur.

In Table 2.03 the forces are classified as:

1. Externally-applied forces which act on the machine as a whole, from without. They are transmitted to the rotor-bearing system via the foundations or machine casing. Such forces are experienced in aerospace maneuvers, in explosion-proof, blast-proof, and shock-proof, and earthquake-proof designs, notably power plants and delicate measuring apparatus. The impulsive nature of the loading is attenuated to some extent by the rotor-supporting structure, including the bearings, before it reaches the rotor. The effects may range from transient-initiated instabilities in the motion which either are sustained or decay, to bearing touching accompanied by shaft deformation followed by severe unbalance whirling. A knowledge of the forces involved in shock motions is important in the design of all delicate, high-reliability, and accurate position-control equipment.
2. Forces generated by the rotor motion. These forces are absent from the environment when the machine is not operating. In each instance, the specific nature of the equipment determines the forces involved. Usually, a number of these forces act together. The overall motion is then determined by their relative magnitudes. Specific effects are discussed in detail in the following chapters, and methods for overcoming related problems are indicated.
3. Forces applied to rotor. These forces occur during operation, and are applied by the system in which the rotor operates. These include drive torques; steady, accelerating, oscillating, or transient; radial or tangential rotor forces existing from drive application or transmission, and field forces either gravity or electromagnetic; and axial or normal applied forces resulting from the balance of

pressures required for the machine operational functioning, or for component function such as high load accurate position hydrostatic bearings.

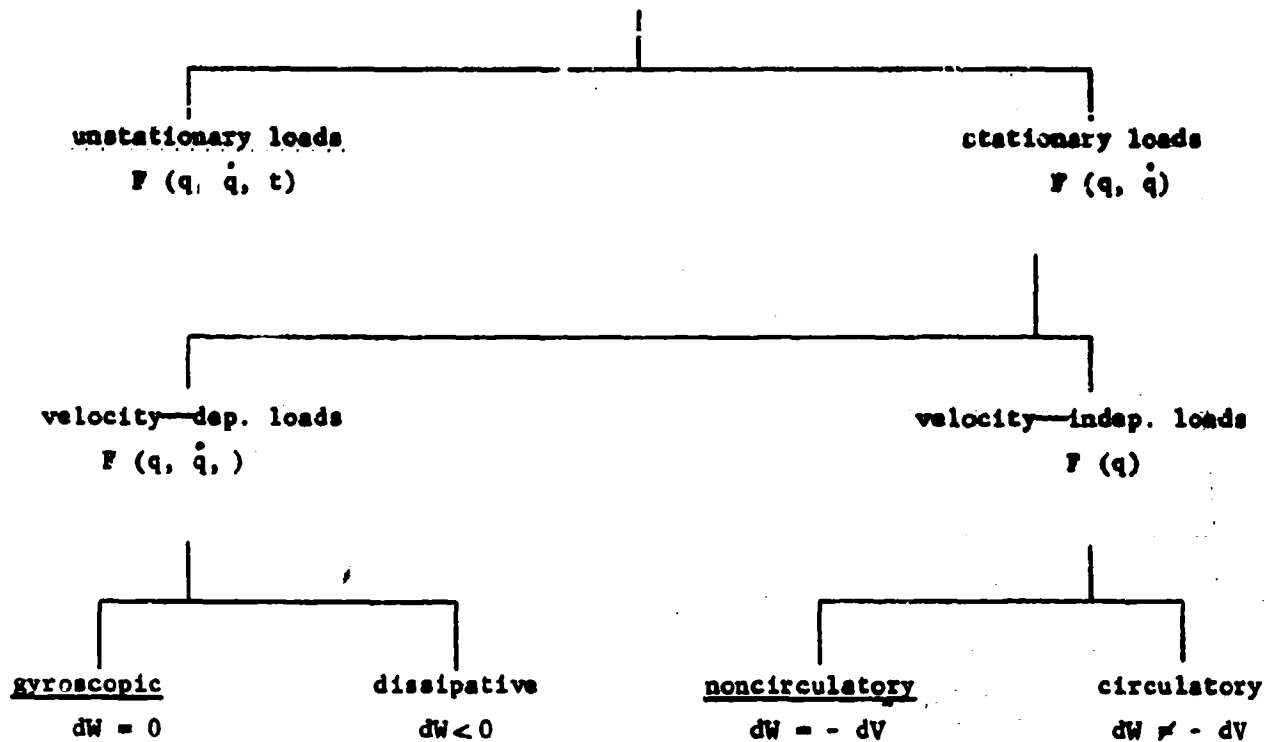
In calculating the dynamic performance of a rotor in bearings, the only forces usually required are the rotor unbalance value, its location, and the bearing forces corresponding to the operating eccentricity. These forces allow the amplitude response and transmitted bearing force, and the rotor-bearing stability properties to be calculated for the system. From this information the rotor performance characteristics may be optimized at the design stage. If the rotor encounters operational problems such as half-frequency whirl, synchronous whirl, Coulomb friction whirl, or resonant whipping, the above dynamic performance data allows these problems to be diagnosed, providing the action of the forces which promote these motions is clearly understood. A detailed knowledge of all the forces which act on a rotor is not required for design, but recognition of the significant forces occurring in an operational environment is essential for the diagnosis of rotor-bearing system problems. Finally, the analytical formulation of any rotor-bearing problem also requires an appreciation of all the forces involved in the motion. The influence of the forces listed in Table 2.03 on rotor motions is discussed in the following chapters.

Table 2.01 Spring and Damping Coefficients

	$\epsilon$	$K_{xx}$	$K_{xy}$	$K_{yx}$	$K_{yy}$	$C_{xx}$	$C_{xy}$	$C_{yz}$	$C_{yy}$	$S$
Plain Cylindrical L/D = 1.0	0.2	1.283	5.492	-4.610	2.22	10.72	1.95	2.29	9.77	0.665
	0.5	2.06	3.23	-1.07	2.04	6.02	2.00	2.17	3.40	0.189
	0.7	3.59	3.38	0.02	1.99	6.23	1.95	2.13	2.00	0.081
Four-Axial Groove L/D = 1.0	0.2	2.10	5.21	-3.85	0.927	10.18	0.825	0.408	3.6	1.922
	0.5	3.07	2.74	-0.249	0.86	3.92	-0.94	1.405	0.293	0.47
	0.7	5.28	3.62	3.67	1.20	2.67	-1.587	-0.006	-0.004	0.1296
Elliptical Bearing L/D = 1.0	0.2	4.12	6.80	-4.99	0.583	16.04	-0.15	-1.95	3.88	
	0.5	3.92	3.50	-0.203	1.44	7.08	1.61	1.66	1.25	
	0.7	18.40	6.84	1.54	1.85	13.21	1.94	1.98	76.10	
L/D = 1.0 M = 1.0	0.2	12.4	7.73	-6.50	0.057	27.2	-2.24	-8.41	1.51	
	0.5	15.8	4.20	-2.19	0.887	11.72	-0.100	-1.43	1.98	
	0.7	117.5	41.7	12.32	7.38	33.6	3.69	4.12	0.765	
150 Degree Partial Arc	0.2	-1.279	4.54	-2.542	3.647	8.234	5.674	5.674	6.620	0.264
	0.6	0.3085	1.943	-1.632	3.084	2.081	2.605	2.604	6.725	0.062
	0.09	0.8015	3.043	-0.618	10.31	0.896	2.03	2.034	9.331	0.0134

Spring and damping coefficients for tilting-pad bearings are given in chart form in Lund (Ref. 81).

Classification of Loads  
active forces



Classification of Reactions  
reactive forces

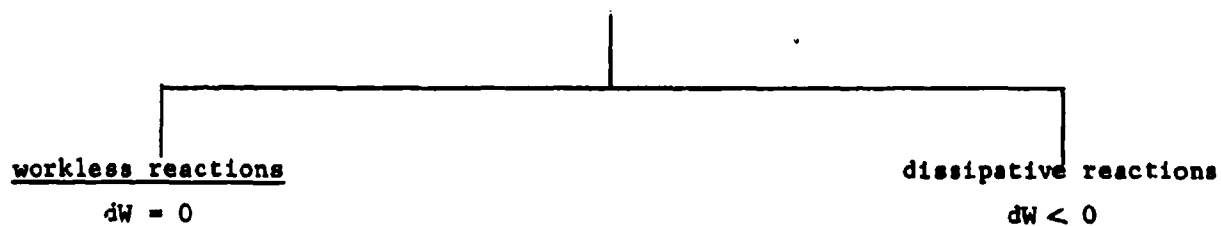


Table 2.02 Classification of Forces and of Reaction

Table 2.03 Forces Acting on Motor-Bearing Systems

Source of Force	Description	Application
1. Forces transmitted to foundations, casing, or bearing pedestals.	Constant, unidirectional force Constant force, rotational Variable, unidirectional Impulsive forces Random forces	Constant linear acceleration. Rotation in gravitational or magnetic field. Impressed cyclic ground- or foundation-motion. Air blast, explosion or earthquake. Nearby unbalanced machinery. Blows, impact.
2. Forces generated by rotor motion.	Rotating unbalance: Residual, or bent shaft. Coriolis forces Elastic hysteresis of rotor  Coulomb friction  Fluid friction  Hydrodynamic forces, static.  Hydrodynamic forces, dynamic. Dissimilar elastic beam Stiffness reaction forces  Gyroscopic moments	Present in all rotating machinery  Motion around curve of varying radius. Space applications. Rotary-coordinated analyses. Property of rotor material which appears when rotor is cyclically deformed in bending, torsionally or axially. Construction damping arising from relative motion between shrunk fitted assemblies. Dry-friction bearing whirl. Viscous shear of bearings Fluid entrainment in turbomachinery. Windage. Bearing load capacity Volute pressure forces Bearing stiffness and damping properties. Rotors with differing rotor lateral stiffnesses. Slotted rotors, electrical machinery. Keyway. Abrupt speed change conditions Significant in high-speed flexible rotors with disks.
3. Applied to rotor	Drive torque Cyclic forces  Oscillating torques  Transient torques Heavy applied rotor force  Gravity Magnetic field, stationary or rotating. Axial forces	Accelerating or constant-speed operation Internal combustion engine torque and force components. Misaligned couplings. Propellers. Fans. Internal combustion engine drive Gears with indexing or positioning errors Drive gear forces Misaligned 3-or-more rotor-bearing assembly. Non-vertical machines. Non-spatial applications. Rotating electrical machinery  Turbomachine balance piston. Cyclic forces from propeller, or fan. Self-excited bearing forces. Pneumatic hammer.

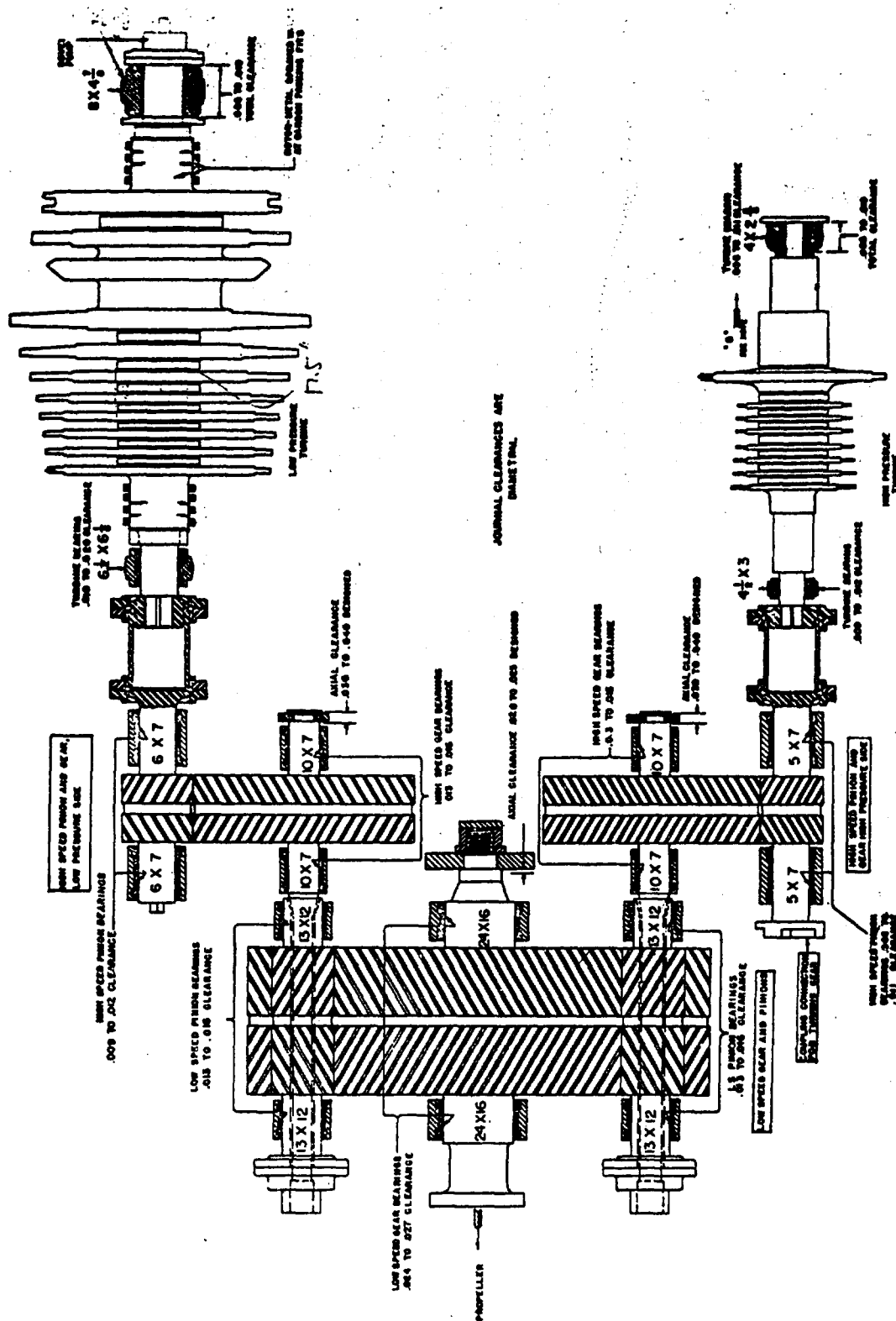
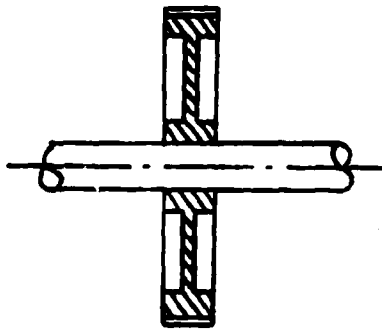
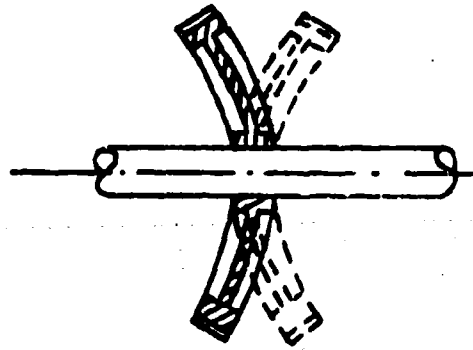


Fig. 2.01 Geared System Susceptible to Bending and Torsional Motions

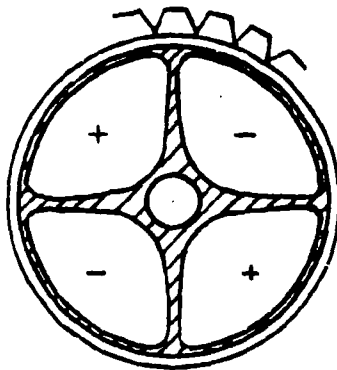
Reprinted from THE EFFECT OF FLEXIBILITY OF SUPPORT UPON THE CRITICAL SPEEDS OF HIGH SPEED ROTORS, Figure 6, by Frank C. Linn and M. A. Prohl for The Society of Naval Architects and Marine Engineers. November 1951



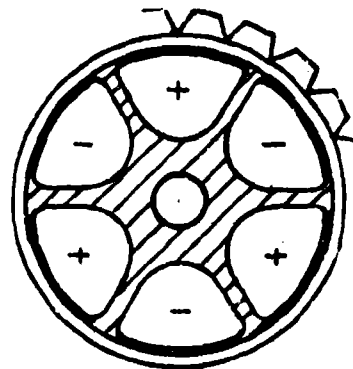
(a) Gear on Shaft



(b) Fundamental (Umbrella) Mode



(c) Two-Diameter Mode



(d) Three-Diameter Mode

Fig. 2.02 Plate Mode Vibrations. Umbrella and Diameter Modes

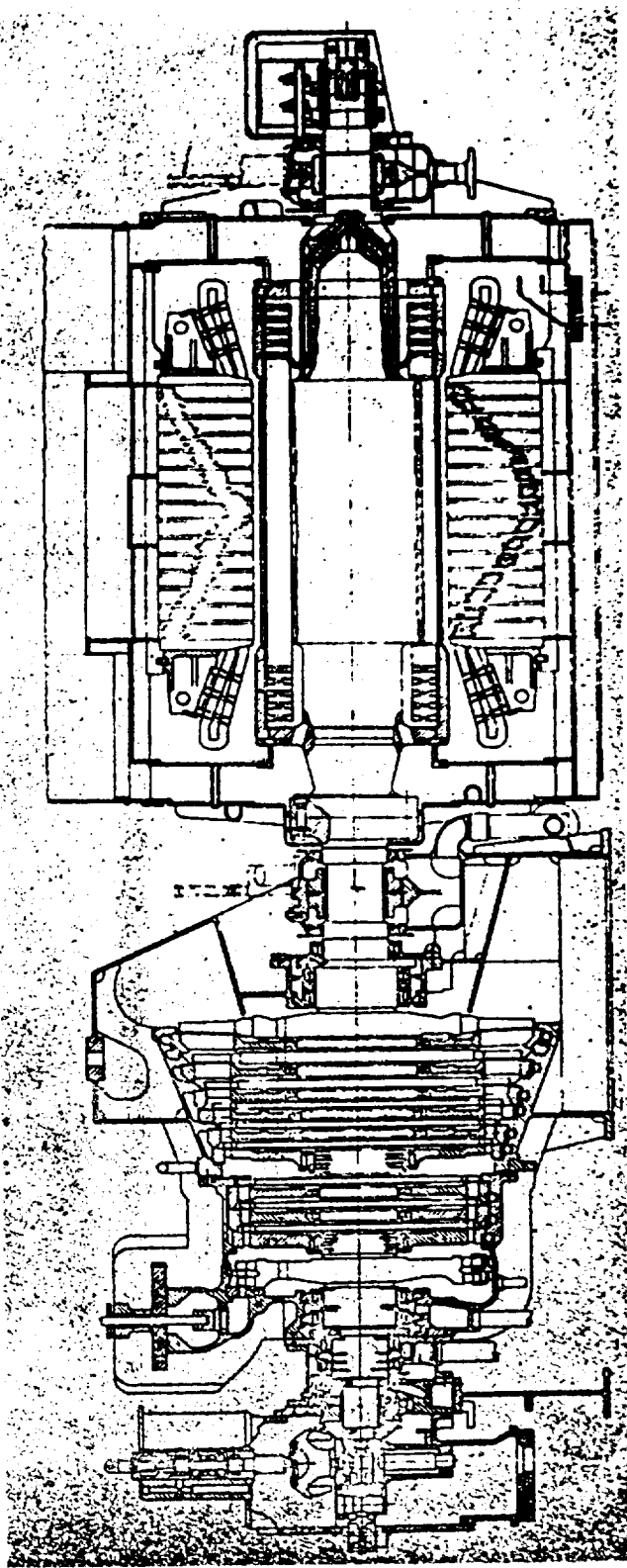
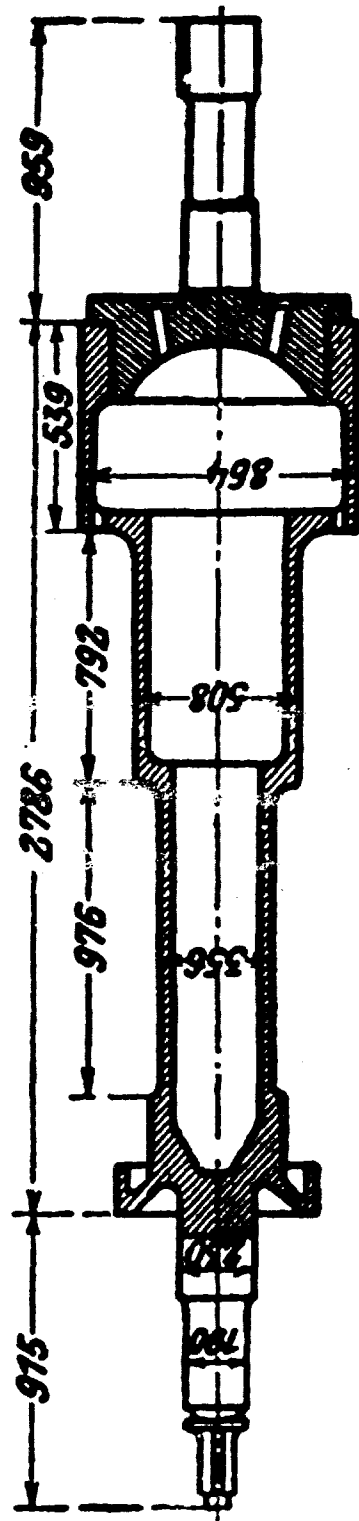


Fig. 2.03 Turbogenerator Rotor, Section Showing Marine Components

Reprinted from THE EFFECT OF FLEXIBILITY OF SUPPORT UPON THE CRITICAL SPEEDS OF HIGH SPEED ROTORS, Figure 4, by Frank C. Linn and M. A. Prohl for The Society of Naval Architects and Marine Engineers. November 1951



Dimensions are in mm.

Fig. 2.04 Drum-Type Rotor

Reprinted from STEAM AND GAS TURBINES WITH  
A SUPPLEMENT ON THE PROSPECTS OF THE THERMAL  
PRIME MOVER, Figure 387, by Dr. A. Stodola  
Volume 1, McGraw Hill Book Company, Inc.  
New York, N.Y. 1927

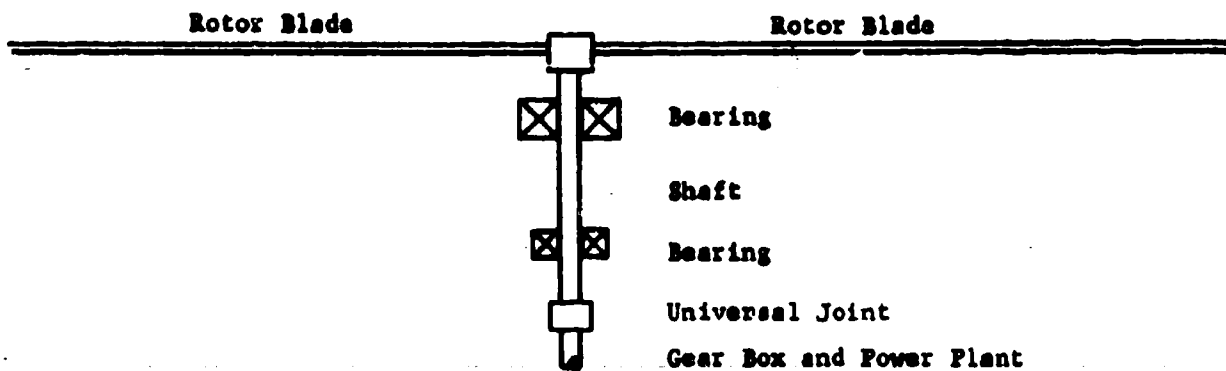


Fig. 2.05 Helicopter Rotor. Flexible Blades and a Flexible Shaft

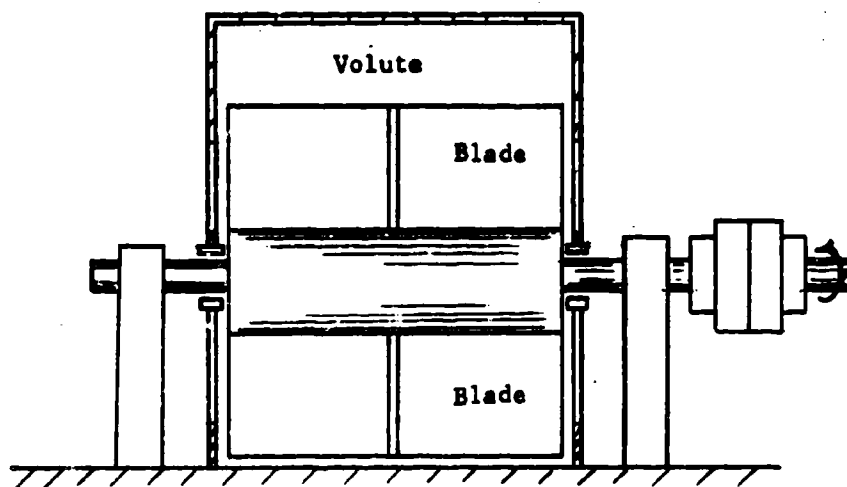


Fig. 2.06 Ventilation Fan Rotor

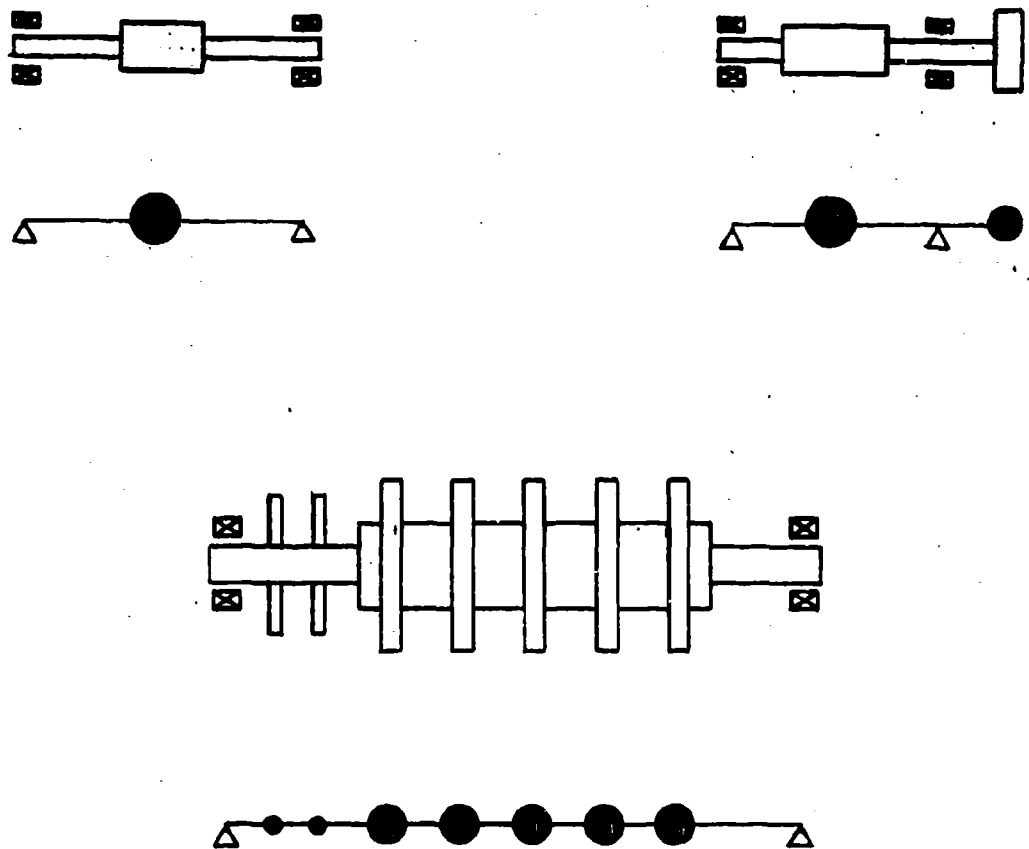


Fig. 2.07 Representation of Actual Rotor by Analytical Model

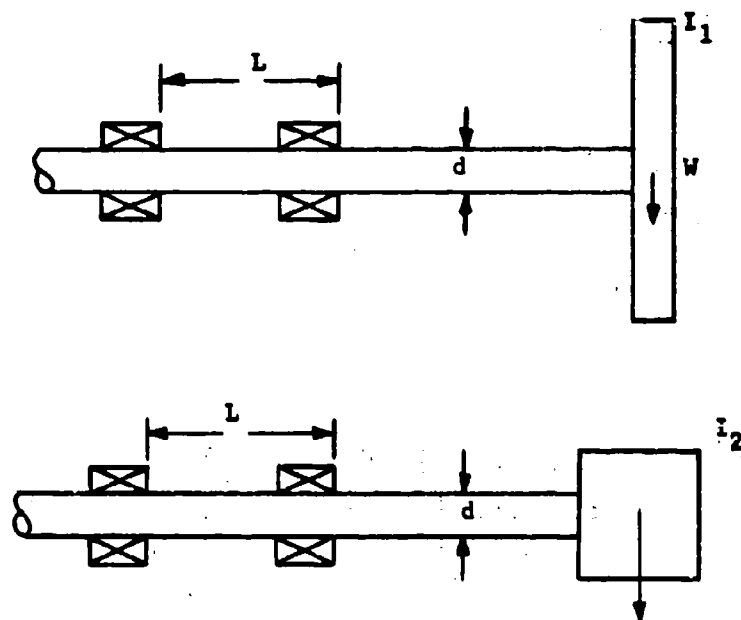


Fig. 2.08 Equal Mass-Stiffness, Differing Inertia Systems (After Den Hartog)

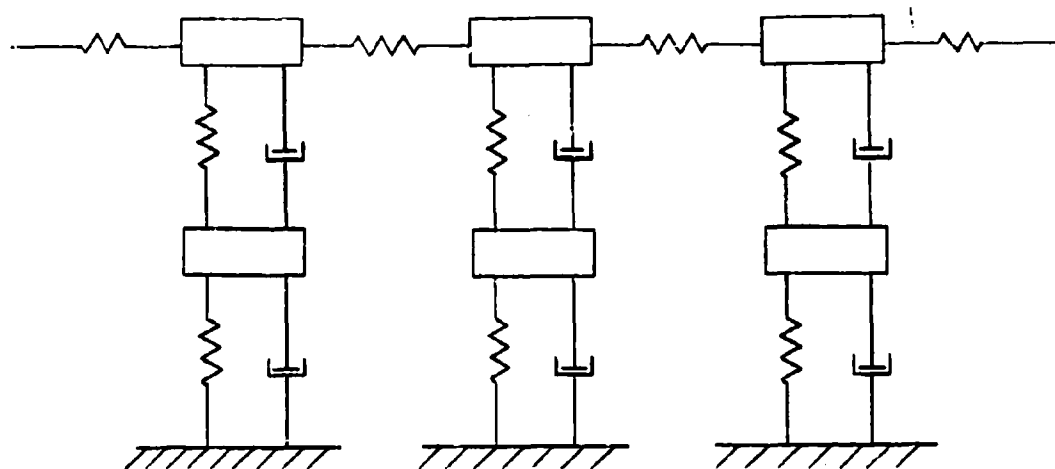
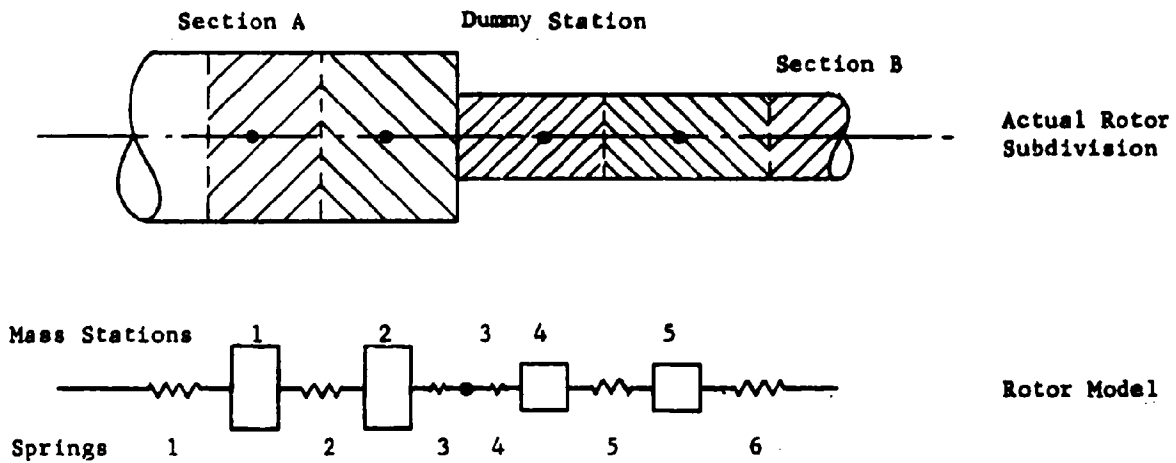
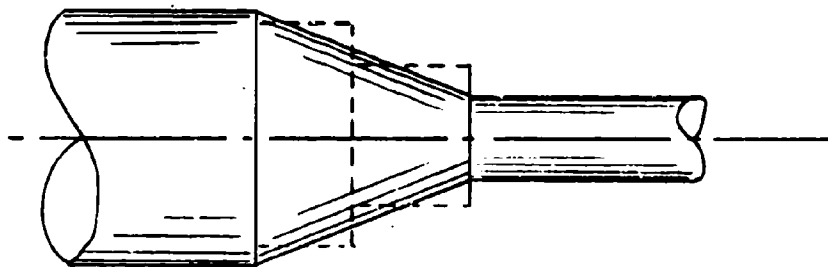


Fig. 2.09 Mass Elastic-Bearing Rotor Representation



- (a) Representation of Abrupt Section Change Using Uniform Shaft Sections by Introducing a Dummy Mass Station At 3



- (b) Representation of Conical Section by Two Equivalent Cylindrical Sections

Fig. 2.10 Methods for Representing Rotor Section Changes

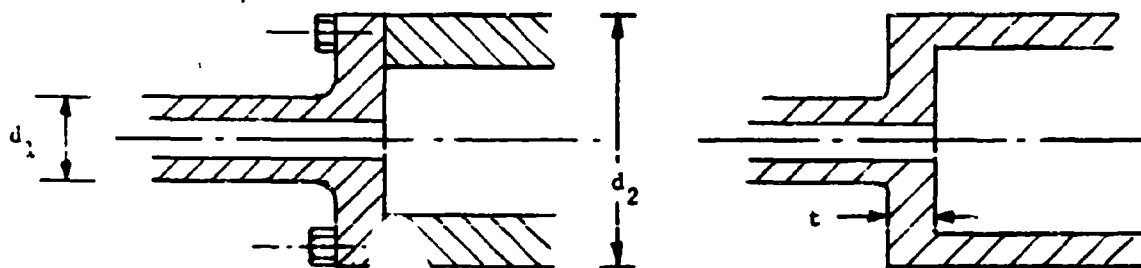
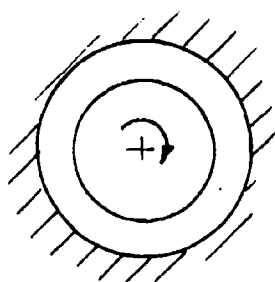
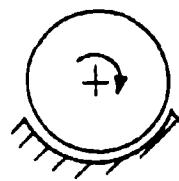


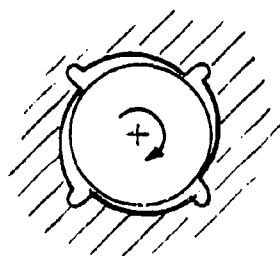
Fig. 2.11 Representation of Bolted Joint



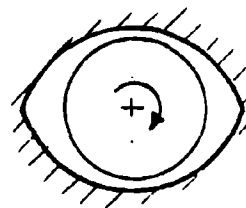
(a) Full Cylindrical



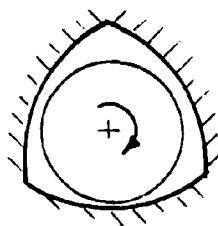
(b) Partial Arc



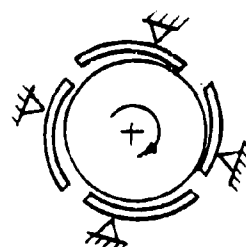
(c) Four-Axial Groove



(d) Elliptical



(e) Three-Lobe



(f) Tilting-Pad

Fig. 2.12 Hydrodynamic Bearing Types

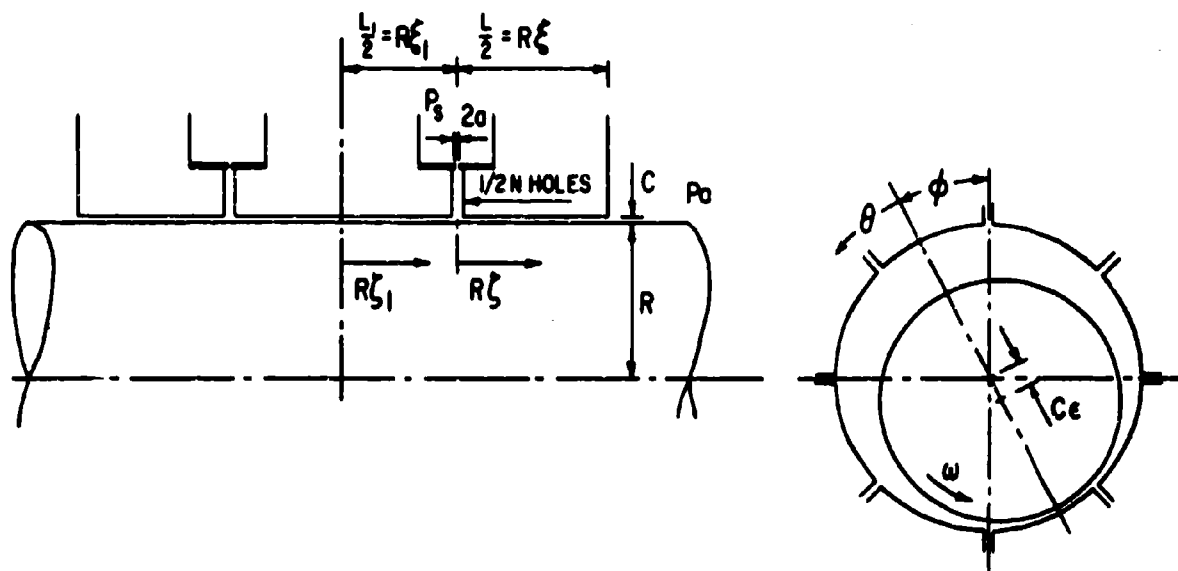


Fig. 2.13 Principle of Hydrostatic Bearing

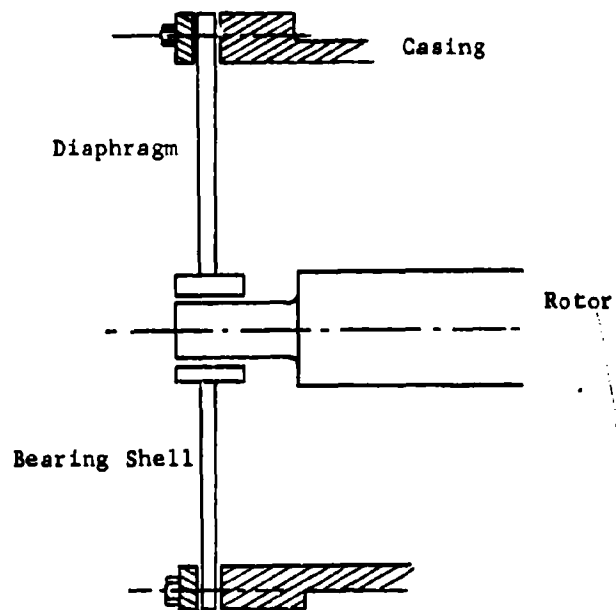
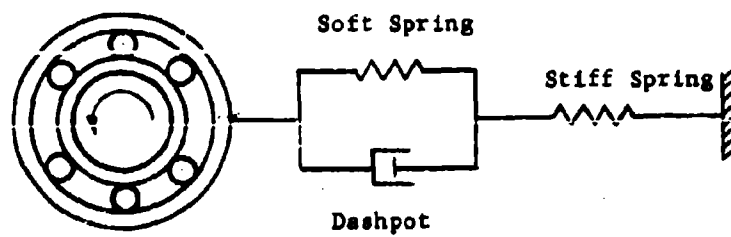
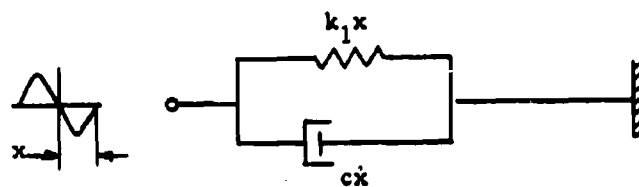


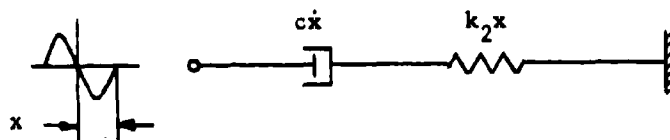
Fig. 2.14 Diaphragm-Supported Rotor



(a) Constant Stiffness Support



(b) Effective System at Low Speed



(c) Effective System at High Speed

Fig. 2.15 Damped Support System for Attenuating Vibrations

### III

#### DYNAMIC RESPONSE OF UNBALANCED FLEXIBLE ROTORS

##### Introductory Remarks on the Influence of Unbalance

All rotors retain some degree of residual unbalance. The purpose of this section is to discuss the effects produced by unbalance on a rotor-bearing system. Each system has, through its shape or construction, a number of specific features such as shaft cross-section, friction, bearing properties, pedestal properties, and so on, which influence the rotor motion. The effect of some features is known in advance, at least qualitatively. Here, rotordynamic analysis seeks to make these effects predictable, and so to optimize their overall contribution to system performance. Other effects such as high-speed balancing involve several system parameters simultaneously, and so may not be predicted readily by experience or intuition. In these cases, systematic investigation of parameter interaction is provided. This is accomplished through the analysis of a rotor-bearing system which contains the mechanical features required to simulate the effects observed in practice.

Rotor amplitude and transmitted bearing force are both governed by rotor unbalance — where the motion is stable. When the variation of amplitude with operating speed is known at critical stations along the rotor throughout the speed range, it is then possible to decide on other aspects of the mechanical design, such as: degree of balance necessary for machine operation, suitability of bearing design, possibility of rotor fatigue and creep-induced permanent bowing at high operating temperatures, and others. The level of bearing-transmitted force may be significantly modified by the type of bearing used. This, in turn, influences the rotor motions, and, therefore, may determine the degree of balance required for operation at high speeds. Also, by attenuating the transmitted force through bearing design, the structural noise level is reduced.

Very few rotors operate in "rigid" bearings. Heavily loaded hydrodynamic bearings come the closest to this condition, but even these bearings possess a degree of flexibility and damping which influences the motion, particularly the critical speeds. The simple vertical rotor, consisting of a single unbalanced central disk mounted on a flexible undamped circular shaft, and which operates in short rigid bearings, has been considered initially in order to simplify the analysis

of certain more basic effects of unbalance on rotor whirl. Later, this simple concept is modified to include horizontal operation, the bearing properties, and rotor asymmetry. The gyroscopic effect is considered in Section 4- Critical Speeds, since its main effect is to dynamically stiffen the rotor and raise the rotor natural frequency in bending. Likewise, certain effects of friction and of rotor shape, which concern the stability of rotor-bearing motions, are discussed in Section 5.

The distribution of the unbalance in an actual machine cannot be predicted in advance. It is known through its effects on rotor amplitude and bearing-transmitted force. These effects are commonly discussed in terms of "static" unbalance, where the disturbing forces lie in a single plane; and "dynamic" unbalance, where there may be several disturbing forces - each acting in its own plane. Both static and dynamic unbalance are usually present in a given machine. Unbalance is customarily thought of as being the whole or portion of the rotor weight,  $W$ , acting at a small eccentricity,  $a$ , from the elastic axis. The unbalance is thus referred to as  $W.a$  oz.in. in each plane. This is shown in Figure 3.01. Balancing of rotors is more fully dealt with in Section 7.

#### Nature of Whirl Motions

During its rotation, a rotor is said to whirl when the mass center of any portion of it travels around a circle or any other closed curve - instead of remaining at a fixed point. If identical whirl orbits are traced out with successive rotations, the whirl is said to be stable. When the whirl orbit is growing or decaying, the whirl is transient and may be unstable. Stable whirls alone are discussed in this section.

Any rotating force which acts on the rotor will induce a whirl. If the rotor c.g. is eccentric with respect to the axis about which it rotates, a radial force will exist which rotates in synchronism with the rotor during operation. This will cause the rotor to assume a deflected shape in the direction of the rotating force, and this shape then whirls about the axis of rotation at all speeds. All forces which act on the rotor, including applied forces and those induced by the whirl motion, contribute to the overall resultant motion.

At the critical speed, the viscous friction which is present in practical rotor-bearing systems acts in the tangential direction and is in equilibrium with the rotor unbalance force. The system is then stable. This is shown in Figure 3.07. The initial phase of the motion causes a transient whirl consisting of two components which rotate in opposite directions with a frequency equal to the system natural frequency. In systems which have viscous damping, these transients decay, irrespective of whether the rotor operating speed is above or below the system critical, leaving only the unbalance whirl motion. For systems which have hysteretic damping, the whirl motion is again made up of two counter-rotating transients with system critical frequency together with a steady synchronous component. Below the critical speed this system is stable, and the transients decay with time. However, above the critical speed, the forward transient component becomes a sustained whirl of increasing amplitude, and the system is unstable. This is caused by the friction force which changes direction as the rotation speed exceeds the natural frequency of the system, and drives the unbalance motion instead of opposing it.

A rotor which has different lateral stiffnesses gives rise to a growing transient within the speed range between the natural frequencies corresponding to the stiffnesses. These unstable motions become stabilized by the inclusion of viscous friction damping, but may be worsened by the presence of hysteretic damping, for operation above the first critical speed.

Flexibility of the rotor supports and foundations does not itself cause whirling, but it may greatly modify the whirling characteristics of the system. In cases where the support stiffnesses are dissimilar, two system critical speeds exist and the rotor exhibits backward precession in the speed range between them. These motions are stable.

A rotor which is supported in fluid-film bearings may whirl at a frequency around half the operating speed of the machine when operating in the order of twice the system critical speed. This whirl becomes resonant with the corresponding system critical speed. The large whirl amplitude which develops is known as resonant whipping and is a self-sustained motion of the journal within the bearing. For further increases in speed, the whirl frequency continues at

the system critical frequency and the large amplitude motions usually persist. Only in rare cases has the resonant whipping condition been passed through.

### Whirling of a Simple Undamped Rotor

The simple rotor shown in Figure 3.01 consists of a single massive disk mounted on a flexible circular shaft. The disk mass,  $m$ , is concentrated at its center of gravity,  $G$ , which is distance  $a$  from the point of attachment,  $E$ , between disk and shaft. The shaft has stiffness,  $k$ , and elastic shaft force is applied to the disk at  $E$ , which is referred to as the elastic center. Any outwardly-directed radial displacement of the shaft from its position of equilibrium causes an opposing radial force,  $F_E$ , in proportion to the displacement. In the case of a vertical shaft, the static equilibrium position is the bearing axis,  $OZ$ . A horizontal shaft has a static deflection line about which it rotates. In both cases, the bearing axis is a convenient datum from which displacements will be measured. Gyroscopic and gravitational influences are excluded from the rotor motion. These effects are considered later.

In establishing the basic features of the rotor motion, a rotor without friction will be considered first. Figure 3.02 shows a simple, undamped rotor whirling about its static equilibrium position under the effects of centrifugal unbalance. The whirl motion acts in synchronism with the externally-applied rotation,  $\omega$ , which drives the rotor. Referring this motion to the stationary coordinates  $x$ ,  $y$ , and writing the displacement coordinates of  $G$  gives:

$$x_G = x + a \cos \phi$$

$$y_G = y + a \sin \phi$$

(3.01)

The equations of motion of the disk are:

$$m\ddot{x} + kx = ma\omega^2 \cos \phi$$

$$m\ddot{y} + ky = ma\omega^2 \sin \phi$$

$$I\ddot{\phi} + ka [x \sin \phi - y \cos \phi] = T_0 \quad (3.02)$$

For constant speed of rotation  $\dot{\phi} = \omega t$ , and  $\ddot{\phi} = T_0 = 0$  since there is no angular acceleration and no energy dissipation. From this, it follows that for harmonic motions where the solution to the above equations has the form:

$$x = A \cos \omega t$$

$$y = B \sin \omega t \quad (3.03)$$

The moment equation shows that:

$$\frac{y}{x} = \tan \omega t = \tan \phi$$

which indicates that OE and EG fall on the same straight radial line for an undamped rotor which is whirling about its static equilibrium position. This indicates that the rotor whirl frequency,  $\nu$ , is the same as the rotor speed,  $\omega$ , (i.e., the whirl is in synchronism with the rotation). Equations 3.02 are linearly independent, and may be solved individually or combined by recalling that  $x + iy = r$ ,  $i = \sqrt{-1}$ , to give the general solution for the whirl radius,  $r$ , of the elastic center. Writing:

$$\omega_c = \sqrt{\frac{k}{m}} \quad (3.04)$$

where  $\omega_c$  is the frequency of the natural transverse vibrations of the system. This allows the solution to be written as:

$$\begin{aligned} x &= A_1 e^{i\omega_c t} + A_2 e^{-i\omega_c t} + \frac{\Omega^2}{1-\Omega^2} a \cos \omega t \\ y &= B_1 e^{i\omega_c t} + B_2 e^{-i\omega_c t} + \frac{\Omega^2}{1-\Omega^2} a \sin \omega t \end{aligned} \quad (3.05)$$

where  $\Omega = \frac{\omega}{\omega_c}$  is the dimensionless speed ratio.

The general solution shows that the total motion of E is made up of three component motions. The first and second terms represent counter-rotating transient vibrations in the radial direction which rotate along with

with the synchronous whirl (Fig. 3.03). The frequency of vibration is shown by the exponent to be the natural frequency of the rotor,  $\omega_c$ , and is independent of speed of rotation. The transient amplitude is determined by the conditions under which the motion was initiated. Although the above transients are sustained by the absence of friction, this condition only occurs under certain conditions in practical rotors. The influence of friction on rotor motion including transients is discussed in the following sections. The third term describes the synchronous whirling of the elastic center, E, in a circular orbit about O due to unbalance. The orbit radius, OE, is given by:

$$r = x + iy = \frac{a\Omega^2}{1-\Omega^2} [\cos \omega t + i \sin \omega t]$$

thus

$$\frac{r}{a} = \frac{\Omega^2}{1-\Omega^2} \quad (3.06)$$

The dimensionless transmitted force, F, depends on the elastic displacement of the rotor, r, and is therefore:

$$\frac{F_E}{ka} = \frac{1}{2} \cdot \frac{\Omega^2}{1-\Omega^2} \quad (3.07)$$

Similarly, the orbit radius of G is given by:

$$r_G = r + a = \frac{a}{1-\Omega^2}$$

or

$$\frac{r_G}{a} = \frac{1}{1-\Omega^2} \quad (3.08)$$

Synchronous whirl radius thus depends on speed and eccentricity. If unbalance can be minimized by design and construction, and eliminated by accurate balancing, the whirl must disappear for all speeds, except when  $\Omega = 1$ , i.e., when  $\omega = \omega_c$ . At this speed, the forcing frequency,  $\omega$ , of the whirl becomes resonant with the

transverse natural frequency,  $\omega_c$ , of the rotor. Sustained resonant operation must lead to the buildup of large whirl amplitudes, and also to heavy transmitted forces at the bearings as can be seen from Equation 3.07. This condition is known as "critical" whirling, and the speed at which it takes place is known as the critical whirling speed. As the motion is characterized by bending of the rotor shaft, this type of critical whirl is commonly referred to as the flexural or bending critical whirl mode of the rotor. Sustained operation at any critical speed may lead to: large whirl amplitude and the danger of rotor-stator contact; heavy dynamic bearing loads, touching and wear; increased seal wear; and undesirable levels of structure-borne vibration and noise.

Below the critical speed, the static equilibrium position, O, the elastic center, E, and the center of gravity, G, form a single, straight line OEG, as shown in Figure 3.04 (a). As the rotor passes through the critical speed, the radius changes from positive to negative, as  $\Omega$  changes from  $<1$  to  $>1$ . This can be concluded from Equation 3.06 and corresponds to a phase change of 180 degrees. Physically, as the rotor passes steadily through the critical speed, it may be seen to "shudder" as the whirl radius changes from positive, Figure 3.04 (a), through the critical position with the eccentricity leading the radius by 90 degrees, Figure 3.04 (b), to negative where the elastic center, E, whirls at a greater radius than the elastic center. For undamped motions the super-critical whirl is a straight-line OGE, Figure 3.04 (c).

The dimensionless whirl radius,  $\frac{r}{a}$ , as a function of speed ratio,  $\frac{\omega}{\omega_c}$ , is shown in Figure 3.05. Negative  $\frac{r}{a}$  values for  $\omega > \omega_c$  are plotted positive for convenience.

#### Critical Whirling of a Simple, Undamped Rotor

Although Equations (3.02) apply at all speeds, the solutions (3.05) are invalid at  $\omega = \omega_c$ . Rewriting the equations of motion for this case as:

$$\begin{aligned}\ddot{x} + \omega_c^2 x &= a \omega_c^2 \cos \omega_c t \\ \ddot{y} + \omega_c^2 y &= a \omega_c^2 \sin \omega_c t\end{aligned}\tag{3.02}$$

In this instance, the quasi steady-state solutions are:

$$\begin{aligned} x &= a \frac{\omega_c t}{2} \sin \omega_c t \\ y &= -a \frac{\omega_c t}{2} \cos \omega_c t \end{aligned} \quad (3.09)$$

These expressions indicate that the whirl radius does not become infinite at the instant the critical speed is reached, but rather it grows linearly with time as the shaft continues to rotate at the critical speed. Note that this result is true even where there is no viscous damping in the system. The time-path is a growing logarithmic cycle as shown in Figure 3.06. In this condition, there is a phase difference of 90 degrees as the centrifugal unbalance leads the whirl radius, OE.

The complete solution to Equations (3.02) also includes sustained transient motions to which the previous remarks again apply. In the above analysis, the rate of growth of the whirl radius is assumed to be small so that the motion is not significantly influenced by Coriolis forces. A rigorous analysis should include these effects to allow all growth rates to be investigated.

#### Influence of Viscous Friction on Rotor Motion

Viscous friction effects in a rotor-bearing system may arise from fluid-film action in the bearings and from the drag of the gas or liquid in which the machine rotates. For the present it is convenient to represent the viscous friction forces as being linearly dependent on velocity with a coefficient,  $c$ , and in the case of the single-disk rotor to consider their effect as being concentrated at the shaft center, O. The forces which act on the disk are then as shown in Figure 3.07. Gyroscopic and gravitational effects are again negligible in the motion considered. Again, employing the coordinate equations (3.01) for the disk c.g. gives the equations of motion for a damped, elastic rotor operated at constant speed,  $\omega$ , as:

$$\begin{aligned} m\ddot{x} + c\dot{x} + kx &= m\omega^2 \cos \omega t \\ m\ddot{y} + c\dot{y} + ky &= m\omega^2 \sin \omega t \end{aligned} \quad (3.10)$$

The damping force opposes the coordinate motion. Where motion is outward, the damping force is inwardly directed and vice versa. Assuming a solution of the form:

$$\begin{aligned}x &= A \cos (\omega t - \alpha) \\y &= B \sin (\omega t - \alpha)\end{aligned}\tag{3.11}$$

leads to the coordinate solutions:

$$\begin{aligned}x &= A_1 \exp \left[ -\frac{ct}{2m} \right] \exp \left[ i(qt + \gamma_1) \right] + A_2 \exp \left[ -\frac{ct}{2m} \right] \exp \left[ -i(qt + \gamma_1) \right] \\&+ \frac{a\omega^2 \cos (\omega t - \beta)}{\sqrt{\omega_c^2 - \omega^2} + b^2 \omega^2} \\y &= B_1 \exp \left[ -\frac{ct}{2m} \right] \exp \left[ i(qt + \gamma_2) \right] + B_2 \exp \left[ -\frac{ct}{2m} \right] \exp \left[ -i(qt + \gamma_2) \right] \\&+ \frac{a\omega^2 \sin (\omega t - \beta)}{\sqrt{\omega_c^2 - \omega^2} + b^2 \omega^2}\end{aligned}\tag{3.12}$$

where

$$q = \left[ \omega_c^2 - \left( \frac{c}{2m} \right)^2 \right]^{\frac{1}{2}} ; \quad \gamma_1, \gamma_2 = \text{constants} ; \quad i = \sqrt{-1}$$

and

$$\beta = \arctan \left[ \frac{\frac{c\omega}{k}}{1 - \Omega^2} \right] , \quad \Omega = \frac{\omega}{\omega_c} , \quad \omega_c = \sqrt{\frac{k}{m}}$$

The first two terms in Equations 3.12 represent damped transient vibrations of the rotor in the radial direction, occurring with a frequency,  $q$ , rad/sec, i.e., the damped natural frequency of the rotor in the transverse direction. As in the previous case, these transients rotate in opposite directions, along with the main unbalance whirl, until damped out. The actual value of the damping coefficient,  $c$ , need not be large enough to effect a rapid decrease in vibration amplitude, and also a sizable change in the amplitude build-up near the critical speed. For small to moderate values of the damping coefficient,  $c$ , the damped

natural frequency,  $q$ , is slightly less than  $\omega_c$ . The size and significance of these transients depends on the initial conditions of the motion. This feature is discussed further in Section 6.

The third term in Equations 3.12 is the synchronous whirl amplitude, the radius of which is given by  $(x^2 + y^2)^{\frac{1}{2}}$ , or:

$$\frac{a\omega^2}{\sqrt{(\omega_c^2 - \omega^2)^2 + c^2\omega^2}} \left[ \cos^2(\omega t - \beta) + \sin^2(\omega t - \beta) \right]^{\frac{1}{2}}$$

$$\frac{a\omega^2}{\sqrt{(\omega_c^2 - \omega^2)^2 + c^2\omega^2}}$$

or

$$\frac{r}{a} = \frac{\Omega^2}{\sqrt{(1 - \Omega^2)^2 + 4\Omega^2\zeta^2}} \quad (3.13)$$

where

$$\zeta = \frac{c}{c_c} ; \quad c_c = 2\sqrt{mk}$$

For a shaft in rigid bearings with identical lateral stiffnesses, the whirl is, therefore, circular about the static equilibrium position with radius  $r$ . The dimensionless whirl radius  $(\frac{r}{a})$  depends on the speed ratio,  $\Omega$ , and the damping ratio,  $\zeta$ , and its variation with both these factors is shown in Figure 3.08. Negative  $(\frac{r}{a})$  values occurring when  $\Omega > 1$  are plotted positive for convenience. The whirl radius reaches a maximum, but finite value when:

$$\frac{\omega}{\omega_c} = \sqrt{1 + \zeta^2}$$

Damping, therefore, increases the critical speed in a system which has frequency-dependent excitation.

The term, "critical damping",  $c_c$ , refers to the degree of viscous damping required to just permit a mass to return to its initial position without oscillation following a displacement. The dimensionless damping ratio,  $\zeta$ , expresses the ratio (actual-to-critical) damping,  $(c/c_c)$ .

The phase relationship between the rotor eccentricity,  $a$ , and the whirl radius is given by:

$$\tan \beta = \left[ \frac{c\omega}{k} \right] \frac{1}{1-\Omega^2} \quad (3.14)$$

As the rotor passes through the critical speed, the phase angle again changes as shown in Figure 3.04, but with damping the change is continuous throughout the speed range. With low damping values, the abruptness of the inversion is similar to that indicated by the undamped rotor results. Figure 3.09 shows the relationship between speed, damping and phase angle.

The above results verify that practical rotors also whirl with the c.g. situated beyond the point of attachment between disk and shaft where  $\omega < \omega_c$ , also  $\omega > \omega_c$ , the c. occupies a position between the point of attachment and the whirl center. As the speed becomes higher and higher, the c.g. moves still closer towards 0. Hence, it is said that beyond the critical speed a rotor is "self-balancing" and that it tends to "whirl about its c.g.". Practical rotors possess a number of critical speeds each of which has the above tendencies to some degree. The true situation in a given case is a matter for dynamic analysis of the particular rotor-bearing system.

#### Force Transmitted from an Unbalanced Rotor with Viscous Damping

Although a damped rotor whirls rather than vibrates, the force transmitted to the bearings varies cyclically in both x-y directions. This is a source of both structural vibration and noise generation, as well as bearing fatigue. The magnitude of the transmitted force in any direction for a system with a rotating unbalance and viscous damping is given by:

$$2F_x = kx + c\dot{x}$$

$$\text{as } x = r \cos (\omega t - \alpha)$$

$$r \text{ constant}$$

Hence

$$2F_x = r \sqrt{k^2 + c^2 \omega^2} \cdot \cos (\omega t - \epsilon)$$

where

$$r = \frac{a \Omega^2}{\sqrt{(1-\Omega^2)^2 + 4\zeta^2 \Omega^2}}$$

$$\epsilon = \alpha - \arctan \frac{c\omega}{k}$$

$$= \arctan \frac{2\zeta \Omega^3}{(1-\Omega^2) + 4\zeta^2 \Omega^2}$$

The amplitude of the transmitted force in the x-direction is therefore:

$$2F_x = m\omega^2 \sqrt{\frac{1 + 4\zeta^2 \Omega^2}{(1-\Omega^2)^2 + 4\zeta^2 \Omega^2}} \cdot \cos(\omega t - \epsilon) \quad (3.15)$$

The dimensionless maximum transmitted force

$$\frac{2F_x}{m\omega^2} = \frac{2F_x}{ka\Omega^2} = \sqrt{\frac{1 + 4\zeta^2 \Omega^2}{(1-\Omega^2)^2 + 4\zeta^2 \Omega^2}}$$

is plotted as a function of speed ratio  $\Omega$  in Figure 3.10. The phase angle,  $\beta$ , is shown as a function of speed and damping in Figure 3.11.

### Influence of Internal Friction on Rotor Whirl Motion

The laws of elastic hysteresis on the basis of existing experimental data do not permit a simple formulation suitable for analysis of rotor motions. However, by the use of certain approximations it is possible to develop a rational theory which can be used to explain the rotor behavior where internal friction forces are present. Internal friction effects arise from elastic hysteresis of the rotor material, and from any interface Coulomb slippage between the components of a built-up rotor. In both instances, the resulting energy loss gives rise to a tangential force acting on the rotor. When the rotor speed,  $\omega$ , is below the whirl speed,  $v$ , the tangential force opposes the rotation, and the rotor is stable; but, where the rotor speed exceeds the whirl speed, the tangential force reverses direction and tends to drive the rotor. In this condition, the whirl radius increases with time unless arrested by some additional system force. The stability of this system is discussed at greater length in Section 5.

Investigators from Rowett (Ref.21) to Lazen (Ref.22) and in particular Kimball (Ref.23) in the case of rotors have found that:

1. The energy loss is independent of the cyclic frequency, and
2. Energy loss is approximately proportional to the square of the maximum cyclic amplitude, for a steadily vibrating system with a stabilized hysteresis loop.

Built-up rotors, where there is relative slip between the assembled components, show a similar cyclic hysteresis loss of energy, resulting from interface Coulomb friction. A typical hysteresis loop is shown in Figure 3.12.

The loss of energy arises from some form of vibration, and not from the steady whirl motion itself. It may be generated through the transient rotor motions which, as stated previously, are radial vibrations that rotate along with the synchronous whirl motion; another source is the deflected rotor shape of horizontal rotors. When at rest, the rotor is stressed as a beam by gravity. Unbalance whirling about this static equilibrium position results in a cyclic stressing of the rotor material and leads to a loss of energy by hysteresis. Any action which disturbs the dynamic equilibrium of the rotor, such as a speed change, cyclic torque variation, or an external impulse or a blow, may initiate hysteretic whirling under suitable circumstances.

The following analysis concerns the dynamic behavior of a simple rotor in rigid bearings acted on by internal friction. The laws of hysteretic damping stated above are used to describe the energy dissipation, expressed as

$$F_H = c \frac{dr}{dt}$$

Consider the rotor whirl configuration shown in Figure 3.13 in which the  $x, y$  axes are stationary, and the  $\xi, \eta$  axes rotate with the shaft. The whirl radius,  $r$ , in rotating coordinates is given by:

$$r = \xi e^{i\omega t} \quad \text{where } r = x + iy$$

Differentiation gives

$$\begin{aligned} \dot{r} &= (\dot{\xi} + i\omega\xi)e^{i\omega t} \\ \ddot{r} &= (\ddot{\xi} + 2i\omega\dot{\xi} - \omega^2\xi)e^{i\omega t} \end{aligned}$$

Substituting these expressions into Equations 3.02 gives the equations of motion for a simple undamped rotor in rotating coordinates:

$$\ddot{\xi} + 2i\omega\dot{\xi} + \left(\frac{k}{m} - \omega^2\right)\xi = \frac{ka}{m} \quad (3.16a)$$

In these coordinates, the shaft is stationary and any small radial motion of the shaft due to the rotating unbalance (similar to a spring with an eccentric load rotating at velocity  $\bar{v} = \omega$ ), gives rise to the hysteretic damping force  $c\dot{\xi}$ . Including this damping force in the above system equation gives:

$$\ddot{\xi} + \left(\frac{c}{m} + 2i\omega\right)\dot{\xi} + \frac{k}{m}\left(\frac{c}{m} - \omega^2\right)\xi = \frac{ka}{m} \quad (3.16b)$$

The  $x, y$  coordinate equations are now obtained as follows:

$$\xi = re^{-i\omega t}; \quad \dot{\xi} = (\dot{r} - i\omega r)e^{-i\omega t}; \quad \ddot{\xi} = (\ddot{r} - 2i\omega\dot{r} - \omega^2 r)e^{-i\omega t}$$

Thus:

$$\begin{aligned} \ddot{r} + \frac{c}{m}\dot{r} + \left(\frac{k}{m} - i\omega\frac{c}{m}\right)r &= \frac{ka}{m}e^{i\omega t} \\ \ddot{x} + \frac{c}{m}\dot{x} + \frac{k}{m}x + \frac{c\omega}{m}y &= \frac{ka}{m}\cos\omega t \\ \ddot{y} + \frac{c}{m}\dot{y} + \frac{k}{m}y - \frac{c\omega}{m}x &= \frac{ka}{m}\sin\omega t \end{aligned}$$

From the above, it can be seen that the internal friction in the complex equation for  $r$  in stationary coordinates is characterized by the term:

$$\frac{c}{m} \dot{r} - i\omega \frac{c}{m} r$$

The total integral of this equation is

$$r = A \exp [i\Lambda_1 t] + B \exp [-i\Lambda_2 t] + \frac{a}{1-\Omega^2} \exp [i\omega t]; \quad \Omega = \frac{\omega}{\omega_c} \quad (3.17)$$

The third term of this solution describes the synchronous whirling of the shaft to unbalance. The critical speed of the rotor is again  $\omega_c = \sqrt{\frac{k}{m}}$ , as may be seen from the form of the denominator. Internal friction does not influence the unbalance whirl motion for there is no radial oscillation to invoke the hysteretic damping force. For this reason, internal damping cannot limit the critical speed resonant whirl amplitude, and so a system which has hysteretic damping alone experiences heavy vibrations if the passage through the critical speed is slow and if operation at the critical speed or in its vicinity is sustained, the danger of rotor damage is considerable. Fortunately, practical rotors usually possess a certain amount of viscous damping due to their environment. The viscous drag of the surrounding medium, and of the bearings acts along with the unbalance whirl motions to inhibit amplitude build-up and transmitted bearing force.

The first two terms of Equation 3.17 describe the transient radial vibrations which arise from the initial conditions of the motion, or from a radial disturbance as discussed above. The frequencies of vibration  $\Lambda_1, \Lambda_2$  are determined from the roots of the characteristic equation:

$$\Lambda^2 - i \frac{c}{m} \Lambda - \left[ \frac{k}{m} - i\omega \frac{c}{m} \right] = 0 \quad (3.18)$$

From which:

$$\Lambda_{1,2} = \pm \lambda + i\alpha_{1,2}$$

Where

$$\lambda = \omega_c \left[ \frac{(1 - 4\zeta^2) + \sqrt{(1 - 4\zeta^2)^2 + 4\zeta^2\Omega^2}}{2} \right]^{\frac{1}{2}}$$

$$\alpha = \omega_c \left[ \left( \frac{\omega}{k} \right) \left( \frac{1}{2\Omega} \right) + \left\{ \frac{-(1 - 4\zeta^2) + \left[ (1 - 4\zeta^2)^2 + 4\zeta^2 \Omega^2 \right]^{\frac{1}{2}}}{2} \right\}^{\frac{1}{2}} \right]$$

$$\text{and } \zeta = \frac{c}{c_c}; \quad c_c = 2\sqrt{k m}, \quad \Omega = \frac{\omega}{\omega_c}, \quad \omega_c = \sqrt{\frac{k}{m}}$$

as previously.

The above expressions for the transient vibration frequencies  $\Lambda_1, \Lambda_2$  were obtained by Dimentberg (Ref. 1), and are explained as follows: The complex nature of the expressions indicates vibrations in which the amplitude varies, according to the amount of damping present.  $\lambda$  is the natural frequency which, for small values of  $\zeta$  is equal to  $\omega_c$ . This is then the hysteretic whirl frequency of the rotor.  $\alpha_1$  and  $\alpha_2$  are the variations in the transient amplitude. The coefficient  $\alpha_1$  may be positive or negative, and so the transient vibrations are accompanied by damping and amplitude variation depending on whether the sign is plus or minus. Examining the formula indicates that the difference, i.e., the sign of  $\alpha$  will be positive when  $\omega < \omega_c$  and negative when  $\omega > \omega_c$ . The physical meaning of this result is that the motion is stable where the speed of rotation,  $\omega$ , is less than the critical speed,  $\omega_c$ , i.e., where the index is negative, and that the motion is unstable where  $\omega$  is greater than  $\omega_c$ . In this latter condition, the friction forces will increase due to the increasing transient vibration, and their direction will be to drive the rotor and thereby increase the whirl radius until limited by some other external constraint.

#### Rotor Dynamic Characteristics with Viscous and Hysteretic Damping

The results of the two previous sections are that: (1) viscous friction tends to promote stable operation at all times, with finite amplitudes at the critical speed; also, that the whirl is synchronous with the speed of rotation, and (2) that hysteretic damping causes the rotor to whirl at its critical speed. The whirl is stable below the critical speed, but unstable above it, causing the whirl amplitude to grow. Several questions immediately arise: How does a practical rotor behave, possessing as it does both viscous and hysteretic damping? What are the conditions under which the viscous damping will maintain stable whirling at speeds above the critical? And, at which speed will the rotor whirl, the critical speed or at synchronous speed; or between?

The equations of motion for this case are obtained by introducing a viscous damping term  $c_1$  with the hysteretic damping term  $c_2$  into the coordinate equations for the elastic-center, E. Doing this for stationary coordinates gives:

$$\begin{aligned} m\ddot{x} + (c_1 + c_2) \dot{x} + kx + c_2 \omega y &= m\omega^2 \cos \omega t \\ m\ddot{y} + (c_1 + c_2) \dot{y} + ky - c_2 \omega x &= m\omega^2 \sin \omega t \end{aligned} \quad (3.19)$$

Considering the homogeneous portion of these equations, and reformulating gives:

$$\begin{aligned} \ddot{x} + a_1 \dot{x} + a_2 y + a_3 x &= 0 \\ \ddot{y} + a_1 \dot{y} - a_2 x + a_3 y &= 0 \end{aligned}$$

This may be written as

$$\ddot{x} + 2a_1 \dot{x} + (2a_3 + a_1^2) \ddot{x} + 2a_1 a_3 \dot{x} + (a_2^2 + a_3^2) x = 0 \quad (3.20)$$

The primitive is a quartic polynomial as found on substituting  $x = A e^{i\Lambda t}$ , with  $\Lambda$  complex e.g.,

$$\Lambda^4 + A_3 \Lambda^3 + A_2 \Lambda^2 + A_1 \Lambda + A_0 = 0$$

where

$$\begin{aligned} A_3 &= 2a_1 = \frac{c_1 + c_2}{2m} \\ A_2 &= 2a_3 + a_1^2 = 2\omega_c^2 + \left[ \frac{c_1 + c_2}{4m} \right]^2 \\ A_1 &= 2a_1 a_3 = \omega_c^2 \left( \frac{c_1 + c_2}{2m} \right) \\ A_0 &= a_2^2 + a_3^2 = \omega_c^4 + \frac{(\omega_c^2 c_2^2)}{16m^2} \end{aligned}$$

The stability of the system may be examined by Routh's criterion which for a quartic polynomial requires

$$A_1 A_2 A_3 > A_1^2 + A_0 A_3^2$$

for a negative real part in  $\Lambda = \lambda + i\alpha$ . This condition reduces to the stability condition:

$$\omega < \omega_c \left[ 1 + \frac{c_1}{c_2} \right] \quad (3.21)$$

### Influence of Unsymmetrical Bearing Stiffness on Rotor Motions

A large proportion of practical bearings have stiffness properties which vary according to the radial direction from which the bearing load is applied. This can be due to: (1) shape of the bearing, for example, a partial-arc journal bearing (2) whether the rotor-bearing system operates horizontally or vertically, or (3) differing transverse stiffness properties of the bearing pedestal. Rolling-element bearings, vertical cylindrical journal bearings, and vertical multi-pad journal bearings have stiffness symmetry.

The influence of unsymmetrical bearing stiffness on the motion of the rotor which they carry is as follows. Consider again a simple vertical rotor which consists of an unbalanced circular disk which is centrally mounted on a light, flexible, circular shaft. The rotor is mounted in undamped flexible bearings which have different stiffnesses in the  $x$ ,  $y$  directions. The principal features of the rotor-bearing system are shown in Figure 3.14 and Figure 3.15 shows the displacement of the rotor c.g from the bearing centerline  $OZ$ .

The equations which govern the translatory motions are:

$$\begin{aligned} m\ddot{x} + k(x - x_0 - a \cos \omega t) &= 0 \\ m\ddot{y} + k(y - y_0 - a \sin \omega t) &= 0 \\ k(x_0 - x) + k_1 x_0 &= 0 \\ k(y_0 - y) + k_2 y_0 &= 0 \end{aligned} \quad (3.22)$$

Simplifying these expressions and introducing the expressions

$$q_1 = \frac{2kk_1}{2k_1 + k} \quad q_2 = \frac{2kk_2}{2k_2 + k}$$

leads to the equations

$$\begin{aligned} m\ddot{x} + q_1 x &= q_1 a \cos \omega t \\ m\ddot{y} + q_2 y &= q_2 a \sin \omega t \end{aligned} \quad (3.23)$$

This shows that the coordinate motions are independent, each having its own critical speed at

$$\omega_1 = \left[ \frac{g_1}{m} \right]^{\frac{1}{2}} \quad \omega_2 = \left[ \frac{g_2}{m} \right]^{\frac{1}{2}}$$

Solving Equations 3.23 and combining their steady-state unbalance whirl components by writing  $r = x + iy$  leads to the following expression for the motion of G about Oz:

$$r = \frac{\omega_1^2 \omega_2^2 - \frac{\omega_1^2 + \omega_2^2}{2} \omega^2}{(\omega_1^2 - \omega^2)(\omega_2^2 - \omega^2)} a e^{i\omega t} + \frac{\frac{\omega_2^2 - \omega_1^2}{2} \omega^2}{(\omega_1^2 - \omega^2)(\omega_2^2 - \omega^2)} a e^{-i\omega t}$$

The motion of the elastic center Z is found from:

$$\begin{aligned} r_Z &= r - a e^{i\omega t} \\ &= a \omega^2 \left[ \frac{\frac{\omega_2^2 + \omega_1^2}{2} - \omega^2}{(\omega_1^2 - \omega^2)(\omega_2^2 - \omega^2)} e^{i\omega t} + \frac{\frac{\omega_2^2 - \omega_1^2}{2}}{(\omega_1^2 - \omega^2)(\omega_2^2 - \omega^2)} e^{-i\omega t} \right] \quad (3.24) \end{aligned}$$

Equation 3.24 shows that the whirl motion relative to a stationary coordinate system is made up of two separate whirls which rotate in opposite directions with angular velocity  $\omega$ . The rotation of the first vector consists of forward translatory precession of the disk in the direction of shaft rotation; whereas, the second vector represents backward precession in the reverse direction to shaft rotation. The length of each whirl vector is fixed for any given speed.

$$\omega = \left[ \frac{\omega_1^2 + \omega_2^2}{2} \right]^{\frac{1}{2}}$$

However, when the length of the forward whirl vector becomes zero, the length of the backward whirl vector becomes:

$$\frac{(\omega_2^4 - \omega_1^4) a}{(\omega_1^2 - \omega^2)(\omega_2^2 - \omega^2)}$$

At this speed, therefore, the motion will be pure reverse precession of the shaft center, despite the presence of excitation by the unbalance in the forward direction. This motion is sustained up to the second critical speed. For speeds below the first critical, the first term in the above expression is larger than the second, and so the forward precession whirl dominates the motion; also, for speeds beyond the second critical, this term again becomes predominant.

The presence of the two critical speeds, and the variation in whirl direction between forward and backward precession has been examined using models by Downham (Ref. 24) and by Hull (Ref. 25). Hull's results are shown in Figure 3.16 and this author discusses the physical origin of the backward whirl. This motion becomes necessary when the machine is operating above the critical speed in one direction, and below the critical speed in the other, due to the 180 degree phase shift which occurs in the position of the disk c.g. in one plane, but not in the other.

#### Whirling of a Rotor Having Unsymmetrical Stiffnesses

The most important dynamic feature of a rotor which has dissimilar transverse moments of inertia is the inherent instability which exists at speeds which lie between the two bending critical speeds — corresponding to the two stiffnesses. For this reason, this section is limited to a brief discussion of the rotor motion, including the derivation of the required equations of motion. The stability of this motion is discussed in Section 5.

The rotor consists of a single, massive disk in which the c.g. is eccentric from the elastic axis of the shaft by an amount,  $a$ , and is located at an angle  $\beta$  to the stiffer transverse axis of the shaft. The shaft operates in rigid bearings and has dissimilar stiffnesses in the transverse direction. Aligning the principal inertia axes with the rotating coordinates  $\xi, \eta$  as shown in Figure 3.17, the deflection  $OE = r_E$  of the whirling elastic axis at the disk location gives rise to the deflecting force components  $k_1 r_E \cos x$  and  $k_2 r_E \sin x$ . Both force components may be resolved radially and tangentially to give respectively the total radial force:

$$F_R = r_E \left[ k_1 \cos^2 \alpha + k_2 \sin^2 \alpha \right]$$

and the total tangential force

$$F_T = r_E (k_2 - k_1) \sin \alpha \cos \alpha$$

writing

$$q_1 = (k_2 + k_1)/2 \quad \text{and} \quad q_2 = (k_2 - k_1)/2$$

and substituting in the above gives

$$F_R = r_E (q_1 - q_2 \cos 2\alpha)$$

$$F_T = r_E q_2 \sin 2\alpha$$

A viscous damping force is considered to act opposing the whirl at the elastic center. To obtain the total vector deflecting force on the shaft expressed in terms of the stationary coordinate system, note that the reflection of  $\bar{r}_E$  about the rotating axis  $\xi$  is  $\bar{r}_E''$  which leads  $\bar{r}_E$  by angle  $2\alpha$ . Thus,  $\bar{r}_E''$  is parallel to, but opposite in direction to, the vector  $q_2 \bar{r}_E$  showing in Figure 3.18. The vector deflecting force in rotating coordinates is, therefore,  $(q_1 \bar{r}_E - q_2 \bar{r}_E')$ . Use is now made of the property that the reflection of  $\bar{r}_E$  in the stationary axis  $x$  is  $\bar{r}_E'$  which is the same as  $\bar{r}_E$  except for a phase lead of  $2\omega t$ . This leads to the relationship:

$$\bar{r}_E'' = \bar{r}_E' e^{i2\omega t}$$

From this, the force exerted on the disk by the shaft is

$$\bar{F} = -q_1 \bar{r}_E + q_2 \bar{r}_E' e^{i2\omega t} \quad (3.26)$$

The vector damping force equation is

$$\bar{D} = -c \dot{\bar{r}}_E$$

The equation of motion for the shaft center may now be written, firstly neglecting the influence of gravity for simplicity. This step reveals uniquely the influence of dissimilar stiffness on the rotor motion, which is:

$$m\ddot{\bar{r}}_G = \bar{F} + \bar{D}$$

$$\ddot{\bar{r}}_G = \ddot{\bar{r}}_E + \ddot{\bar{a}} = \ddot{\bar{r}}_E - \omega^2 e^{i(\omega t + \beta)}$$

Thus,

$$m\ddot{\bar{r}}_E + c\dot{\bar{r}}_E + q_1\bar{r}_E - q_2\bar{r}_E' e^{i2\omega t} = me\omega^2 e^{i(\omega t + \beta)} \quad (3.27)$$

which is the equation of motion of a damped unbalanced rotor with dissimilar stiffnesses in stationary coordinates.

As a trial solution, select

$$\bar{r}_E = \bar{R} e^{i\omega t}$$

$$\bar{R} = X + iY$$

$$\bar{R}' = X - iY$$

Here, X and Y are constants to be evaluated by substitution. Introducing the following ratios for speed, damping and dissymmetry:

$$\Omega = \frac{\omega}{\omega_c}$$

$$\frac{c}{c_c} = 2\sqrt{q_1 m} = \zeta$$

$$\theta = \frac{q_2}{q_1}$$

$$\omega_c^2 = \frac{q_1}{m}$$

The scalar value of the deflection (or half amplitude)  $r_E$  is then obtained from

$$r_E = [X^2 + Y^2]^{1/2}$$

Thus,

$$\frac{r_E}{a} = \frac{\Omega^2 \left[ (1-\Omega^2)^2 + 4C_c^2 \Omega^2 + \Theta^2 + 2\Theta(1-\Omega^2)\cos 2\beta + 4C_c \Omega \Theta \sin 2\beta \right]^{\frac{1}{2}}}{(1-\Omega^2)^2 + 4C_c^2 \Omega^2 - \Theta^2} \quad (3.28)$$

The phase angle  $\Phi$  is obtained from

$$\tan \Phi = \tan (\Phi - \beta) = \frac{Y}{X} = \frac{[(1-\Omega^2 - \Theta)\sin \beta - 2C_c \Omega \cos \beta]}{[(1-\Omega^2 + \Theta)\cos \beta + 2C_c \Omega \sin \beta]} \quad (3.29)$$

These expressions for amplitude and phase angle assume simpler forms where the unbalance angle  $\beta$  has some simple numerical values, such as 0, 30, 45, 60, 90, etc., degrees. Further simplifications result from zero damping, and zero dissymmetry leads to previously obtained solutions.

The critical speeds of the system occur where  $(r_E/a)$  is a maximum; this condition may be found from

$$\frac{d}{d\Omega} \left[ \frac{a}{r_E} \right] = 0 \quad ; \quad \frac{d^2}{d\Omega^2} \left[ \frac{a}{r_E} \right] = +ve$$

Taylor (Ref 8) has obtained an approximate result for the critical speed condition by equaling the denominator of Equation 3.28 to zero, viz.,

$$\Omega_{1,2} = \left[ (1 - 2\zeta^2) \pm \sqrt{\Theta^2 - 4\zeta^2(1 + \zeta^2)} \right]^{\frac{1}{2}} \quad (3.29)$$

but is in error when he suggests that a damped critical speed may have infinite amplitude and also when he attempts to obtain it by the above operation, except where  $\zeta = 0$ . In this case:

$$\Lambda_{1,2} = \sqrt{1 \pm \Theta^2}$$

which leads to:

$$\omega_1^2 = \frac{k_1}{m} \quad ; \quad \omega_2^2 = \frac{k_2}{m}$$

For moderate damping,  $\zeta$  is small and the system critical speeds will fall close to these values. The question of stability of the motion between these critical speeds is discussed in Section 5.

Theoretical results for average whirl amplitude  $r_g$  obtained by Taylor are shown in Figure 3.19, for the case of a shaft with moderate dissymmetry  $H = 0.03$  and moderate damping  $\zeta = 0.035$ . Note that the amplitude is finite at all speeds. The influence of the phase angle,  $\beta$ , leading the rotor motion is to cause the critical speed to occur at a lower speed ratio. A considerable increase in amplitude is associated with  $\rho = 45^\circ$ , and where  $\beta = -45$  the rotor amplitude is lowest. The amplitude build-up for a circular shaft is in keeping with the moderate damping present,  $\frac{r_g}{a} = 1/2 \zeta \approx 14$ .

Figure 3.20 shows the results for large dissymmetry  $H = 0.09$ , damping again  $\zeta = 0.035$ . The greater dissymmetry has promoted larger whirl amplitudes and also widened the unstable speed range between the two critical speeds. The rotor amplitude in this zone, however large, is, in fact, finite where the system possesses viscous damping. Figure 3.21 presents more of the speed range for several values of dissymmetry  $H = 0, 0.5$  and  $0.09$  and with the same damping  $\zeta$ . The half frequency critical speed is discussed in the following section.

A series of experiments were made to confirm the above findings using a 5300 lb. rotor, 66 in. long and 7.75 in. in diameter, carrying several masses. This is shown in Figure 3.22 together with results obtained for a circular shaft. Results for an unsymmetrical shaft are shown in Figure 3.23 for a range of unbalance weights and unbalance angles. The critical speed amplitude build-up in both the horizontal direction and the vertical direction were detected with the horizontal properties occurring as usual in practice at a somewhat lower speed. Results indicated that horizontal amplitude build-up is always larger; the 45 degree unbalance angle gives the greatest amplitude build-up; and both horizontal and vertical amplitudes are finite, though large, in all cases. The damping ratio  $\zeta$  was 0.07, determined experimentally, and due mainly to the fluid-film bearings used. The motion of a rotor which has its mass-elastic properties uniformly distributed along its length and dissimilar lateral stiffnesses has been studied by Kellenberger (Ref. 26)

### Subharmonic Whirling

During run-up and run-down, it is noticed with certain machines that a minor vibration of the machine occurs at precise sub-multiples of the critical speed such as  $\omega_c/2$ ,  $\omega_c/4$ , and so on. The  $\omega_c/2$  subharmonic amplitude is noticed quite frequently, and the other smaller amplitude subharmonics are seen less often. These motions may be caused by: (1) dissimilar lateral stiffness properties of the rotor, (2) gravity causing a twice-per-cycle fluctuating torque to act on the rotor unbalance, and (3) any other source of cyclic torque fluctuation in the rotor drive with a frequency  $n$  times the rotor speed. The relative significance of these three sources was evaluated by Soderberg (Ref. 27), who, with a linearized solution to a very complex analysis, established that the predominant effect was stiffness dissymmetry.

The influence of stiffness dissymmetry and gravity may be considered using the equations developed in the previous section, as follows: Consider the rotor to be perfectly balanced and operating in the horizontal position. Here  $G$  coincides with  $E$ , and the gravitational force vector  $\bar{W} = -\bar{I}mg$  is included into the equation of motion to give:

$$m\ddot{\bar{r}}_G = \bar{F} + \bar{D} + \bar{W} = m\ddot{\bar{r}}_E$$

Thus,

$$m\ddot{\bar{r}}_E + c\dot{\bar{r}}_E + q_1\bar{r}_E - q_2\bar{r}_E e^{i2\omega t} + \bar{I}mg = 0 \quad (3.30)$$

For a trial solution, assume that the vector amplitude  $\bar{r}_E$  consists of a stationary vector  $\bar{C}$ , plus a double-frequency vector  $\bar{R}$ , or:

$$\bar{r}_E = \bar{C} + \bar{R}e^{i2\omega t}$$

where

$$\bar{C} = X_1 + iY_1$$

$$\bar{R} = X_2 + iY_2$$

By substituting in Equation 3.30 the values of  $X_1$ ,  $Y_1$ ,  $X_2$ , and  $Y_2$  are obtained. The amplitude of the double-frequency vector  $\bar{R}$  is found from:

$$\bar{R} = [X_1^2 + Y_1^2]^{1/2}$$

Employing the same dimensionless ratios  $\Omega$ ,  $\zeta$  and  $\Theta$  given previously, the amplitude  $R$  is found to be:

$$R = \left( \frac{y_1 - y_2}{2} \right) \cdot \frac{[1 - \Theta^2]}{\sqrt{(1 - 4\Omega^2 - \Theta^2) + 16\zeta^2\Omega^2}} \quad (3.31)$$

For  $\Omega = 0$ ,  $R = (y_1 - y_2)/2$ , i.e. the 'static' whirl mentioned by Robertson (Ref 28). The amplitude of  $R$  becomes infinite by large where:

$$\Omega = \frac{\omega}{\omega_c} = 0.5 \sqrt{\frac{1 - \Theta^2}{1 - 4\zeta^2}}$$

For small damping  $\frac{\omega}{\omega_c} = 0.5 \sqrt{1 - \Theta^2}$

$$\approx 0.5$$

for small  $\Theta$ , the usual case. This explains the half-critical subharmonic observed in almost-symmetrical systems. The experiments conducted by Taylor also showed the half-critical peaks at 600 rpm quite prominently (not included). Laffoon and Rose (Ref. 29) also show results for the half-critical speed.

The lower subharmonics do not appear in the above theoretical result. They were excluded by the type of solution chosen,  $\bar{R}^{12\omega t}$ . They are revealed in a more detailed analysis which included non-linear effects. Den Hartog (Ref. 17) gives an introduction to this problem, which involves Mathieu's equation. The solution of Mathieu equations is discussed by Stoker (Ref. 30) and McLaughlin (Ref. 31).

### Operation of Rotors in Fluid-Film Bearings

The motions of a flexible rotor which operates in fluid-film bearings are determined by the interaction between the rotor mass-elastic properties and bearing elastic-damping properties. The bearing characteristics depend on geometry and proportions and on lubricant viscosity, rotor operating speed, and bearing load. For small vibratory movements of the system, these characteristics may be linearized to represent the bearing as an arrangement of springs and dashpots as shown in Figure 3.24. The derivation of these bearing coefficients is given in Appendix A, together with tables of values for several bearing types. The same general bearing representation applies for hydrodynamic and hydrostatic bearings, liquid or gas bearings, and laminar or turbulent bearing operation.

As in the case of the elastically supported rotor considered previously, the elasticity of the fluid film contributes to the overall system flexibility, and the critical speeds of the system occur at lower speeds of rotation. Critical whirl amplitudes of the rotor are reduced as a result of the damping properties of the fluid-film, but for higher speeds the damping causes larger whirl amplitudes. As the bearing stiffness and damping coefficients vary with speed, due to changes in bearing operating eccentricity, one of the problems in designing high-speed machinery is to select the bearing properties so that the critical speed occurs within the most suitable range, and the maximum attenuation of transmitted force occurs at the critical speed. Force attenuation depends on bearing flexibility, but so does whirl amplitude. A compromise solution must, therefore, be found in which the transmitted force is minimized in keeping with journal whirl amplitudes of practical magnitude for a given level of unbalance. Attempts to optimize rotor-bearing attenuation usually involve a lower system critical speed, and the machine operating range is often such that two or more critical speeds may be involved. Minimum force transmission at the operating speed may then result in large amplitudes and forces at the criticals which lie within the range. In the following analyses, the design problems of the flexible, high-speed rotors in damped, flexible bearings are discussed in detail. A vertical unbalanced rotor with uniform elastic properties is assumed in all cases in order to consider the problems associated with unbalance synchronous whirl in fluid-film machinery. The stability of rotors in fluid-film bearings is discussed in Section 5.

### Single-Disk Elastic Rotor in Fluid-Film Bearings

Lund and Sternlicht (Ref.32) have examined the rotor dynamic performance of the simple elastic rotor operating in fluid-film bearings shown in Figure 3.25. The effect of rotor mass is taken to be concentrated at mid-span and located at G, which is eccentric from the shaft center, E, by a. The shaft is massless and has symmetrical elastic properties but no damping. The bearings possess both elastic and damping properties which are linear for small displacements. Both supporting pedestals are rigid. Thus, the rotor whirls as shown about O in synchronism with the shaft rotation,  $\omega$ . The equations of motion for G are

$$m\ddot{x} + k(x - x_1) = m\omega^2 \cos \omega t$$

$$k(x - x_1) = 2K_{xx} x_1 + 2C_{xx} \dot{x}_1 - 2K_{xy} y_1 - 2C_{xy} \dot{y}_1$$

$$m\ddot{y} + k(y - y_1) = m\omega^2 \sin \omega t$$

$$k(y - y_1) = 2K_{yy} y_1 + 2C_{yy} \dot{y}_1 - 2K_{yx} x_1 - 2C_{yx} \dot{x}_1 \quad (3.32)$$

writing

$$\omega_o^2 = \frac{k}{m}$$

$$\kappa = \frac{1}{2} \frac{\omega_o^2}{\omega_o^2 - \omega^2}$$

or in dimensionless form

$$\bar{\kappa} = \frac{\frac{1}{2} k}{\left(\frac{\lambda \omega_o}{C}\right)} \cdot \frac{\frac{\omega}{\omega_o}}{1 - \left(\frac{\omega}{\omega_o}\right)^2} = S \cdot \frac{\frac{B|B|}{B_o}}{1 - \left(\frac{B|B|}{B_o}\right)^2}$$

where S is the bearing number. Taking the solution to the above equations in the form

$$x = A \cos \omega t + B \sin \omega t$$

$$x_1 = \frac{A \omega_0^2 + a \omega^2}{\omega_0^2 - \omega^2} \cos \omega t + \frac{B \omega_0^2}{\omega_0^2 - \omega^2} \sin \omega t \quad (3.33)$$

$$y = E \cos \omega t + F \sin \omega t$$

$$y_1 = \frac{E \omega_0^2}{\omega_0^2 - \omega^2} \cos \omega t + \frac{F \omega_0^2 + a \omega^2}{\omega_0^2 - \omega^2} \sin \omega t \quad (3.34)$$

Substituting Equations (3.33) and (3.34) into (3.32) yields a matrix in terms of the eight bearing coefficients which may be reduced to a matrix of the same form as the one for a rotor without cross-coupling terms. Such a rotor has only four spring and damping coefficients denoted by  $K_x$ ,  $C_x$ ,  $K_y$  and  $C_y$ . The reduced matrix is:

$\frac{A}{\kappa \delta}$	$\frac{B}{\kappa \delta}$	$\frac{C}{\kappa \delta}$	$\frac{D}{\kappa \delta}$	
$(K_x - \kappa)$	$\omega B_{x..}$	0	0	1
$-\omega B_x$	$(K_x - \kappa)$	0	0	0
0	0	$(K_y - \kappa)$	$\omega B_y$	0
0	0	$-\omega B_y$	$(K_y - \kappa)$	1

(3.35)

The relationship between the above four bearing coefficients and the original eight coefficients is:

$$K_x = K_{xx} - \left( \frac{1}{\psi_x} \right) \left[ \zeta K_{xy} + \eta \omega C_{xy} \right]$$

$$C_x = C_{xx} + \left( \frac{1}{\psi_x} \right) \left[ \eta K_{xy} - \zeta \omega C_{xy} \right]$$

$$K_y = K_{yy} - \left( \frac{1}{\psi_y} \right) \left[ \xi K_{yx} - \eta \omega C_{yx} \right]$$

$$C_y = C_{yy} - \left( \frac{1}{\psi_y} \right) \left[ \eta K_{yx} - \xi \omega C_{yx} \right] \quad (3.36)$$

where

$$\psi_x = \left[ K_{xy} - \kappa + \omega C_{xy} \right]^2 + (K_{xy} - \omega C_{yy})^2$$

$$\psi_y = \left[ K_{xx} - \kappa - \omega C_{yx} \right]^2 + (K_{yx} + \omega C_{xx})^2$$

$$\xi = \left[ K_{xx} - \kappa - \omega C_{yx} \right] \left[ K_{xy} - \omega C_{yy} \right] + \left[ K_{yy} - \kappa + \omega C_{xy} \right] \left[ K_{yx} + \omega C_{xx} \right]$$

$$\eta = \left[ K_{xx} - \kappa - \omega C_{yx} \right] \left[ K_{yy} - \kappa + \omega C_{xy} \right] - \left[ K_{xy} - \omega C_{yy} \right] \left[ K_{yx} + \omega C_{xx} \right] \quad (3.37)$$

Solving Equations 3.35 for the coefficients A, B, E and F gives

$$\frac{A}{a} = \frac{\kappa(K_x - \kappa)}{(K_x - \kappa)^2 + (\omega C_x)^2}$$

$$\frac{B}{a} = \frac{\kappa(\omega C_x)}{(K_x - \kappa)^2 + (\omega C_x)^2}$$

$$\frac{E}{a} = \frac{-\kappa(\omega C_y)}{(K_x - \kappa)^2 + (\omega C_x)^2}$$

$$\frac{F}{a} = \frac{\kappa(K_y - \kappa)}{(K_y - \kappa)^2 + (\omega C_y)^2} \quad (3.38)$$

These expressions allow the rotor whirl coordinates to be obtained from Equation 3.33 and 3.34. The whirl path of G is an ellipse (Figure 3.26) and the motion may be comprehended more concisely by determining the geometric proportions of this orbit. These are found to be

Major axis

$$\bar{r}_a = \sqrt{\frac{1}{2} \left[ \left( \frac{A}{a} \right)^2 + \left( \frac{B}{a} \right)^2 + \left( \frac{C}{a} \right)^2 + \left( \frac{F}{a} \right)^2 \right] + \frac{1}{2} \left[ \left( \frac{A}{a} \right)^2 + \left( \frac{B}{a} \right)^2 + \left( \frac{C}{a} \right)^2 + \left( \frac{F}{a} \right)^2 \right]^2 - \left[ \left( \frac{A}{a} \right) \left( \frac{F}{a} \right) - \left( \frac{B}{a} \right) \left( \frac{C}{a} \right) \right]^2} \quad (3.38)$$

Minor axis

$$\bar{r}_b = \sqrt{\frac{1}{2} \left[ \left( \frac{A}{a} \right)^2 + \left( \frac{B}{a} \right)^2 + \left( \frac{C}{a} \right)^2 + \left( \frac{F}{a} \right)^2 \right] - \frac{1}{2} \left[ \left( \frac{A}{a} \right)^2 + \left( \frac{B}{a} \right)^2 + \left( \frac{C}{a} \right)^2 + \left( \frac{F}{a} \right)^2 \right]^2 - \left[ \left( \frac{A}{a} \right) \left( \frac{F}{a} \right) - \left( \frac{B}{a} \right) \left( \frac{C}{a} \right) \right]^2} \quad (3.39)$$

Angle of inclination

$$\tan 2\beta = \frac{2 \left[ \left( \frac{A}{a} \right) \left( \frac{C}{a} \right) + \left( \frac{B}{a} \right) \left( \frac{F}{a} \right) \right]}{\left[ \left( \frac{A}{a} \right)^2 + \left( \frac{B}{a} \right)^2 - \left( \frac{C}{a} \right)^2 - \left( \frac{F}{a} \right)^2 \right]} \quad (3.40)$$

The force transmitted to the bearing pedestal is given by

$$F_x = K_x x_o + C_x \dot{x}_o$$

$$F_y = K_y y_o + C_y \dot{y}_o$$

Introducing Equations 3.38 and 3.39 and simplifying gives

$$\frac{F_x}{K_x} = \sqrt{\frac{K_x^2 + (\omega C_x)^2}{(K_x - \kappa)^2 + (\omega C_x)^2}} \cos \left[ \omega t - \phi_x + \gamma_x \right] \quad (3.41)$$

where

$$\tan \phi_x = \left[ \frac{\omega C_x}{K_x - \kappa} \right]$$

$$\tan \gamma_x = \frac{\omega C_x}{K_x}$$

and

$$\frac{F_y}{K_y} = \sqrt{\frac{Z_y^2 + (\omega C_y)^2}{(K_y - K)^2 + (\omega C_y)^2}} \sin [\omega t - \phi_y + \gamma_y] \quad (3.42)$$

where

$$\tan \phi_y = \left[ \frac{\omega C_y}{K_y - K} \right] \quad \tan \gamma_y = \frac{\omega C_y}{K_y}$$

The force transmitted to the bearing pedestals also varies in an elliptical manner with the maximum and minimum values corresponding to the major and minor axes of the force ellipse. These values may be found in a similar manner to that described for calculating the whirl ellipse proportions.

The above analysis has been applied in the case of several important bearing profiles to determine the effect of the fluid film on rotor whirl amplitude and bearing transmitted force. Results are given in Figures 3.27 and 3.28 for the cylindrical journal bearing and the four-axial-groove bearing, for a range of bearing eccentricity ratios. The single rotor-bearing system critical speed,  $\omega_c$ , follows directly from the simple rotor-bearing model considered.

## Two-Mass Rotor in Damped Flexible Bearings

The results of the previous analysis are limited in their application to the vicinity of the fundamental critical speed of the rotor-bearing system. The operating speed range of many high-speed machines includes several critical speeds, and in order to obtain adequate design information for these cases, it is necessary to consider a rotor which has several degrees of freedom in translatory motion.

A two-mass rotor has been analysed by Warner and Thoman (Ref. 33) using bearing data obtained by Warner (Ref. 34) for 150-degree partial-arc bearings. This rotor is shown in Figure 3.29, and certain results for transmitted force and rotor amplitude are given in Figure 3.30 (a)(b)(c) and (d). The results given in this paper cover maximum transmitted bearing force,  $\left[ \frac{F}{\xi_{\text{max}}^2} \right]$ , maximum journal displacement,  $\frac{x_2 \xi}{a}$ , and maximum mass displacement  $\frac{x_1}{a}$ , over a speed range,  $\left( \frac{\omega}{\omega_c} \right)$ , 0.05 to 5.00, and for a range of bearing operating eccentricity,  $\eta$ , from

0.05 through 0.95. By means of a device,  $\xi$ , the charts apply to either the fundamental mode or to the second mode - according to the value of  $\xi$ , used in the dimensionless system parameters. For mode 1,  $\xi = 1.00$ , and the rotor is in a state of "static" unbalance in which the eccentric masses act in phase. For mode 2,

$$\xi = \frac{\text{distance from center of discrete mass to center of span}}{\text{half span length}}$$

and the rotor is in a state of "dynamic" unbalance in which the two eccentric masses act in anti-phase, 180 degrees apart, as indicated in Figure 3.29. The results given in this paper cover a very wide range of machine proportions and operating conditions, and are directly applicable to high-speed rotor design. In discussing this paper, Lund (Ref. 35) has shown how the results may be condensed into a single diagram by a different choice of parameters. The basic equations given by Warner and Thoman are

$$\begin{aligned} \frac{k}{\alpha_{11}} [x_1 - \xi x_2] &= K_x x_2 + B_{xx} \dot{x}_2 - D_x y_2 + B_{xy} \dot{y}_2 \\ \frac{k}{\alpha_{11}} [y_1 - \xi y_2] &= D_y x_2 + B_{xy} \dot{x}_2 + K_y y_2 + B_{yy} \dot{y}_2 \end{aligned} \quad (3.43)$$

where  $K_x$ ,  $K_y$ ,  $D_x$  and  $D_y$  are the direct and cross-coupled bearing stiffnesses,  $B_{xx}$ ,  $B_{yy}$ ,  $B_{xy}$  and  $B_{yx}$  are the direct and cross-coupled damping coefficients, and  $\alpha_{11}$  is an influence coefficient. As  $x_1$ ,  $x_2$ ,  $y_1$  and  $y_2$  are complex displacements, writing

$$\begin{aligned} \frac{x_1}{a} &= \frac{\frac{\xi x_2}{a} - 1 \left( \frac{\omega}{\omega_c} \right)^2}{1 - \left( \frac{\omega}{\omega_c} \right)^2} \\ \frac{y_1}{a} &= \frac{\frac{\xi y_2}{a} + \left( \frac{\omega}{\omega_c} \right)^2}{1 - \left( \frac{\omega}{\omega_c} \right)^2} \end{aligned} \quad (3.44)$$

where

$$\omega_c^2 = \frac{1}{m\alpha_{11}}$$

allows the above equations to be written in terms of the basic parameters as follows:

$$\begin{Bmatrix} \left[ \frac{CK_x}{W} - \kappa + 1 \frac{C\omega B_{xx}}{W} \right] & \left[ -\frac{CD_x}{W} + 1 \frac{C\omega B_{xy}}{W} \right] \\ \left[ \frac{CD_y}{W} + 1 \frac{C\omega B_{yx}}{W} \right] & \left[ \frac{CK_y}{W} - \kappa + 1 \frac{C\omega B_{yy}}{W} \right] \end{Bmatrix} \begin{Bmatrix} \frac{\xi x_2}{a} \\ \frac{\xi y_2}{a} \end{Bmatrix} = \kappa \begin{Bmatrix} -1 \\ 1 \end{Bmatrix} \quad \text{where } \kappa = \frac{c\xi^2}{W} \frac{\left( \frac{\omega}{\omega_c} \right)^2}{1 - \left( \frac{\omega}{\omega_c} \right)^2} \quad (3.45)$$

Hence,  $\kappa$  is the only basic variable whereas in the paper by Warner and Thomas this has been treated as two separate variables,  $\frac{\omega\alpha_{11}}{C\xi^2}$  and  $\frac{\omega}{\omega_c}$ . Likewise, the

dimensionless transmitted force becomes:

$$\frac{CF}{aW} = \left[ \frac{C\xi^2}{W\alpha_{11}} \right] \left[ \frac{F}{\xi m a \omega_c^2} \right]$$

Plotting the transmitted force as a function of  $k$  reduces the figures to a single curve, eliminating the parameter  $\frac{Wx_{11}}{C\xi^2}$ . The same is true for the journal amplitude  $\frac{\xi-2}{a}$ , but not  $\frac{\xi-1}{a}$ . Figure 3.31 is based on these parameters and unifies the Warner-Thomson data into one curve - including the variation of eccentricity ratio  $\eta$  with speed. The physical significance of  $K$  is given by

$$K = \frac{C\xi F_m}{W_a}$$

such that  $K$  is the dimensionless transmitted force when the bearings are rigid. This may be seen from Figure 3.31. The ratio between the dimensionless transmitted force and  $K$  is, therefore, a measure of the force attenuation due to the bearings.

It is of interest to note that when  $\frac{\omega}{\omega_c} = 1$ ,  $K = \infty$ , and  $K$  is thus independent of the rotor parameter. For this case,  $\frac{\xi x_2}{a} = 1$  and  $\frac{\xi y_2}{a} = -1$ , so that the journal whirl path is circular and the maximum displacement is 180 degrees out-of-phase with the unbalance, independent of the bearing eccentricity ratio.

#### Uniform elastic rotor in damped flexible bearings

The results of Lund and Sternlicht allow an operating eccentricity to be chosen so that attenuation of the bearing transmitted-force is a maximum, in the vicinity of the first critical speed. General rotor operating characteristics including attenuation were investigated by Rieger (Ref. 36) for speed ratios,

$\left(\frac{\omega}{\omega_c}\right)$  up to 25. The results obtained cover the operating speed range for all

but the most exotic machines. A uniform elastic rotor with distributed mass operating in cylindrical fluid-film bearings and having a rotating unbalance located at some point along its length was considered. The influence of: stiffness ratio,  $v$ , (shaft/bearing), bearing eccentricity ratio,  $\eta$ , and unbalance position  $\mathcal{L}$  on transmitted force, rotor displacement, and journal displacement

was investigated throughout the speed range. Typical results for  $\eta = 0.7$  with a central unbalance  $\mathcal{L} = 0.5$  are shown in Figures 3.32 (a)(b) and (c). This static unbalance condition gives rise to symmetrical condition gives rise to symmetrical modes alone, due to symmetry. Superposition of two unbalance solutions with a 180 degree phase difference between the unbalance loads situated at  $\mathcal{L} = 0.45$  and  $\mathcal{L} = 0.55$  corresponds to a dynamic unbalance condition. Results are given in Figure 3.33 (a) and (b). Mode shapes for static unbalance are shown in Figure 3.34 and for dynamic unbalance in Figure 3.35.

Since the mass and elasticity of the rotor are uniformly distributed along its length, the solutions obtained include the influence of all rotor modes on each particular motion directly. The rotor-bearing system does not apply to any specific machine configuration. The results obtained bring out the relative influence of each parameter on the motion for a wide ranges of the variables chosen.

In general, the results show that rotor motions are principally determined by the interaction between rotor stiffness and bearing stiffness and by the type of unbalance (static or dynamic) which is present in the system. A flexible rotor tends to adopt a whirl configuration which is determined by the rigidity of the bearings. A rigid rotor whirls as a rigid body within its bearings at low speeds; but, at higher speeds where bending effects predominate its motions are similar to those of a free-free beam. The operating eccentricity corresponding to maximum transmitted force attenuation depends on the system stiffness ratio,  $v^1$ , the nature of the unbalance (static or dynamic), and on the speed of operation. In the low speed range,  $\eta = 0.5$  gives the greatest attenuation; however, at higher speeds, the condition for optimum operation must be selected to suit each case individually and depends on the machine operating requirements. A different eccentricity will be required for best overall performance throughout the speed range as opposed to minimum transmitted force at a specific operating speed.

---

1. The notation of this reference.

## Development of Rotor-Bearing Dynamics

Present understanding of the operation of rotors in bearings is based on a long and arduous development. The copious subject literature reflects both the wide range of applications requiring consideration and the difficulties which have been surmounted in obtaining the present level of technological development. The present section is intended as a guide to the more important of these literature contributions. A complete discussion would require a special volume. The most necessary purpose will be served by indicating those works which have pioneered further developments, and also by mentioning a number of other works which contain either erroneous or misleading information. The basic mechanics of several aspects of the subject have given rise to controversial debate, and the fresh reader until now has been left to find the resolution of each aspect without guidance.

Rotor dynamic analysis was initiated by Rankine (Ref.37), who studied the un-damped radial motion of a flexible shaft. From this work it was concluded erroneously that no rotor could survive the sustained infinitely-large amplitude build-up caused by the fundamental transverse natural frequency of the shaft, the 'critical' speed. This result limited the design of rotating machinery until DeLaval in 1889 demonstrated experimentally that stable operation beyond the critical speed was possible, and that the supposed instability threshold was manifest only as a zone of large amplitude. Rankine's analysis was extended by Foppl (Ref.38) who demonstrated that dynamic equilibrium was restored beyond the critical speed by the inversion of the rotor, e.g. between the elastic and the wheel axis. Greenhill (Ref.39) investigated the elastic stability of a rotating shaft subjected to a combination of axial thrust and applied torque, and obtained critical speed formulas for several kinds of end support. The extensive investigation of systems and methods of calculation for critical speeds made by Dunkerley (Ref.40) emphasized the analytical complexity involved with all but uniform rotors with the simplest layouts. The question of applicability and accuracy of the simple method suggested by Dunkerley was soon taken up by eminent analysts such as Chree (Ref.41), Jeffcott (Ref.42), and Morley (Ref.43). At that time, analysis of rotor critical speed phenomena as stated by Chree was based on the fallacious elastic stability concept wherein the action of the rotor centrifugal forces is to reduce the elastic restoring forces to zero, so that at the critical speed the natural frequency of the

shaft diminishes to zero.

This concept eventually gave rise to a vigorous controversy when Kerr (Fig. 44) published theoretical and experimental critical speed results for two machines which could not be reconciled. Although the disagreement now seems to have been due to neglecting the dynamic bearing properties, it re-opened the question of the mechanics of rotor behavior, and received attention from Chree (Ref. 44), Stodola (Ref. 44), and Jeffcott (Ref. 44), amongst several others. Jeffcott (Ref. 42) finally resolved the controversy by considering an eccentric unbalance as the exciting force, and included the effect of viscous (velocity) damping in his analysis. Thus the radial and tangential effects were considered simultaneously. This analysis forms the basis of the rotor dynamic theory given in the present chapter. Jeffcott's basic concept of a rotor which whirled about its static equilibrium position was restated and extended by Rogers (Ref. 45) in discussing the existence of the critical speeds of  $\omega_c/2$  (Stodola) and at  $\omega_c/\sqrt{2}$  (Kerr). This latter critical is the result of an incorrect physical concept in which the elastically unstable rotor is assumed to whirl about the bearing axis. Howland (Ref. 46) also discussed these critical speeds, but in attempting to derive the basic equations in rotating coordinates he omitted Coriolis effects, thus invalidating the subsequent analytical conclusion, as indicated by Robertson (Ref. 47). In a series of classical papers, Robertson discussed the nature and occurrence of shaft whirling phenomena (Ref. 48), analyzed the static and dynamic aspects of shafts with dissimilar lateral stiffnesses (Ref. 28), collated the existing data on shaft hysteretic whirling (Ref. 49), analyzed the nature of transient whirl motions arising from a disturbance of dynamic equilibrium with supporting experiments and developed a graphical method of analysis (Ref. 50), discussed the influence of speed oscillations on inducing shaft whirling (Ref. 51), and established, without solving, the basic equations of an infinitely long rigid rotor in a full cylindrical journal bearing, using Sommerfeld's lubrication theory (Ref. 52).

In the course of development of a high-speed turbo-blower, Newkirk and Kimball encountered large amplitude whirling motions which could not be eliminated by more refined rotor balancing. The rotors operated in rolling-element above their bending critical speed, and it was noted that although the whirl motion was synchronous with the rotation, at speeds beyond the critical, the rotor whirl was constant at the critical rotor speed, and the rotor amplitude grew

to dangerously large proportions. Kimball (Ref. 23) (Ref. 53), found that shrink-fitted assemblies with inadequate contact pressure gave rise to a cyclic energy loss, and showed that this loss generated a tangential force, which, at speeds above the critical, reversed in direction to promote an unstable whirl motion of increasing amplitude. Immediately following this discovery, a second outbreak of rotor instability occurred in the same machine works to which neither refined balance nor improved shrink-fit design made any improvement. Further experiments conducted by Newkirk (Ref. 54) established that this second type of whirling commenced at speeds in the order of twice the bending critical speed, and that at still higher speeds the whirling persisted accompanied by very large amplitudes of the rotor within the fluid-film bearings. Moreover, the whirl frequency was again the rotor bending critical frequency, which led to the earlier (incorrect) supposition that this was a further case of hysteretic whirling. Newkirk and Taylor (Ref. 55) subsequently noted that this second type of whirl was predominantly hydrodynamic in nature and could be suppressed by diminishing the bearing clearance, and by increasing the viscosity of the lubricating oil. Rotor motions of this type came to be known as resonant whipping. Newkirk and Grobel (Ref. 56) experimented with the geometry of the bearing surfaces to develop a complex "non-whirling" bearing. Although valuable experimental work was done on hydrodynamic whirl during this period, the only significant analytical achievement was the rigid-rotor full-bearing work of Robertson (Ref. 52) who inferred (correctly) for the case considered that the full journal bearing was inherently unstable, without solving the equations which had been derived. These developments were reviewed by Newkirk (Ref. 57) and later by Newkirk (Ref. 58). At the same time Swift (Ref. 59, and later Ref. 60) had analysed the influence of higher harmonic components on the infinitely-long full journal bearing using the Sommerfeld theory, in connection with crankshaft wrist-pin lubrication. This work led to the important observation that the load-carrying capacity of the oil-film vanishes when the frequency of the applied force is exactly twice the rotational frequency. This finding corroborated the results of Newkirk for the onset of resonant whipping at twice the critical speed. The level of knowledge was greatly extended by Burwell (Ref. 61)(Ref. 62)(Ref. 63) and Shawki (Ref. 64) (Ref. 65)(Ref. 66), both of whom conducted more detailed experimental and theoretical analyses of this problem, including the application of the digital computer to the solution of the hydrodynamic equation with time-dependent forces.

For a long time the principal rotor dynamic characteristic of any system was the fundamental flexural critical speed and calculations were based on methods given by Dunkerley (Ref. 40), Rayleigh (Ref. 67), Morley (Ref. 43) as documented in detail in Stodola (Ref. 18). Critical speed calculations for complex rotors were done in rare cases by hand calculation until Prohl (Ref. 68) developed the discrete mass rigid bearing analysis and prepared it first for punch card machine calculation. Myklestad (Ref. 69) gave a similar method at approximately the same time. These methods are adaptations of the Holzer method of vibration analysis, for massive flexible beams, and include the effects of bending gyroscopic moments and where necessary, shear. Further work using this discrete mass approach was carried out by Lund (Ref. 70) who developed an unbalance amplitude and transmitted force response program for a generalized rotor in damped flexible bearings. The effects of pedestal stiffness and damping are also included. A sub-program of this analysis gives critical speeds. Thus, at present it is possible to calculate accurately the dynamic response to any specified unbalance for any rotor which can be represented by an equivalent discrete mass system, operating in bearings of known dynamic characteristics.

Where rotor performance is significantly affected by the bearing characteristics, these properties must be known in advance. The first data was obtained by Stodola (Ref. 18) and more refined values were given by Hagg (Ref. 71) Hagg and Warner (Ref. 72), Hagg and Sankey (Ref. 73), and when the digital computer was applied to the bearing problem during the 1950's, Sternlicht (Ref. 74) obtained complete elastic and damping coefficients for the cylindrical bearing. Lund and Sternlicht (Ref. 32) obtained similar properties for other bearing types. These properties also allowed rotor bearing analyses to be made for simple rotors on damped elastic bearings and the results of such analyses were then presented as non-dimensional charts for amplitude response, transmitted force and rotor stability. Recently, Warner and Thoman (Ref. 33) have investigated the dynamic response of a two-mass rotor in partial-arc bearings and given design charts. For a similar rotor, Lund (Ref. 75) has extended the analysis to include pedestal mass, stiffness and damping, again in charts from which the dynamic characteristics of the rotor may be determined directly.

Whirling and instability arising from dissimilar lateral stiffnesses of a rotor have been troublesome, and investigation to determine the dynamic performance have been made by Taylor (Ref. 76) Foote, Foritsky and Siele (Ref. 77), Kallenburger (Ref. 26) and Dimentberg (Ref. 1 ). Although the rotor models used were simple to facilitate analysis, the results are general and provide a guide for design, and also for diagnosis of troublesome rotor whirling for which the cause is to be determined.

Rotors which operate beyond their bending critical speeds are susceptible to large amplitude build-up on passing through the critical speed. Although it was recognized towards the end of last century that operation in the post-critical range was possible, the first detailed study of transition of a rotor through its critical speed was made by Lewis (Ref. 78). After solving the equations of motion by a graphical method, results were obtained for various rates of transition, and for various amounts of damping present in the system. More recently, Dimentberg (Ref. 1 ) has investigated this problem more completely using an analytical method based on Fresnel integrals, including damping and flexible bearings. This method is discussed in detail in Chapter 6 and the analytical results are compared with experimentally obtained data, indicating good correlation.

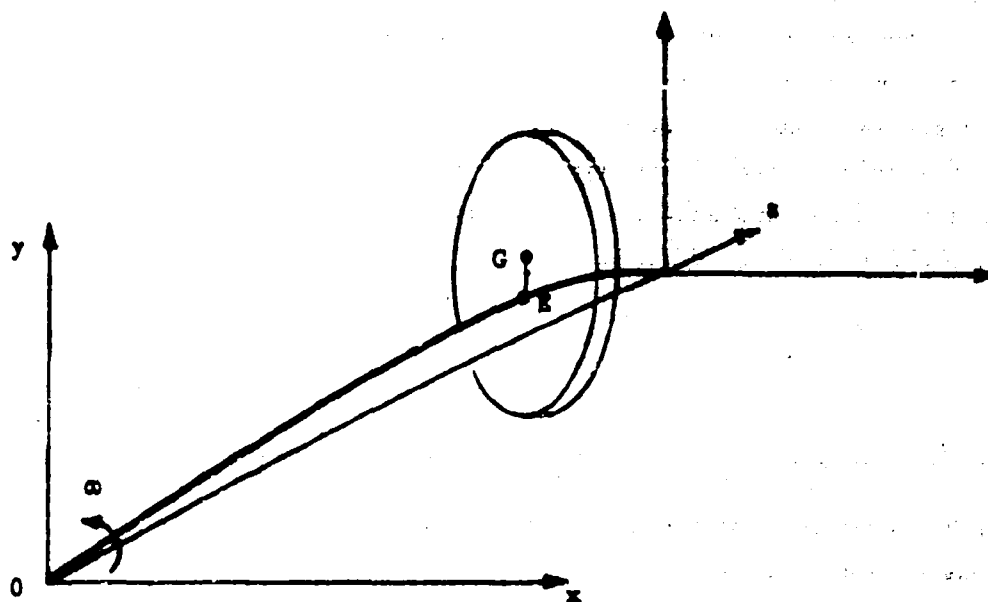


Fig. 3.01 Simple Rotor and Coordinate System

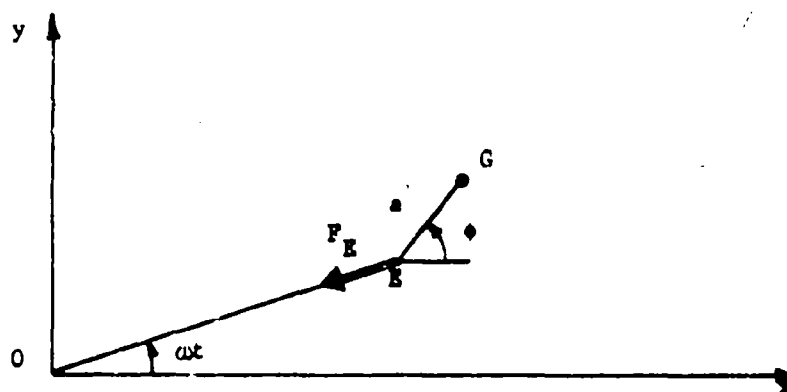


Fig. 3.02 Geometry of the Whirling Rotor

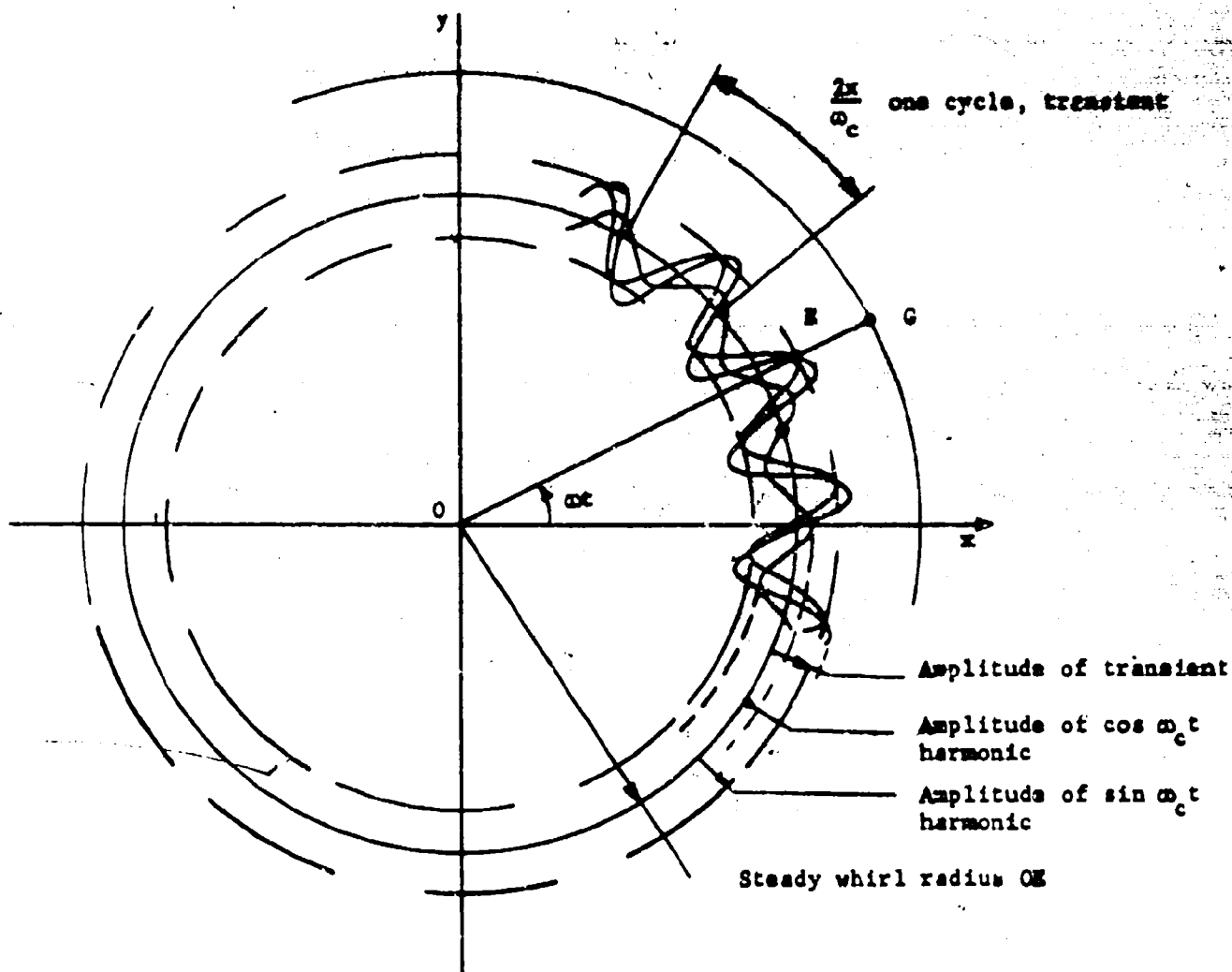
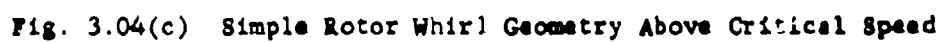
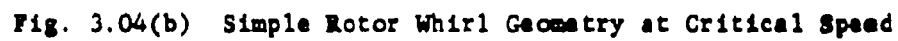
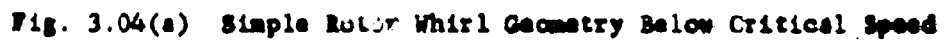


Fig. 3.03 Steady Whirl Motion with Sustained Transient  
 Simple Undamped Vertical Rotor  $\omega < \omega_c$



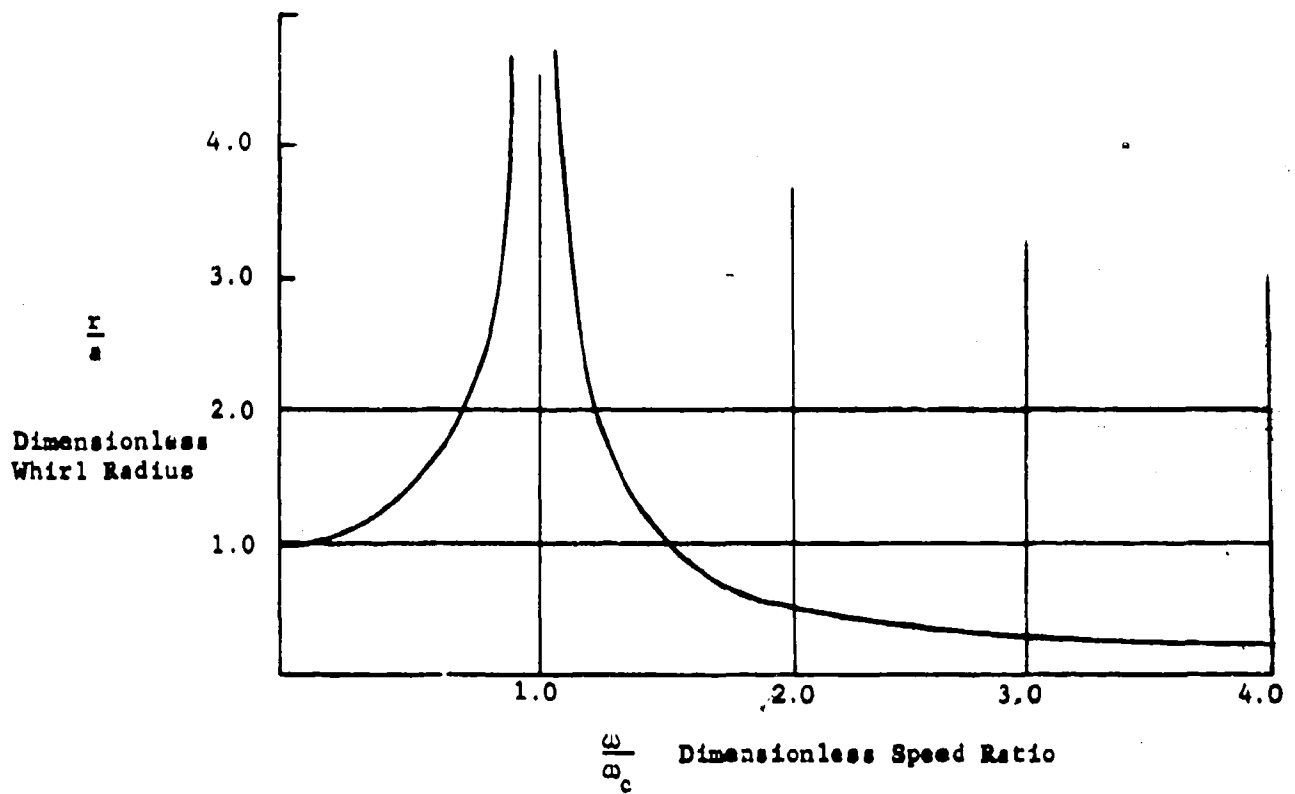


Fig. 3.05 Dependence of Whirl Radius on Rotor Speed

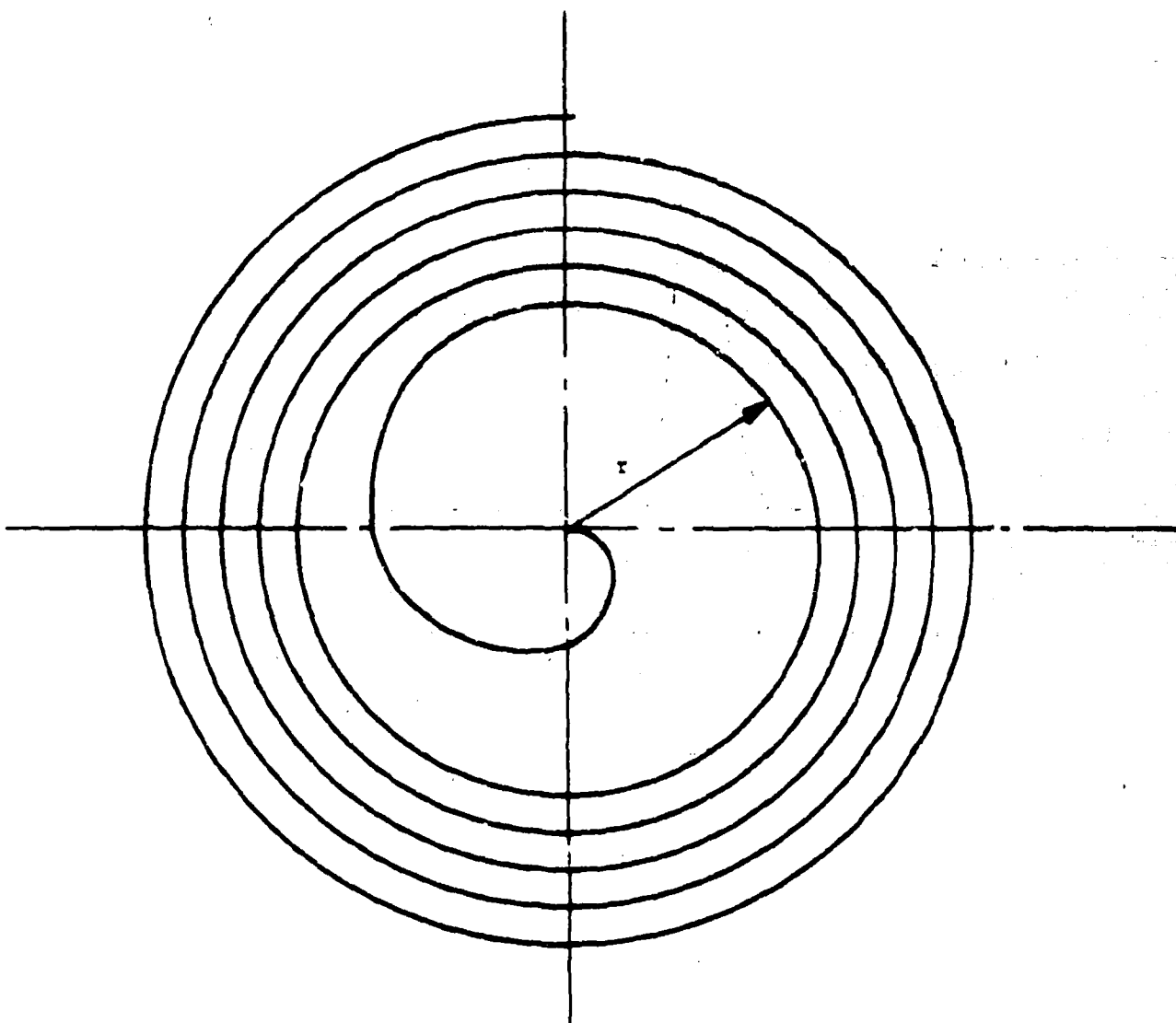


Fig. 3.06 Orbit Growth at Rotor Critical Speed,  $\omega = \omega_c$

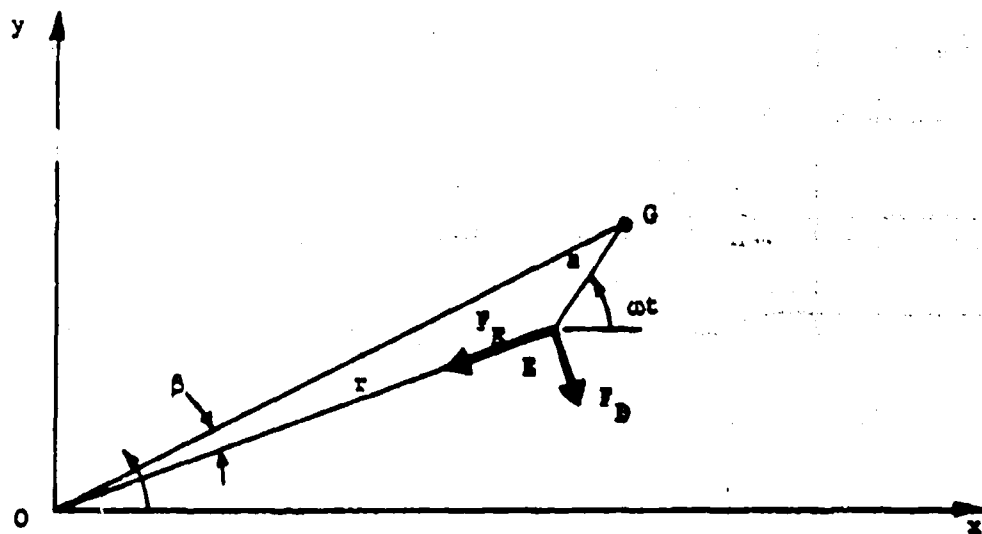


Fig. 3.07 Geometry of the Whirling Rotor With Viscous Damping

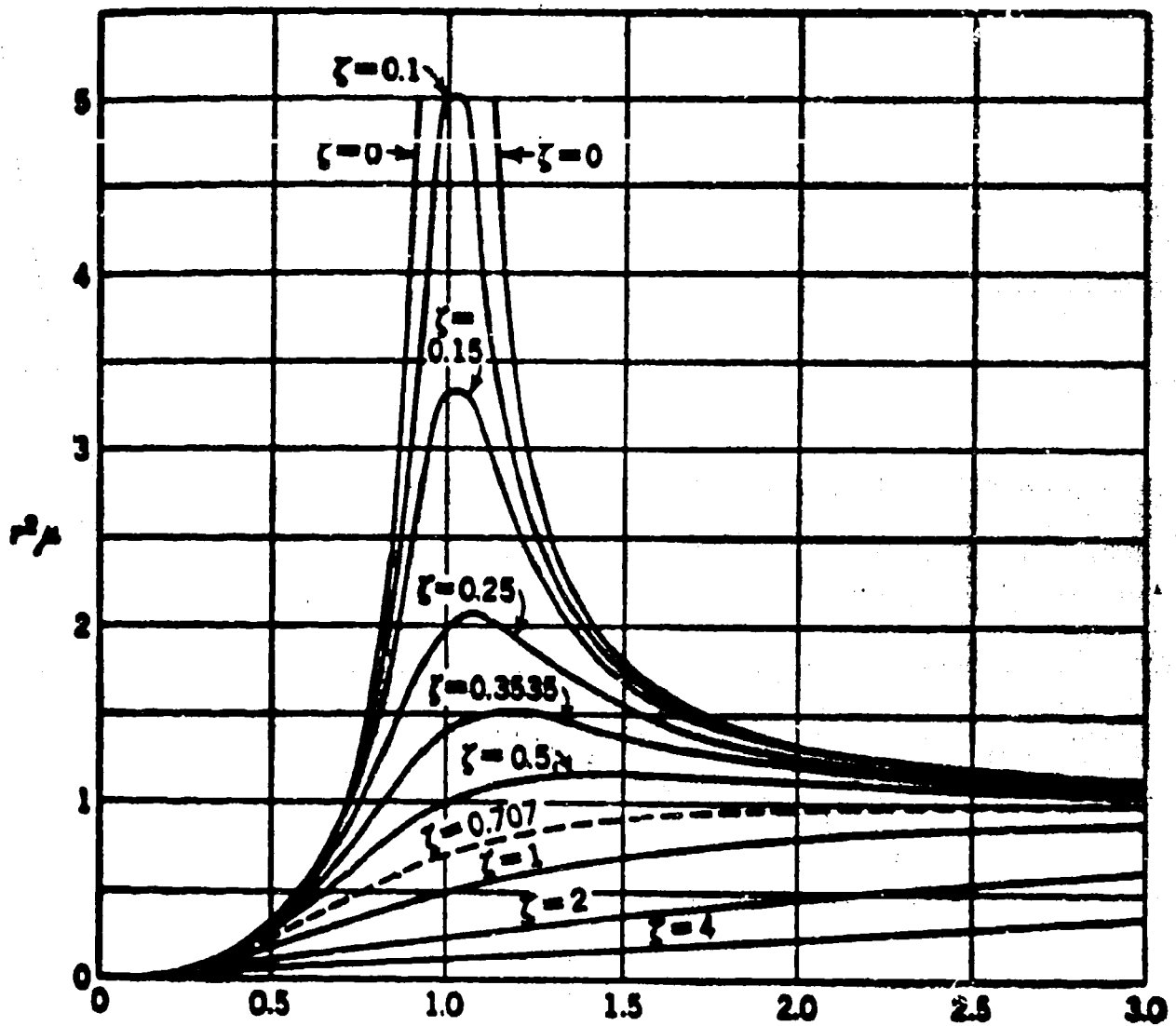


Fig. 3.08 Amplitude Ratio Versus Speed for Rotating Unbalance

Reprinted from FUNDAMENTALS OF VIBRATION ANALYSIS,  
Fig. 9-15, by N. O. Myklestad. McGraw-Hill Co.  
New York, N.Y. 1956.

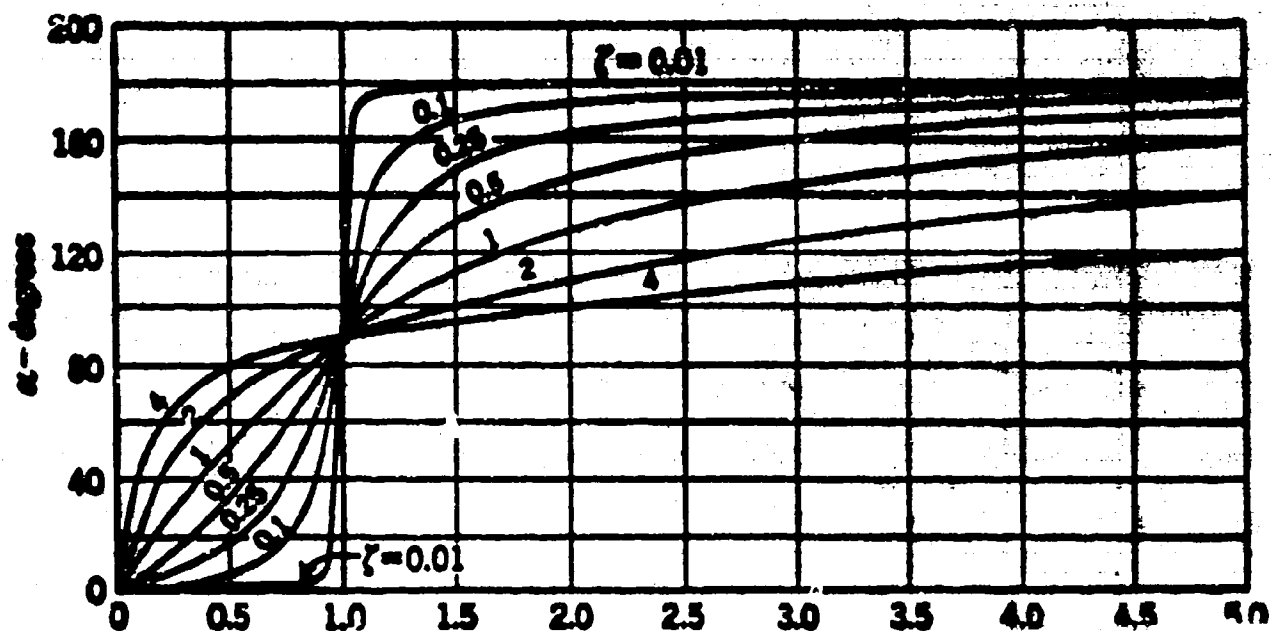


Fig. 3.09 Amplitude Phase Angle Versus Speed

Reprinted from FUNDAMENTALS OF VIBRATION ANALYSIS,  
Fig. 9-4, by N. O. Myklestad. McGraw-Hill Co.  
New York, N.Y. 1956

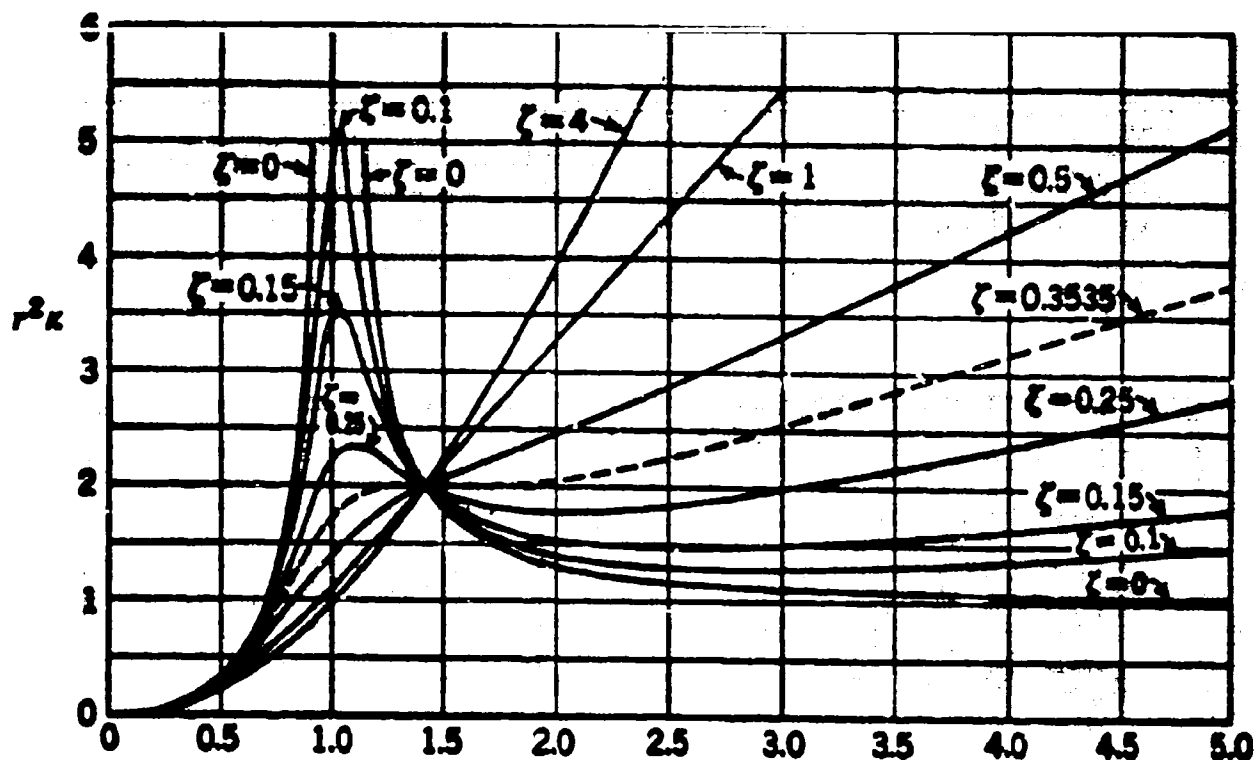


Fig. 3.10 Force Transmissibility Ratio Versus Speed  
for Rotating Unbalance Load

Reprinted from FUNDAMENTALS OF VIBRATION ANALYSIS,  
Fig. 11-5, by N. O. Myklestad. McGraw-Hill Co.  
New York, N.Y. 1956

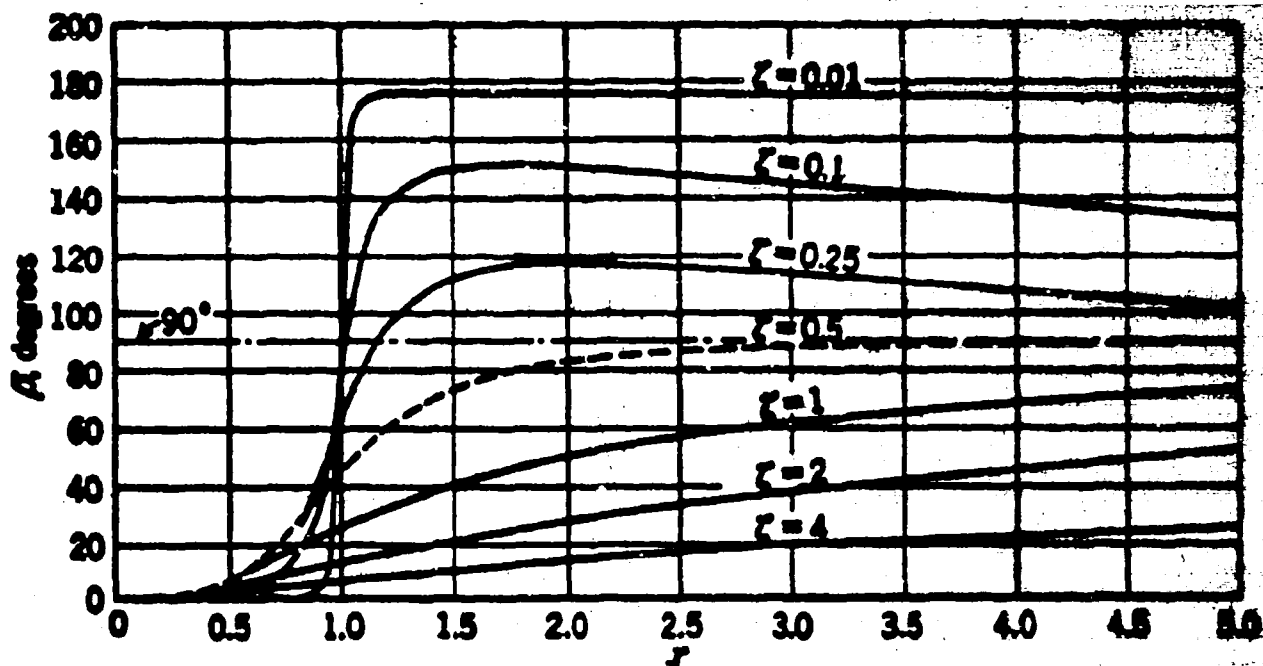


Fig. 3.11 Force Phase Angle Versus Speed

Reprinted from FUNDAMENTALS OF VIBRATION ANALYSIS,  
Fig. 11-3, by N. O. Myklestad. McGraw-Hill Co.  
New York, N.Y. 1956

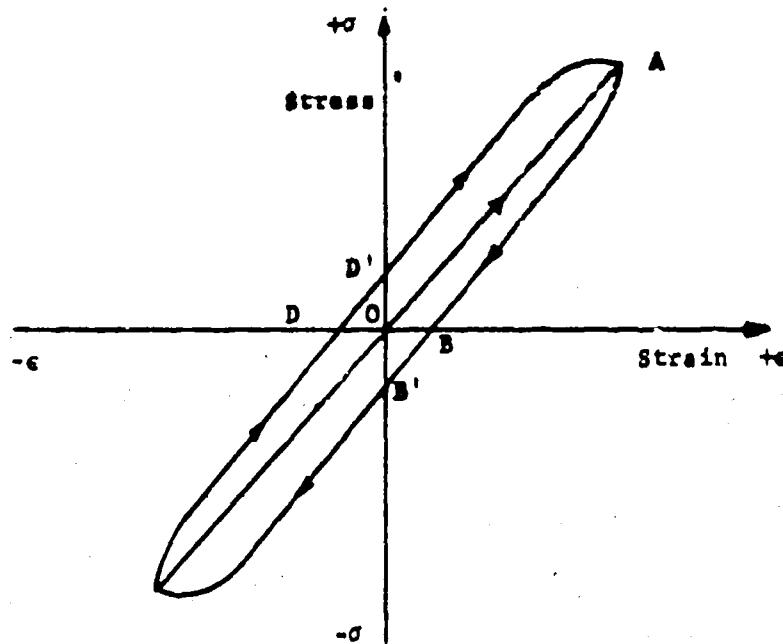


Fig. 3.12 Elastic Hysteresis Loop

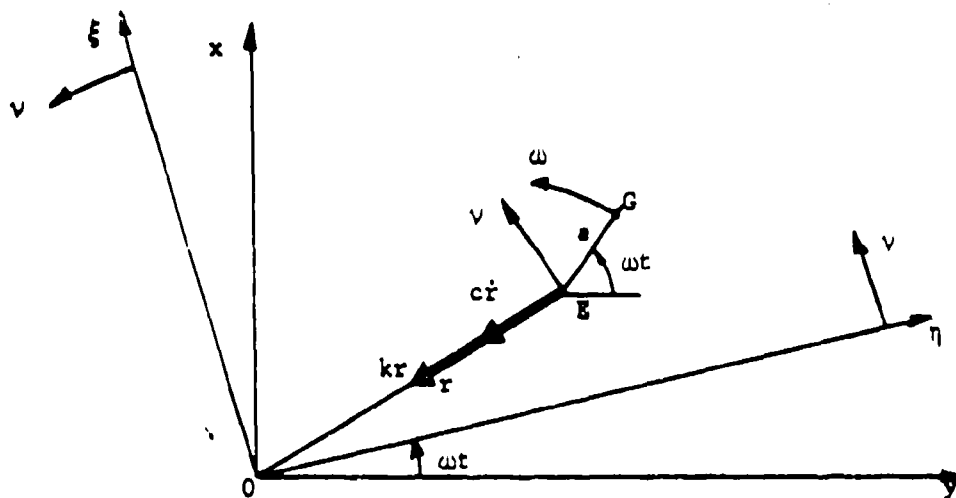


Fig. 3.13 Rotor Whirl Geometry. Internal Friction Damping  
Fixed and Rotating Coordinates

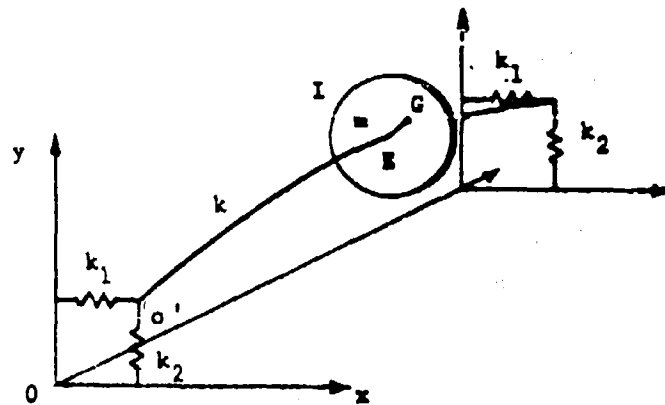


Fig. 3.14 Whirling of a Flexible Rotor in Bearings With Dissimilar Stiffness

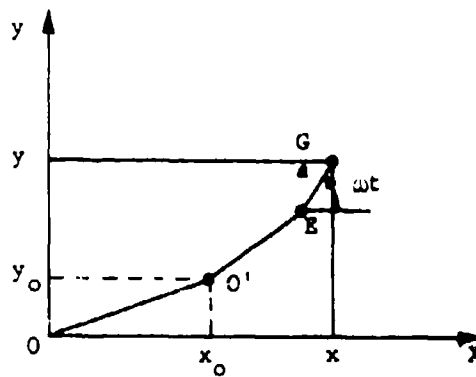


Fig. 3.15 Whirl Geometry of Flexible Rotor in Bearings With Dissimilar Stiffnesses

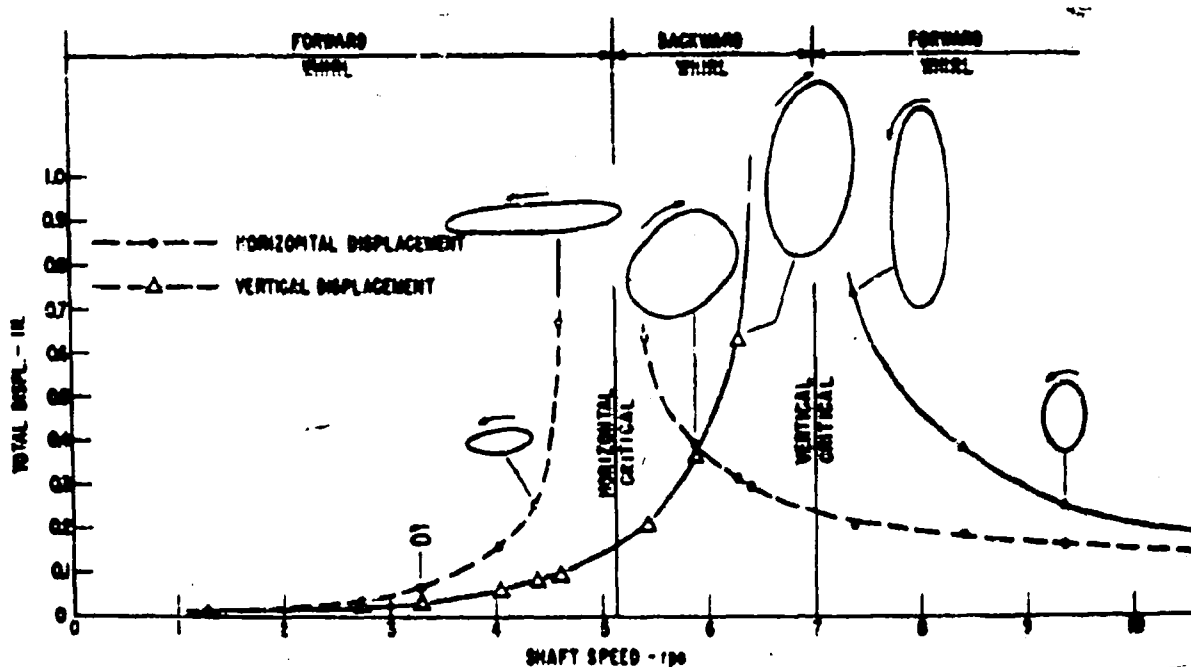


Fig. 3.16 Vertical and Horizontal Displacement versus Shaft Speed Symmetrical Shaft in Unsymmetrical Stiffness Bearings

Reprinted from SHAFT WHIRLING AS INFLUENCED BY STIFFNESS ASYMMETRY, Fig. 3, by E. H. Hull. Journal of Engineering for Industry. May 1961

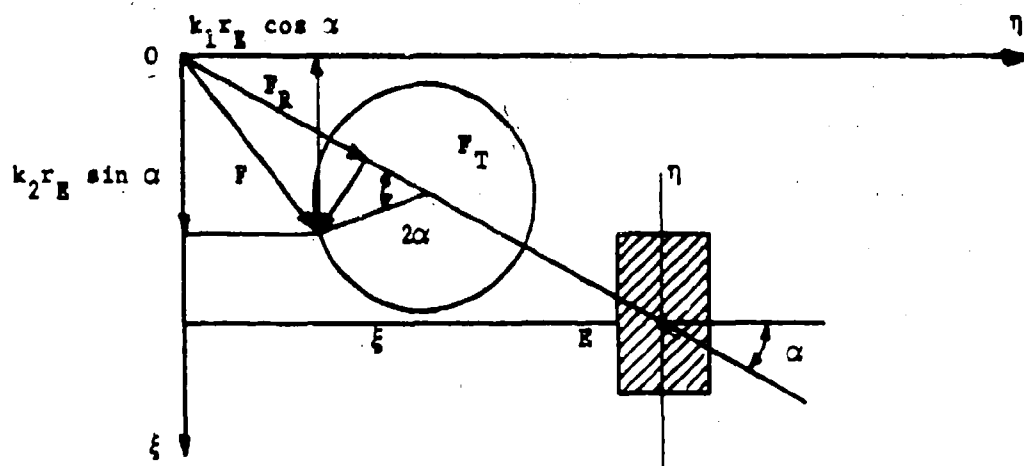


Fig. 3.17 Deflection and Force Geometry for Shaft with Dissimilar Stiffness

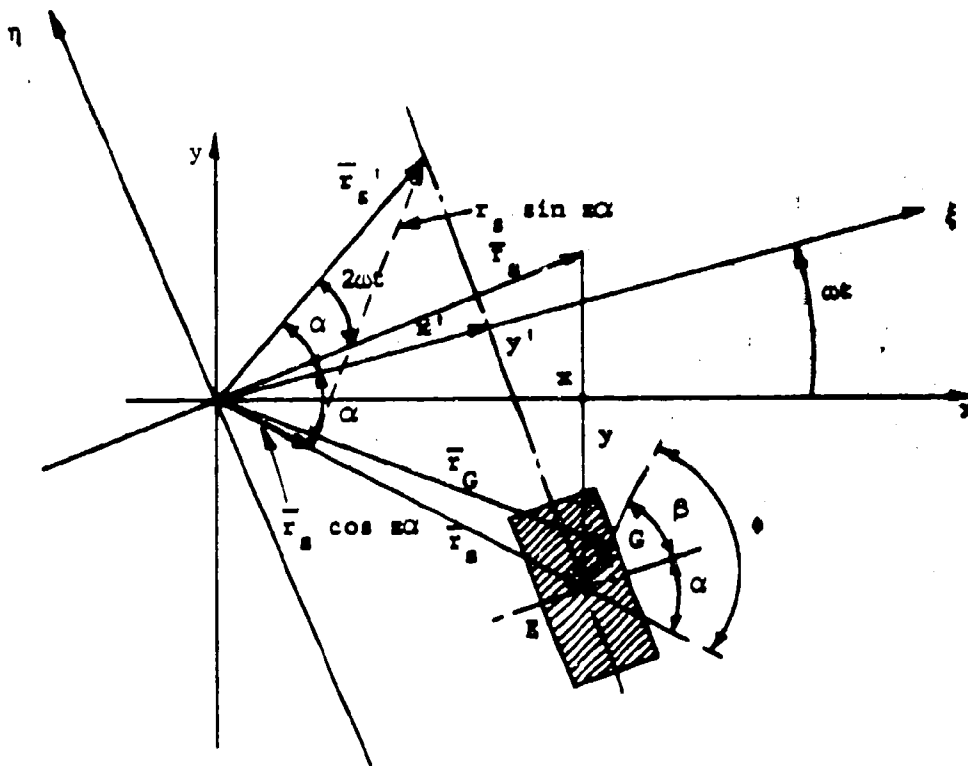


Fig. 3.18 Rotor Whirl Geometry for Shaft with Dissimilar Lateral Stiffnesses

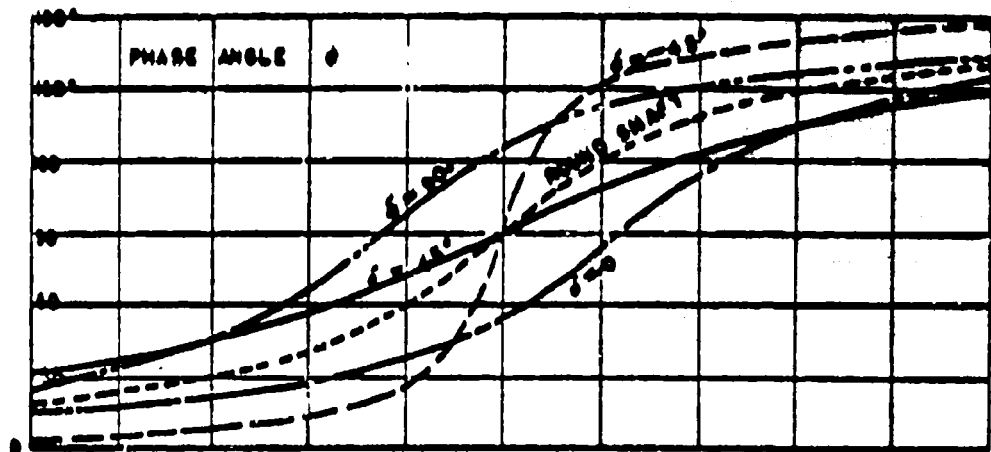
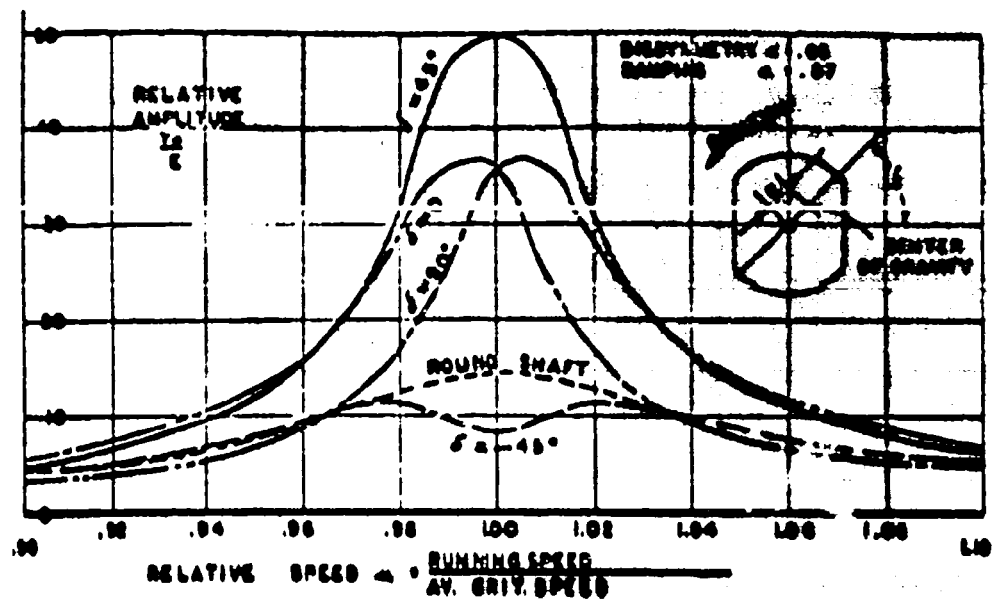


Fig. 3.19 Resonance Curves for Shaft with Moderate Stiffness Asymmetry

Reprinted from CRITICAL-SPEED BEHAVIOR OF UNSYMMETRICAL SHAFTS, Fig. 4, by H. D. Taylor. Journal of Applied Mechanics. June 1940

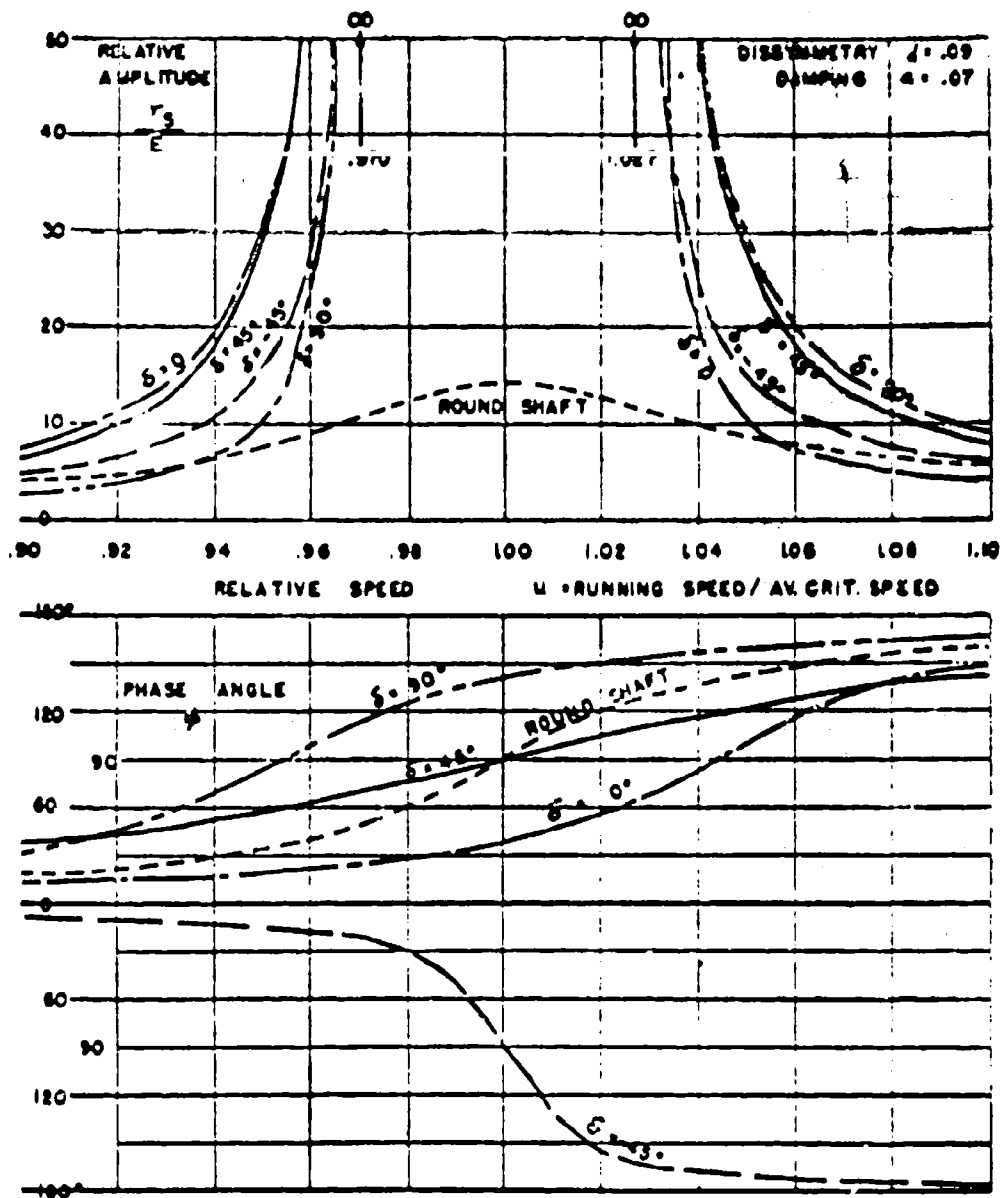


Fig. 3.20 Resonance Curves for Shaft with Relatively Large Stiffness Asymmetry

Reprinted from CRITICAL-SPEED BEHAVIOR OF UNSYMMETRICAL SHAFTS,  
Fig. 6, by H. D. Taylor. Journal of Applied Mechanics. June 1940

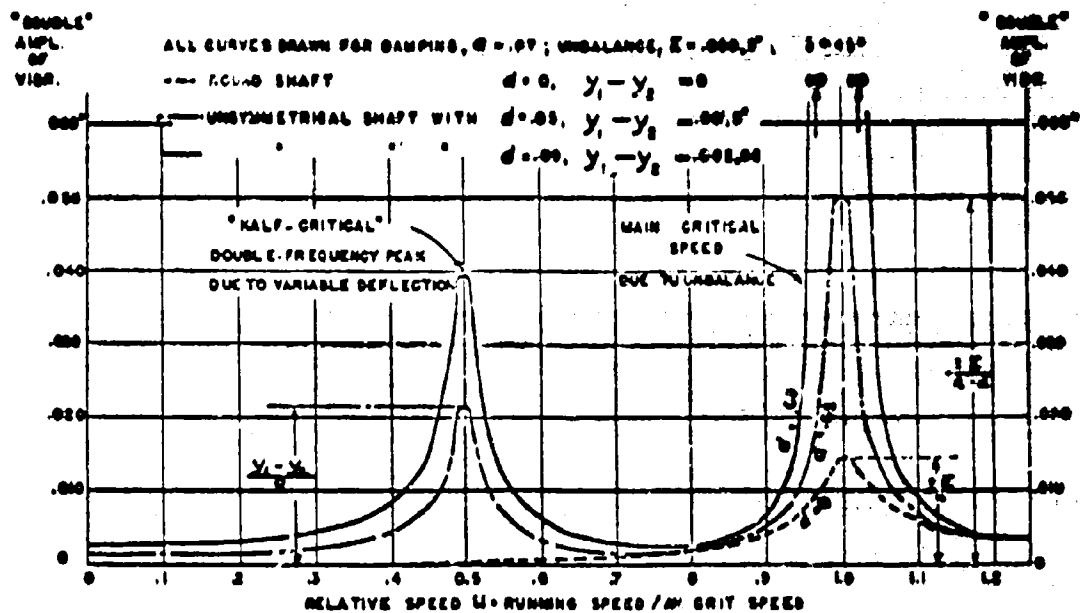


Fig. 3.21 Effects of Stiffness Assymetry on Amplitude

Reprinted from CRITICAL-SPEED BEHAVIOR OF UNSYMMETRICAL SHAFTS,  
 Fig. 7, by H. D. Taylor. Journal of Applied Mechanics. June 1940

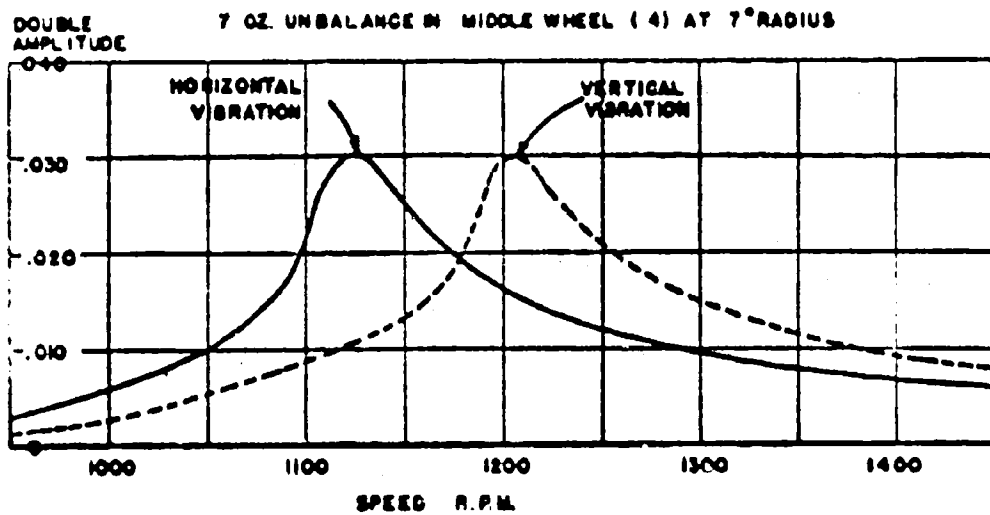
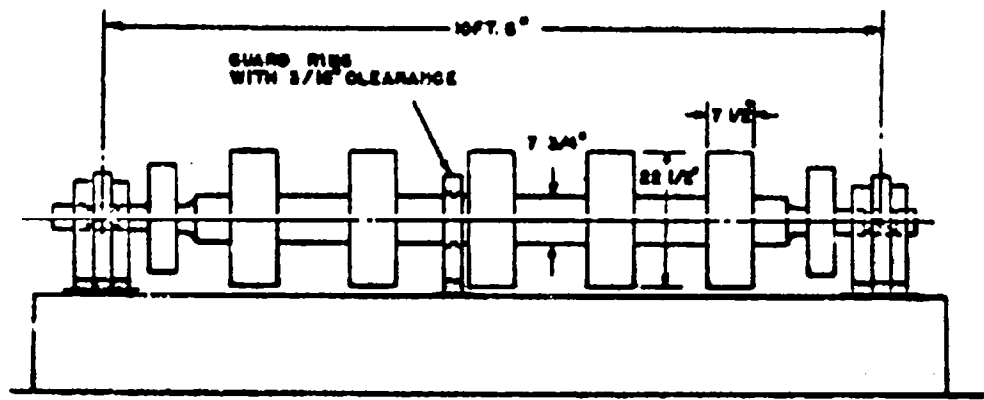


Fig. 3.22 Test Rotor with Round Shaft and Amplitude-Speed Results

Reprinted from CRITICAL-SPEED BEHAVIOR OF UNSYMMETRICAL SHAFTS, Figs. 8 and 9, by H. D. Taylor. Journal of Applied Mechanics. June 1940.

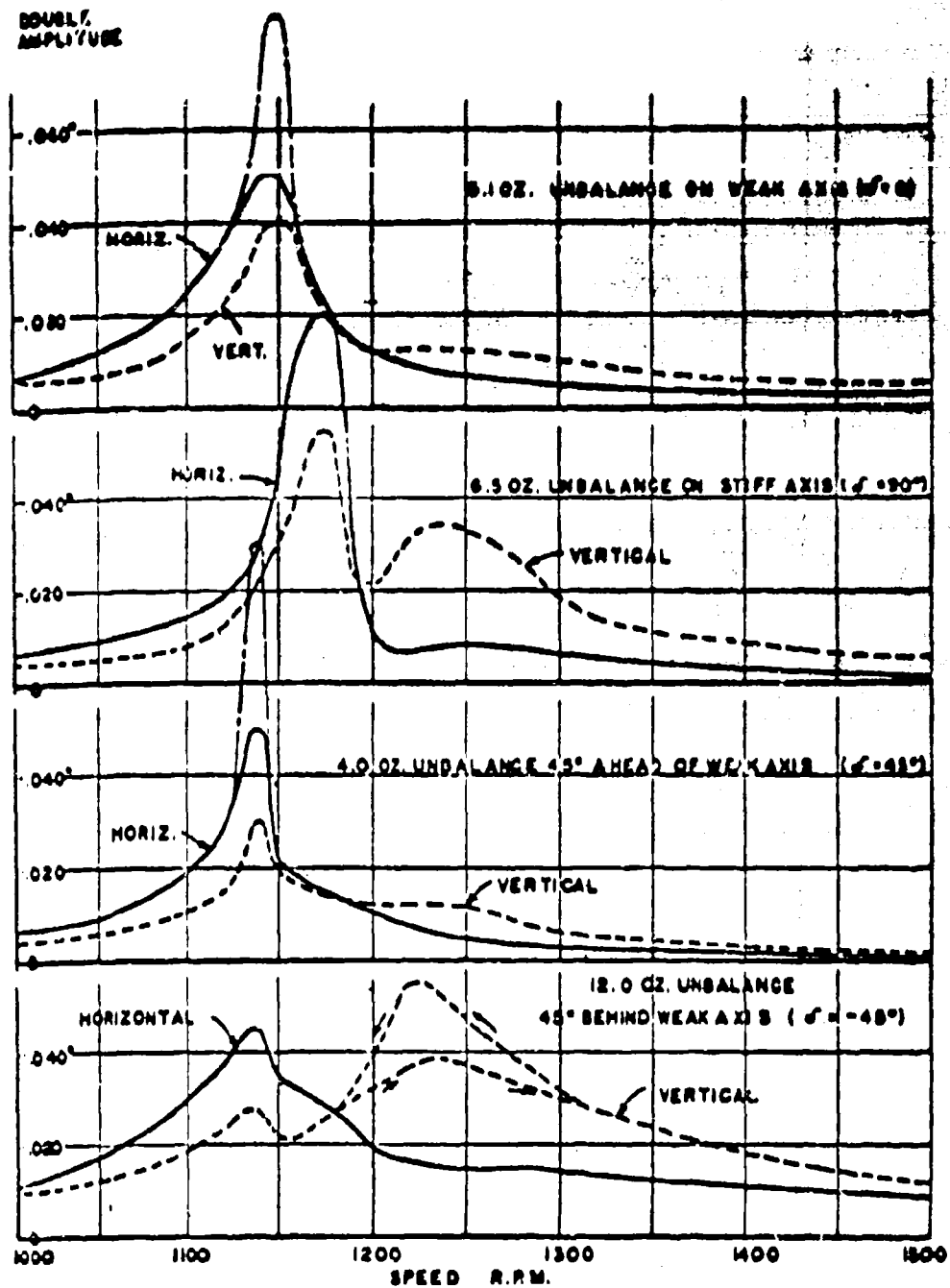


Fig. 3.23 Amplitude-Speed Response of Test Rotor with Flats Cut on Shaft

Reprinted from CRITICAL-SPEED BEHAVIOR OF UNSYMMETRICAL SHAFTS,  
Fig. 10, by H. D. Taylor. Journal of Applied Mechanics. June 1940

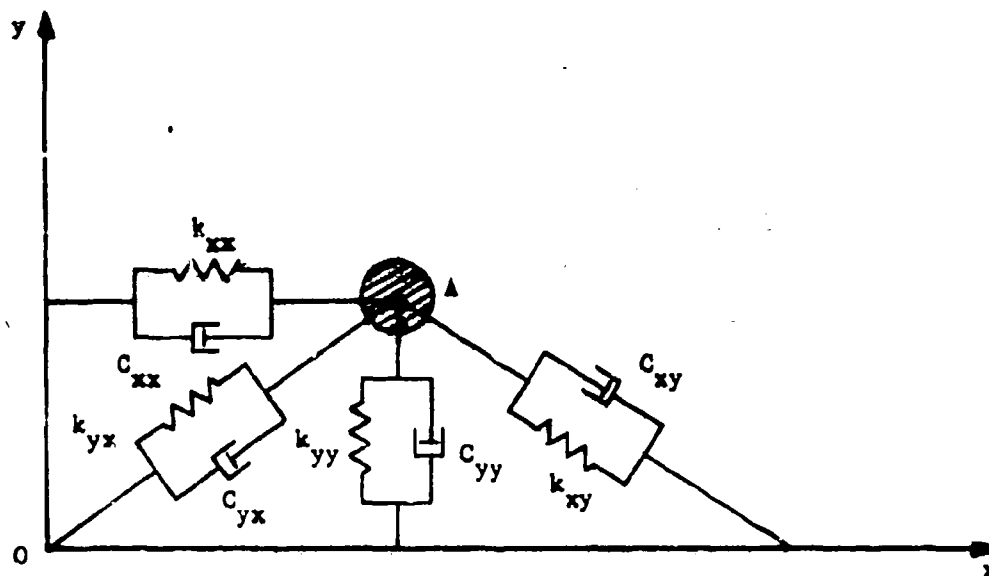


Fig. 3.24 Schematic Representation of Elastic-Damped Bearing

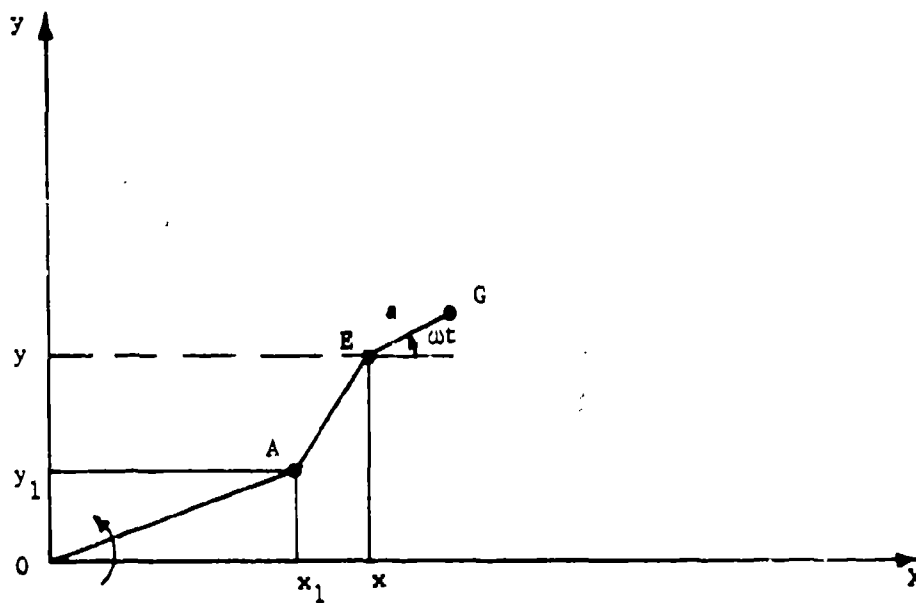


Fig. 3.25 Synchronous Whirl Geometry. Unbalanced Rotor in Flexible Bearings

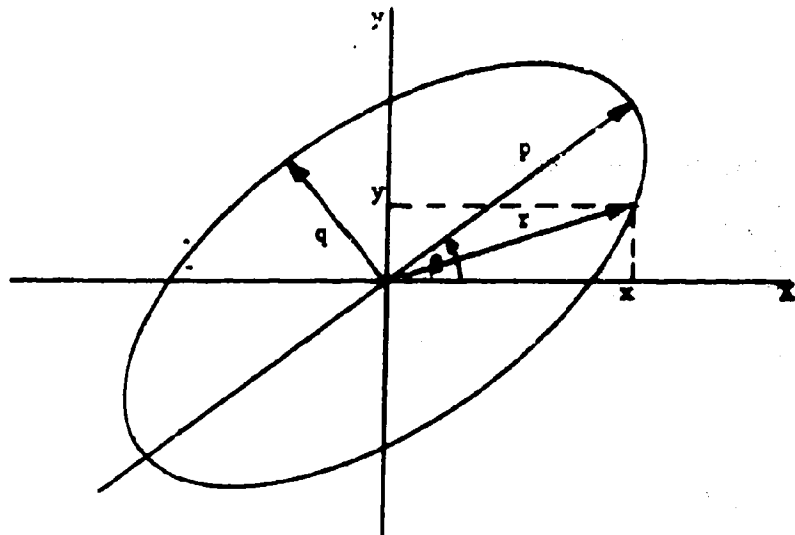


Fig. 3.26 Unbalance Whirl Ellipse, Rotor Center of Gravity

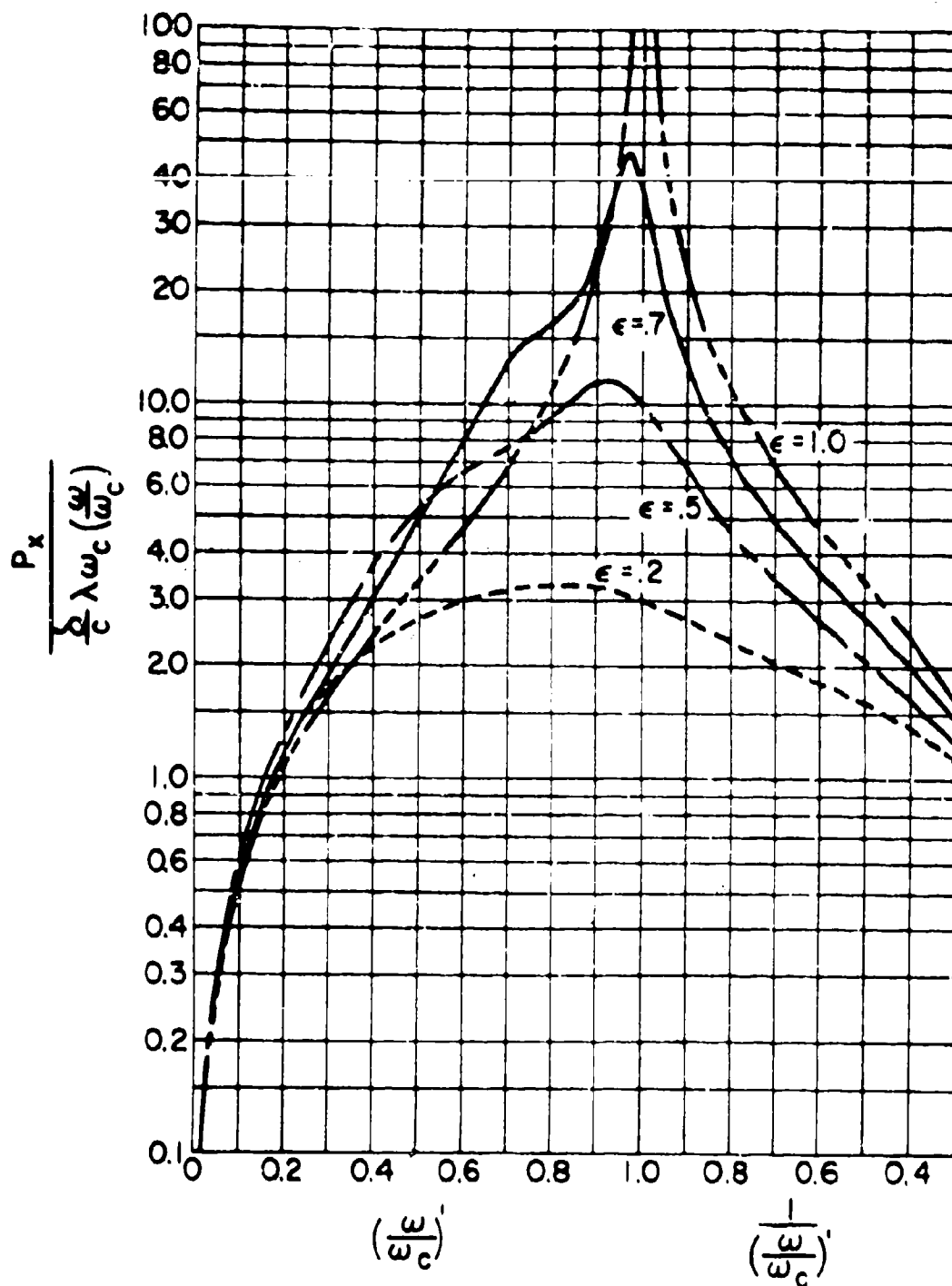


Fig. 3.27 Dimensionless Transmitted Force in Vertical Direction Versus Speed Ratio, Plain Cylindrical Bearing  $L/D = 1/2$

Reprinted from ROTOR-BEARING DYNAMICS WITH EMPHASIS ON ATTENUATION, Fig. 2, by J. W. Lund and B. Sternlicht. ASME Paper No. 61-WA-68

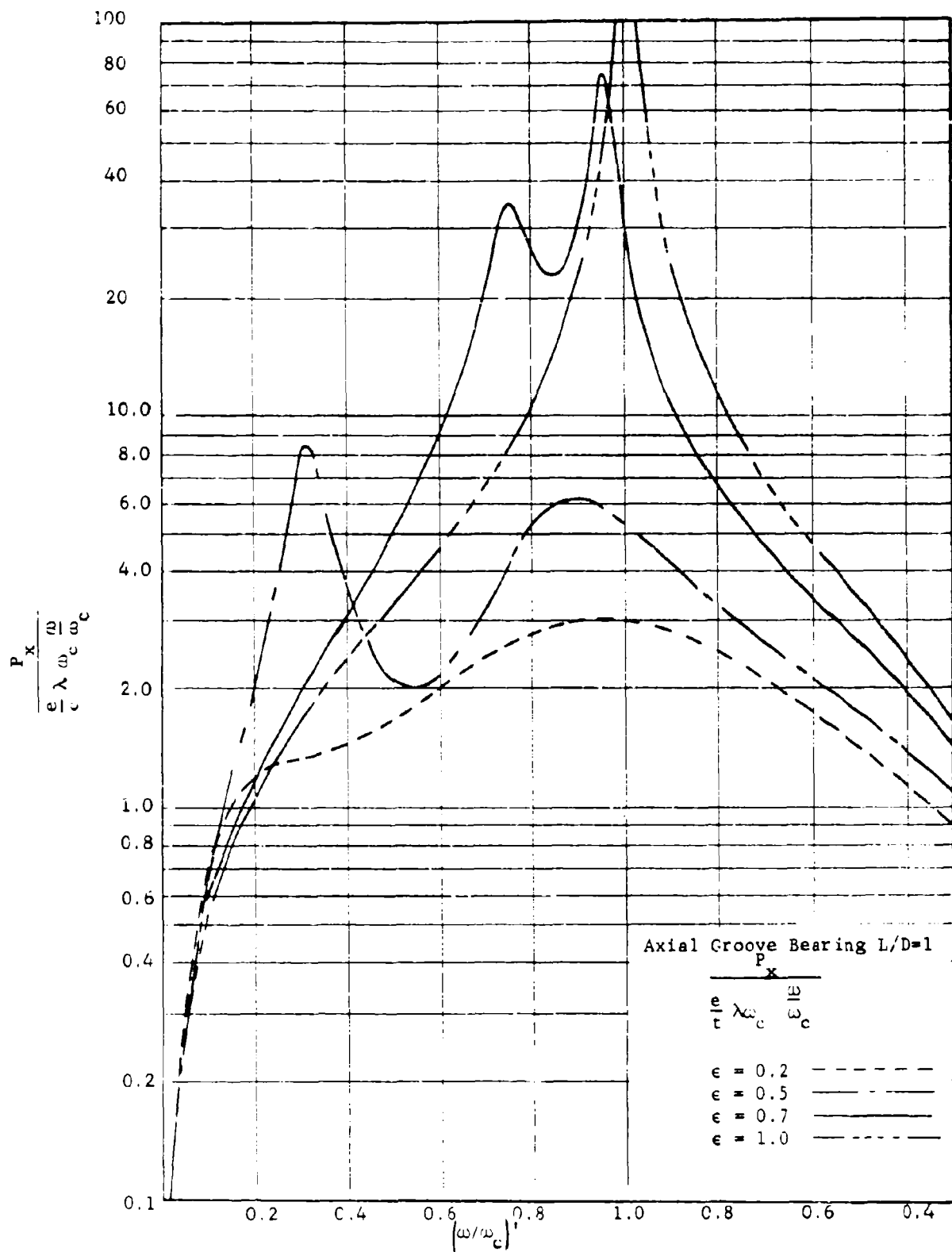
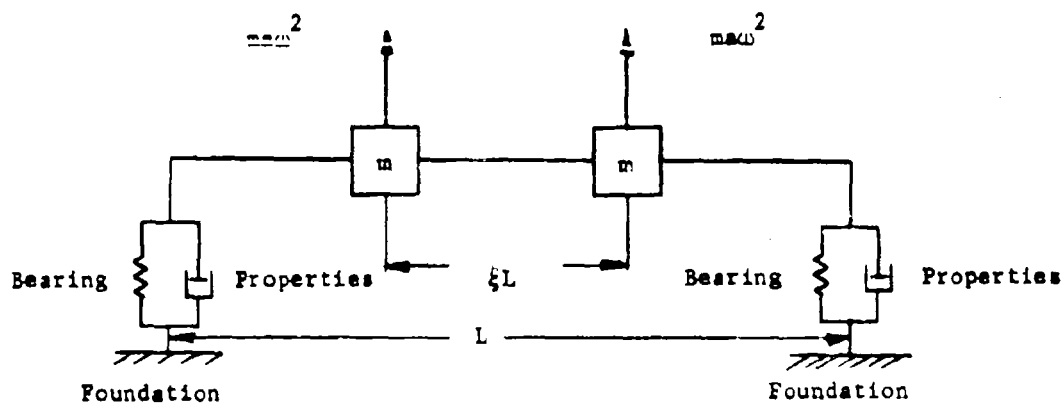
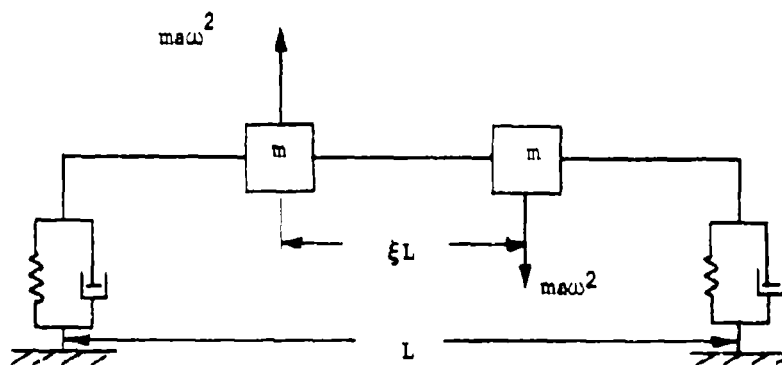


Fig. 3.28 Dimensionless Transmitted Force in Vertical Direction Versus Speed Ratio, For Axial Groove Bearing  $L/D = 1$

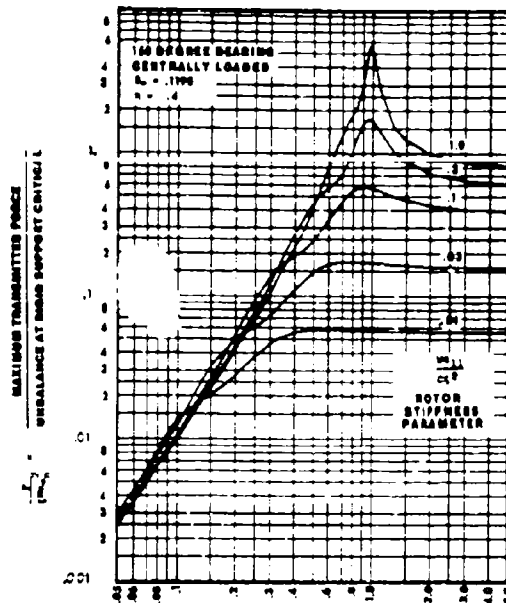


(a) Static Unbalance

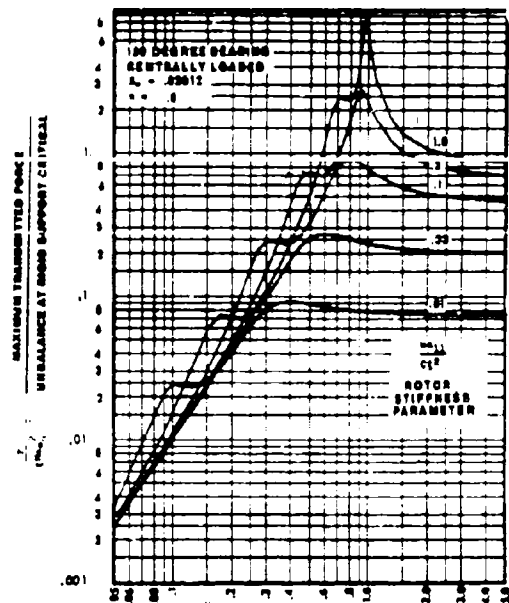


(b) Dynamic Unbalance

Fig. 3.29 Two-Mass Rotor. Static and Dynamic Unbalance

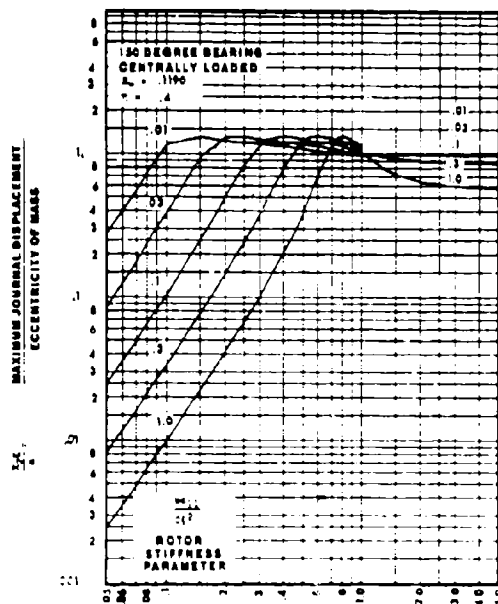


(a)

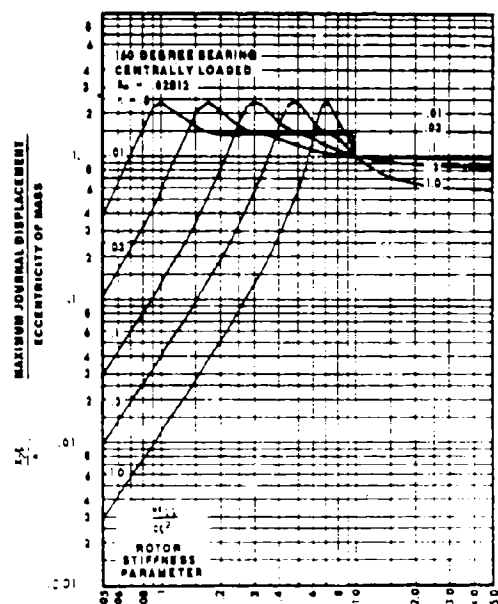


(b)

Transmitted Force Versus Speed. Partial Arc Bearing



(c)



(d)

Journal Amplitude Versus Speed. Partial Arc Bearing

Figure 3.30

Reprinted from THE EFFECT OF THE 150 DEGREE PARTIAL BEARING ON ROTOR-UNBALANCE VIBRATION. Figs. 6, 8, 14, 16. by P. C. Warner and R. J. Thoma. ASME Paper No. 63-LubS-6

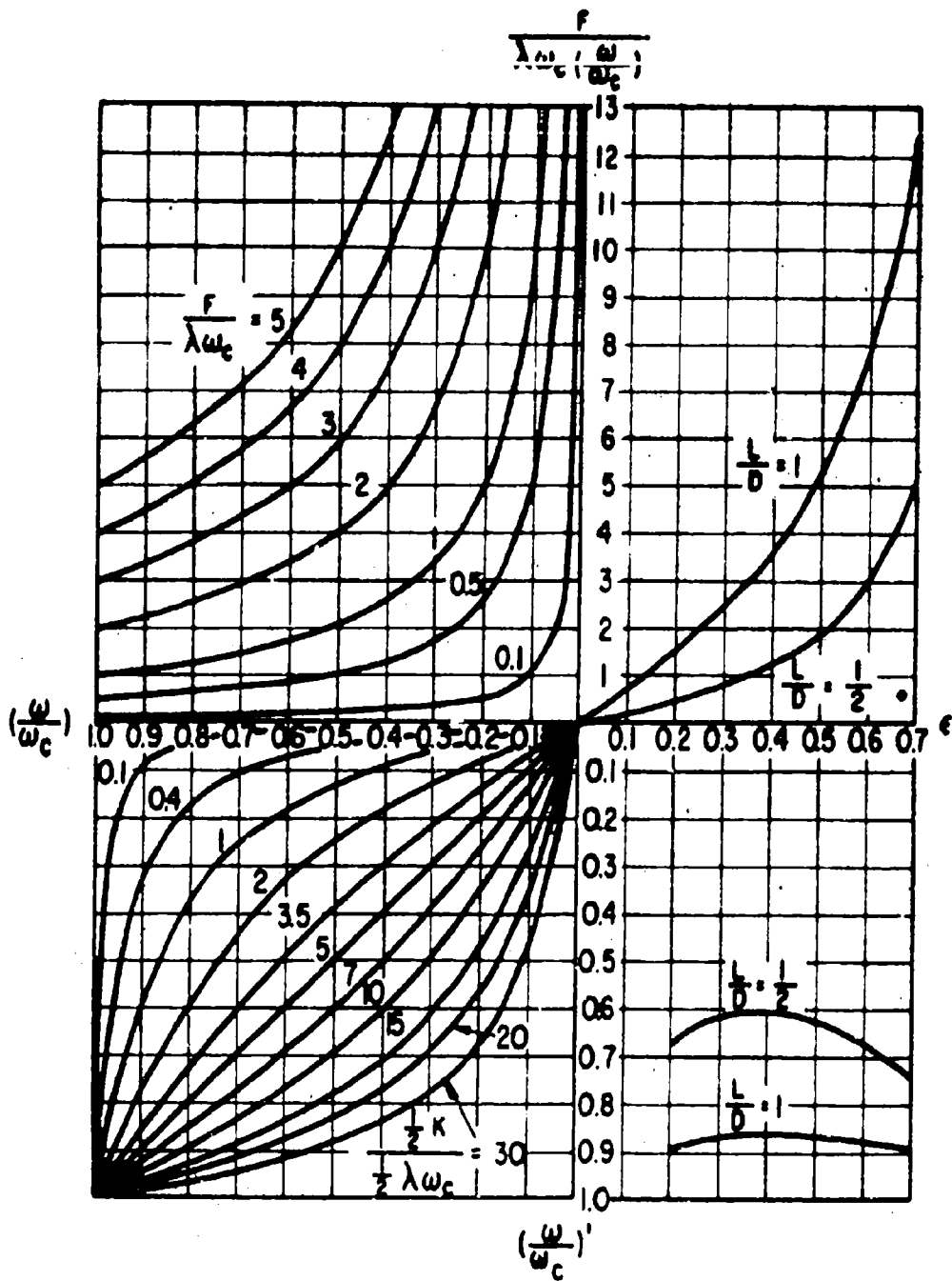


Fig. 3.31 Critical Speed of Flexible Rotor in Fluid-Film Bearings

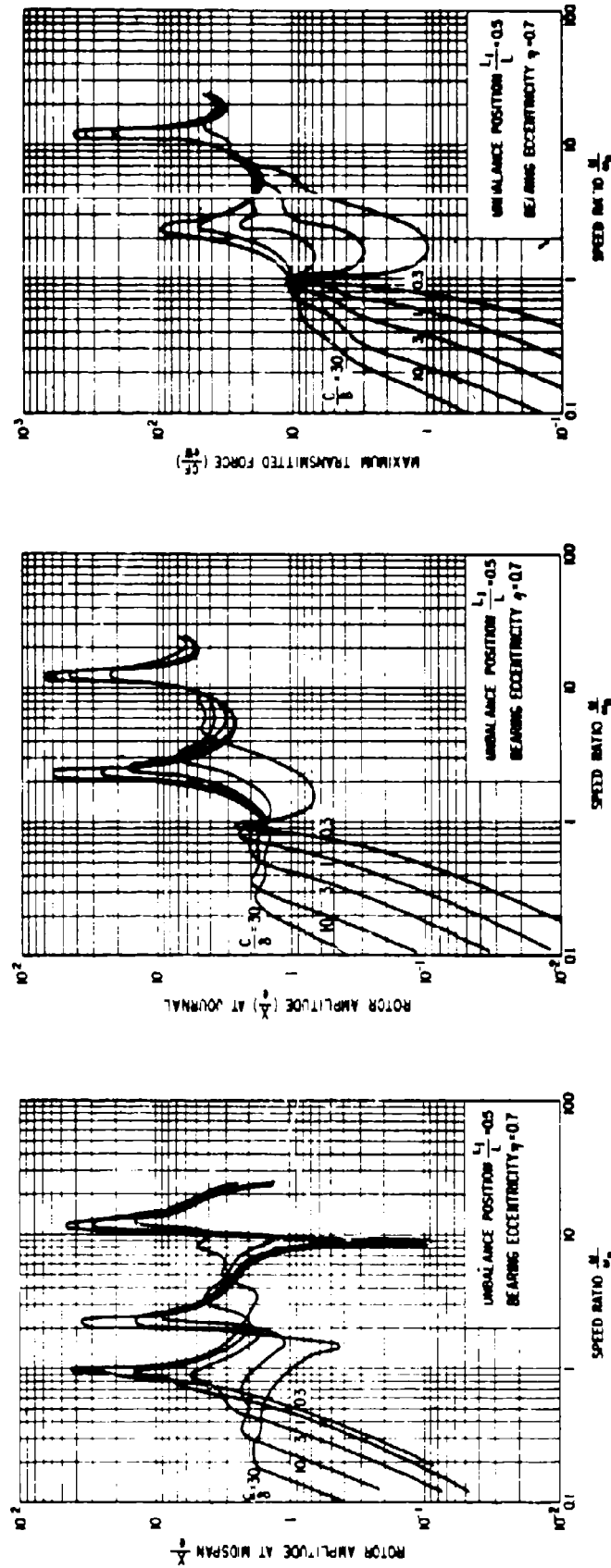


Fig. 3.32 Amplitude and Transmitted Force Versus Speed. Uniform Elastic Rotor, Static Unbalance

Reprinted from ATTENUATION OF BEARING TRANSMITTED NOISE, Vol. 2, Figures 8, 11 and 21. August 1964. Performed in conjunction with Subcontractor Mechanical Technology Incorporated in fulfillment of Contract No. NOBS-86914. Bureau of Ships. Department of Navy. United States of America. Westinghouse Electric Corporation, Lester, Pennsylvania

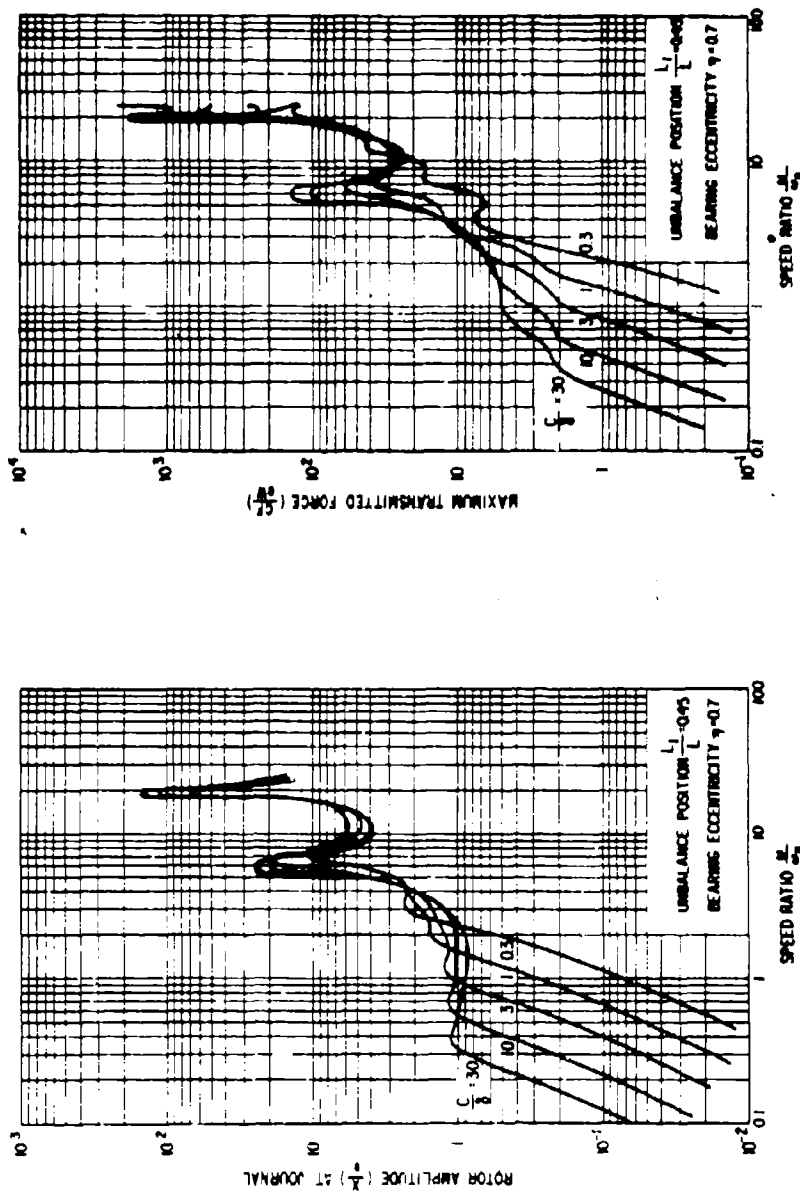


Fig. 3.33 Amplitude and Transmitted Force Versus Speed. Uniform Elastic Rotor, Dynamic Unbalance

Reprinted from ATTENUATION OF BEARING TRANSMITTED NOISE, Vol. 2, Figures 17 and 24. August 1964. Performed in conjunction with Subcontractor Mechanical Technology Incorporated in fulfillment of Contract No. NOBS-86914. Bureau of Ships. Department of Navy. United States of America. Westinghouse Electric Corporation, Lester, Pennsylvania

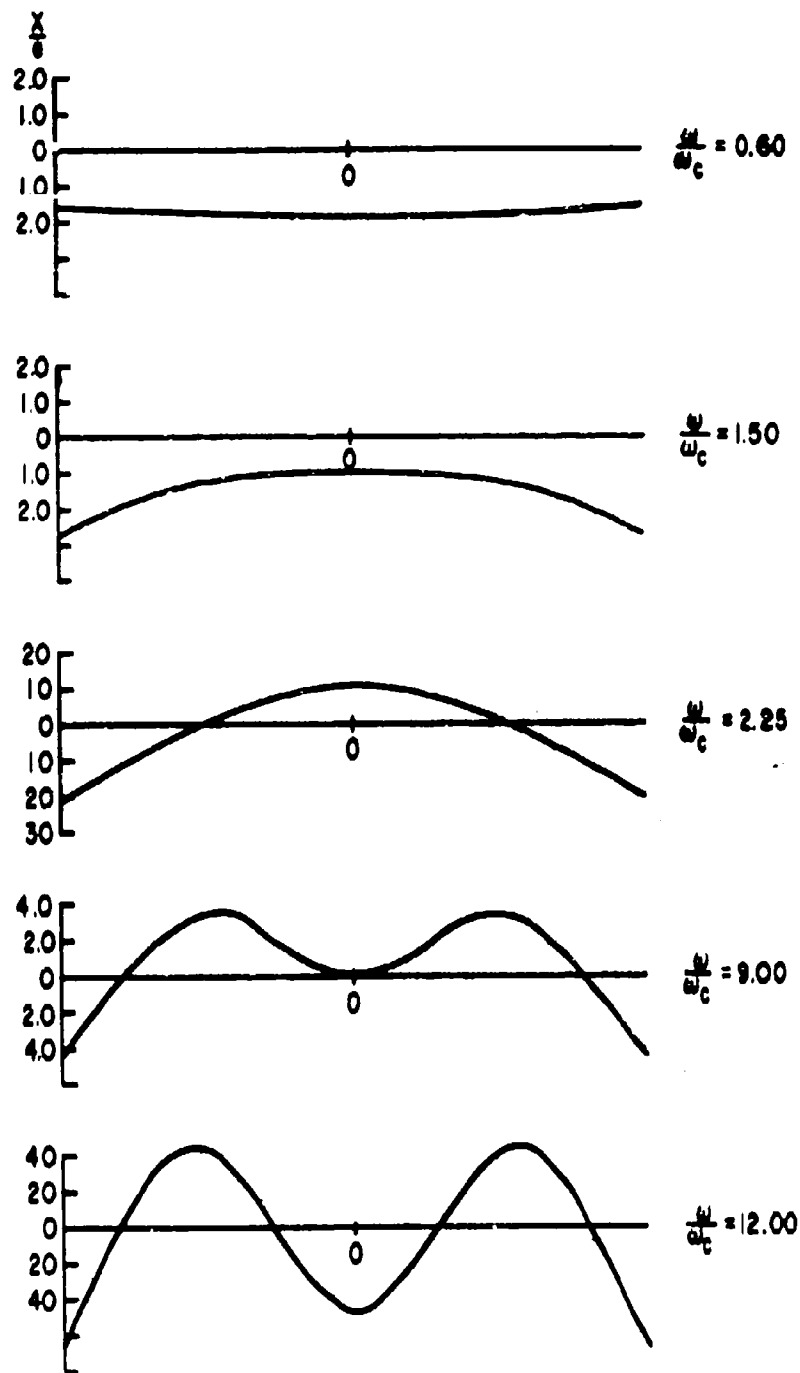


Fig. 3.34 Mode Shapes for Symmetrical Unbalance. Uniform Elastic Rotor

Reprinted from ATTENUATION OF BEARING TRANSMITTED NOISE, Vol. 2, Fig. 26, August 1964. Performed in conjunction with Subcontractor Mechanical Technology Incorporated in fulfillment of Contract No. NOBS-86914. Bureau of Ships. Department of Navy, United States of America Westinghouse Electric Corporation, Lester, Pennsylvania

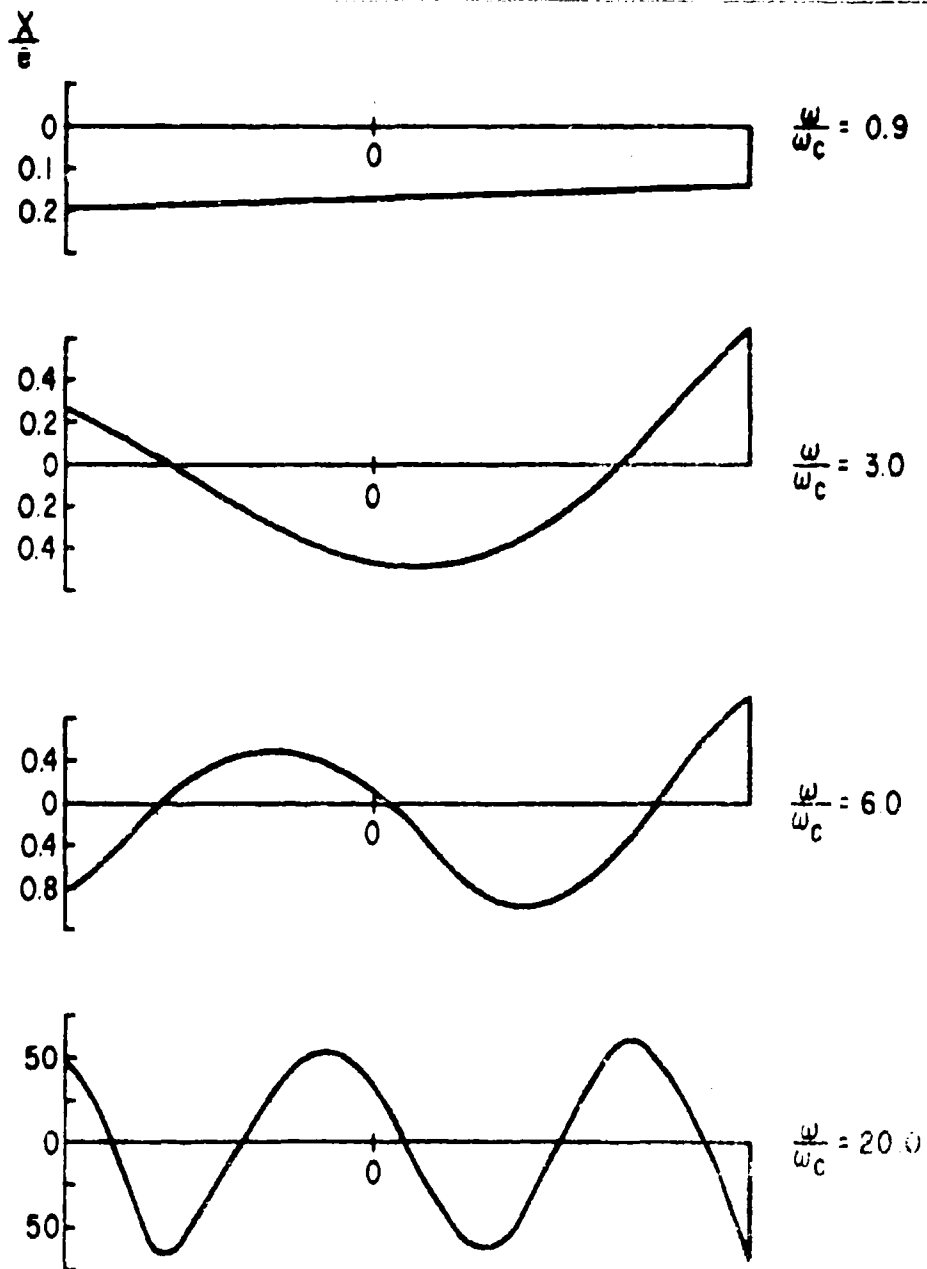


Fig. 3.35 Mode Shapes for Asymmetrical Unbalance. Uniform Elastic Rotor

Reprinted from ATTENUATION OF BEARING TRANSMITTED NOISE, Vol. 2, Fig. 27, August 1964. Performed in conjunction with Subcontractor Mechanical Technology Incorporated in fulfillment of Contract No. NOBS-86914. Bureau of Ships. Department of Navy, United States of America. Westinghouse Electric Corporation, Lester, Pennsylvania

## IV

### CRITICAL SPEED

#### Calculation of Critical Speed

Critical speeds are of great importance since in any mode they correspond to zones in which the rotor amplitude buildup and transmitted bearing forces are at a local maximum. Once the critical speeds of a particular machine layout are known, other design aspects influenced by amplitude and transmitted force may be considered. Good dynamic design requires the critical speeds to be removed from speeds at which sustained operation takes place. To achieve this may require substantial modifications in the layout of rotor-bearing stiffness and mass — leading to component redesign. Synchronous whirl amplitude, rotor balance, bearing dynamic forces, structure-borne noise, and the threshold of resonant whipping are all determined by the critical speed of the machine. Where the rotating unbalance has been minimized and adequate damping has been provided, the machine critical speeds may often be passed through unnoticed, and non-critical operation is very smooth.

#### Whirling Modes of Elastic Systems

A rotor which is whirling at a critical speed adopts the characteristic deflected mode shape associated with that particular whirl mode. The operating speed range of a given machine may contain a number of critical speeds — each corresponding to a different mode shape. All whirling modes are potentially dangerous to machine operation because of the large transverse displacements involved. The occurrence of any mode is determined by the prevailing speed and the dynamical constants of the system (such as inertia, stiffness and damping), which are usually speed dependent. Several commonly-occurring modes are shown in Figure 4.01. The most important transverse rotor modes are: the so-called rigid-body modes, translatory and conical; and the bending modes, of which there may be several. Axial and torsional rotor motions also occur. These are dealt with in Section 8.

The extent to which the modes shown in Figure 4.01 occur in the actual rotor motion depends on the relationship between rotor flexural stiffness and bearing radial stiffness, at a particular speed. For example, pure rigid-body modes occur where the rotor is relatively stiff compared with the bearings. This is the case with gas-film bearings. Alternatively, where the bearings are stiff compared with the rotor, pure bending modes with nodes at the bearings may occur. This is the case with radially-preloaded rolling element bearings or with extremely stiff externally-pressurized, fluid-film bearings. At very high speeds, the rotor may have a bending critical speed corresponding to its free-free mode if the bearing radial forces are relatively small at these speeds.

In general, there is considerable overlap, or coupling, between the various modes, where the rotor and bearing stiffnesses are of comparable magnitude. Any differences between the bearing stiffnesses, or axial mass-elastic variation, tends to reinforce the tendency toward modal coupling. The influence of coupling is included in the solution of any system in which the number of degrees of freedom prescribed for the analytical rotor-bearing model are adequate to describe all modes anticipated within the operating speed range.

#### Influence of Rotor-Bearing Properties on Critical Speed

The important dynamic properties of the rotor and its bearings have been discussed in Section 2. This section discusses the manner in which these properties affect the various critical speed modes.

##### 1. Rotor

In most instances, accurate values for critical speeds can be obtained using analytical representations of the rotor which are simpler than the actual component. Suitable rotor formulation depends on anticipation of the number of critical speeds which the speed range will contain. For a discrete-mass rotor representation, the number of masses into which the rotor is subdivided may not be less than the number of critical speeds to be calculated, and preferably should be somewhat greater to preserve accuracy. Where the critical speed occurs in the low-speed range, gyroscopic effects may be neglected except where these have an obviously strong influence on the motion. Shear deformations of the rotor may be ignored

except for the most refined calculations on short, stubby rotors at very high speeds.

Both hysteretic and viscous damping are present in actual rotors; but, invariably the magnitude is small enough to have little effect on the value of the calculated critical speed.

## 2. Bearing

Both radial and tangential stiffness and velocity-damping properties influence the critical speed. Rolling-element bearings and gas-lubricated bearings possess little damping, and so it is customary to calculate the critical speed of such systems considering the radial stiffness alone. A procedure for calculating rolling element bearing radial stiffness has been given by Palmgren (Ref.79), (and is also part of the present program) which includes speed, preload, and applied load effects. For rolling-element bearings, the stiffness will vary little due to changes in the machine speed and applied load conditions, and so the critical speed may be calculated directly from a frequency equation. But, with gas- and liquid-lubricated bearings, the radial stiffness is a function of speed, and so the critical speed is also speed-dependent. In this case a preliminary estimate may be used to locate the critical speeds. Specific stiffnesses corresponding to each approximate critical speed may then be used to refine the calculations. The need for refinement depends on the stiffness change, 'initial' to 'refined', and on the extent to which the bearing stiffness determines the system motion. This extent is greater for rigid-body criticals than for bending criticals. Frequently, a plot is made of critical speed versus bearing stiffness, and of bearing stiffness versus speed. Using bearing stiffness as a common abscissa, the point where the two curves intersect determines the critical speed. This procedure is shown in Figure 4.02. The influence of bearing flexibility on mode shape is shown diagrammatically in Figure 4.03. This diagram shows how the fundamental critical speed of a rigid-rotor flexible-bearing combination may be raised by stiffening the bearings. Zero stiffness bearings induce a rigid-rotor critical at zero rpm. With stiffer bearings, the rotor bends and the critical speed is raised. Further stiffening eventually leads to rigid-bearings, for which the fundamental critical speed

$$\text{is } N_c = 9.55 \left( \frac{\pi}{L} \right)^2 \sqrt{\frac{EI}{WA}}$$

In the second whirl mode, the influence of stiffening from zero to rigid changes the conical whirl at zero speed to the second rigid bearing critical mode. The rotor whirls with a mid-span node, as shown. The zero stiffness third critical is the fundamental free-free bending mode of the rotor. Stiffening the bearings eventually constrains the rotor to whirl in its third rigid bearing mode. These properties are presented quantitatively in Figure 4.04 in terms of the critical speed ratio ( $N/N_c$ ) for the uniform elastic rotor in elastic undamped bearings. The abscissa  $(N_c/1000)(1000W/K)^{1/2}$  represents increased bearing flexibility. Where the bearing pedestals are not massless, their effect is to replace the original critical speed with two critical speeds, one above and one below the former value. Motions of the system shown are similar to those of a tuned vibration absorber. The rotor is considered to be uniform and rigid, with flexibility included in  $K_R$  which also includes the bearing stiffness. The pedestal (or foundation) flexibility is  $K_S$ , and  $W_S$  is the pedestal weight. The pedestal natural frequency is  $N_S = 187.7 \sqrt{\frac{K_S}{W_S}}$ . For convenience the overall flexibility  $K$  is expressed by:

$$\frac{1}{K} = \frac{1}{K_R} + \frac{1}{K_S} \cdot \frac{1}{1 - N^2} \quad (4.01)$$

where

$$N = \frac{N}{N_S}$$

For  $N < 1$ ,  $K$  is positive; for  $N > 1$  the second term is negative and for a flexible support may make  $K$  negative. Figure 4.05 again expresses the critical speed ratio  $N$  for positive  $K$ ; for negative  $K$  Figure 4.04 should be used. The effect of a negative  $K$  value is the same as adding a mass  $1/2 m$  to each end of the rotor, where  $m\omega^2 = K$ .

In calculating the free-free mode of a rotor in its bearings, account should be taken of the bearing angular stiffness, in addition to radial stiffness. An estimate of angular stiffness has been made by Lund (Ref. 7).

### 3. Foundation

Types of foundation range from steam turbine pedestals, supported on a structural gridwork or on monolithic concrete, to the outer pressure-casing of an encapsulated pump. Foundation flexibility may influence the motions of the rotor if its magnitude is comparable to that of the pedestal, lubricant film (if any), or the rotor. The method discussed above may also be used to determine the influence of foundation flexibility on the lowest system critical speed. Frequently, the foundation coordinate stiffnesses are dissimilar. This induces an elliptical whirl orbit, and may promote two critical speeds if the difference is great. The stiffness of a lightweight foundation acts in series with the pedestal, lubricant film, and rotor. If the inertia effects are large, the system equations must include this effect. Stodola (Ref. 18) discussed the problem of foundation flexibility and its effect on the critical speed of a flexible rotor. He concluded that the system acted as a double pendulum with critical speeds away from the rigid foundation resonance. Geiger (Ref. 19) also consider this problem for a rigid rotor. Tondl (Ref. 80) has obtained experimental and theoretical results for a flexible rotor in oil bearings, and Lund (Ref. 75) has considered the dynamic response and stability of a flexible rotor in gas bearings, seeking the conditions of optimum attenuation, with the foundation mass as a variable. In instances where a high fundamental bending critical speed is desired, the rotor may be designed to assume its free-free mode. From Figure 4.03 this requires very low bearing angular stiffness. Where stiff bearings are needed for stability, a very flexible foundation in the form of a diaphragm may be used to give the same effect, with low inertia bearing shells. Aside from metal fatigue considerations, the ability of the bearing shell to follow the rotor whirl is an important design feature in which low diaphragm angular stiffness is most important. Anti-phase resonance across a gas film is a highly dangerous condition which must be avoided.

### 4. Damping

Rotor damping may be viscous, hysteretic, or Coulomb. In general, although the basic rubbing or slipping mechanism may be sufficient for fretting corrosion to occur, and the damping may be sufficient to limit rotor resonant amplitudes to safe values, it is still too small to influence the actual speed at which the critical whirl takes place. Common damping ratio values for rotor materials

range from  $\zeta = 0.005$  to  $0.010$ . For a single disk rotor,  $\omega_c = \omega_0 \sqrt{1 + \zeta^2}$ , i.e., a maximum increase of 0.5 percent. Laminated rotors occur in electrical machinery, and where the operating speed differs from the whirl speed there can be considerable internal hysteretic damping present. This effect is discussed in Section 5. Other rotors such as those of turbomachinery, and certain ship propeller shafts, operate immersed in a process fluid, and due to entrainment of the fluid during rotation, considerable viscous damping is introduced into the system. Stodola (Ref. 18) noted that the critical speed of a long shaft remained unchanged despite total immersion in water, but that the water reduced the whirl amplitude to negligible proportions. Bearing damping depends on speed, lubricant, operating geometry, and bearing type. Rolling-element bearings operating efficiently have extremely low damping values, even when very heavily loaded. However, lubricant flooding greatly increases the power loss and damping present. Hydrodynamic gas bearings have a small inherent damping capacity. Hydrostatic gas bearings have somewhat higher properties. Moderate unbalance and low eccentricity correspond to maximum fluid-film damping capacity which is due to both squeeze-film and rotational effect. The damping in liquid-lubricated bearings may reach critical-damping proportions when the Sommerfeld number (sec/min) exceeds 100, as shown by Hagg and Sankey (Ref. 73) and Lund (Ref. 81) for a variety of common bearing types. Critical damping conditions are to be anticipated in lightly-loaded (particularly vertical) high-speed rotors. Under these circumstances, the usual critical speed amplitude buildup is suppressed, and the 'critical' speed disappears, as shown in Figure 4.06.

Pedestal and foundation damping for small motions is usually taken as being proportional to velocity. The magnitude depends on foundation type, ranging from  $\zeta = 0.005$  to  $0.010$  for a structural gridwork, with a minimum of bolted construction to induce Coulomb damping, through  $\zeta = 0.010$  to  $0.100$  for monolithic concrete, to  $\zeta = 0.100$  to  $0.5$  or more for clay-soil foundations. For accurate values under the latter condition, site test values are needed.

In summary, damping may be neglected in the case of solid rotors in rolling-element or gas bearings operating in a gas or a vacuum, and the calculated critical speeds will still be accurate. However, care is required in the case

of liquid-film bearings, particularly in the case of lightly-loaded high-speed rotors which may generate critical damping under certain circumstances. If the damping is shown to be high, it should be allowed for by either a supplementary spring force in parallel or by the actual effect expressed as viscous damping in the calculations. A lower limit only will be obtained for the critical speed of a rotor when significant system damping is ignored.

### Exact Methods

Simple rotors are characterized by uniform prismatic shape, few disks, and simple support conditions. These features are readily handled mathematically, and so there are available a large number of formulae for the calculation of critical speeds of simple rotor-bearing systems. Insofar as the mathematical conditions represent the rotor, these solutions are both exact and free from method inaccuracies.

Exact methods discussed in the following sections are of two types: (1) discrete mass systems which operate by breaking down the rotor into a suitable number of constituent masses which are linked by massless flexible shafts; and (2) continuous systems in which the distribution of mass-elastic properties may be either constant or uniformly varying along the rotor length. These methods formulate the critical speed problem from the basic equations, and result in a critical speed or frequency equation which may be polynomial or transcendental. The discussion which follows is more concerned with the techniques and their capabilities, application and limitations, than in the solution of the frequency equation.

The exact method has the advantage that it also allows the higher critical speeds of the system to be calculated from the basic frequency equation. Ritz's method is the only approximate method which determines harmonic critical speeds with good accuracy. With the aid of a computer, the labor of solving a complicated system determinant is removed; instead, a computer program must be written and checked out. High-speed machines which pass through several critical speeds must be analyzed according to this procedure, whereas low-speed machines may often be analyzed by some less-involved technique.

### Discrete-Mass Systems

A rotor which carries a number of massive disks on a flexible shaft may often be represented by a discrete-mass system, Figure 4.07. The calculation of the critical speeds of such a system is performed as follows. The mass,  $m_i$  of each disk is assumed to be concentrated at its c.g., and rotor flexural stiffness is wholly due to the aggregate stiffness of the shaft sections,  $k_{ij}$ , between the disks. Where the motions are free of gyroscopic and torsional influences, the equations of motion for an n-mass system without damping are:

$$\begin{aligned}
 m_1 \ddot{x}_1 + k_{11}x_1 + k_{12}x_2 + \dots + k_{1n}x_n &= m_1 a_1 \omega^2 \cos(\omega t + \epsilon_1) \\
 m_2 \ddot{x}_2 + k_{21}x_1 + k_{22}x_2 + \dots + k_{2n}x_n &= m_2 a_2 \omega^2 \cos(\omega t + \epsilon_1) \\
 \dots &= \dots \\
 m_n \ddot{x}_n + k_{n1}x_1 + k_{n2}x_2 + \dots + k_{nn}x_n &= m_n a_n \omega^2 \cos(\omega t + \epsilon_1) \\
 m_1 \ddot{y}_1 + k_{11}y_1 + k_{12}y_2 + \dots + k_{1n}y_n &= m_1 a_1 \omega^2 \sin(\omega t + \epsilon_1) \\
 m_2 \ddot{y}_2 + k_{21}y_1 + k_{22}y_2 + \dots + k_{2n}y_n &= m_2 a_2 \omega^2 \sin(\omega t + \epsilon_2) \\
 \dots &= \dots \\
 m_n \ddot{y}_n + k_{n1}y_1 + k_{n2}y_2 + \dots + k_{nn}y_n &= m_n a_n \omega^2 \sin(\omega t + \epsilon_2) \quad (4.02)
 \end{aligned}$$

writing

$$r_i = x_i + iy_i$$

and noting that

$$e^{i(\omega t + \epsilon_1)} = e^{i\omega t} \cdot e^{i\epsilon_1} = \alpha_i e^{i\omega t}$$

leads to the system of equations

$$\begin{aligned}
m_1 \ddot{r}_1 + k_{11} r_1 + k_{12} r_2 + \dots + k_{1n} r_n &= \alpha_1 m_1 a_1 \omega^2 e^{i\omega t} \\
m_2 \ddot{r}_2 + k_{21} r_1 + k_{22} r_2 + \dots + k_{2n} r_n &= \alpha_2 m_2 a_2 \omega^2 e^{i\omega t} \\
\dots &= \dots \\
m_n \ddot{r}_n + k_{n1} r_1 + k_{n2} r_2 + \dots + k_{nn} r_n &= \alpha_n m_n a_n \omega^2 e^{i\omega t}
\end{aligned} \tag{4.03}$$

Selecting solutions of the form

$$r_i = A_i e^{i\omega t}$$

leads to

$$\begin{bmatrix} (k_{11} - m_1 \omega^2) & k_{12} & \dots & k_{1n} \\ k_{21} & (k_{22} - m_2 \omega^2) & \dots & k_{2n} \\ \dots & \dots & \dots & \dots \\ k_{n1} & k_{n2} & \dots & (k_{nn} - m_n \omega^2) \end{bmatrix} \begin{Bmatrix} A_1 \\ A_2 \\ \dots \\ A_n \end{Bmatrix} = \omega^2 \begin{Bmatrix} \alpha_1 m_1 a_1 \\ \alpha_2 m_2 a_2 \\ \dots \\ \alpha_n m_n a_n \end{Bmatrix}$$

or in matrix notation

$$[K] - \omega^2 [I] [M] \{A\} = \omega^2 \{Cma\} \tag{4.04}$$

where  $I$  is the unit diagonal matrix. The complex amplitudes  $A_i$  are obtained from the above expression, except where the denominator

$$[K] - \omega^2 [I] [M] = 0 \tag{4.05}$$

For a given system  $[K]$  and  $[M]$  are fixed and so the above condition is satisfied by particular values of  $\omega^2$ , corresponding to the critical speeds of the system. For an  $n$ -mass system there are  $n$  critical speeds. Equation 4.05 is independent

of the right-hand column matrix, indicating that the critical speeds occur independently of the unbalance properties of any disk.

#### Methods of Solution

If the system involves relatively few masses, Equation 4.05 may be expanded and solved: (1) exactly by a standard algebraic method, (2) graphically, by substitution using Newton's method, or (3) numerically, by Graeffe's method, or by the technique given in Duncan and Collar (Ref. 82). Where many masses are involved, a digital computer is usually required to facilitate the matrix algebra, at least for computing values of the matrix over a range of  $\omega^2$  for graphical solution, and preferably with a program which seeks out the eigenvalues automatically.

#### Example 1: Single disk, flexible shaft, rigid bearings

The simple rotor shown consists of a single thin disk mounted centrally on a massless flexible shaft, Figure 4.08. The equation of motion derives from Equation 4.05 and is:

$$m\ddot{r} + kr = cm\omega^2 e^{i\omega t} \quad (4.06)$$

As above, the critical speed is obtained from the homogeneous equation, and is

$$\omega_c = \left[ \frac{k}{m} \right]^{1/2}$$

For inelastic bearings the system flexibility is the flexibility of the shaft. In the present case,

$$k = \frac{48 EI}{L^3}$$

The critical speed is therefore:

$$\omega_c = \left[ \frac{48 EI}{mL^3} \right]^{1/2} \quad (4.07)$$

Furthermore, note that the static deflection  $\delta_s$  of the rotor c.g. under the action

of gravity is

$$\delta_s = \frac{WL^3}{48EI}$$

Substituting in Equation 4.07 and writing  $W = mg$ , gives

$$\omega_c = \left[ \frac{g}{\delta_s} \right]^{1/2}$$

Substituting the appropriate units leads to the expression:

$$N_c = \frac{187.3}{\sqrt{\delta_s}}$$

where  $N_c$  is the rotor critical speed in rpm, and  $\delta_s$  is the static deflection of the disk c.g. in inches. This formula may be used to find the critical speed of any single mass system, in rigid or flexible bearings, once  $\delta_s$  is known.<sup>1</sup>

#### Example 2: Unsymmetrical rotor, single disk, flexible bearings

Figure 4.09 shows the deflection geometry of this system. The shaft deflection is

$$\delta_s = \frac{3 EIL}{W a^2 b^2}$$

The effective bearing displacement at the rotor is

$$\delta_b = \left( \frac{W}{K_1} \right) \left( \frac{b}{L} \right) \left[ 1 + \left( \frac{a}{b} \right) \left( \frac{a}{b} \cdot \frac{k_1}{k_2} - 1 \right) \right]$$

The total displacement of the rotor c.g. due to system flexibility is

1. In the case of a uniform shaft with a uniformly distributed load, it may be shown from fundamentals that the lowest critical speed is given by

$$N_c = \frac{221.8}{\sqrt{\delta}}$$

For simple supported ends,

$$\delta = \frac{5}{384} \cdot \frac{wL^4}{EI}$$

For a cantilever shaft,

$$\delta = \frac{1}{8} \frac{wL^4}{EI}$$

$$\delta = \delta_s + \delta_b$$

Hence,

$$N_c = \left[ \frac{A}{b} \right]^{1/2}$$

In this particular case, if the transverse inertia  $I_T$  of the disk were significant, this would introduce a second critical speed with a conical or rocking mode. An exact solution would, therefore, involve simultaneous solution of the translatory and rocking equations of motion, including the influence of gyroscopic forces.

### Example 3: Symmetrical two-mass rotor in rigid bearings

Equations of motion 4.04 apply directly to the rotor shown in Figure (4.10), i.e.,

$$\begin{bmatrix} (k_{11} - m_1 \omega^2) & k_{12} \\ k_{21} & (k_{22} - m_2 \omega^2) \end{bmatrix} \begin{Bmatrix} A_1 \\ A_2 \end{Bmatrix} = \omega^2 \begin{Bmatrix} \alpha_1 m_1 a_1 \\ \alpha_2 m_2 a_2 \end{Bmatrix}$$

The critical speed condition is that the determinant of coefficients of the  $A_i$  is zero. Multiplying out gives:

$$\omega^4 - \left[ \frac{k_{11}}{m_1} + \frac{k_{22}}{m_2} \right] \omega^2 + \left[ \frac{k_{11}k_{22} - k_{12}k_{21}}{m_1 m_2} \right] = 0 \quad (4.08)$$

This may be solved directly as a quadratic in  $\omega^2$ . A total of four roots are obtained of which the two positive roots alone are of physical significance.

### Continuous Systems

Rotors which have their mass-elastic properties distributed uniformly along their length or portion of it may also have their critical speeds calculated exactly. In these cases, the basic equation governing the whirling motion is:

$$\frac{\partial^2}{\partial z^2} \left[ EI \frac{\partial^2 R}{\partial z^2} \right] = - \frac{wA}{g} \frac{\partial^2 R}{\partial t^2} + F(t) \quad (4.09)$$

where

$$R = X + iY \quad i = \sqrt{-1}$$

For a uniform shaft free from external forces,  $F(t) = 0$ , and the  $x, y$ , coordinate equations have solutions of the form:

$$\begin{aligned} X &= x(z) e^{i\omega t} \\ Y &= y(z) e^{i\omega t} \end{aligned} \quad (4.10)$$

where  $x(z)$ ,  $y(z)$  are functions of length and frequency of vibration only.

Substituting leads to the solutions:

$$\begin{aligned} x(z) &= A \cos \lambda z + B \sin \lambda z + C \cosh \lambda z + D \sinh \lambda z \\ y(z) &= E \cos \lambda z + F \sin \lambda z + G \cosh \lambda z + H \sinh \lambda z \end{aligned} \quad (4.11)$$

where  $A, B, C, D, E, F, G, H$ , are integration constants to be determined from the boundary conditions of particular cases, and:

$$\lambda^4 = \left[ \frac{wA\omega^2}{gEI} \right]$$

Continuous systems have an infinite number of degrees of freedom, and so there exists an infinite number of  $\lambda L$  solutions (eigenvalues) to the characteristic equations listed in Table 4.01. Each eigenvalue corresponds to a particular critical whirling mode.

**Example 1: Uniform rotor in rigid supports**

The characteristic equation may be determined through either  $x(z)$  or  $y(z)$ .

Considering motions in the  $x$ - $z$  plane, the boundary conditions for this case are:

$$\text{At } z = 0: \quad (y) = EI \left( \frac{d^2 y}{dz^2} \right) = 0$$

$$\text{At } z = L: \quad (y) = EI \left( \frac{d^2 y}{dz^2} \right) = 0 \quad (4.12)$$

Substituting and reducing leads to the frequency equation for this case:

$$\sin \lambda L = 0 \quad (4.13)$$

The corresponding eigenvalues in this case are  $0, \pi, 2\pi, \dots, n\pi$ ,  $n$  integer.

**Example 2: Uniform rotor, rigid supports, with overhang (Figure 4.11)**

Again considering motions in the  $x$ - $z$  plane, the rotor equation must be integrated separately in the two domains  $0 \leq z_1 \leq l_1$ ,  $0 \leq z_2 \leq l_2$ , leading to eight integration constants. The boundary conditions for these two domains are:

$$\begin{aligned} \text{At } z_1 = 0: \quad & (y_1) = 0 & EI \left( \frac{d^2 y_1}{dz_1^2} \right) &= 0 \\ \text{at } \left\{ \begin{array}{l} z_1 = l_1: \\ z_2 = 0: \end{array} \right. & \left\{ \begin{array}{l} (y_1) = 0 \\ (y_2) = 0 \end{array} \right. & \left\{ \begin{array}{l} EI \left( \frac{d^2 y_1}{dz_1^2} \right) = M \\ EI \left( \frac{d^2 y_2}{dz_2^2} \right) = M \end{array} \right\} \\ z_2 = l_2: & EI \frac{d^2 y_2}{dz_2^2} = 0 & EI \left( \frac{d^3 y_2}{dz_2^3} \right) &= 0 \end{aligned} \quad (4.14)$$

Substituting into the solutions:

$$x(z_1) = A_1 \cos \lambda z_1 + B_1 \sin \lambda z_1 + C_1 \cosh \lambda z_1 + D_1 \sinh \lambda z_1$$

$$x(z_2) = A_2 \cos \lambda z_2 + B_2 \sin \lambda z_2 + C_2 \cosh \lambda z_2 + D_2 \sinh \lambda z_2$$

Eliminating and reducing leads to the system frequency equation.

$$\begin{aligned} & [\cosh \lambda L_1 \sin \lambda L_1 - \sinh \lambda L_1 \cos \lambda L_1] [\cosh \lambda L_2 \sin \lambda L_2 - \sinh \lambda L_2 \cos \lambda L_2] \\ & - 2 \sinh \lambda L_1 \sin \lambda L_1 [1 + \cosh \lambda L_2 \cos \lambda L_2] = 0 \end{aligned} \quad (4.15)$$

Solutions to this transcendental may be obtained by writing:

$$\lambda L_2 = L \cdot \lambda L_1 \quad (4.16)$$

where

$$L = (L_2/L_1)$$

Plotting values of Equation 4.15 against  $\lambda L_1$  leads to the required eigenvalues. Alternatively, an analytic solution may be achieved by perturbing on an approximate known solution  $(\lambda L)'$ . Writing:

$$\lambda L_1 = (\lambda L)' + \epsilon; \quad \lambda L_2 = L [(\lambda L)' + \epsilon]$$

where  $\epsilon$  is small and unknown. Substituting, expanding, and rejecting powers higher than the first leads to an expression for  $\epsilon$ , and hence, allows the required  $\lambda L_1$  values to be calculated. Table 4.02 contains results given by Dunkley (Ref.40) for the fundamental mode of this case.

It is apparent that the exact solution of continuous systems rapidly become complicated in both derivation and solution for all but the simplest systems. A number of methods exist for overcoming this, of which the Receptance method is presently the most highly developed in its application to beam and rotor problems. A set of 'receptance' functions has been prepared, corresponding to certain basic beam vibration cases. The desired properties of more complex systems

TABLE 4.01

Frequency Equations. Uniform Rotor. Various End Conditions

<u>End Condition</u>	<u>Frequency Equation</u>
Sliding-Sliding	$\sin \lambda L = 0$
Pinned-Pinned	$\sin \lambda L = 0$
Clamped-Clamped	$\cos \lambda L \cosh \lambda L - 1 = 0$
Clamped-Free	$\cos \lambda L \cosh \lambda L + 1 = 0$
Clamped-Pinned	$\cos \lambda L \sinh \lambda L - \sin \lambda L \cosh \lambda L = 0$
Clamped-Sliding	$\cos \lambda L \sinh \lambda L + \sin \lambda L \cosh \lambda L = 0$
Free-Free	$\cos \lambda L \cosh \lambda L - 1 = 0$

TABLE 4.02

Value of  $\lambda L_1$  as Function of L. Fundamental Mode

<u>Ratio L</u>	<u><math>\lambda L_1</math></u>
1.00	1.506
0.75	1.902
0.50	2.507
0.33	2.905
0.25	3.009
0.20	3.044
0.163	3.060
0.143	3.069
0.125	3.071
0.111	3.073
0.100	3.078
0	3.143

including frequency equations may be obtained by combining these functions according to certain laws. This procedure is described by Bishop (Ref. 83) and has been applied to flexible rotors by Gladwell and Bishop (Ref. 34).

#### Approximate Methods

Many practical systems cannot be adequately represented by a simple mathematical rotor model for which an exact solution is available. In these instances, such a representation gives only an estimate of the critical speed. Where an exact solution would require an inordinate amount of effort, an approximate calculation using one of the methods outlined in the present section will usually yield a result of acceptable or good accuracy in a fraction of the calculation time.

The most useful approximate methods employed in rotor-bearing dynamics are:

- |                       |  |
|-----------------------|--|
| 1. Rayleigh's Method  | A general calculation method based on the energy principle. The results are always high.   |
| 2. Ritz's Method      | A refinement of Rayleigh's method giving more exact results, based on the minimum principle.   |
| 3. Stodola's Method   | An iterative technique based on recalculations of the deflection curve, and hence the critical speed.  |
| 4. Morley's Method    | Another iterative technique with more rapid convergence than Stodola involving comparison of the mean deflection curve.  |
| 5. Southwell's Method | Gives a lower frequency limit for specific systems subjected to a number of separate external influences.  |
| 6. Dunkerley's Method | The critical speed is obtained by subdividing the system into a number of simple standard cases, and summing those effects in accordance with a special formula. |

In all cases, the fundamental bending critical speed alone is calculated. Certain methods exist for the calculation of harmonics, and several of the given methods may be adapted to harmonics. In general, however, the accuracy is considerably less for the calculation of harmonics than for the fundamental mode, and it becomes worse as the modes become higher.

The following sections discuss each of the above methods in detail, indicating the principle on which the method is based, the theoretical background necessary for its application, and giving examples of importance using the method for further clarification. The references cited apply to the original sources or to conveniently-available explanations of it. Important instances of special application are also mentioned.

#### Rayleigh's Method

The fundamental critical speed of an elastic rotor-bearing system may be obtained from the energy properties of the system. A method for doing this was developed by Rayleigh and is based on the fact that the distribution of the kinetic and potential energies in the fundamental mode of vibration is such as to make the frequency a minimum. The great practical utility of this method is due to the relatively small errors which are introduced by assuming any similar deflection profile for the modal form in order to simplify the analysis. As the method applies to the fundamental mode alone, the true modal form may be readily visualized. An approximate analytic representation may then be prescribed.

For a multi-mass system, such as a shaft carrying several massive disks, the configuration of the system at any instant is completely specified by the values of a finite set of coordinates  $q_1, q_2, \dots, q_n$ , measured from some equilibrium datum such as the undeflected shaft centerline. The elastic restoring force is proportional to these coordinates, and so the potential energy,  $V$ , of the deflected shaft is a quadratic function of displacement, i.e.,

$$V = \frac{1}{2} (k_1 q_1^2 + k_2 q_2^2 + \dots + k_n q_n^2) \quad (4.17)$$

where  $k_1, k_2, \dots, k_n$  are the system stiffnesses corresponding to each displacement. The kinetic energy  $T$  is a function of the coordinate velocities and takes the form

$$T = \frac{1}{2} (m_1 \dot{q}_1^2 + m_2 \dot{q}_2^2 + \dots + m_n \dot{q}_n^2) \quad (4.18)$$

For harmonic motions, the coordinate displacements and velocities may be written as

$$q_k = x_k \cos (\omega_k t + \epsilon_k) \quad k = 1, 2, \dots, n$$

$$\dot{q}_k = -\omega_k x_k \sin (\omega_k t + \epsilon_k)$$

As the system is conservative, the potential and kinetic energies over a cycle are equal in steady motion. Considering any mode of frequency,  $\omega$ , the mean values of the kinetic and potential energies are

$$\bar{V} = \frac{1}{4} (k_1 x_1^2 + k_2 x_2^2 + \dots + k_n x_n^2)$$

$$\bar{T} = \frac{1}{4} \omega^2 (m_1 x_1^2 + m_2 x_2^2 + \dots + m_n x_n^2)$$

The frequency is thus obtained from

$$\omega^2 = \frac{k_1 x_1^2 + k_2 x_2^2 + \dots + k_n x_n^2}{m_1 x_1^2 + m_2 x_2^2 + \dots + m_n x_n^2} \quad (4.19)$$

and is a function of the amplitudes of the motion. If the gravity deflection curve is chosen to represent the modal form,  $F_k = k_k x_k = m_k g$ , and hence

$$\omega^2 = g \frac{(m_1 x_1 + m_2 x_2 + \dots + m_n x_n)}{(m_1 x_1^2 + m_2 x_2^2 + \dots + m_n x_n^2)}$$

In the case of a shaft with distributed mass and elasticity where  $I(z)$  and  $w(z)$  are functions of  $x$ , the potential energy due to bending is given by

$$\bar{V} = \frac{1}{2} \int_0^L EI(z) \left( \frac{d^2 w}{dz^2} \right)^2 dz \quad (4.20)$$

and the kinetic energy is

$$\bar{T} = \frac{\omega^2}{2g} \int_0^L w(z) x^2 dz \quad (4.21)$$

In addition, both end thrust  $P$  and torque  $T$  may act on the shaft. The thrust causes a reduction in the potential energy of

$$V_1 = -\frac{1}{2} P \int_0^L \left( \frac{dx}{dz} \right)^2 dz \quad (4.22)$$

whereas the torque increases the potential energy by amount

$$V_2 = \frac{1}{2} C \int_0^L \left( \frac{d\phi}{dz} \right)^2 dz \quad (4.23)$$

in which  $C$  is the torsional rigidity of the cross section and  $\phi$  is the angle of twist per unit length. The presence of torque in the system constraints gives rise to the additional bending moments

$$M_x = T \frac{dy}{dz} ; \quad M_y = -T \frac{dx}{dz}$$

on the elemental length, as shown in Figure 4.12. The corresponding strain energy is

$$\begin{aligned} V_x &= \frac{1}{2} T \int_0^L \left( \frac{dy}{dz} \right) \left( \frac{d^2 x}{dz^2} \right) dz \\ V_y &= \frac{1}{2} T \int_0^L \left( \frac{dx}{dz} \right) \left( \frac{d^2 y}{dz^2} \right) dz \end{aligned} \quad (4.24)$$

In this case, the system must be solved in both coordinate directions simultaneously.

The effect of 'imposing' an approximate deflection curve on the rotor causes it to conform to an additional constraint, and the implied stiffening causes the critical speed as calculated by the Rayleigh Method to always be a few percent in excess of the true value. The assumption of the gravity deflection line, although quite close, never exactly simulates the dynamic deflection line in the fundamental mode. This may be seen from the following:

The static deflection is governed by the equation

$$EI \frac{d^4 x}{dz^4} = w \quad (4.25)$$

For a simply supported shaft under uniform load, this leads to

$$x = \frac{16}{5} x_1 \left[ \left( \frac{z}{L} \right)^4 - 2 \left( \frac{z}{L} \right)^3 + \left( \frac{z}{L} \right) \right] \quad (4.26)$$

where  $x_1$  is the center deflection. The dynamic deflections are obtained from the equation

$$EI \frac{d^4 x}{dz^4} = \frac{w}{c} \omega^2 y$$

For the same simply-supported uniform shaft the deflection equation is

$$x = x_1 \sin \frac{\pi z}{L}$$

comparison between the two profiles will reveal their similarity and their difference. Both theory and engineering application of Rayleigh's method are discussed in the book by Temple and Bickley (Ref. 85). Several examples will now be given to present the application and scope of Rayleigh's Method.

#### Example 1: Cantilever rotor with end mass

The cantilever rotor and its fundamental mode shape are shown in Figure 4.13. The modal form may be represented by the deflection equation:

$$x = x_0 \left[ 1 - \cos \frac{\pi z}{2L} \right] \quad (4.27)$$

This expression satisfies the boundary conditions of  $x = 0$  at  $z = 0$  and  $x = x_0$  at  $z = L$ .

Potential energy:

$$\bar{V} = \frac{1}{2} EI \int_0^L x_0^2 \left( \frac{\pi}{2L} \right)^2 \cos^2 \left( \frac{\pi z}{2L} \right) dz =$$

Kinetic energy:

$$\begin{aligned} \bar{T} &= \frac{W\omega^2}{2g} \int_0^L x_0^2 \left[ 1 - \cos \frac{\pi z}{2L} \right]^2 dz + \frac{W\omega^2 x_0^2}{2g} \\ &= \frac{\omega^2 x_0^2}{2g} 0.226 WL + W \end{aligned}$$

Rayleigh formula:

$$\omega^2 = g \frac{\int_0^L EI(x''')^2 dz}{\int_0^L w x^2 dz} = \frac{3.04}{1 + 0.226 W} \frac{EIg}{WL^3}; \quad \bar{W} = \frac{WL}{W}$$

If  $w(z) = 0$ , the critical speed formula reduces to

$$\omega^2 = 3.04 \frac{EIg}{WL^3} \quad (4.28)$$

From discrete mass methods the exact formula is

$$\omega^2 = 3.00 \frac{EIg}{WL^3} \quad (4.29)$$

representing a difference of 1.3 percent between the two methods.

#### Example 2: Simply supported rotor with end thrust

The simple uniform rotor in rigid bearings has a central disk,  $W$ , distributed shaft weight,  $w$ , per unit length and an end thrust,  $P$ . Its mode shape is sinusoidal, similar to the deflection line under gravity load, i.e.,

$$x = x_1 \sin \frac{\pi z}{L} \quad (4.30)$$

where  $x_1$  is the deflection at the central disk.

Potential energy. Bending

$$\begin{aligned} V_1 &= \frac{1}{2} EI \int_0^L x_1^2 \left( \frac{\pi}{L} \right)^4 \sin^2 \left( \frac{\pi z}{L} \right) dz \\ &= \frac{\pi^4 EI}{4L^3} x_1^2 \end{aligned}$$

End thrust

$$\begin{aligned} V_2 &= -\frac{1}{2} P \int_0^L x_1^2 \left( \frac{\pi}{L} \right)^2 \cos^2 \left( \frac{\pi z}{L} \right) dz \\ &= -\frac{\pi^2 P}{4L} x_1^2 \end{aligned}$$

Kinetic energy

$$\begin{aligned} \bar{T} &= \frac{\omega^2}{2g} \int_0^L x_1^2 \sin^2 \left( \frac{\pi z}{L} \right) dz + \frac{\omega^2 x_1^2}{2g} \\ &= \frac{\omega^2 x_1^2}{2g} (W + 0.5 \omega L) \end{aligned}$$

Rayleigh's formula:

$$\omega^2 = \frac{\int_0^L EI (\ddot{x})^2 dz - P \int_0^L (\dot{x})^2 dz}{\int_0^L \omega x^2 dz}$$

which simplifies to

$$\omega^2 = \frac{\pi^4 EI g}{2WL^3} \left[ \frac{1 - (P/P_c)}{1 + 0.5 \bar{W}} \right]; \quad P_c = \frac{\pi^2 EI}{L^2}; \quad \bar{W} = \left( \frac{\omega L}{g} \right) \quad (4.31)$$

In cases where the end thrust is a significant portion of the Euler buckling load of the shaft, the critical speed may be lowered considerably. This may become an important design feature of single disk, their flexible shaft machines in which the critical speed is naturally fairly low. Where  $P = 0$  the critical speed formula for a massive disk on a uniform heavy shaft is obtained:

$$\omega^2 = \left[ \frac{48.7}{1 + 0.5 \bar{W}} \right] \cdot \frac{EI g}{WL^3} \quad (4.32)$$

If the shaft weight is small compared with the disk weight, the critical speed formula becomes

$$\omega^2 = \frac{48.7 EI g}{WL^3} \quad (4.33)$$

The critical speed-deflection formula  $\omega^2 = g/\delta$  derived previously gives

$$\omega^2 = \frac{48 EI g}{WL^3}$$

for this case, a difference of 1.4 percent between the exact and approximate methods.

### Example 3: Uniform rotor with section change

The stepped-section rotor shown in Figure 4.14 is a common type, but the section change makes exact critical speed analysis cumbersome. An approximate critical speed may be obtained by assuming a deflected profile of the form:

$$x = x_1 \sin \frac{\pi x}{L} \quad (4.34)$$

which has the effect of ignoring the additional rotor deflection which results from the greater flexibility of the end sections. This flexibility may be included by adding a second term to the above expression, e.g.,

$$x = x_1 \sin \frac{\pi x}{L} + x_3 \sin \frac{3\pi x}{L} \quad (4.35)$$

Superposition of these curves, together with suitable coefficients  $x_1$ ,  $x_3$  leads to a good representation of the deflection lines of actual cases. Where the deflection line is known, the critical speed may be found directly from the Rayleigh formula obtained from the second expression

$$\omega^2 = \frac{4g}{\pi} \cdot \frac{x_1 + \frac{x_3}{3}}{x_1^2 + x_3^2} \quad (4.36)$$

Where the deflection line must be calculated, the graphical area-moment method is well-suited to rotors with changes of section. A numerical example will illustrate this.

A rotor of Figure 4.14 has the dimensions shown. Region 1 refers to the small diameter end section. Region 2 refers to the central tube. Both bearings are rigid and the span between them is 168 inches. The tube O.D. is 10.25 inches, and the wall thickness is 0.5 inches. The material is steel throughout.

Calculations based on these dimensions give:

$$w_1 = 2.348 \text{ lb/in}, \quad w_2 = 4.334 \text{ lb/in}$$

$$I_1 = 5.47 \text{ in}^4; \quad I_2 = 182.47 \text{ in}^4$$

Dividing the beam into the section shown and calculating the  $\frac{M}{EI}$  diagram due to the gravity, Figure 4.15, load allows the deflection curve to be calculated based on the moment of the areas about the left-hand end. The Rayleigh Table based on the deflection at the centroid of each section is shown below.

Section	W lb.wt.	$y_1 \times 10^4$ in.	$y_1^2 \times 10^8$ in <sup>2</sup>	$Wy_1 \times 10^4$ lb.wt.in.	$Wy_1^2 \times 10^8$ lb.wt.in <sup>2</sup>
1	14.08	8.69	75.55	122.44	1,064.34
2	14.08	23.92	572.37	337.00	8,062.54
3	26.00	33.88	1148.03	881.12	29,855.00
4	26.00	42.54	1810.18	1106.42	47,074.30
5	26.00	50.78	2578.88	1320.61	67,064.54
6	26.00	58.48	3420.86	1520.99	88,960.43
7	26.00	65.57	4299.43	1705.16	111,807.89
8	26.00	71.94	5176.28	1870.98	134,610.58
9	26.00	77.54	6013.27	2016.58	156,376.70
10	26.00	82.30	6774.14	2140.36	176,163.45
11	26.00	86.17	7426.10	2240.99	198,117.89
12	26.00	89.11	7941.15	2317.41	206,511.93
13	26.00	91.08	8297.24	2368.79	215,771.96
14	26.00	92.06	8475.44	2394.10	220,407.55

$$\Sigma y_1 = 22,343.04 \times 10^{-4} \quad \Sigma Wy_1^2 = 105.68 \times 10^{-4}$$

$$N_c = \frac{30}{\pi} \sqrt{\frac{8 \Sigma W_1 y_1}{\Sigma Wy_1^2}} = \frac{30}{\pi} \sqrt{\frac{(386.4)(2.234)}{(1.657)(10^{-2})}}$$

$$= 2179 \text{ rpm}$$

Curves for the calculation of critical speeds of stepped shafts are given by Rieger in Ref. 86. These curves give  $N_c = 2166 \text{ rpm}$  when applied to the above example.

Substitution of  $x_1, x_3$  deflection values obtained from the above calculation in Equation 4.36 gives  $N_c = 2167$  rpm by that method.

### Ritz's Method

An extension of Rayleigh's method made by Ritz diminishes the inaccuracy introduced by the assumed deflection curve not exactly matching the true whirling form of the rotor at a critical speed, as follows: Let  $\phi_1(z), \phi_2(z), \dots, \phi_n(z)$  be a set of  $n$  linearly independent functions each of which satisfies the boundary conditions of a given case. Combine these functions in the form

$$X(z) = a_1 \phi_1(z) + a_2 \phi_2(z) + \dots + a_n \phi_n(z) \quad (4.37)$$

to represent the deflection curve of the rotor, in which the  $a_1, a_2, \dots, a_n$  are coefficients. The essential feature of Ritz's method is that these coefficients are to be selected in such a manner as to make the calculated frequency a minimum.

In the case of a whirling shaft subjected to bending and centrifugal forces alone, the frequency equation, based on energy considerations and incorporating the above expression, is:

$$\omega^2 = g \cdot \frac{\int_0^L EI(z)(x^{11})^2 dz}{\int_0^L w(z) A(z)(x)^2 dz} \quad x^{11} = \frac{d^2 x}{dz^2} \quad (4.38)$$

The Ritz minimum condition will be satisfied if

$$\frac{\partial}{\partial a_1} \frac{\int_0^L I(z)(x^{11})^2 dz}{\int_0^L A(z)(x)^2 dz} = 0 \quad i = 1, 2, \dots, n$$

Reforming the differentiation gives

$$\int_0^L A(z)(x)^2 dz \cdot \frac{\partial}{\partial a_1} \int_0^L I(z)(x^{11}) dz - \int_0^L I(z)(x^{11}) dz \cdot \frac{\partial}{\partial a_1} \int_0^L A(z)(x)^2 dz = 0 \quad (4.39)$$

But from the Rayleigh frequency equation

$$\int_0^L I(z)(x^{11})^2 dz = \frac{\omega^2}{gE} \int_0^L A(z)(x^2) dz \quad (4.40)$$

This leads to the minimum expression

$$\frac{\partial}{\partial a_1} \int_0^L \left[ I(z)(x^{11})^2 - \frac{\omega^2}{gE} A(z)(x)^2 \right] dz = 0 \quad (4.41)$$

In application, equating the above expressions to zero leads to a linear homogeneous equations in  $a_1, a_2, \dots, a_n$ . When the determinant of these coefficients is equated to zero, the frequency equation for the system is obtained. Actual values of the coefficients  $a_i$  are not required in setting up the frequency equation. The basic requirement is that each term in the original series satisfies the boundary conditions of the problem being considered. In the case of a simple-supported rotor, a trigonometric series

$$x = a_1 \sin \frac{\pi z}{L} + a_3 \sin \frac{3\pi z}{L} + a_5 \sin \frac{5\pi z}{L} + \dots$$

fulfills this requirement. Likewise, a cantilever rotor may be investigated using a cosine trigonometric series, or with a polynomial expression

$$x = a_1 \left[ 1 - \frac{z}{L} \right]^2 + a_2 \frac{z}{L} \left[ 1 - \frac{z}{L} \right]^2 + a_3 \left( \frac{z}{L} \right)^2 \left[ 1 - \frac{z}{L} \right]^2 + \dots$$

The complete Fourier series may be applied to more complicated cases. This method of critical speed analysis has been discussed by Inglis (Ref. 87).

The Ritz method requires that the boundary conditions should be satisfied by all terms individually in the series. It has been applied with excellent accuracy to rotors of both constant and smoothly varying cross sections. However, with a rotor in which the section changes abruptly, the method fails when a series satisfying the end conditions alone is chosen, because the smoothly varying deflection line fails to meet the moment and shear requirements at the abrupt section variations.

### Iterative Methods

Stodola (Ref. 18) describes a method which allows accurate results to be obtained for the fundamental mode using a simple iterative procedure, as follows:

1. Assume an initial deflected form for the shaft. This is frequently the gravity deflection curve, determined analytically or graphically, but it may be any form which satisfies the end conditions.
2. From this deflection curve, obtain deflection values  $x_1, x_2, \dots, x_n$  corresponding to the distribution of weight carried by the rotor  $w_1, w_2, \dots, w_n$ . Rotors with uniformly distributed weight may be broken down into an appropriate number of discrete weights.
3. Assume an angular velocity,  $\omega$ . This may be any value whatsoever. It is simply required for calculation.
4. Calculate the centrifugal force acting on each weight  $w_i$  due to the whirl radius  $x_i$ , at assumed speed,  $\omega$ .
5. Calculate a second deflection curve, due to the centrifugal forces acting as static loads on the shaft. The deflections at  $w_1, w_2, \dots, w_n$  will then be denoted  $x'_1, x'_2, \dots, x'_n$  for this curve.
6. Calculate the critical speed  $\omega_c$  from the ratio of the assumed deflection  $x_1$  to the calculated deflection  $x'_1$ , i.e.,

$$\omega_c = \omega \sqrt{\frac{x_1}{x'_1}}$$

The validity of the above formula is due to the fact that if the centrifugal forces were now recalculated using  $\omega_c$  instead of  $\omega$ , these forces would be increased in the ratio  $x_1/x'_1$  and the static-centrifugal deflection curve would also be increased in amplitude by this amount. If this deflection curve, thus enlarged, is exact it will precisely match the initially assumed deflection curve. This may only occur where the calculated speed  $\omega_c$  is the true critical whirling speed at which the centrifugal forces are in fact sufficient to retain the whirling form of the shaft against elastic restoring forces.

If the curves do not match, the calculated critical speed is not the true value, and the procedure must be continued, as follows:

7. Using the static-centrifugal deflection curve, calculate a second set of centrifugal forces corresponding to  $W_1$ ,  $x_1$  and  $\omega$ .
8. Applying these second centrifugal forces to the shaft, recalculate the deflection curve. The deflections will then be  $x_1''$ , corresponding to  $W_1$ .
9. Calculate the critical speed  $\omega_c$  from

$$\omega_c = \omega \sqrt{\frac{x_1}{x_1''}}$$

This procedure may be continued until the difference between successive values of  $\omega_c$  is as small as desired. Experience has shown this method to be rapidly convergent, consistent with Rayleigh's principle that a considerable error in the deflected form introduces but a small error in the value of  $\omega_c$ . The method is widely used and is quite general; it may be applied to a rotor for which a reasonable, approximate representation of the deflected profile in the fundamental mode may be obtained. Borowicz (Ref.88) has investigated the application of this method to the critical speeds of multi-span rotors. Morley (Ref.89) has given a similar iterative method for which very rapid convergence is claimed. From the exact formula for the critical speed of the fundamental mode,

$$\omega_c^2 = \frac{g E W x}{\sum W x^2} = \frac{g}{x_m} \quad (4.42)$$

where  $x_m$  is the mean deflection value. But, for an arbitrarily assumed deflection profile,  $x'$ , the above formula is an approximation justified in application by Rayleigh's principle. If it is assumed that  $x$  has values  $x'$  proportional to those produced by gravity, the formula becomes

$$(\omega_c')^2 = \frac{g E W x'}{\sum W (x')^2} = \frac{g}{x_m'} \quad (4.43)$$

where

$$\bar{x}_m' = \frac{\sum W(x')^2}{\sum W(x')'} \quad (4.44)$$

A mean value of the deflections,  $\bar{x}'$ , and is a first approximation to the value  $x_m$  in Equation (4.42), and so  $\omega_c'$  is a first approximation to the value  $\omega_c$ . Distributed loads may be included using the corresponding formulas

$$\int w \left( \frac{dx}{dz} \right)^2 dz \quad \text{and} \quad \int w \left( \frac{d^2x}{dz^2} \right)^2 dz \quad (4.45)$$

The method is as follows:

1. Assume a deflected profile for the rotor with a maximum deflection  $x_m$ . Calculate  $\omega_c$  from Equation (4.42).
2. Calculate the centrifugal force for each rotor weight  $W_i$  corresponding to the assumed deflection  $x_i$ , at the calculated speed  $\omega_c$ .
3. Calculate the shaft deflection profile corresponding to these centrifugal forces acting statically on the rotor. Call the  $W_i$  deflection  $x_i$  in this case.
4. Recalculate the critical speed corresponding to new deflections.

Here,

$$\omega_c' = \frac{g \sum W_i x_i'}{\sum W_i (x_i')^2}$$

5. If the difference between  $\omega_c$  and  $\omega_c'$  is too great, the above procedure is repeated, recalculating the centrifugal force, the deflection curve, and so the centrifugal force  $\omega_{c11}$ .

The convergence of the above procedure is claimed to be very rapid, and very few cycles are necessary. This is due to using the mean deflection,  $\bar{x}_m'$ , (Equation 4.44) rather than comparing the deflection at a single point

$\omega_c' = \omega_c \sqrt{\frac{\bar{x}}{x}}$ , as in Stodola's method. More computation is required at each step, but the convergence is more rapid.

### Southwell's method

Where two or more external effects contribute to the overall motion of the fundamental mode, a method due to Southwell may be used to determine approximately the net effect on the critical speed of the system. This method states that if  $\alpha_1, \alpha_2, \dots$  are the eigenvalues for each of the effects acting separately, the eigenvalue for all effects acting together satisfies the inequality

$$\alpha > \alpha_1 + \alpha_2 + \dots \quad (4.46)$$

The inequality sign indicates that the critical speed obtained by this method may be lower than the true value; in practice this is usually the case.

The proof of this inequality is given in Southwell (Ref. 90).

It has been demonstrated that this method gives accurate results in cases where the vibrating structure itself remains unaltered, but where this structure is subjected to several types of loading, e.g. centrifugal force, torque, shear end load, gyroscopic loading. Substantial inaccuracies may result where the system itself changes, such as adding a discrete mass to a distributed mass to form a system. This is due to the nature of the method which is based on synthesis of potential energy.

#### Example 1: Influence of end loading on critical speed, simple-supported uniform shaft

The fundamental critical speed of the shaft without end load is:

$$\omega_1^2 = \pi^2 \frac{EIg}{wL^4}$$

The natural frequency of the bar due to a tensile force  $p$  neglecting flexural stiffness, is:

$$\omega_2^2 = \pi^2 \frac{Pg}{wl^2}$$

By Southwell's theorem:

$$\alpha \geq \alpha_1 + \alpha_2$$

or

$$\omega^2 \geq \omega_1^2 + \omega_2^2 \quad (4.47)$$

The critical speed with both effects acting together is therefore:

$$\omega^2 \geq \frac{\pi^4 EI g}{w L^4} + \frac{\pi^2 p g}{w l^2} \quad (4.48)$$

In the case of end thrust, where  $p$  is negative,

$$\omega^2 \geq \frac{\pi^4 EI g}{w L^4} - \frac{\pi^2 p g}{w l^2} \quad (4.49)$$

which may be written

$$\left(\frac{\omega}{\omega_c}\right)^2 \geq 1 - \frac{P}{P_c} \quad (4.50)$$

where  $\omega_c$  is the critical speed of the shaft without end load and  $P_c$  is the Eulerian critical thrust.

Temple and Bickley (Ref. 85) have drawn attention to the generality of the form of the above inequality, indicating that where a system has several critical numbers, such as end thrust  $\frac{P}{P_c}$ , applied torque  $\frac{T}{T_c}$ , flexural critical speed  $\left(\frac{\omega}{\omega_c}\right)^2$ , and so on, the general result may always be presented in the form of an equality of the above type. Thus,

$$1 \leq \frac{P}{P_c} + \frac{T}{T_c} + \left(\frac{\omega}{\omega_c}\right)^2 \quad (4.51)$$

applies to the above system, agreeing with the results of Southwell and Gough (Ref. 91) for this case. The following formulas have been obtained by Greenhill (Ref. 39) for the critical torque:

Shaft of length  $l$ , running in two short end bearings;  $T_c = 2\pi EI/l$

Shaft of length  $l$ , running in two long end bearings;  $T_c = 2C EI/L$

where

$$C = 4.493$$

Using Southwell's method together with Rayleigh's method allows the critical speed to be established within specific bounds.

### Dunkerley's Method

A convenient method for the fundamental critical speed calculation of systems which consist of a number of components such as gears, compressor or turbine disks, flywheels, etc., mounted on a basic shaft has been presented by Dunkerley (Ref.40). The method consists of reducing the actual system into a number of simple sub-systems, each of which may be calculated directly by standard formulae. The critical speeds  $\omega_1, \omega_2, \dots, \omega_n$  they combine according to the law

$$\frac{1}{\omega^2} = \frac{1}{\omega_1^2} + \frac{1}{\omega_2^2} + \dots + \frac{1}{\omega_n^2} \quad (4.52)$$

to give the actual critical speed  $\omega$  of the system. In the above,  $\omega_1$  may be the critical speed of an unloaded shaft in its bearings, while  $\omega_1, \omega_2, \dots$  represent the critical speeds of the various loads, ignoring the mass of the shaft. The approximation is usually very close, for shafts which are mounted in two bearings, especially where there is no overhang.

### Example 1: Uniform cantilever shaft with end mass

For the unloaded shafts:

$$\omega_1^2 = 12.36 \frac{EIg}{wL^4}$$

Massless shaft, with end mass

$$\omega_2^2 = 3.00 \frac{EIg}{WL^3}$$

By Dunkerley's rule

$$\frac{1}{\omega^2} = \frac{1}{\omega_1^2} + \frac{1}{\omega_2^2} = \frac{wL^4}{EIg} \left[ \frac{1}{12.36} + \frac{1}{3} \frac{W}{wt} \right]$$

Thus,

$$\omega^2 = \frac{12.36}{1 + 4.12K} \cdot \frac{EIg}{wL^4} \quad K = \frac{W}{wl} \quad (4.53)$$

This may be compared with the result obtained previously by Rayleigh's method, i.e.,

$$\omega^2 = \frac{EIg}{wL^4}$$

In general, results of good accuracy may be obtained by following the above procedure. Any number of masses may be considered, and the shaft section may vary although this introduces the analytical complications associated with stepped shafts discussed earlier. Where rotating inertia and gyroscopic forces appear likely to influence the motion, these factors should be included in the sub-system calculations. The formulae for simple cases have been corrected for rotatory inertia (but omitting the gyroscopic effect) by Morley (Ref. 43). Dunkerley used two exact methods and the above approximate method to calculate a wide variety of systems. Various end conditions were examined for one-, two-, and three-span shafts. One- and two-pulley shaft systems were examined. An extensive series of experiments was conducted to verify the analytical findings. The apparatus consisted of long thin shafts carrying heavy pulleys, mounted in short oil-lubricated bearings. Maximum error found using the empirical method was 4.6 percent, for an extreme case. The general order of accuracy was around 2.0 percent high. Several analyses by other authors, notably Chree (Ref. 41), Morley (Ref. 43), and Jeffcott (Refs. 92 and 93), have discussed both the accuracy and the applicability of Dunkerley's method. Morley's findings are discussed in the following section.

#### Effect of Disk Gyroscopic Action on Critical Speed

When the diameter of a disk is large in relation to its thickness, it is necessary to include the influence of gyroscopic action in calculating the critical speeds of the system. Where this inertia is sufficiently large, it may give rise to a number of critical speeds. Stodola (Ref. 18) discussed both positive and

and negative synchronous precession of a simple cantilever rotor. His results were confirmed by Foppl (Ref.94). A discussion of the gyroscopic effects in a number of rigid-bearing rotors has been given by Green (Ref.95).

Consider a thin balanced disk mounted on a flexible massless shaft which rotates at speed  $\omega$  about the OZ axis as shown in Figure 4.16. As the shaft whirls, the inclination of the disk changes cyclically. This causes a gyroscopic moment to act in opposition to the radial whirl forces, tending to reduce rotor deflections. The instantaneous small angles of inclination  $\beta$ ,  $\gamma$  in the x-y and y-z planes each brings about an angular momentum component, the rate of change of which causes the gyroscopic moments  $M_y$  and  $M_x$ . One principal inertia axis of the disk coincides with the direction of the elastic axis of the shaft at the disk. Since the disk is circular, the other two axes may be selected parallel to the x and y axis respectively. Denoting the principal moments of inertia as  $I_p$  along the shaft axis and  $I_T$  in both the x and y axis, for small values of  $\beta$  and  $\gamma$ , the gyroscopic moments in the x-z and y-z planes are given by:

$$M_x = \frac{d}{dt} [I_p \omega \beta - I_T \dot{\gamma}] \quad M_y = \frac{d}{dt} [I_p \omega \gamma + I_T \dot{\beta}] \quad (4.54)$$

These moments also cause the shaft to deflect, modifying the whirling form of the rotor. The equations of motion of the system must, therefore, include the gyroscopic effect. Under the action of the force P and the moment M, Figure 4.17, the deflection and rotation at E are

$$y = \frac{a^2 b^2}{3EIL} P + \frac{ab(a-b)}{3EIL} M$$

$$\beta = \frac{ab(a-b)}{3EIL} - \frac{(a^2 - ab + b^2)}{3EIL} M \quad (4.55)$$

Thus

$$P = 3EIL \left[ \left( \frac{a^2 - ab + b^2}{a^3 b^3} \right) y + \left( \frac{a-b}{a^2 b^2} \right) \beta \right] = \alpha_{11} y + \alpha_{12} \beta$$

$$M = 3EIL \left[ -\frac{(a-b)}{2b^2} y - \frac{1}{ab} \beta \right] = -\alpha_{21}y - \alpha_{22}\beta \quad (4.56)$$

From Figure 4.17 the equations of motion are:

$$\begin{aligned} m\ddot{x} &= -P_x = -\alpha_{11}x - \alpha_{12}\beta \\ m\ddot{y} &= -P_y = -\alpha_{11}z - \alpha_{12}\gamma \end{aligned} \quad (4.57)$$

and from Equations 4.56

$$\begin{aligned} I_p \omega \dot{\beta} - I_T \ddot{\gamma} &= \alpha_{21}x + \alpha_{22}\gamma \\ I_p \omega \dot{\gamma} + I_T \ddot{\beta} &= -\alpha_{21}y - \alpha_{22}\beta \end{aligned} \quad (4.58)$$

These four equations may be solved for the critical speed by choosing a solution of the form  $e^{pt}$  which gives four linear homogenous equations for the above balanced shaft.

Substituting

$$x = r \cos \omega t \quad y = r \sin \omega t \quad \beta = \phi \cos \omega t \quad \gamma = \phi \sin \omega t \quad (4.59)$$

and considering  $r$  and  $\phi$  constant for any particular speed to obtain the boundary conditions for the instant when the whirl plane of the shaft coincides with the  $y$ - $z$  plane:

$$\begin{aligned} \beta &= \phi & \dot{\beta} &= 0 & \ddot{\beta} &= -\phi \omega^2 \\ \gamma &= 0 & \dot{\gamma} &= \omega & \ddot{\gamma} &= 0 \\ x &= r & \dot{x} &= 0 & \ddot{x} &= -r \omega^2 \\ y &= 0 & \dot{y} &= r \omega & \ddot{y} &= 0 \end{aligned} \quad (4.60)$$

reduces the equations of motion to

$$m\ddot{x} + \alpha_{11}x + \alpha_{12}\beta = 0$$

$$(I_p - I_T)\omega^2\beta - \alpha_{21}y + \alpha_{22}\beta = 0 \quad (4.61)$$

The above equations indicate the effect of centrifugal force ( $m\omega^2x$ ), and of gyroscopic moment  $(I_p - I_T)\omega^2\beta$  on the shaft deflection. To solve these equations substitute

$$y = r \cos \omega t \quad \beta = \phi \cos \omega t \quad (4.62)$$

The critical speed of the above system under the influence of gravity is then obtained from the determinant of the coefficients of  $y, \beta$ . This is

$$\omega^4 - (p^2 + q^2)\omega^2 - p^2q^2(1 - c) = 0 \quad (4.63)$$

where

$$p^2 = \frac{\alpha_{11}}{m}$$

$$q^2 = \frac{\alpha_{22}}{I_p - I_T}$$

$$c = \frac{a^2 - 2ab + b^2}{a^2 - ab + b^2} \quad (4.64)$$

For  $a, b$  real,  $c < 1$ , Equation 4.63 has only one real root,  $\omega$ , corresponding to forward precession. This is the condition which occurs most frequently in practice. The gyroscopic effect stiffens the shaft and raises the critical speed, due to the forward precession of the disk.

In the above discussion, it has been assumed that the whirl velocity of the shaft is  $\omega$ , the speed of shaft rotation. If it is not, and the rotor whirl velocity is  $v$ , substituting

$$x = r \cos Vt \quad y = r \sin Vt \quad \beta = \phi \cos Vt \quad \gamma = \phi \sin Vt \quad (4.65)$$

gives

$$m\ddot{x} + \alpha_{11}x + \alpha_{12}\beta = 0$$

$$\left[ I_p \omega v - I_T v^2 \right] \beta - \alpha_{21}x + \alpha_{22}\beta = 0 \quad (4.66)$$

when  $V = \omega$  the previous result is obtained. If  $V = -\omega$ , the second equation becomes

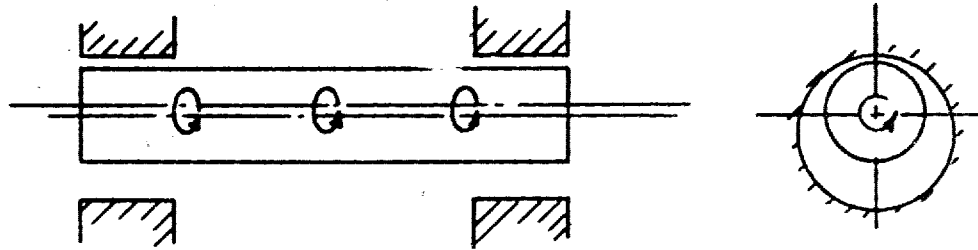
$$- \left[ I_p + I_T \right] \omega^2 \beta - \alpha_{21}x + \alpha_{22}\beta = 0 \quad (4.67)$$

and the gyroscopic effect becomes positive and tends to increase the shaft deflection. This negative precession does not occur naturally but may be initiated by an external cyclic disturbance. The increased deflection lowers the system critical speed.

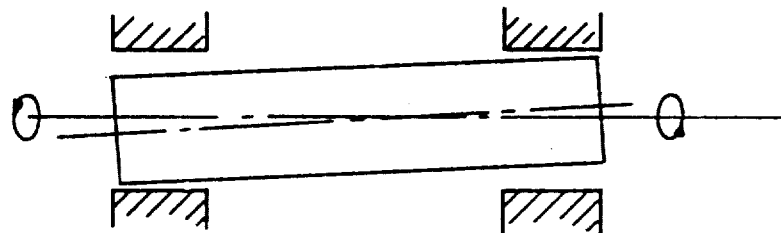
Green (Ref.95) has given solutions in chart form for the cantilevered disk, the simply supported disk (considered above), a two-disk system, and multidisk systems.

Dimentberg (Ref. 1) has considered the two-bearing overhung disk with both balanced and unbalanced operation. This treatment is then extended to include the effect of internal friction and external friction — individually and then simultaneously. It is shown in this work that the number of critical speeds for a given case depends on the disk proportions. For a circular disk, in general, there are three critical speeds as  $I_p = 2I_T$ , one with forward precession, and two with backward precession. Where  $I_p < I_T$  there are four critical speeds, two forward and two backward precession, corresponding to the roots of the quartic characteristic equation.

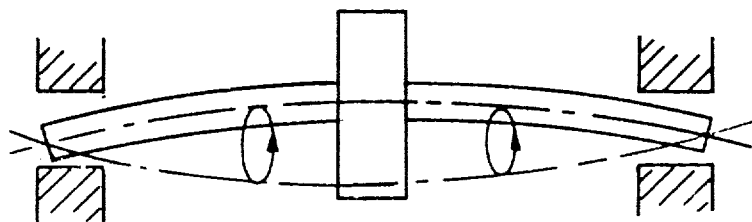
Yamada (Ref. 96) has investigated the case of an unsymmetrical cantilevered plate,  $I_1 > I_2 > I_3$  both analytically and experimentally. The results indicated that where the circular disk undergoes a circular whirl, the asymmetrical plate gave elliptical whirl orbits. Two forward synchronous precessional motions occurred in contrast with single forward precession with a circular disk, and the speed range between these motions was unstable.



(a) Rigid Body Translatory Mode



(b) Rigid Body Conical Mode



(c) Bending Mode or Flexible Rotor

Figure 4.01

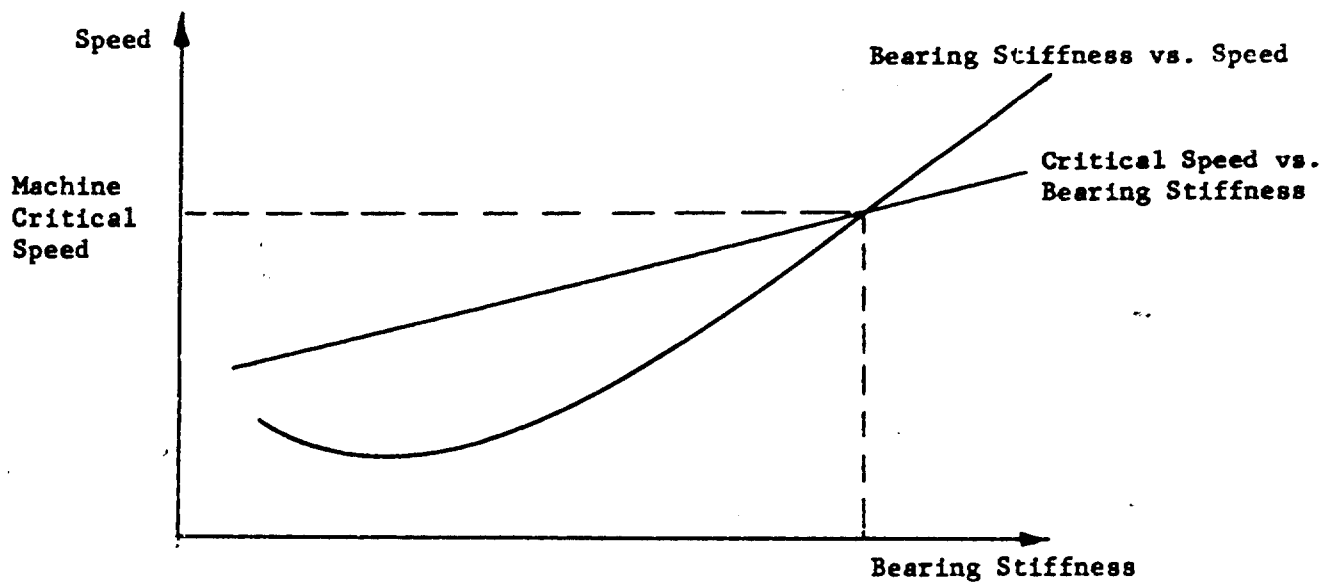


Fig. 4.02 Determination of Critical Speed  
for Variable Stiffness Bearings

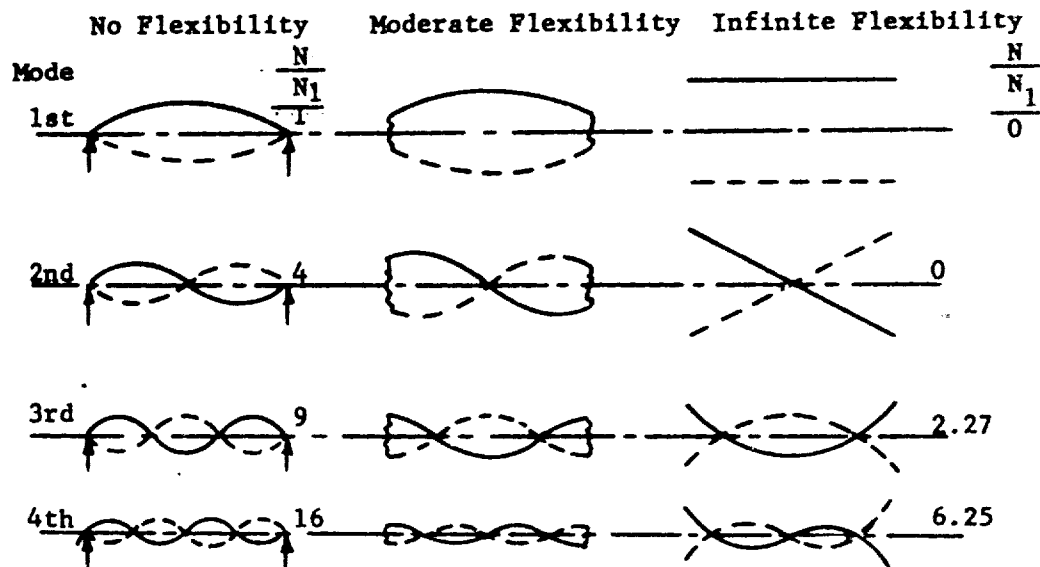


Fig. 4.03. Influence of Bearing Flexibility on Critical Speed for Flexible Rotor

Reprinted from THE EFFECT OF FLEXIBILITY OF SUPPORT UPON THE CRITICAL SPEEDS OF HIGH SPEED ROTORS, Figure 10, by Frank C. Linn and M. A. Prohl for The Society of Naval Architects and Marine Engineers. November 1951

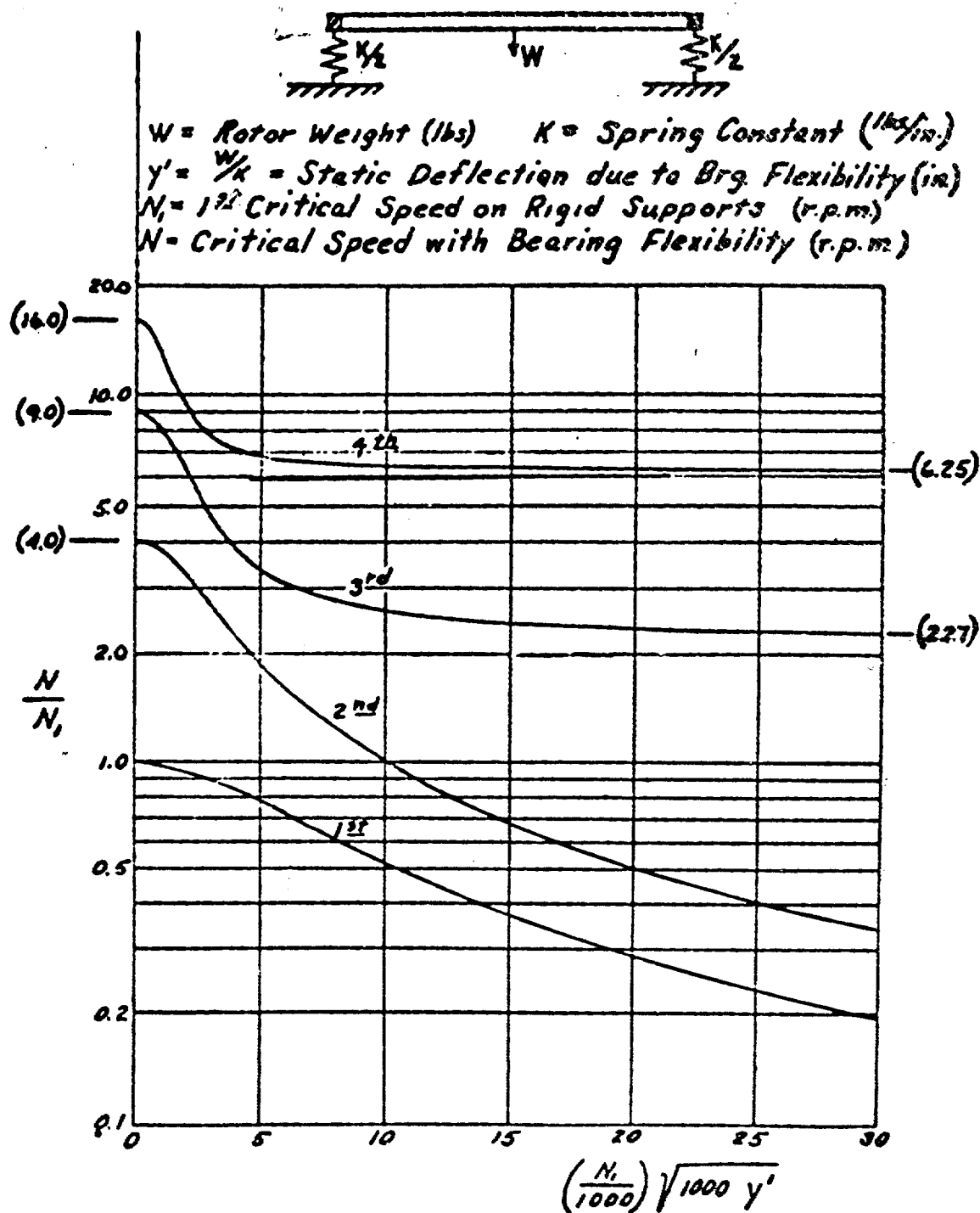


Fig. 4.04 Influence of Bearing Mass and Flexibility on Critical Speed

Reprinted from THE EFFECT OF FLEXIBILITY OF SUPPORT UPON THE CRITICAL SPEEDS OF HIGH SPEED ROTORS, Figure 9, by Frank C. Linn and M. A. Prohl for The Society of Naval Architects and Marine Engineers. November 1951

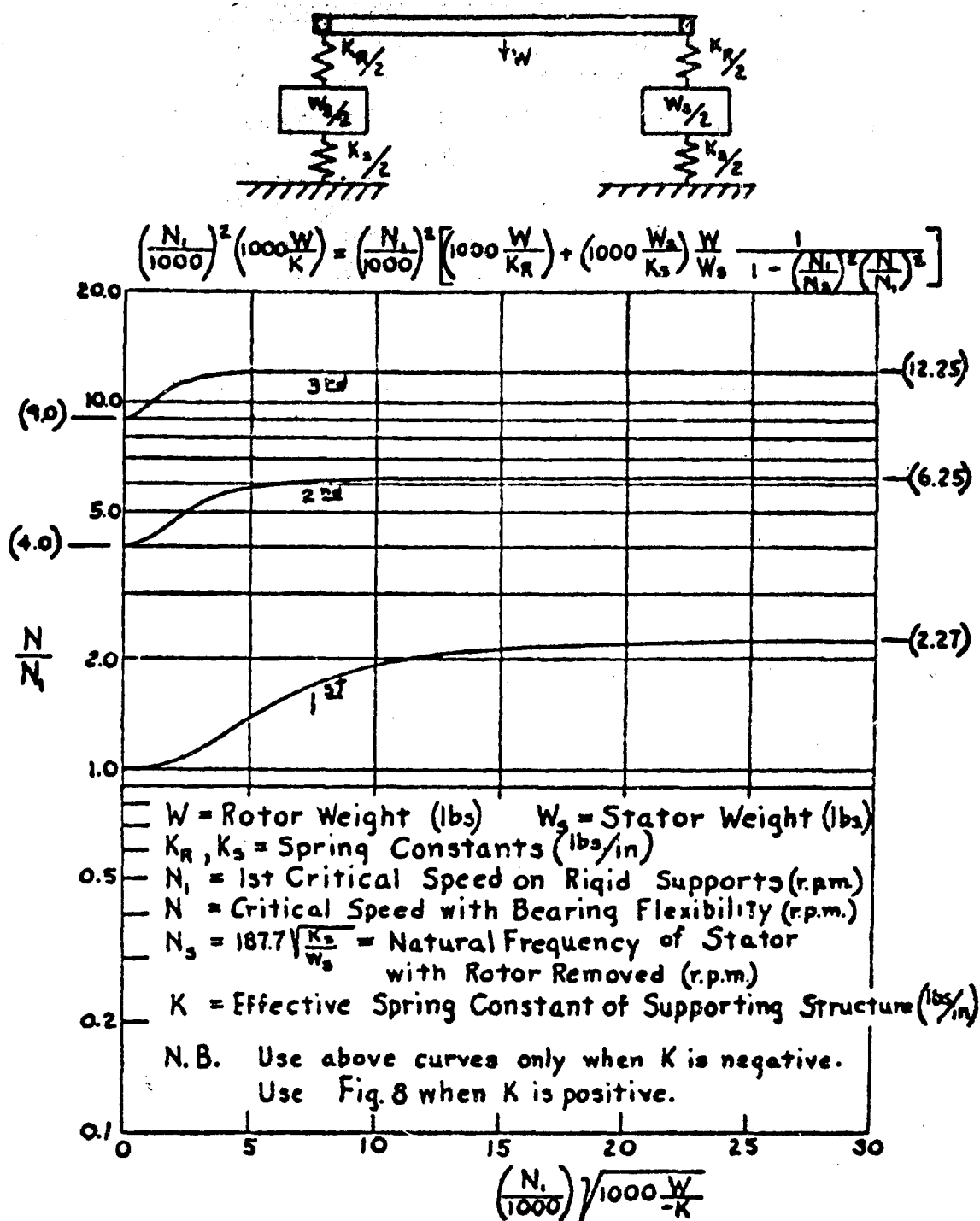


Fig. 4.05 Influence of Bearing Mass and Flexibility on Critical Speed

Reprinted from THE EFFECT OF FLEXIBILITY OF SUPPORT UPON THE CRITICAL SPEEDS OF HIGH SPEED ROTORS, Figure 11, by Frank C. Linn and M. A. Prohl for The Society of Naval Architects and Marine Engineers. November 1951

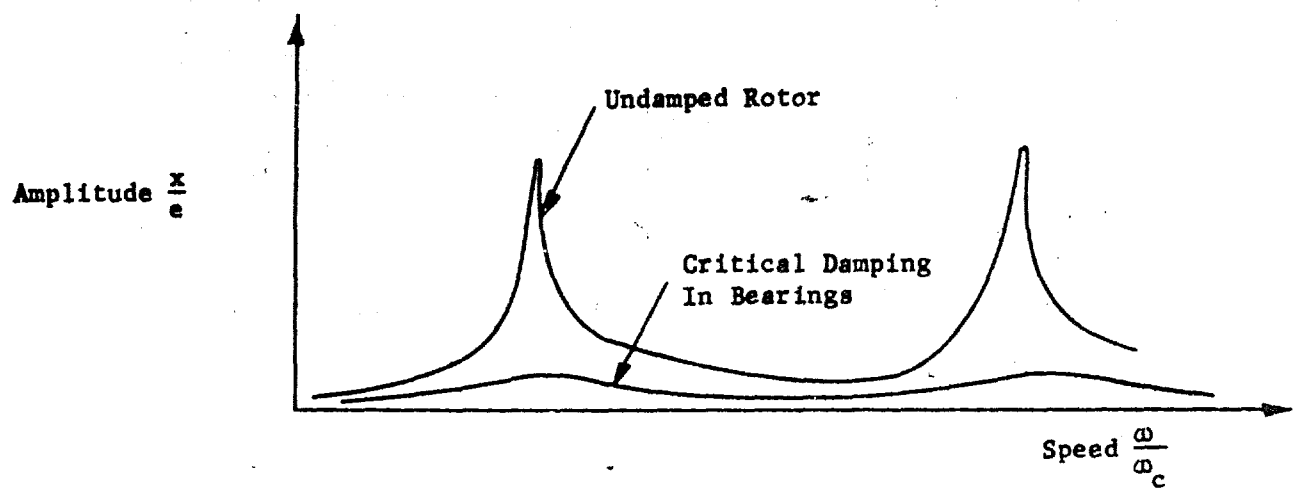


Fig. 4.06 Influence of Bearing Damping on Critical Speed

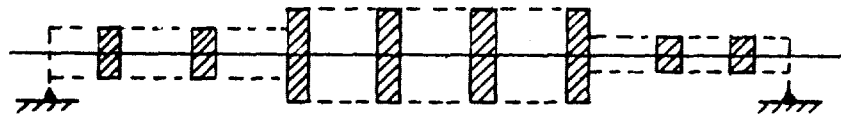


Fig. 4.07 Discrete Mass Representation of Massive Flexible Rotor

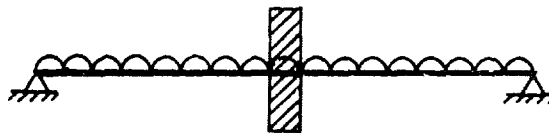


Fig. 4.08 Single Disk Rotor on Massive Flexible Shaft

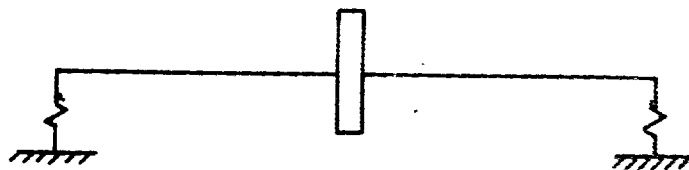


Fig. 4.09 Flexible Single Disk Rotor in Flexible Bearings



Fig. 4.10 Symmetrical Two Mass Rotor in Rigid Bearings

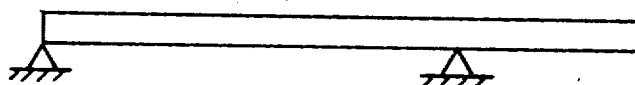


Fig. 4.11 Uniform Rotor With Overhang in Rigid Supports

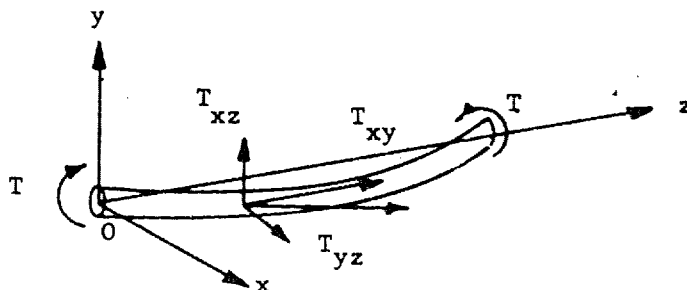


Fig. 4.12 Additional Bending Moments Due to End Torque in Flexible Shaft

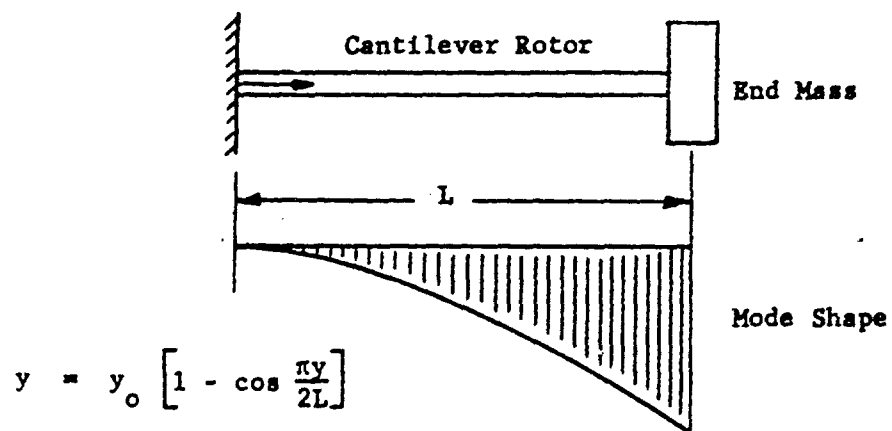


Fig. 4.13 Cantilever Rotor with End Mass Showing Fundamental Mode Shape

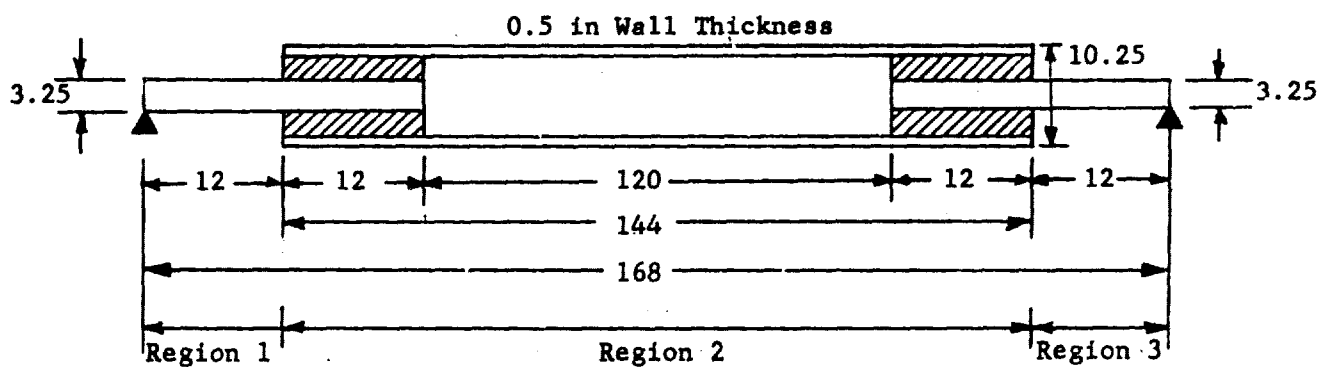


Fig. 4.14 Uniform Rotor With Stiffened Central Section

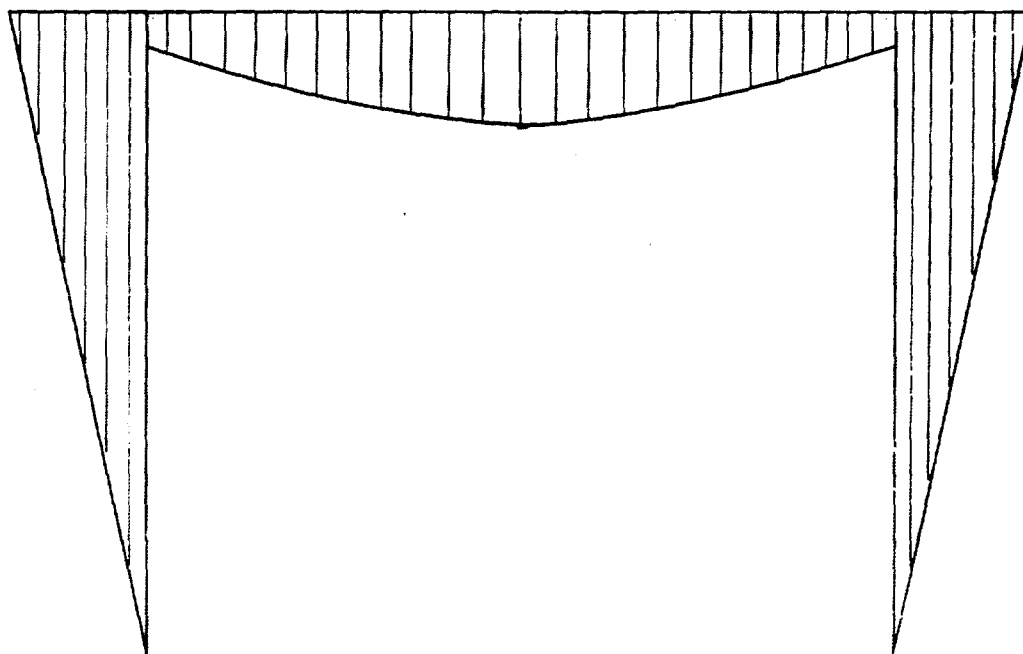


Fig. 4.15 M/EI Diagram for Stiffened Shaft Based on Gravity Deflection

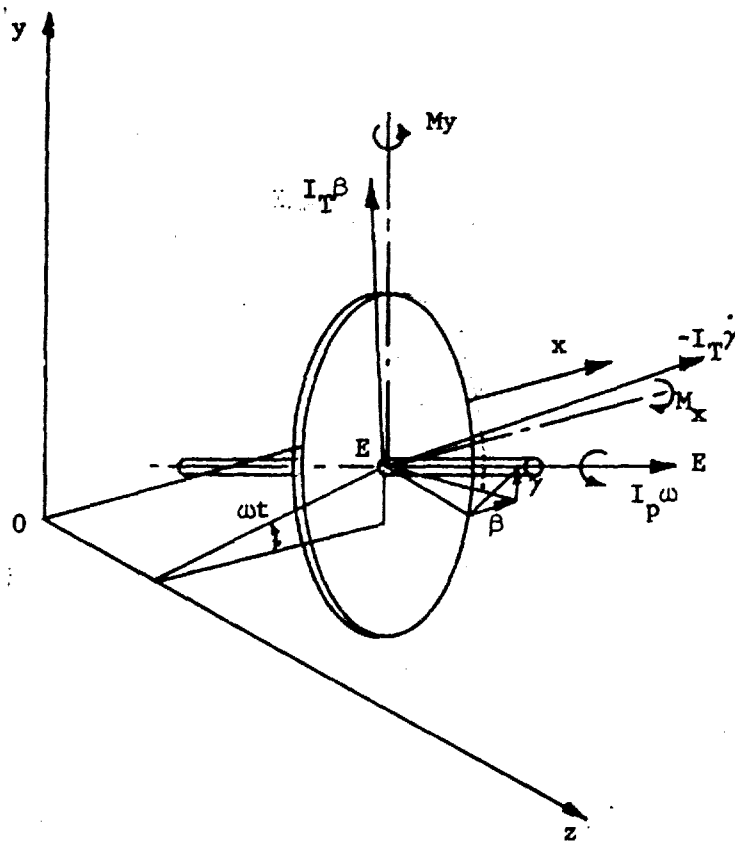


Fig. 4.16 Moments Acting on a Balanced Disk Mounted on a Flexible Shaft

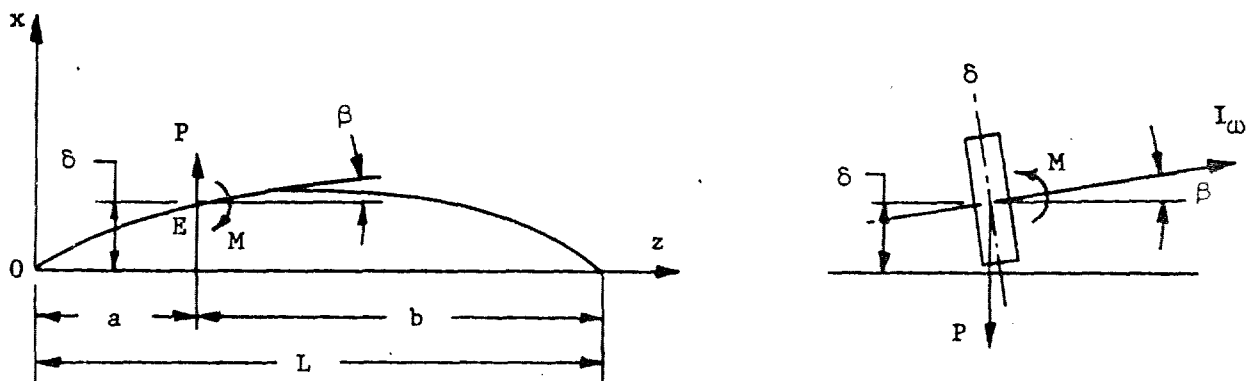


Fig. 4.17 Moment and Force Acting on Shaft due to Disk Gyroscopic Action

STABILITYThe Nature of Whirl Motions

When the radius of the whirl orbit traced out by the c.g. of a rotor tends to increase with time following a small displacement from the equilibrium position, the rotor motion is said to be unstable. A stable rotor will tend to return to its original whirl orbit with a damped oscillatory motion following the removal of the disturbance. If the disturbance persists, such as an additional unbalance or cyclic force, a stable rotor will adopt a new whirl orbit in keeping with the new operating conditions; whereas, the whirl radius of a rotor in unstable equilibrium will continue to grow with time until restrained by some other constraint. These conditions are illustrated in Figure 5.01. The form of the whirl orbit is determined by the collective action of all forces acting on the rotor. The simplest orbit is circular about the undisturbed rotor axis. This arises from the action of an inwardly-directed radial force of constant magnitude such as the rotor elastic force. The simultaneous presence of a constant negative tangential force which rotates along with the radial force does not disturb the form of the orbit and confers stability on the motion at the rotor critical speed. Where the tangential force is positive, such as in the case of hysteretic friction above the rotor critical speed and with hydrodynamic bearings above twice the system critical speed, tangential equilibrium does not exist. The motion is unstable and the rotor whirl path is a spiral whose radius increases with time. This spiral whirl growth also occurs in the case of a simple rotor in rigid bearings, when running at its critical speed.

Rotors which have dissimilar lateral moments of inertia have two critical speeds corresponding to the two stiffnesses. Below the lower critical and above the higher critical, the rotor unbalance whirl is stable, and the whirl orbit is elliptical with the major and minor axes corresponding to the principal rotor stiffness directions. At speeds between these criticals the rotor motion is unstable and the whirl radius is again a growing spiral. This instability is independent of rotor unbalance and cannot be eliminated by more refined balancing. The unsymmetrical rotor stiffness also appears as a twice-per-

revolution variation as shown in Figure 5.02 which gives rise to a whirl at twice shaft speed, even when the rotor balance is perfect. This whirl becomes resonant when the rotor runs at half each critical speed. For a rotor with small stiffness dissymmetry, the proximity of these two whirls may cause a noticable sub-harmonic resonant amplitude peak.

Simple elasticity of the rotor supports does not itself induce whirling, but it may exert a strong influence upon the shape of the whirl orbit. If the stiffness is not symmetrical, the orbit will be elliptical rather than circular. In addition, fluid-film bearings possess complex direct and cross-coupled stiffness and damping properties which depend on the operating eccentricity of the journal within the bearing. During operation, therefore, the bearing stiffness and damping properties are not symmetrical about the journal axis. The fluid-film damping diminishes the rotor whirl motions up to a certain threshold speed which occurs at approximately twice the system critical speed. Beyond this threshold, the journal whirls within the clearance with a frequency equal to half the whirl threshold speed. The resonant nature of this motion may lead to dangerously large whirl amplitudes. This is known as resonant whipping, and it is sustained by the fluid-film forces themselves. Only in isolated instances has it been possible to run through the resonant whipping condition because once established, the large-amplitude whirl motions sustain themselves for all higher speeds and machine operation is hazardous. The accompanying changes which take place in the bearing coefficients, and, hence, in the motion, due to the large amplitudes, are not fully understood at present.

A number of minor whirl conditions associated with torque and speed fluctuations exist. Gravity acting on an unbalanced rotor may be sufficient by initiating a small whirl at twice rotational speed which may become resonant when the rotor operates at half the system critical speed. A similar condition results from externally imposed torque fluctuations — such as those from a reciprocating engine or pump. When applied at integer multiples of the system critical speed, these torques may develop further sub-harmonic resonant whirl motions.

In each of the above whirl instances, the presence of viscous friction in the system acts to stabilize and limit any whirl motions which occur. It is the

absence of effective frictional forces in the bearing which leads to resonant whipping. Both hysteretic and viscous friction are frequently present simultaneously in large built-up rotors with dissimilar lateral stiffnesses. The hysteretic damping accentuates the inherent whirl instability of these rotors between the critical speeds, whereas the viscous damping tends to suppress the whirl at all speeds. A considerable amount of viscous damping in the bearings of such a rotor may be required to assure stable whirl amplitudes of moderate proportions throughout the speed range.

### Stability of a Simple Rotor in Rigid Bearings

Below the critical speed,  $\omega < \omega_c$ , it is well known that all practical rotor motions are stable below the first critical speed. No major source of instability becomes troublesome below this speed, and the inherent sources of rotor-bearing damping are usually adequate to deal with any sub-harmonic whirls which occur. At all speeds away from the critical, the synchronous unbalance whirl is inherently stable, irrespective of friction damping. This may be as in the following demonstration.

Consider the undamped, flexible, single-disk rotor shown in Figure 3.01. It has been shown in Chapter 3. that the points OEG lie in the same radius for this case. For  $\omega < \omega_c$  a radial force balance gives:

$$m\omega^2 [r + a] = kr \quad (5.1)$$

Now let a small disturbance be impressed on the equilibrium condition such that the variables  $r$  and  $\omega$  become  $r + \Delta r$  and  $\omega + \Delta\omega$ . All other system properties remain constant. This gives

$$m [\omega + \Delta\omega]^2 [(r + \Delta r) + a] = [k r + \Delta r]$$

or

$$\Delta r \left[ \omega_c^2 - \omega^2 \right] + \left[ r (\omega_c^2 - \omega^2) - a\omega^2 \right] = \Delta\omega \left[ 2\omega(r + a) \right] \quad (5.2)$$

The terms in square parentheses are constant. This means that if  $\Delta\omega = 0$ ,  $\Delta r$  must also be zero for equilibrium, and so there can be no radius increase without a corresponding increase in speed. Each speed has a definite equilibrium whirl

radius which the system will seek if displaced and, hence, the system is stable. The above demonstration ignores Coriolis forces, but is a reasonable illustration if the radius increase is considered to take place slowly.

#### Above the Critical Speed $\omega > \omega_c$

A similar demonstration indicates that the system is also stable above the critical speed for small displacements. The points OGE lie along the same radius as shown in Figure 3.04c. A force balance gives:

$$m\omega^2 [r - a] = kr$$

or

$$\Delta r [\omega^2 - \omega_c^2] + \Delta \omega [2\omega(r - a)] = - [r [\omega^2 - \omega_c^2] - a\omega^2] \quad (5.3)$$

The terms in the square parentheses are constant and positive — except quite close to  $\omega_c$ . Therefore, when  $\Delta \omega = 0$ ,  $\Delta r$  must also equal zero. For  $\Delta r$  to be a positive increase in radius,  $\Delta \omega$  must be negative, i.e., the speed must decrease. Again, each speed has a definite equilibrium whirl radius, and the system considered is stable.

A rigorous investigation of stability above the critical speed for this system has been made by Foppl (Ref. 97) and is quoted by Stodola (Ref. 18).

#### Stability at the Critical Speed $\omega = \omega_c$

The equations of motion for a simple undamped rotor given in Chapter 3 are:

$$\begin{aligned} m\ddot{x} + kx &= m\omega^2 \cos \omega t \\ m\ddot{y} + ky &= m\omega^2 \sin \omega t \end{aligned} \quad (3.02)$$

If  $\omega = \omega_c$ , the steady-state solutions are:

$$\begin{aligned} x &= + \frac{1}{2} a \omega_c t \sin \omega_c t \\ y &= - \frac{1}{2} a \omega_c t \cos \omega_c t \end{aligned} \quad (3.09)$$

These expressions apply to a logarithmic spiral with radius increasing with time. The undamped rotor is, therefore, inherently unstable at its critical speed. The instability manifests itself as a steady growth in the whirl radius, proportional to the degree of residual unbalance in the rotor. A finite time is, therefore, required for the dangerous effects of this instability to become manifest.

### Stability of a Damped Rotor in Rigid Bearings

A rotor in which the damping is predominantly viscous in nature may experience large amplitude whirling, but the motions themselves will always be stable. This is explained by the nature of viscous friction, in which the force is generated by the relative motion, and always acts in opposition to it. Thus, the viscous friction force opposes the shaft rotation at all times; it never tends to drive the rotor, radially or tangentially. The viscous friction force depends on velocity, and hence, it increases linearly with the whirl radius to oppose any amplitude growth.

The rotor equations for the simple unbalanced rotor with viscous damping are Equations 3.10. Combining these using  $r = x + iy$  give the shaft center equation:

$$m\ddot{r} + b\dot{r} + kr = m\omega^2 e^{i\omega t} \quad (5.4)$$

The solution to this equation is:

$$r = A \exp \left[ -\frac{b}{2m} t \right] \cdot \exp \left[ i \sqrt{\omega_c^2 - \frac{b^2}{4m^2}} \cdot t \right] + B \exp \left[ -\frac{b}{2m} t \right] \cdot \exp \left[ -i \sqrt{\omega_c^2 - \frac{b^2}{4m^2}} \cdot t \right] + \frac{\Omega^2 e^{i\omega t}}{\sqrt{(1-\Omega^2)^2 + \left(\frac{c\omega}{m\omega_c}\right)^2}} \quad (5.5)$$

The whirl radius is stable if it possesses no positive-real time exponents to cause either the transients or the steady-state solution to grow with the passage of time. The exponents are reviewed in the following table.

Term	Exponent	Properties	Stability Comment
First Transient	$-(\frac{b}{2m})$	Negative, real	Stable, Amplitude decays with time. Independent of speed.
First Transient	$1 \quad (1-\Omega^2)^2 + (\frac{c\Omega}{2m\omega_0})^2$	Positive, Imaginary	Stable. Harmonic variation of ampli- tude with time. Varies with speed.
Second Transient	$-(\frac{b}{2m})$	Negative, real	Stable. Amplitude decays with time. Independent of speed.
Second Transient	$-1 \quad (1-\Omega^2)^2 + (\frac{c\Omega}{2m\omega_0})^2$	Negative, Imaginary	Stable. Harmonic variation of ampli- tude with time. Varies with speed.
Steady-State	$i\omega$	Positive, Imaginary	Stable. Harmonic variation of ampli- tude with time. Varies with speed.

Thus, the transients both decay with time, while the steady-state whirl remains constant in amplitude for any given speed. If the speed is varied, the amplitude also varies, passing through a zone of finite maximum amplitude at the system bending critical speed.

#### Influence of Internal Friction on Rotor Stability

The rotor dynamic aspects of internal friction have been discussed in Section 3. This part of Section 5 concerns the stability of a simple, balanced rotor in rigid bearing and indicates in greater detail the mechanism by which the whirl-inducing tangential force,  $F$ , occurs. The stability of a simple rotor with internal friction damping is then examined from the solution to the equations of motion.

The presence of a tangential force arising from elastic hysteresis of the material during motion may be demonstrated by considering a simple balanced vertical rotor in rigid bearings, Figure 5.03a. For an elastic shaft of spring

constant  $\alpha$ , a displacement,  $r$ , from the equilibrium position corresponds to a displacing force,  $F_c$ , acting on the disk such that:

$$r = \alpha F_c \quad (5.6)$$

Due to  $F_c$ , the shaft is bent and the convex surface ABC is in tension while the concave surface CDA is in compression. The neutral axis is AC. If the shaft is now rotated with speed  $\omega$  about E; while the plane of bending containing E does not rotate, the shaft material will be subjected to cyclically varying stresses due to its rotation in the displaced condition. As the material is not perfectly elastic, the distribution of bending stresses over the shaft cross section is not independent of the rotation, but is influenced by the hysteretic lag in strain between the loading and unloading portions of the hysteresis cycle, shown in Figure 3.12. As a surface element rotates from A to C, its flexural stresses change from tension to compression, along the lower portion of the ABC. As the cycle is completed, the stress reverses along the upper portion of the loop CDA. Due to material hysteresis, the tensile stress falls to zero where positive strain still acts at B'. The half-cycle is completed to full compressive stress at C. A similar condition occurs during the remaining half-cycle as the compressive stress falls to zero with a negative strain acting at D'. This has the effect of shifting the angular position of the neutral axis from BD to B'D'. Observe that the same effect would be produced with a perfectly elastic shaft if a small force, Q, acted on the shaft at point B as shown — together with the deflecting force, P. To evaluate Q note that the work done by this force per whirl revolution of the shaft is:

$$W = 2\pi r.Q \quad (5.7)$$

This is equal to the energy loss, E, per cycle due to hysteresis. Recalling that this loss is proportional to the square of the limiting cyclic amplitude and independent of frequency gives

$$E = 2\pi D r^2 \quad (5.8)$$

where D is a constant which depends on the hysteresis characteristic of the shaft material. Equating W and E gives

$$Q = Dr \quad (5.9)$$

This is the value of the tangential force required to prevent whirling of the shaft about O. It is proportional to the radial displacement and depends on the properties of the shaft material in the case of elastic hysteresis and on the stick-slip Coulomb friction characteristics of the joints in the case of a built-up rotor. If this restraining force is removed, the rotor is free to whirl about the undeflected shaft axis.

Consider the case where the rotor is whirling freely about O with angular velocity,  $\nu$ , where  $\nu < \omega$  — the shaft rotational speed. The whirl configuration is shown in Figure 5.03b. The coordinates of E, coincident with G in a balanced rotor, are

$$\begin{aligned} x &= r \cos \phi \\ y &= r \sin \phi \end{aligned} \quad (5.10)$$

The equation of motion for the disk in stationary coordinates are

$$\begin{aligned} m\ddot{x} &= -kx - Q \sin \alpha \\ m\ddot{y} &= -ky + Q \cos \alpha \end{aligned} \quad (5.11)$$

From the previous  $Q = Dr$ , substituting gives

$$\begin{aligned} m\ddot{x} + kx + Dy &= 0 \\ m\ddot{y} + ky - Dx &= 0 \end{aligned} \quad (5.12)$$

These equations are coupled and may be solved simultaneously by taking a solution of the form

$$\begin{aligned} x &= x_0 e^{i\Lambda t} \\ y &= y_0 e^{i\Lambda t} \end{aligned} \quad (5.13)$$

This leads to the characteristic equation

$$\Lambda^4 - 2k\Lambda^2 + (k^2 + D^2) = 0 \quad (5.14)$$

This is a quartic in  $\Lambda$ , the roots of which are complex and may be written

$$\Lambda_1 = \lambda + i\alpha_1$$

$$= \pm \left[ \frac{-k}{m} \pm i \frac{D}{m} \right]^{\frac{1}{2}}$$

Thus

$$\lambda = + \frac{\sqrt{-k + \sqrt{k^2 + D^2}}}{2m}$$

$$\alpha_1 = + \frac{\sqrt{k + \sqrt{k^2 + D^2}}}{2m}$$

The solution to Equation 5.12 is therefore:

$$x = Ae^{\lambda t} \cos(\alpha_1 t + \phi_1) - Be^{-\lambda t} \cos(\alpha_1 t + \phi_2)$$

$$y = Ae^{\lambda t} \sin(\alpha_1 t + \phi_1) + Be^{-\lambda t} \sin(\alpha_1 t + \phi_2) \quad (5.15)$$

where  $A, B, \phi_1$  and  $\phi_2$  are constants to be determined. Observing that force  $Q$  is always small compared with  $P$ , it follows that  $(\frac{D}{k})$  must also be small. This leads to the approximations:

$$\lambda = \frac{D}{2\sqrt{km}} \quad ; \quad \alpha_1 = \sqrt{\frac{k}{m}} = \omega_c$$

The second expression shows that the internal friction whirl takes place at a constant speed which coincides with the critical speed of the rotor. As the speed of rotation,  $\omega$ , must be greater than the whirl speed,  $\nu$  ( $=\omega_c$ ), for the force  $Q$  to drive the shaft around the whirl orbit, this means that the shaft will tend to whirl at speeds above the rotor critical speed. Also, the exponent  $\lambda$ , in the first exponential is positive, indicating growth of the whirl amplitude with time.

The results of the above indicate that a perfectly balanced rotor will not whirl at speeds below the critical since the damping force is constant and acts in opposition to the whirl motion. Above the critical speed, the rotor whirls with increasing amplitude, unless restrained by some other effect such as viscous

friction. The whirl frequency is independent of speed of rotation and occurs at the bending critical speed of the rotor.

Internal friction whirl has been particularly troublesome in the case of built-up rotors with inadequate interference fits between disks and shaft. It has also occurred in electrical machinery with laminated cores. This whirl motion can be minimized by providing tight contact between the mating surfaces, the length of which should be kept to a minimum, (see Figure 5.04). Kimball and Lovell (Ref. 23) and Newkirk (Ref. 54) have discussed this problem in detail. In a given machine, internal damping is rarely the only source of damping, although it may be the largest source for small amplitude motions. Both bearing friction and viscous drag of the surrounding fluid are also present. Both these effects are dissipative and uni-directional and depend on speed. Eventually, an equilibrium whirl configuration may form between all system forces at a finite radius.

#### Whirling of a Shaft with Unsymmetrical Stiffness

While the majority of rotors have axial symmetry in their stiffness properties, there are certain important types such as two-pole turbogenerator rotors where the stiffness properties of the cross section are not symmetrical. This asymmetry affects the rotor whirl motion and gives rise to two critical speeds corresponding to the individual stiffnesses, between which the motion is unstable unless the system possesses sufficient viscosity. This effect has been studied by Stodola (Ref. 18), Robertson (Ref. 28), Taylor (Ref. 76), Foote, Poritsky and Slade (Ref. 77) and others. These authors have observed the following characteristic features in the rotor motion:

1. The rotor has two critical speeds corresponding to the two principal stiffness values of the cross section. Where the rotor mass is distributed throughout its length, two critical speeds occur in the vicinity of the symmetrical rotor criticals.
2. Between the two critical speeds the motion is unstable, and whirl amplitude tends to increase with time.
3. Rotor whirl stability between the critical speeds does not depend on the degree of rotor unbalance, and stability cannot be conferred on the system by more refined balancing.

4. Whirl amplitude below the first critical and above the second critical depends on the level of rotor unbalance.
5. The whirl frequency is constant between the two critical speeds.
6. Viscous friction damping reduces the whirl amplitude, and where sufficient, viscous friction is present, the whirl motion between the critical speeds becomes stable. Coulomb friction has the reverse effect, and tends to promote instability.
7. Sub-harmonic critical speeds occur at  $\frac{\omega_1}{2}$  and  $\frac{\omega_2}{2}$ . For moderate stiffness inequality, the proximity of these sub-harmonics, particularly when influenced by friction, gives rise to a single sub-harmonic critical amplitude peak.

The motions of a damped, unbalanced, single-disk rotor with dissimilar lateral stiffnesses have been considered in Section 3 and expressions for amplitude response and phase angle have been obtained. The following stability analysis considers the undamped, perfectly balanced, single-disk rotor in rigid bearings, to determine the conditions of inherent instability. Designate the shaft natural frequencies  $\omega_1$  and  $\omega_2$  corresponding to vibrations in the two lateral principle directions, such that

$$\omega_1^2 = \frac{k_1}{m}, \quad \omega_2^2 = \frac{k_2}{m}$$

Let the rotating axis be  $\xi, \eta$ , and let these directions correspond with the planes of maximum and minimum stiffness, as shown in Figure 5.05. Writing the rotor whirl radius as

$$r = \xi \bar{i} + \eta \bar{j} \quad (5.16)$$

where  $\bar{i}, \bar{j}$  are unit vectors in the  $\xi, \eta$  directions, gives the radial acceleration of the disk c.g. as

$$\ddot{r} = \left[ \ddot{\xi} - 2\omega\dot{\eta} - \omega^2\xi \right] \bar{i} + \left[ \ddot{\eta} + 2\omega\dot{\xi} - \omega^2\eta \right] \bar{j}$$

The equations of motion, Figure 5.05b, for a simple undamped rotor become, on substituting the above,

$$\begin{aligned} m \left[ \ddot{\xi} + 2\omega\dot{\eta} - \omega^2\xi \right] &= -k_1\xi \\ m \left[ \ddot{\eta} + 2\omega\dot{\xi} + \omega^2\eta \right] &= -k_2\eta \end{aligned} \quad (5.17)$$

These equations have constant coefficients, but the variables  $\xi, \eta$  are not separable. Selecting a solution of the form:

$$\xi = \xi_0 e^{\Lambda t}, \quad \eta = \eta_0 e^{\Lambda t} \quad (5.18)$$

leads to the characteristic equation:

$$\left[ \Lambda^2 - \omega^2 + \omega_1^2 \right] \left[ \Lambda^2 - \omega^2 + \omega_2^2 \right] + 4\omega^2\Lambda^2 = 0 \quad (5.19)$$

This is a quadratic in  $\Lambda^2$ . The motion of the disk will be stable when both roots are negative. Writing Equation 5.19 as

$$\Lambda^4 + 2b\Lambda^2 + c = 0 \quad (5.20)$$

where

$$b = \omega^2 + \frac{\omega_1^2 + \omega_2^2}{2}$$

$$c = (\omega_1^2 - \omega^2)(\omega_2^2 - \omega^2)$$

gives the roots as

$$\Lambda^2 = -b \pm \sqrt{b^2 - c} \quad (5.21)$$

Substituting leads to the conclusion that the radicand is always  $> 0$ , and so the roots are always real. If  $c$  is positive, then both roots are negative; if  $c$  is negative, some roots of Equation 5.20 will also be positive, giving unstable motions. This occurs when

$$\omega_1^2 < \omega^2 < \omega_2^2$$

This result leads to the conclusion that the speed range between the two critical speeds corresponding to the maximum and minimum transverse stiffnesses is unstable for an undamped rotor. In this range, the rotor whirl amplitude will grow steadily with time unless otherwise restrained. This instability has been shown to be independent of the residual unbalance of the rotor; but, as this unbalance may promote synchronous rotor whirl amplitude growth at all speeds below the upper critical,  $\omega_c$ , the greater residual rotor unbalance, the more rapidly will the unstable rotor amplitude grow. As in the case of a simple rotor at its critical speed, the whirl amplitude growth path within the unstable range is an increasing spiral, Figure 3.06. At speeds below the first critical, the rotor motion is a stable synchronous whirl; and at speeds above the second critical, the rotor is again stable with the c.g. between the whirl axis and the elastic center.

These conditions apply to the undamped rotor. The presence of viscous friction in the system tends to stabilize these motions and to limit the whirl amplitude between the two critical speeds. If the rotor also has hysteretic damping, this tends to promote instability above the critical speed as noted previously. The combined effect of viscous and hysteretic damping on the motions of such a rotor within the unstable range depends on the extent of each damping present.

### Hydrodynamic Instability

Rotors which operate in fluid-film bearings are susceptible to a particular form of instability in which the journals of the rotor whirl within the bearing clearance. The severity of this whirl may range from a mild increase in rotor amplitude to a vigorous and growing oscillation which is capable of destroying the bearing, if allowed to persist. In this latter case, further increase in machine speed is impossible, and so the speed at which this hydrodynamic whirl sets in represents an upper limit for machine operation. This whirl is a property of the rotor-bearing system alone, and occurs independently of the state of balance of the rotor.

The hydrodynamic stability of a rotor in its bearings at a given speed depends on the operating eccentricity and the type of bearing used. In general, high operating eccentricity ratios are conducive to stable operation; whereas low eccentricities, as in a vertical rotor, are not. High speeds decrease the operating eccentricity of hydrodynamic bearings, and so a speed exists, known as the threshold of instability, beyond which the rotor begins to whirl with a frequency  $\nu$  which is usually somewhat less than half its speed of rotation. It is common for the threshold of instability to occur around twice the first critical speed of the rotor-bearing system.

Hydrodynamic instability is a known operating hazard with both hydrodynamic and hybrid gas bearings, although external pressurization considerably extends the speed range over which stable operation is possible. As the rotor is usually very rigid compared with the gas film, it is the film stiffness which determines the whirl threshold speed. Gas bearing hydrodynamic instability is commonly referred to as 'half-frequency' whirl for hydrodynamic bearings, and 'fractional-frequency whirl' for hybrid bearings.

Liquid-film hydrodynamic bearings may also become unstable, particularly where the lubricant viscosity is low, as in the case of water and mercury. Hydrostatic liquid bearings are stable throughout the operating range of all present-day rotating machinery. For liquid-lubricated bearings, hydrodynamic instability is usually referred to as resonant whipping, although other titles such as oil whip, resonant fluid-film whipping, are sometimes used.

Circular cylindrical bearings have inherently poor hydrodynamic stability properties. Tilting-pad bearings have the best stability properties of all bearing types, as the pad tilting allows the bearing to 'follow' the rotor oscillations, and so preserve the rotor force: film force equilibrium required for stability. This type of bearing loses its stability when the pad 'flutters' and fails to follow, at extremely high speeds. Elliptical bearings, offset bearings, two and three-lobe bearings are other types with good stability properties.

#### Mechanics of Hydrodynamic Instability

In order to clarify the physical phenomena which underlie the problem of hydrodynamic stability, the forces which give rise to the motion will first be considered.

##### Vertical rigid rotor

First consider the rigid rotor shown in Figure 5.06 which operates in vertical, plain cylindrical bearings with the clearance space filled with lubricant. Hydrodynamic action confers both stiffness and damping properties on the bearings, and so the rotor is capable of two types of whirl motion, translatory and conical, as shown in Figure 4.01. For simplicity, the following remarks are confined to the translatory mode.

If a constant load,  $W$ , is applied to the rotor, it will adopt a steady-state equilibrium position as shown in Figure 5.06a in which the rotor is displaced a small distance  $OG$  from the bearing center. Hydrodynamic action within the convergent portion of the fluid-film gives rise to a pressure distribution. The force component  $F$  of this pressure distribution acts through  $G$  and is sufficient to support the applied load,  $W$ , without the journal touching the bearing surface. The angle between the line of centers and the load balance is  $\phi$ , the attitude angle. Consider now the case where the vertical shaft is not loaded, but is displaced an identical distance  $OG$ , for example, by a blow. Hydrodynamic action again generates the force component  $F$  through  $G$ . But no steady-state equilibrium may result in this case, and so force  $F$  tends to drive the rotor into an orbit around the bearing center. As long as  $O$  and  $G$  are not coincident with the rotor

motionless, a driving force will continue to be generated by the relative displacement, as shown in Figure 5.06b and the whirl will continue. Since both the hydrodynamic action and the whirl motion generate friction forces which oppose motion, bearing stability and whirl radius, both depend on the damping characteristics of the system.

#### Horizontal rigid rotor

A situation similar to the vertical rotor case exists except that the static equilibrium condition is as shown in Figure 5.07a. Here, the rotor is displaced a distance OG from the bearing center and the fluid-film pressures support the rotor weight, W, through the component F. If now the rotor center is given a second displacement to G', the fluid-film force F' corresponding to the new film shape will no longer exactly balance W. The force balance may be thought of as shown in Figure 5.07b where  $F' = F + F''$  and  $F = W$  as before. The component F'' which cuts through G is therefore, free to promote whirling of the rotor about G. The nature of the motion which follows is again determined by the damping properties of the fluid film.

#### Rigid Rotor in Fluid-Film Bearings

The influence of bearing stiffness and damping properties on the rotor motions is most significant where the rotor is rigid, as then these properties alone determine the rotor amplitude and stability during operation. The possibility of instability due to the fluid-film was recognized by Stodola (Ref. 18) and was investigated by his co-worker Hummel (Ref. 98). Their analysis is based on the assumption that the eccentricity locus is a semi-circle. By examining the nature of the geometry of an arbitrary displacement from the equilibrium operating position expressions for the x,y coordinate stiffnesses of the fluid-film were obtained. Substituting in the equations of motion then led to a stability equation which was examined for real root, corresponding to unstable (amplitude-increasing) operating conditions.

The results indicated that for any operating eccentricity ratio  $\epsilon > 0.65$ , two frequencies existed for which the motion would be unstable. For eccentricities below 0.65, Hummel found the motion inherently unstable, and therefore did not consider this region further. This region has since been investigated by Cameron (Ref. 99) who found a single threshold frequency for instability rather than the inherently unstable domain inferred by Hummel. Cameron and Solomon (Ref. 100) experimentally confirmed the existence of the predicted low-eccentricity instability threshold for  $\epsilon$ -values down to 0.18. The correlation of this theory with half-frequency whirl is a deduction from practice and not a consequence of the analysis which sheds little light on the mechanics of fluid-film whirl. Further extension of this approach to cover flexible rotors has been made by Parzewski and Cameron (Ref. 101).

This method is simple and direct and the results have been formulated as a stability threshold chart. Experimental correlation is quite good as far as it goes. At both high and low eccentricities, grave inaccuracies are to be anticipated due to the omission of damping from the analysis. At low eccentricities the results predict a high (or infinite) stability threshold frequency whereas it is well known that in this condition most bearing types have serious instability problems. This condition is important in predicting the performance of vertical machines. At high eccentricities, the complex interaction between bearing stiffness and damping cannot be neglected, and the damping term alone may become very large. Most large horizontal rotors operate with eccentricities within the Hummel limits  $0.65 < \epsilon < 1.00$  where this shortcoming is manifest. The upper frequency threshold predicted by the theory is of no practical significance. Once whirling has been initiated, operation at higher speeds is rarely possible as the resulting large-amplitude motions violate the assumptions upon which all linear analyses rest, and further analysis must therefore include the neglected non-linearizing terms. In practice, only in rare instances has it been possible to pass through the range of resonant whipping with liquid bearings, and never with gas bearings. The approach used in these papers has since been superseded by more accurate and more general methods, and their value lies in providing rapid approximate answers within the range  $0.2 < \epsilon < 0.8$ , in cases where the cavitation status of the bearing is known and where the eccentricity locus is known to be approximately semi-circular.

Newkirk and Taylor (Ref.55) describe the first recorded practical encounter with whirling which is significantly influenced by the bearing fluid-film properties. In a series of experiments it was shown that the rotor whirled within its bearings with a frequency somewhat less than half the speed of rotation, and that the whirl became resonant above twice the system critical speed. This latter is the resonant whipping condition, and most subsequent experimental investigations with liquid-film bearings have been concerned with bearing developments which would suppress it, or extend the range of stable operation. These developments are discussed later under investigations of the resonant whipping condition. Newkirk and Taylor detected the rigid-body whirl motions, which they called oil-film resonance. These motions received no further attention at that time as their amplitudes were small, due to damping, compared with the resonant whip amplitudes.

The first attempt to investigate the motion of a rigid journal within a bearing using hydrodynamic theory was made by Harrison (Ref.102), who derived expressions for the radial and tangential components of the fluid-film force due to the journal displacement. These expressions are based on the Reynolds' assumptions, and apply to an infinitely-long, full (no cavitation) bearing using an incompressible lubricant, as follows:

$$\begin{aligned} F_{\theta} &= \frac{12\pi \mu a^3}{c^2} \cdot \frac{\epsilon}{(2 + \epsilon^2)(1 - \epsilon^2)^{1/2}} \cdot (\omega - 2\Omega) \\ F_r &= - \frac{12\pi \mu a^3}{c^3} \cdot \frac{1}{(1 - \epsilon^2)^{3/2}} \cdot \frac{de}{dt} \end{aligned} \quad (5.22)$$

where  $a$  is the journal radius,  $c$  is the radial clearance,  $e$  is the radial displacement of the journal center, and  $\epsilon$  is the eccentricity ratio ( $e/c$ ).

For a stationary journal center  $F_r$  reduces to zero while:

$$F_{\theta} = \frac{12\pi \mu a^3}{c^2} \cdot \frac{\epsilon}{(2 + \epsilon^2)(1 - \epsilon^2)^{1/2}} \cdot \omega \quad (5.23)$$

This constitutes a force on the journal which is perpendicular to the displacement of the center, urging it to whirl in the direction of rotation. In practice, both radial and tangential force components have been shown to exist simultaneously. The discrepancy arises from the Sommerfeld assumptions which neglect the influence of cavitation. In the case of a full cylindrical vertical bearing, the theoretical conditions are all present and the prediction of

whirl instability from zero speed upwards is realized in this case, see Boeker and Sternlicht (Ref. 103). Robertson (Ref. 52) reconsidered Harrison's case, and indicated the omission of radial motion effects on the tangential component of surface velocity. This is considered negligible by Poritsky (Ref. 104). Robertson deduced that the journal has an inherent tendency to whirl with a frequency equal to half the speed of rotation. This work also contains the shortcomings associated with infinitely-long full cylindrical bearing theory, and so only applies to vertical bearings operating at small eccentricities.

Hagg (Ref. 71) collated the then-existing knowledge of the problem, and pointed out several important features requiring incorporation into the quest for a meaningful stability criterion which would reconcile the experimentally observed effects with the available simple theory and its unacceptable prediction of inherent instability. Considering the continuity conditions for a journal whirling with a full film, the amount of fluid passing some point A, Figure 5.08, must equal the volume passing point B plus the volume required to fill the void left by the receding journal. For zero side leakage it follows that

$$\frac{a\Omega}{2} (c + a) = \frac{a\Omega}{2} (c - a) + 2a\omega c \quad (5.24)$$

and hence  $\omega = \frac{\Omega}{2}$

This establishes that the whirl speed is related to the speed of rotation as shown correlating the result obtained by Robertson (Ref. 52). Hagg further discussed the stability of a rigid rotor in fluid-film bearings, considering the system equations of motion.

$$m\ddot{x} + c\dot{x} + k_1x - D_1y = 0 \quad k_1D_2 : x \text{ direction} \quad (5.25)$$

$$m\ddot{y} + c\dot{y} + k_2y + D_2x = 0 \quad k_2D_1 : y \text{ direction}$$

where  $c$  is the bearing damping constant, and  $k_1$ ,  $k_2$ ,  $D_1$ , and  $D_2$  are the fluid-film stiffness properties. Applying Routh's stability criterion this leads to the result that the system will be stable when

$$(k_1 - k_2)^2 + 2c^2 (\omega_1^2 + \omega_2^2) > 4D_1D_2 \quad (5.26)$$

where  $\omega_1^2 = (k_1/m)$        $\omega_2^2 = (k_2/m)$ .

This expression defines the whirl threshold speed in terms of the operating eccentricity ratio  $e_0$ . This value corresponds to a particular Sommerfeld Number for the particular bearing geometry. An experimental program verified the conclusion  $\omega = \Omega/2$ , but was not extended to cover the stability criterion at that stage, although it had been corroborated with field observations on actual rotors.

Hagg gave a simple evaluation of the damping capacity of a tilting pad bearing, and later, Hagg (Ref.105), gave curves for spring and damping constants for 120 degree partial-arc bearings, together with a simple stability chart. Later work by Hagg and Rankay (Ref.73 and 106) gave more complete data on spring and damping constants for partial-arc and tilting-pad bearings for small-amplitude whirl, determined experimentally. At both low and high Sommerfeld numbers these curves are in error, as in these zones they have been obtained by extrapolation. Accurate values for the cylindrical bearing have been obtained by Sternlicht (Ref.74), for the 150 degree partial bearing by Warner (Ref.34), and for the tilting-pad bearing by Lund (Ref.81). Each of these analyses applies to incompressible lubricants, and may be applied to compressible lubricants at low ( $\alpha < 1.0$ ) compressibility numbers. Hagg and Warner (Ref.72) extended the earlier work on the stability threshold speed, using an electric analog to study the stability limit. This work gave good qualitative correlation with both test results and with data obtained from an industrial turbine set, but the absolute values were often considerably different to the test results. The criterion given above, Equation 5.09, was extended to cover rotor flexibility more completely than in Ref. 71. This is

$$(k_1 - k_2)^2 + \frac{2}{m} \left[ \frac{c_1^2 k_1}{1 + k_1/k_s} + \frac{c_2^2 k_2}{1 + k_2/k_s} \right] > 4 D_1 D_2 \quad (5.27)$$

where  $k_s$  is the rotor spring constant  $m\omega_c^2$ ,  $\omega_c$  is the rigid-bearing rotor critical rad/sec, and  $c_1$  and  $c_2$  are the bearing damping coefficients in the x and y directions respectively. Plotting  $(CN_c^2/g)$  versus Sommerfeld Number S with parameter  $(cN_c^2/g)$  where C is the radial clearance of the bearing, N is the journal rpm, and  $N_c$  is the rotor rigid-bearing critical speed rpm allows the analog stability results to be presented in chart form for 120-degree partial-arc bearings, for  $L/D = 1.0$  and 0.67. Lower  $L/D$  ratios increase the stable operating region, and the effectiveness of a central circumferential groove in raising the stability threshold is explained on this basis. Three bearing types were tested (a) full cylindrical bearing, (b) full bearing with circumferential groove, and (c) 160 degree partial bearing. The speeds at which resonant whipping developed and at which it disappeared differed by an average of ten percent. Typical oscillograms obtained are shown in Figure 5.10, with the rotor whirl frequency  $\omega = 0.43\Omega$ . The upper curve shows a well developed whirl; the lower curve shows transition from whirl to stable running, with decreasing speed. At the stability

threshold the frequency of the resonant whipping corresponds to a natural frequency of the system. Hagg and Warner concluded that this may be either the system bending critical frequency, involving motion of the rotor, bearings and supporting structure; or it may be a rigid-body motion of the rotor on the elastic oil films; or it may correspond to the rigid-bearing rotor critical speed. The frequency in all cases was less than  $0.5\Omega$ , i.e. half rotational frequency. They also concluded that the final question of stability depends on all elements of the system that are involved in the motion, and that factors such as machine alignment, oil supply pressure, oil-film extent, oil-film temperature, and loading may alter the theoretical conditions. It was observed that unbalance vibration usually inhibits resonant whipping. This is equivalent to an increase in bearing operating eccentricity, but may lead to self-excited subharmonic elastic whirling at exactly  $1/2$ ,  $1/3$ ,  $1/4$ , and so on, of running speed. Friction in non-rotating parts may act to give a stable system, whereas friction in rotating parts tends to promote instability. These latter observations endorse the comments on friction and stability made earlier in the present section and in Section 3. Shortcomings in using the simple criterion developed in this work are (a) incomplete formulation as the cross-damping terms are neglected, (b) the criterion is approximate, being based on experimental data. Inaccuracies in its general application are to be expected, and these are evident in the correlation shown.

The basic concepts of the theory of hydrodynamic whirl were given by Poritsky (Ref. 104) who showed that the discrepancy between observed results and those predicted by the Sommerfeld-Harrison infinitely-long full-bearing theory of hydrodynamic lubrication arose from neglecting the cavitated region in the bearing film. Poritsky showed that when a radial force component was included in the equations of motion for a rigid journal, stability was predicted at speeds below the rotor critical speed, while at speeds above twice the critical speed the rotor becomes unstable and whirls at the rotor critical frequency in accordance with observed performance. This led to the stability criterion

$$m\omega^2 \left[ \frac{1}{k_s} + \frac{1}{k} \right] < 4 \quad (5.28)$$

where  $k_s$  and  $k$  are the shaft stiffness and bearing stiffness respectively. Recalling that the critical speed  $\omega_c$  of an elastic rotor on elastic bearings is given by

$$= \left[ \frac{1}{k_s} \right] + \frac{1}{k} = \frac{1}{\omega_s^2}$$

it is evident that the rotor whirl frequency is given by  $(\omega/\omega_s) < 2$ , as given by Hagg (Ref.71). The results are also in agreement with the practical observation that the whirl proceeds in the direction of rotor rotation. Poritsky's analysis neglected the influence of fluid-film damping, and no attempt was made to determine the value of the fluid-film stiffnesses, except to postulate that these would be linear with displacement for small amplitude motions. Later investigations into the elastic and damping properties of the cavitated fluid-film by Boeker and Sternlicht (Ref.103) and by Sternlicht (Ref.74) verified the existence of the radial force component, and also provided values for all four spring and damping-coefficients. When damping is included, the predicted whirl frequency is always less than 0.50, in agreement with practical observations. It is important to note at this stage that the linearization of the bearing forces is valid only where the rotor whirl amplitudes are small within the bearing clearance. This assumption is justified on the grounds that the rotor operates at a stable eccentricity below the whirl threshold speed, and that at the initiation of instability the rotor motions will indeed be small. Large-amplitude non-linear modes have been considered by Huggins (Ref.107). Poritsky also considered briefly the influence of gravity, and displacements due to periodic forces.

Translatory fluid-film whirl of a vertical rigid rotor was investigated experimentally by Boeker and Sternlicht (Ref.103) to define the occurrence of the whirl threshold speed. Correlation of the results with Poritsky's theory was also attempted. Two types of bearing were tested (a) plain cylindrical and (b) grooved shaft in plain cylindrical. Both air and water were used as lubricants. In air, the plain bearing whirled at all speeds, i.e., the whirl threshold speed was zero for this case. The ratio of whirl frequency to shaft rotational frequency ranged from 0.41 to 0.50. When operating with water as the lubricant, the whirl threshold was at 130 rpm with one shaft, and at 220 rpm with another more flexible shaft. With the grooved-shaft plain-bearing combination, whirl commenced at 2700 rpm, and disappeared at 2400 rpm with water as the lubricant. This 'lag' was also observed by Hagg and Warner, as mentioned above. Using the experimental eccentricity locus, (Fig. 5.11),

the stabilizing radial component in the fluid film was observed to be zero for the plain bearing at zero eccentricity. This is the Sommerfeld-Harrison full bearing condition leading to a theoretical zero speed whirl threshold and continued whirling at all speeds beyond. This conclusion is therefore confirmed, and so the plain cylindrical bearing, operated vertically is an inherently unstable bearing. With the modified bearing locus, Figure 5.12, the radial force component at zero eccentricity has a finite value, and hence the rotor motion is stable at zero speed and beyond, up to the whirl threshold. The theoretical analysis given agrees with Poritsky's result, and predicts a whirl threshold speed

$$\omega = 2 \sqrt{\frac{k}{m}}$$

for the rigid rotor, the numerical value of which ranged from 2260 rpm to 2910 rpm, and was between 2400 rpm and 2600 rpm from the slope of the eccentricity locus at the origin. Experimental whirl threshold speed was 2700 rpm. Whirl frequency was slightly less than  $1/2 \Omega$ . These experiments confirmed the Poritsky hypothesis that a stabilizing radial force existed in the fluid film, and indicated that where this was absent, or vanished, the rotor became unstable and whirled at approximately half rotational speed.

The need for data on the dynamic properties of bearings was met by Hagg and Sankey as noted previously, and by Sternlicht (Ref. 74) who applied the digital computer to the calculation of the spring and damping coefficients  $k_{xx}$   $k_{xy}$   $k_{yy}$   $k_{yx}$ ,  $c_{xx}$   $c_{xy}$   $c_{yy}$   $c_{yx}$  of a plain cylindrical bearing for the case of an incompressible lubricant, recognizing that the motion of the journal center was governed by the equations:

$$\begin{aligned} m\ddot{x} &= k_{xx}x + c_{xx}\dot{x} + k_{yx}y + c_{yx}\dot{y} + G \cos(\omega t + \phi) \\ m\ddot{y} &= k_{yx}x + c_{yx}\dot{x} + k_{yy}y + c_{yy}\dot{y} + G \sin(\omega t + \phi) \end{aligned} \quad (5.29)$$

where  $G$  is a rotating force applied to the rigid rotor. In previous analyses the cross-coupled damping terms had been neglected. Sternlicht solved the Reynolds' equation using a finite-difference procedure, for a finite-length bearing, and gave curves showing the variation of the dynamic coefficients as functions of eccentricity  $e$  and  $L/D$  ratio. Both stiffness and damping increase with increase in eccentricity and  $L/D$ . The direct damping coefficients were shown to be of magnitude comparable to the bearing elastic forces, while the cross-coupling damping terms were small.

The application of the computer to problems of rotor-bearing dynamics has since

made possible the solution of many other cases of incompressible and compressible lubrication which are insoluble in closed form. It has also led to the development of several sophisticated analytical approaches such as the Galerkin and linearized ph methods which are capable of solving the stability problem at high eccentricity ratios which would involve an impractical amount of computing time by standard finite-difference procedures. The incompressible dynamic properties of the cylindrical, 4-axial-groove, elliptical and three-lobe bearings have been computed by Sternlicht (Ref.74); the 150 degree partial arc bearing has been computed by Warner; and the tilting pad bearing has been analyzed and calculated by Lund (Ref.81). Properties of the cylindrical bearing and the tilting pad bearing in the turbulent range have been obtained by Orcutt, Ng and Arwas (Ref. 15 and 16).

In the same period as the above development took place, a number of other experimental studies were carried out in an attempt to clarify knowledge on hydrodynamic whirling of rigid and elastic rotors. The non-whirling bearing developed by Newkirk and Grobel (Ref. 56) suppressed rotor vibrations by inducing pressure build-up within the cavitated zone of the bearing, thus preloading the journal and forcing it to run at a higher eccentricity within the bearing. This work provided a cure for a specific application, but revealed little new information about the nature of the problem. A more complete study of the parameters involved in rotor whirling was undertaken by Newkirk and Lewis (Ref.108). With three rotors and five bearings tests were run with oil at various viscosities to determine conditions defining a range of stable operation with cylindrical bearings at speeds above twice critical. It was concluded that short bearings, rather large clearance ratios and moderate unit bearing loads favor a wide range of stable operation. In certain instances, this may extend up to more than five times critical speed. Slight misalignment resulted in a remarkable increase in the stable range. The stable range was never clearly defined with the rotors and test conditions considered, since a jar would cause the severe disturbance to build up at a lower speed in most instances. In a subsequent paper, Newkirk (Ref. 109) reviewed results obtained earlier with a flexible rotor carrying a heavy central disk midway between its bearings, with a unit bearing load of 42.5 psi, and a lowest critical speed (presumably for the system) of 1210 RPM. Within the speed range 2300 to 5000 RPM the rotor whirl with a frequency around 1250 RPM. The severity of the whirl increased with

increasing speed. This result was compared with results obtained with a very stiff rotor for which there was no discernible (bending) critical speed up to 30,000 RPM. The unit bearing load was about 4 psi. This shaft whirled at low speeds with a frequency slightly less than one-half the running speed. It was also noted that the whirl died out at higher speeds, varying from 7000 RPM to 18,000 RPM. Low viscosity oil gave the higher limit. Newkirk concluded correctly that rotor flexibility was the key factor in explaining why the performance of these two machines was so different. He observed that the first rotor whirling was a resonant condition. This was true resonant whipping. However, the conclusion that the motion of the stiffer rotor is 'non-resonant' is not precise. The low unit loading corresponds to a low eccentricity ratio which would induce a rigid body whirl within the bearings at low speed. This is the rigid body instability corresponding to resonant whipping and is induced by the rotor speed exceeding twice the critical speed of the rigid rotor in elastic bearings. It may, therefore, be compared with the investigation made by Sternlicht (Ref.103) for a vertical rotor.

Pinkus (Refs.111 and 112) conducted an experimental study of two rotors having relatively light bearing loads (23.4 psi and 8 psi respectively) and reasonably high critical speeds (4000 and 6100 RPM respectively). The objective was to compare the relative stability of several bearings and included plain cylindrical bearings, axial groove bearings, elliptical bearings, 'pressure' bearings, three-lobe bearings, tilting pad bearings, and hydraulically loaded bearings. He observed that the cylindrical bearings were least stable and the hydraulically loaded bearings were most stable and that with sufficiently high hydraulic pressure, all whipping can be suppressed. Amplitude-speed results obtained in this investigation are shown in Figure 5.13. With the more flexible shaft, the initial amplitude peak corresponds to the rotor unbalance whirl. Resonant whipping sets in at approximately 1.6 times the system bending critical speed, persists with a whirl frequency equal to the critical speed, and tends to disappear around 3.5 times critical speed. The large amplitude build-up in that zone is the second system bending critical speed. The stiffer shaft shows an unbalance whirl peak followed by a steady build-up to full whipping amplitude around three times the system bending critical speed, with no tendency for the whirl to diminish in this case, up to four times the bending critical. The shaft resonant whipping frequency was the system bending critical speed throughout.

Any sub-critical whirling is due to rotor unbalance, occurring at synchronous speed. In this investigation the rotor flexibility is the predominant factor in determining the nature and position of the resonant whipping. No rigid body modes were detected, probably because the bearing stiffness was high compared with rotor stiffness. Thus, the bearings contribute little to determining the location of the whirl threshold speed, but the type of bearing used determines whether whipping will appear or not. Pinkus also noted that higher viscosity oils tended to eliminate whipping. Other investigators (notably Newkirk and Lewis), found the reverse. It seems that both results could be correct as the Sommerfeld Number and the spring and damping properties are the real parameters to be considered. It was confirmed that reduced oil flow eliminates whipping. This induces long operating viscosity, as does a higher clearance bearing which also diminishes the tendency to whirl. Lewis and Fulton (Ref.112) considered flexible rotors and confirmed the higher damping of a more viscous oil in this case, but not the disappearance of whipping at 3.6 times critical speed. Instability always occurred at approximately twice critical speed. This is probably due to near-constant bearing stiffness properties in this instance. Newkirk (Ref. 58) surveyed the available information on journal bearing instability at that time, and compared the Pinkus and Lewis-Fulton results. The conclusions drawn by him are valid, except that half-frequency whirl and resonant whipping are both instability phenomena of which resonant whipping is sustained at the system bending critical speed with flexible rotors because of the inherent tendency for the system to whirl at this speed. The doubtful suggestion regarding half-frequency whirl being damped, and resonant whipping being stimulated by higher oil viscosity is opposed to Pinkus' result. Further investigation would be needed to clarify the situation regarding the effect of oil temperature on rotor bearing stability.

The need for accurate data to predict the performance of higher speed gas bearings led to a large number of investigations on the stability of rotors on compressible fluid films. In this case, the lubricant film is continuous (no cavitation), but the compressible Reynolds' equation is non-linear. Static properties for the cylindrical bearing were obtained by Ausman (Refs.113 and 114) first by a perturbation technique applicable to small eccentricities, and secondly by the 'linearized ph' method which allowed larger eccentricities to be considered. Elrod and Burgdorfer (Ref.115) refined the perturbation method by

using an end-flow factor. Raimondi and Boyd (Ref. 116) and Sternlicht (Ref. 117) used a numerical finite difference method and obtained an iterative solution. This approach has the advantages that (1) the iterations can be continued to give results of any desired accuracy, and (2) the iterative program is directly applicable to bearing geometries other than plain cylindrical. On the other hand, the computing time required to do this is considerable. Each of these methods has given results for load capacity, eccentricity, attitude angle, and friction force.

The limiting factor in the use of gas bearings in high speed applications is half-frequency whirl stability of the journal with the bearing. In most applications the whirl threshold speed represents an upper limit for speed at which the rotor may be operated, as half-frequency whirl, once established, rapidly leads to failure of the bearing by seizure. In order to predict the whirl threshold speed, data on the dynamic bearing properties is required. This data is needed to prepare specific bearing designs, and to compare the suitability of one bearing type with another, for a given application. Sternlicht (Ref. 117) analysed the cylindrical bearing using a "quasi-static" method of solution which was an extension of the numerical finite-difference method employed in Ref. (117). The compressible Reynolds equation for dynamic loading and isothermal conditions is:

$$\frac{\partial}{\partial \theta} \left[ p h^3 \frac{\partial p}{\partial \theta} \right] + R^2 \frac{\partial}{\partial z} \left[ p h^3 \frac{\partial p}{\partial z} \right] = 6 \mu R^3 \left[ \frac{U}{R} \frac{\partial (p h)}{\partial \theta} \right] + 2 V_p + 2 h \frac{\partial p}{\partial t}$$

The last term on the right-hand side of this equation comes from the continuity equation and represents the non-steady flow term. Sternlicht's analysis neglects this term on the grounds that it exerts little effect on the phase angle between restoring force and displacement, and its inclusion greatly complicates the analysis by introducing another parameter for evaluation. The fluid-film force is a function of five parameters:  $\epsilon$ ,  $\epsilon'$ ,  $L/D$ ,  $\Lambda$  and  $\alpha'$ , where  $\epsilon'$  is the time-derivative of eccentricity, and  $\alpha'$  is the dimensionless tangential velocity ( $\alpha/\omega$ ). Results were obtained for the dimensionless force derivatives  $(\partial f_r/\partial \epsilon)$ ,  $(\partial f_t/\partial \epsilon)$ ,  $(\partial f_r/\partial \epsilon')$  and  $(\partial f_t/\partial \epsilon')$  with respect to displacement and velocity for ranges of  $\epsilon$ ,  $L/D$  and  $\Lambda$ .

The time-dependent term  $(\partial p / \partial t)$  requires that the rotor dynamic motion be considered in any rigorous solution to this equation. Sternlicht's quasi-static analysis neglects this term thus uncoupling the lubrication equation from the rotor equations. A method for uncoupling these equations without ignoring the time-dependent effects has been given by Pan (Ref. 119) by assuming that the time-dependence of  $p$  originates from the rotor motion. By supposing that the steady state Reynolds' equation has already been solved such that for each  $L/D$  and steady-state film thickness  $H_0$ :

$$P_0 = P_0(\xi, \theta, \epsilon, \Lambda^*) \quad \xi, \theta: \text{dimensionless rotating coordinates}$$

The time-dependent effects may be considered by a linear perturbation upon  $P_0$  and  $H_0$ , thus:

$$P(\xi, \theta, \tau) = P_0(\xi, \theta) + P'(\xi, \theta, \tau) \quad \tau: \text{dimensionless time}$$

$$H(\xi, \theta, \tau) = H_0(\xi, \theta) + H'(\xi, \theta, \tau)$$

This formulation expresses the dynamic fluid-film pressure as a linear expansion with respect to the radial squeeze-film velocity and the angular whirl acceleration and their time derivatives. Charts of these forces vs  $\Lambda^*$  accompany this work suitable for calculation of dynamic bearing performance and rotor dynamic analysis.

The general problem of stability of rotors in bearings was investigated by Sternlicht, Poritsky and Arwas (Ref. 120). Starting from the assumption that the hydrodynamic bearing forces are functions of the position and velocity vectors of the shaft center, and by treating these forces as constant during a small displacement, these authors obtained stability criteria in terms of the force derivatives with respect to displacement and velocity for small amplitude motions about an equilibrium operation position. The method developed applies to both compressible and incompressible lubricants for any bearing type for which the force derivatives are available. Both rigid and flexible rotors were considered. For small motions, the radial and tangential forces and their derivatives were obtained as functions of  $\epsilon$ ,  $\epsilon'$  and  $L/D$ . The determinantal equation of motion was obtained and examined for conditions under which the

complex frequency  $\nu$  is a pure imaginary number. This indicates a change from a negative (stable) exponent to positive (unstable) exponent in the rotor amplitude,  $e^{\nu t}$ . This analysis is given in the following section on Stability of Small Motions. Equating the real part and the imaginary part of the stability determinant in turn to zero allows the threshold speed ratio  $\delta = \omega/\omega_c$  to be obtained, where  $\omega_c$  is the critical speed of the simple-supported rotor. Tabulated data for the incompressible case in terms of eccentricity ratio, plain bearings and whirl speed ratio is given. This is shown in Table 5.01. The whirl speed ratio is shown also in Table 5.01. A procedure for examining the shaft center locus for large displacement motions of a massless rotor is also included, together with experimental verification of the small motion stability theory.

Rantzeppis and Sternlicht (Ref. 121.) investigated the conditions under which the center of a rigid rotor will remain undisplaced from the equilibrium position, during shaft rotation. To determine the stability bounds, the variational equations of motion were used. These equations are obtained by substituting for the dependent variables radial displacement  $u$  and angular position  $\phi$  of the shaft center the terms  $(\xi_0 + \delta u)$  and  $(\phi_0 + \delta \phi)$ , to obtain the variational equation of motion. If the motion of the shaft center in rotating coordinates is governed by

$$\phi e^{i\phi} = m \left[ (\ddot{\xi} - \dot{\xi}^2) + i(2\dot{\xi}\dot{\phi} + \xi\ddot{\phi}) \right] e^{i\phi} \quad (5.30)$$

where

$$\phi = \phi \left[ \xi, \dot{\xi}, \phi, \dot{\phi}, \omega \right]$$

The variational equations of motion are:

$$\begin{aligned} m\delta\ddot{u} - \phi_{\xi\dot{u}}\delta\dot{u} - (\phi_{\xi u} + m\dot{\phi}_0^2)\delta u - (\phi_{\xi\dot{\phi}} + 2m\dot{\xi}_0\dot{\phi}_0)\delta\phi \\ + (\phi_{\eta} + w \cos \phi_0)\delta\phi = \phi_{\xi\omega}\delta\omega \end{aligned} \quad (5.31)$$

$$\begin{aligned} (2m\dot{\phi}_0 - \phi_{\eta\dot{u}})\delta\dot{u} + (m\ddot{\phi}_0 - \phi_{\eta u})\delta u + m\dot{\xi}_0\delta\dot{\phi} + (2m\dot{\xi}_0 - \phi_{\eta\dot{\phi}})\delta\dot{\phi} \\ - (\phi_{\xi} + w \sin \phi_0)\delta\phi = \phi_{\eta\omega}\delta\omega \end{aligned} \quad (5.32)$$

These equations are linear, and using data from the known "equilibrium" case, the equations may be solved for the variational displacements  $\delta u$  and  $\delta \phi$ . The stability regions bounded by families of load-carrying capacity and operating eccentricity curves, as shown in Figure 5.14, were obtained using the Routh criterion for the quasi-static equilibrium case of a gas-lubricated cylindrical bearing. They show that a minimum zone exists in the stability curves corresponding amongst other things to the worst clearance ratio, at which the stability is a minimum. This conclusion is supported by experimental evidence; see Sternlicht and Winn (Ref.122).

Castelli and Elrod (Ref.123) performed an analysis in which the equation of motion for the rigid rotor and the compressible Reynolds' equation including time-dependent effects were simultaneously integrated on a digital computer to determine the rotor orbital path. The stability or instability of particular cases were established from the growth, stabilization or decay of the orbit. With assumed initial conditions for both the rotor motion and the fluid-film pressure, the influence of incremental displacements on the rotor equations and then on the fluid-film properties were calculated to provide data for the next incremental change. The bearing considered was an infinitely long plain cylindrical bearing, and the Elrod-Bergdorfer (Ref.115) data was used for the equilibrium position about which the perturbations were initiated. This analysis is the most complete solution yet attempted. It provides a basis against which the efficacy of other methods may be evaluated, but for the infinite bearing only. The monumental computational labor involved makes it unsuited for general use. Comparison of this method with other theoretical results and with experimental data is given by Pan and Sternlicht (Ref.124); see later.

Cheng and Trumpler (Ref.125) employed Galerkin's method to solve the non-linear Reynolds' equation with time-dependent effects included. This method reduces the partial differential equation in  $[ph]$  to a set of first-order ordinary differential equations which may be used quite readily with the dynamical equations of rotor motion to examine the stability of the system. This was done on an analog computer for the infinitely-long plain cylindrical bearing. The results gave the threshold speed for instability for each equilibrium operation position, and are presented in the form of a stability chart, Figure 5.15.

In addition, approximate particular solutions for the non-linear dynamical equations were obtained as trajectories of the journal center when it is displaced arbitrarily from the equilibrium position. A significant advantage of this technique lies in the generality of the results for the equilibrium position which are formulated as a series with variable coefficients, particular values of which may be obtained in many cases. By comparison, numerical results give data for one case and set of conditions only in each calculation. This technique was extended by Cheng and Pan (Ref.126) to the case of finite plain cylindrical bearings, but as indicated by Ng (Ref.127) the accuracy of approximation diminishes for certain combinations of  $\Lambda$  and  $L/D$ . Other bearing configurations may also be investigated, for which a representative  $[ph]$  function can be deduced. A stability chart is given in Figure 5.16 and comparison with the results of other theories is given in Figure 5.17.

Ausman (Ref.128) again used the linearized  $[ph]$  method to investigate the stability of a rigid rotor in infinitely long plain cylindrical bearings. This method has the advantage of simplicity without overlooking the time-dependent effects of the fluid-film pressure, and so may also be used to study other bearing types, and more complex bearing-rotor systems. The analysis leads to a six degree stability polynomial which may be solved for the complex eigenfrequency  $\sigma$ . The coupled linearized  $[ph]$  method was further applied by Ng (Ref.127) for finite-length plain cylindrical bearings. Due to the lengthwise pressure variation, the characteristic equation is transcendental in the eigenfrequency, and the Routh-Hurwitz method may no longer be applied to determine the stability threshold. The problem is to determine the whirl frequency ratio such that a single mass parameter will satisfy both the real and imaginary parts of the characteristic polynomial, for a given combination of compressibility number,  $L/D$  ratio, and eccentricity ratio. An initial guess is made, and the approximation leads to a residual. The residual is then minimized. The results given contain data on the stability threshold. Comparison with other analysis is given in Figure 5.18, and with experimental results in Figure 5.19. A paper devoted to comparison amongst analyses, and with experimental results was given by Pan and Sternlicht (Ref.124).

An excellent set of experimental results for plain cylindrical bearings are given in Sternlicht and Winn (Ref.122). These results confirmed the conclusion

that a clearance exists for each bearing design which gives a minimum whirl threshold speed as predicted by Rentzepis and Sternlicht (Ref.121), and also indicated that threshold speed increases with increase in rotor mass, and almost linearly with applied load. Another experimental investigation was made by Sternlicht and Winn (Ref.122) concerning the influence of bearing geometry on half-frequency whirl threshold and on load capacity and attitude angle. Bearing types tested were: plain cylindrical with central orifice; axial groove bearings; axial groove bearing with orifices. It is shown that both the nature and angular position of the geometry change have a significant effect on the whirl threshold. The paper mentions that the pressure of an orifice or groove (correctly positioned) will raise the whirl threshold. This effect is then the same as the non-whirling bearing of Newkirk and Grobel (Ref. 56). No comparison between whirl threshold for plain bearings and for modified bearings is given. Grooved bearings were also studied experimentally by Fisher, Cherubim and Fuller (Ref.130) as part of a development for highly stable bearing types for turbo-machinery systems. Static performance data, unbalance effects on rigid rotors, whirl instability, bearing viscous damping, and pneumatic hammer, and orifice effects were investigated for hydrostatic and hydrodynamic operation. Other studies on grooved plain bearings by Whitley and Betts (Ref.131) also indicated that whirl stability is improved by the pressures of a groove, and that the groove does not affect the load capacity. The effect of variation in transverse inertia, L/D ratio, clearance and gas viscosity on conical whirl threshold was determined experimentally. A basic experimental study of the whirling of a plain unloaded cylindrical journal within the clearance of a vertical oil bearing has been made by Bowman, Collingwood and Midgely (Refs.132 and 134). Curves of whirl threshold and growth are given in the first report, and in the second the stability characteristics of a full bearing which operates with Taylor vortex flow were studied. It is claimed that the whirl threshold speed in the majority of cases was many times the natural frequency of the shaft journal assembly. In Ref. 132, this was determined experimentally, in air. Neglecting the contribution of the fluid-film stiffness and damping at operating speed would readily account for this difference. A considerable decrease in stability threshold speed was found for operation with Taylor vortex flow. Static and dynamic characteristics of plain cylindrical bearings in the turbulent range were investigated by Arwas, Sternlicht and Wernick (Ref. 12). Load capacity, attitude angle and fluid-film stiffness results are presented for the infinite

bearing, corrected for end leakage. Data on damping capacity are required for accurate dynamic analyses of turbulent bearing systems. It was noted that load-carrying capacity, radial stiffness, and power loss were higher with turbulent flow than with laminar flow.

### Synchronous Whirl

The unbalance response of a rigid rotor in gas bearings has received relatively little attention. This problem is less important than the half-frequency whirl problem as in most cases it can be eliminated by good balancing practice. However, in applications such as certain centrifuges where machine operation involves frequent reassembly after cleansing, good balance is difficult to maintain, and synchronous whirling of the rotor in its bearings may then constitute a problem. Sternlicht and Pan (Ref.134) considered the translatory whirl of a vertical rotor in plain cylindrical bearings. Using the steady whirl approximation and removing the time-dependence effect by coordinate transformation, the form of Reynolds' equation for this case is then identical with the static Reynolds' equation, when the compressibility member  $\Lambda$  is replaced by

$$\Lambda^* = \Lambda \left( 1 - \frac{2\dot{\alpha}}{\omega} \right)$$

where  $\dot{\alpha}$  is the angular speed of the whirl. Steady whirl analysis is then used to determine the synchronous whirl motion. Both quasi-static and first-order perturbation analyses lead to incorrect results in this application. For the bearing geometry shown in Figure 5.20, the equations of dynamical equilibrium are

$$\begin{aligned} F_r &= -m \left[ \delta \omega^2 \cos(\beta - \alpha) + \dot{\omega} \sin(\beta - \alpha) + \ddot{e} - e (\dot{\alpha})^2 \right] \\ F_t &= m \left[ \delta \omega^2 \sin(\beta - \alpha) - \dot{\omega} \cos(\beta - \alpha) + e \ddot{\alpha} + 2\dot{e}\dot{\alpha} \right] \end{aligned} \quad (5.33)$$

The fluid film forces in the radial and tangential directions are given by

$$F_r = - \int_{-L/2}^{L/2} dz \int_0^{2\pi} R p \cos \theta d\theta$$

$$F_t = \int_{-L/2}^{L/2} dz \int_0^{2\pi} R p \sin \theta d\theta$$

where  $p$  is determined by the generalized Reynolds' equation. Results indicating the variation of attitude angle between fluid-film force and maximum film thickness with  $\Lambda$  are given and are correlated with experimental results. The results also show that the radial film force decreases to zero when the whirl frequency is half-rotational speed, even for a well balanced rotor. Half-frequency whirl, being thus independent of rotor balance, may not be eliminated by good balancing practice. This analysis neglects the damping properties of the gas film, and so whirl orbit amplitude is not considered. This has been done by Sternlicht and Elwell (Ref.135). Steady whirl analysis is again employed, solving for the case of dimensionless whirl velocity  $\alpha' = (\dot{\alpha}/\omega) = 1.0$  by a numerical iterative procedure, with Reynolds' equation expressed in finite difference form. Using the curves of Figure 5.21 the amplitude and phase angle of a given rotating unbalance may be calculated. A comparison between theoretical and experimental results is given in Figure 5.22. The results confirm that plain cylindrical bearings with good alignment are able to carry significant dynamic loads, and that unbalance in a rotor leading to synchronous whirl tends to suppress half-frequency whirl.

### Hydrostatic Bearings

Rotating shafts are frequently supported in hydrostatic gas journal bearings and where high speeds are involved, the contribution of the hydrodynamic pressures thus generated must be evaluated where bearing stability is important. The static properties of hydrostatic bearings have been studied by Heinrich (Ref.136), while Lund (Ref. 7 ), has considered both static and dynamic performance of a hybrid bearing. The bearing considered is shown in Figure 2.13. Additional load-carrying capacity is generated by harmonic vibrations of the journal, i.e., by the squeeze-film effect. This is important in determining the dynamic stiffness for use in critical-speed and unbalance response calculations, and also for resonant frequency analyses of stationary machines. The vibratory motions considered are around the concentric journal position, and is either a pure translation or a pure rotation around the transverse axis. The

Reynolds' equation is linearized by a first-order perturbation around  $\epsilon = 0$ , and the resulting equations are solved numerically. Values of dimensionless load  $W_D/P_a(L + L_1)/D\epsilon$  and dimensionless moment  $M_D/P_a(L + L_1)D^2(R/C)\alpha$  are given from which the corresponding dynamic translatory and rotational stiffness may be obtained. Sample curves are given in Figure 5.23 and 5.24.

Larson and Richardson (Ref. 137) presented experimental data for the threshold of whirl stability for a short unloaded rigid rotor in hydrostatic compensated gas bearings. The effect of supply pressure and radial clearance on stability were examined. An analysis of rotor motions is given which leads to simple stability criterion for the type of bearing studied. Whirl instability was observed where the frequency of rotation of the shaft lay between two and six times the lowest natural frequency of the rotor-bearing system. Gross (Ref. 138) examined whirl in externally pressurized bearings, and gave some experimental data for dynamic characteristics such as film stiffness and damping. Rotor amplitude speed response up to the stability threshold are given. The form of these curves differs from that obtained by Larson and Richardson (Ref. 137), as here no critical speed peak is apparent. This may be due to better balancing or to the onset of whirl occurring below the rotor-bearing critical speed. A simple analysis for stability threshold speed is presented, and correlated quite well with the experimentally-obtained threshold data. It was found that the whirl path was usually stable, but the whirl amplitude increased rapidly with speed. The threshold for any given supply pressure occurred at about twice the lowest critical speed of the non-rotating system, for film stiffness  $\epsilon = 0$ . Factors which raised the threshold speed were increased pressurization, reduced rotor mass, and to some extent, rotor unbalance. This latter effect has been noted with hydrodynamic bearings, by Sternlicht (Ref. 134).

An extensive analytical and experimental study of hydrostatic gas bearing stability has been made by Licht and Elrod (Ref. 140). Pressure variation with time during the motion is assumed on a "continuous" rather than a "lumped" basis in an attempt to evaluate the squeeze-film effect arising from vibration more accurately. Attention is given to the bearing proportions which should be optimized as follows for stability:

Minimize: Pocket depth; difference between supply and recess pressure  
Effective mass of bearing.

Maximize: Supply nozzle diameter; length of annulus; area ratio of  
annular and pocket regions.

These results are in agreement with those of the analysis given in Section 8. Other studies of stability in both rotating and non-rotating bearings have been given by Roudebush (Ref.140), Licht, Fuller and Sternlicht (Ref.142), and on pneumatic hammer by Licht (Ref.142) and by Fisher, Cherubim and Fuller (Ref.130).

#### Whirling of a Flexible Rotor in Fluid-Film Bearings

Much of the work described in the previous section contains commentary on whirling of flexible rotors in fluid-film bearings, particularly where the results are directed towards the condition known as resonant whipping. In general, flexible rotors become unstable by resonant whipping above twice the system critical speed in bending, whereas rigid rotors in flexible bearings become unstable in half-frequency whirl. The whirl frequency in resonant whipping is constant and occurs at the system bending critical speed, whereas half-frequency whirl occurs at somewhat less than half the rotational speed. This may be observed in the experimental results given by Pinkus (Ref.111) and by Newkirk (Ref.109).

Hagg (Ref. 71) extended his simple criterion of rigid rotor whirl motions to cover the influence of rotor flexibility. The analog results of Hagg and Warner (Ref. 72) refer to the stability of flexible rotors. Poritsky (Ref.104) considered the rotor flexibility in deriving his criterion for whirl threshold speed

$$\omega < 2\omega_0 \frac{1 + k/K_1(\omega)}{1 + k/K_1(\omega_0)} \quad (5.35)$$

where  $k$  is the shaft stiffness (constant) and  $K_1(\omega)$  is the bearing radial stiffness (speed dependent). Pinkus (Ref.111) considered two rotors in which shaft flexibility significantly influenced rotor motions, and Newkirk (Ref.109) concluded that rotor flexibility was the key factor in determining whether a rotor would become unstable by resonant whipping or by half-frequency whirl.

These papers have been discussed in detail in the previous section.

In gas bearings the rotor is customarily so rigid that the bearing stiffness associated with the operating eccentricity determines the whirl threshold speed, and leads to some type of fractional frequency whirl, depending on whether the bearing is hydrostatic or hydrodynamic. In this instability, the amplitude readily becomes dangerously large and safe operation beyond this threshold speed is usually impossible. With liquid bearings half-frequency whirl may be encountered in lightly loaded bearings even where the shaft flexibility is comparable to the bearing flexibility. This effect was observed by Newkirk (Ref.109). It does not necessarily constitute a limiting condition for rotor operation although failures of rotors in liquid film bearings due to half-frequency whirl are not uncommon. The resonant whipping condition sets in at speeds around twice the rotor critical speed. In certain instances speed effects stiffen the bearings between critical speed and twice critical speed. The resonant whip threshold speed will then be higher than twice critical speed.

Poritsky's work emphasized the need for data on the dynamic fluid-film forces instability calculations. This data was first obtained for the plain cylindrical bearing and then for other bearing types, as discussed previously. With this data, and with the concurrent developments in computer applications to rotor and bearing problems plus increased understanding of the overall problem, it became possible to investigate the stability of much more complex rotor-bearing systems. The stability analysis of Sternlicht, Poritsky and Arwas (Ref.120) applies to flexible-rotor, flexible-bearing systems, but for a simple single-mass rotor. The results obtained are reproduced in Table 5.01. No stability charts accompany this paper. Moreover, the formulation of the stability equation in terms of force derivatives of velocity and displacement is inconvenient for direct application to engineering calculations. Recognizing this, Lund (Ref.35) elegantly reformulated the basic stability equations for a two-mass rotor, following the analysis of Warner and Thoman (Ref.33), in terms of the bearing spring and damping coefficients. Later, Lund (Ref.75) extended the two-mass rotor analysis to include the effect of pedestal mass, stiffness, and damping. An extensive range of results and stability charts are included with this work for gas bearing applications, although the analysis itself is perfectly general and applies to both liquid and gas bearing systems.

The analyses given in the parts of this section which follow are derived from the above four papers.

Warner and Thoman (Ref. 33) included a stability chart with their analysis of the rotor dynamic properties of a two-mass rotor in partial-arc bearings. This was obtained by direct application of the Routh-Hurwitz criterion to the basic equations of motion. This approach is equally applicable in any of the other cases quoted above, but becomes extremely complex when the number of variables in the system is large, or when the characteristic equation, resulting from the solution to the equations of motion, is of high order. In such instances, it is usually more convenient to apply Poritsky's approach of examining the nature of the time-exponent in the solution to the equations of motion. The application of this technique has been further discussed in the section on Whirling of a Rigid Rotor, and is given in detail in the following section.

The above analyses have led to a solution of the stability program in flexible rotors which is direct and readily applied. The limitations of this solution are that it applies to small amplitude motions about an equilibrium position, and not to large amplitude motions where the velocity and damping coefficients are no longer constant and the motions are non-linear. In addition, although the analysis indicates when rotor whirl may be anticipated and the frequency at which it will take place as yet it is not possible to determine whether the whirl orbit of a rotor operating its stability threshold is either stable or unstable. It is well known that rotors in liquid film bearings can be operated at many times the system bending critical speed, under resonant whip conditions, without failing the bearings. But at present, it is not possible to design for safe operation in this condition, because data on the stability of the whirl orbit is lacking. Castelli and Elrod (Ref. 123) studied the conditions surrounding the growth or decay of a whirl orbit for a rigid rotor in gas bearings, by a point-by-point amplitude solution for the coupled rotor and bearing equations. As noted, the labor involved was enormous, and this method is unsuited to general design practice. The equations of motion for large amplitude whirl have been formulated by several investigators, Poritsky (Ref. 104) Sternlicht, Poritsky and Arwas (Ref. 120) and others. More recently, the stability of a balanced flexible shaft in cylindrical journal bearings was

studied by Someya (Ref.143) in which the non-linear terms were retained in the equations of motion. The equations were then integrated numerically by the Runge-Kutta method, for rotor amplitude whirl. The rotor was given an initial displacement and the subsequent orbital motion of both rotor and journal were obtained. The results showed that at speeds above twice critical some form of 'external' damping (assumed proportional to the velocity of the rotor center, squared) must exist. The practical source of this damping is not stated. Results are given for the amplitude-speed growth of the whirl orbit below and above the threshold of resonant whipping for a number of cases. The non-linear calculation indicated that instability could exist above twice critical speed even though the linear analysis predicted stable operation. The results obtained by Huggins (Ref.107) for a rigid rotor in short bearings also included the non-linear influences of the fluid-film. This analysis follows the work of Jennings and Ocvirk (Ref.144) who employed an analog computer to study the transient and steady-state whirl paths. This work revealed that where (a) a stable whirl path was achieved the orbit ultimately obtained was independent of the initial disturbance, (b) orbit size is not determined by the static equilibrium position, and (c) orbit size is significantly greater as the mass of the rigid rotor is increased. Reddi and Trumpler (Ref.145) also studied the conditions surrounding orbit formation and growth using a digital computer to solve the equations. The Routh-Hurwitz criterion was used to investigate stability.

### General Theory of Stability of Small Amplitude Motions

When a simple elastic rotor consisting of a single balanced disk mounted on a shaft is operated in elastic, damped, fluid-film bearings, the rotor whirl motions are small until the threshold of stability of the rotor-bearing system is exceeded. Let the rotor be operating initially with a journal eccentricity ratio,  $e_0$ , under a steady external load, such as gravity. This condition is shown in Figure 3.07. For the steady load, the radial and tangential fluid-film forces on the journal are:

$$F_r = -\lambda \omega f_r(e_0, 0)$$

$$F_t = \lambda \omega f_t(e_0, 0) \quad (5.36)$$

where

$$\lambda = \frac{\mu L R}{\pi} \left(\frac{R}{c}\right)^2$$

Now let the journal be displaced a small distance  $de$ ,  $d\alpha$ . The additional forces which result from this displacement are  $dF_r$  and  $dF_t$ . Since  $\omega$  is constant,

$$\begin{aligned} dF_r &= \lambda \left[ 2d\alpha f_r - \omega \left( \frac{\partial f_r}{\partial e} de + \frac{\partial f_r}{\partial e'} de' \right) \right] \\ dF_t &= \lambda \left[ -2d\alpha f_t + \omega \left( \frac{\partial f_t}{\partial e} de + \frac{\partial f_t}{\partial e'} de' \right) \right] \end{aligned} \quad (5.37)$$

where

$$f_r, f_t, \frac{\partial f_r}{\partial e}, \frac{\partial f_t}{\partial e}, \frac{\partial f_r}{\partial e'}, \frac{\partial f_t}{\partial e'}$$

are evaluated at  $e = e_0$ ,  $e' = 0$ .

In the  $x, y$  coordinates,  $X$  and  $Y$  are the additional forces resulting from the displacement. These forces are made up of the above force components in the radial and tangential directions together with contributions from the directional changes  $d\alpha$ , given by

$$F_r d\alpha = -\lambda \omega f_r d\alpha$$

$$F_t d\alpha = \lambda \omega f_t d\alpha$$

The  $f_r$ ,  $f_t$  are again evaluated at  $\epsilon_0$ , 0 for the small displacement. Hence,

$$\begin{aligned} X &= \lambda \left[ -\omega f_r d\alpha - 2 f_t d\alpha + \omega \left( \frac{\partial f_t}{\partial \epsilon} d\epsilon + \frac{\partial f_t}{\partial \epsilon'} d\epsilon' \right) \right] \\ Y &= \lambda \left[ -\omega f_t d\alpha + 2 f_r d\alpha - \omega \left( \frac{\partial f_r}{\partial \epsilon} d\epsilon + \frac{\partial f_r}{\partial \epsilon'} d\epsilon' \right) \right] \end{aligned} \quad (5.38)$$

Writing the components of the small displacement in the x, y directions as  $\xi$ ,  $\eta$ , and measuring  $\alpha$  from the y-axis, for small  $\xi$ ,  $\eta$  there results

$$d\epsilon = \frac{\eta}{c} \quad d\alpha = -\frac{\xi}{\epsilon_0 c}$$

$$d\epsilon' = \frac{d\dot{\epsilon}}{\omega} = \frac{\dot{\eta}}{\omega c} \quad d\alpha' = -\frac{\dot{\xi}}{\epsilon_0 c}$$

The coordinate force expressions may therefore be written:

$$\begin{aligned} X &= \lambda \left[ -\frac{\omega f_r}{\epsilon_0} \frac{\xi}{c} - \frac{2 f_t}{\epsilon_0} \frac{\dot{\xi}}{c} + \omega \frac{\partial f_t}{\partial \epsilon} \frac{\eta}{c} + \frac{\partial f_t}{\partial \epsilon'} \frac{\dot{\eta}}{c} \right] \\ Y &= \lambda \left[ -\frac{\omega f_t}{\epsilon_0} \frac{\xi}{c} + \frac{2 f_r}{\epsilon_0} \frac{\dot{\xi}}{c} - \omega \frac{\partial f_r}{\partial \epsilon} \frac{\eta}{c} - \frac{\partial f_r}{\partial \epsilon'} \frac{\dot{\eta}}{c} \right] \end{aligned} \quad (5.39)$$

The equations of motion for the rotor-bearing system about the stable equilibrium position may now be formed. From Figure 5.25 these are

$$\begin{aligned} m(\ddot{X} + \ddot{\xi}) &= -kx \\ m(\ddot{Y} + \ddot{\eta}) &= -ky \\ kx &= -2X \\ ky &= -2Y \end{aligned} \quad (5.40)$$

where  $k$  is the shaft stiffness and  $m$  is the mass of the disk. The functions  $f_r$ ,

$f_t$  and their derivatives, with respect to  $e$  and  $e'$ , are all evaluated at the equilibrium eccentricity ratio,  $e_0$ , in keeping with the small oscillation theory considered. The stability of any rotor-bearing system may be determined from a knowledge of the steady-state operating eccentricity as follows:

Equations 5.40 are linear in the variables  $x, y, \xi, \eta$ . For harmonic motions the solution is of the form:

$$e^{v\tau}$$

in which  $v$  is a complex, and  $\tau = \omega_c t$ ;  $\omega_c = \sqrt{k/m}$  is the critical speed of the rotor in rigid, undamped bearings. From the first two equations

$$x = -\frac{v^2}{1+v^2} \xi \quad y = \frac{v^2}{1+v^2} \eta \quad (5.41)$$

Substituting these values into the second pair of equations and introducing the dimensionless ratio  $S = (\omega/\omega_c)$ , where  $\omega$  is the rotor angular velocity at the threshold of instability, leads to the stability determinant

$$\omega_c^2 \begin{vmatrix} \left[ S f_r + 2v f_t + \epsilon_0 \xi \right] & \left[ S \frac{\partial f_t}{\partial \epsilon} + \frac{\partial f_t}{\partial \epsilon'} \right] \\ \left[ -S f_t + 2v f_r \right] & \left[ S \frac{\partial f_r}{\partial \epsilon} + v \frac{\partial f_r}{\partial \epsilon'} + \zeta \right] \end{vmatrix} = 0 \quad (5.42)$$

in which

$$A = \frac{\pi k}{2\mu L \omega_0} \cdot \left(\frac{C}{R}\right)^3 \quad \zeta = \frac{A v^2}{1+v^2}$$

As  $\omega_c \neq 0$  for practical systems, this may now be divided out of Equation 5.42.

If the system is to be stable, the real part of  $v$  must be negative; conversally, for dynamic instability, the real part of  $q$  is positive. Thus, the threshold of stability occurs where  $v$  is a pure imaginary number. Taking the imaginary part of Equation 5.42, since  $v \neq 0$ , we have

$$\zeta \left[ 2f_t + \epsilon \frac{\partial f_r}{\partial \epsilon} \right] + S \left[ f_r \frac{\partial f_r}{\partial \epsilon} + f_t \frac{\partial f_t}{\partial \epsilon} \right] + 2S \left[ f_t \frac{\partial f_r}{\partial \epsilon} - f_r \frac{\partial f_t}{\partial \epsilon} \right] = 0$$

During the trivial solution  $S = 0$ , for  $S \neq 0$  this gives:

$$\frac{\zeta}{S} = - \frac{2 \left[ f_t \frac{\partial f_r}{\partial \epsilon} - f_r \frac{\partial f_t}{\partial \epsilon} \right] + \left[ f_r \frac{\partial f_r}{\partial \epsilon} + f_t \frac{\partial f_t}{\partial \epsilon} \right]}{\left[ 2f_t + \epsilon \frac{\partial f_r}{\partial \epsilon} \right]} \quad (5.43)$$

Similarly, taking the real part of Equation 5.42 and considering non-trivial solutions for  $S$  yields

$$\left( \frac{v}{S} \right)^2 = - \frac{\epsilon \left( \frac{\zeta}{S} \right)^2 + \left[ f_r + \epsilon \frac{\partial f_r}{\partial \epsilon} \right] \left( \frac{\zeta}{S} \right) + \left[ f_r \frac{\partial f_r}{\partial \epsilon} + f_t \frac{\partial f_t}{\partial \epsilon} \right]}{2 \left[ f_t \frac{\partial f_r}{\partial \epsilon} - f_r \frac{\partial f_t}{\partial \epsilon} \right]} \quad (5.44)$$

But from Equation 5.43 ,

$$\zeta v^2 - \Lambda v^2 + \zeta = 0$$

Thus, for  $S \neq 0$ ,

$$S^2 \left( \frac{\zeta}{S} \right) \left( \frac{v}{S} \right)^2 - SA \left( \frac{v}{S} \right)^2 + \frac{\zeta}{S} = 0 \quad (5.45)$$

The threshold of instability is defined through this quadratic since  $\omega_c = S\omega_c$ . In order to calculate  $\omega_c$  for any given system, the steady-state operating eccentricity ratio  $\epsilon$  is first obtained from static bearing design consideration, and then the radial and tangential force components and their derivatives corresponding to this eccentricity are determined for the particular bearing type used. The curves given in Table 2.01 and Ref. (32) may be used for the cylindrical journal bearing. Data for the incompressible, partial-arc bearing has been determined by Warner (Ref. 34). Tilting-pad journal bearing values have been given by Hagg and Sankey (Ref. 73) (incompressible) and Lund (Ref. 81), while the elliptical and four axial groove bearing coefficients have been obtained by Lund and Sternlicht (Ref. 32). Substitution of the appropriate coefficients into Equation 5.45 then allows the instability threshold ratio,  $S$ ,

to be determined.

The influence of fluid-film bearing stiffness on the critical speed of the simple rotor-bearing system considered above may now be determined. As bearing stiffness is a function of eccentricity ratio, it is therefore also speed-dependent for any given arrangement. The fluid-film stiffness  $K_2$  is given by

$$K_2 = \frac{dF}{d\epsilon} = \frac{\mu L \omega}{\pi} \left(\frac{R}{c}\right)^3 \left(\frac{df}{d\epsilon}\right)$$

$$= \frac{SK_1}{2A} \frac{df}{d\epsilon}$$

where  $K_1$  is the shaft stiffness. Recalling that for a flexible rotor in flexible bearings

$$\omega_c^2 = \omega_o^2 \frac{1}{1+K}$$

where  $\omega_o$  is the rigid-bearing critical speed  $\left[ \frac{K_1}{m} \right]^{\frac{1}{2}}$   
and  $K$  is the shaft. Bearing stiffness ratio  $\left[ \frac{K_1}{K_2} \right]$

Substitution leads to the expression

$$\omega_c^2 = \omega_o^2 \frac{1}{1 + \frac{A}{S} \frac{df}{d\epsilon}} \quad (5.46)$$

or

$$\left( \frac{\omega_c}{\omega_o} \right)^2 = \frac{\left( \frac{df}{d\epsilon} \right)}{\left( \frac{df}{d\epsilon} + \frac{A}{S} \right)}$$

Subscript r: radial stiffness

The dimensionless system number  $A$  is a function of bearing geometry, shaft stiffness and fluid viscosity. Stability properties have been examined for rotor-bearing systems with values of  $A$  within the range 0.1 to 100 at operating

eccentricities between 0.1 and 0.8, for cylindrical bearing  $(\frac{h}{D})$  ratios 0.3 and 1.0. The results are given in Table 5.01. The results  $\frac{\omega}{\omega_c}$  indicate that for low eccentricities instability sets in at approximately twice the critical speed, but that the threshold of instability occurs at higher values for higher eccentricity ratios. This conclusion is supported by data obtained on actual machines and by experiments, and discussed in the literature review of the previous section. The whirl frequency ratio  $(\frac{\omega}{\omega_c})$  is also listed in Table 5.01. This is the frequency with which the rotor whirls about the static equilibrium position at the threshold of instability, expressed as a fraction of the threshold speed, ratio S, which is related to the rigid bearing critical speed  $\omega_c$ . This value is always below 0.5, and is independent of A. The ratio  $\frac{\omega_c}{\omega_0}$ , system critical speed: rigid bearing critical speed, has also been calculated for the above cases, illustrating the significance of bearing flexibility in system motions.

When the instability threshold has been passed, the whirl amplitudes of the rotor increase rapidly until the whirl frequency coincides with the natural frequency of the system. This resonance usually gives rise to whirl amplitudes which are of such violence that continued operation at or beyond this resonant speed is impossible without damaging the bearings, or even the rotor itself. With liquid-bearing machines, this condition is referred to as resonant whipping and the rotor flexibility contributes to the overall motion. In the case of gas-bearings, the term critical half-frequency whirl is used although the whirl frequency is more frequently some fraction less than one-half the speed of rotation.

The equations developed above to determine the threshold of stability no longer apply when the amplitude of motion becomes large. The analysis of motions which are not restricted to small displacements from the steady-state equilibrium position has been discussed for the simple balanced flexible rotor by Poritsky (Ref. 104), Sternlicht, Poritsky and Arwas (Ref. 120), Huggins (Ref. 107), Someya (Ref. 143), and others.

### Stability of a Two-Mass Rotor with Unbalance

The influence of unbalance on the stability threshold is a question of considerable practical importance, as all practical rotors operate with some degree of unbalance, and all are subjected to transient-initiated displacements away from their operating equilibrium positions. Also, where the normal operating speed is beyond the first system critical speed, some knowledge of the influence of higher harmonic motions on the stability threshold is desirable.

Both questions may be examined by considering the flexible, unbalanced two-mass rotor shown in Figure 3.29, which operates in damped, elastic fluid-film bearings with masses a distance  $\xi L$  apart as shown. In this investigation, the bearing properties are represented by eight spring and damping coefficients, derived in a similar manner to the bearing properties of the previous section such that:

$$\begin{aligned} F_x &= -K_{xx}x - K_{xy}y - C_{xx}\dot{x} - C_{xy}\dot{y} \\ F_y &= -K_{yx}x - K_{yy}y - C_{yx}\dot{x} - C_{yy}\dot{y} \end{aligned} \quad (5.29)$$

Values of the coefficients are given in Table 2.01 for the cylindrical bearing, elliptical bearing, and four-axial groove bearing. Curves for tilting-pad bearings have been given by Hagg and Sankey (Ref. 73) and by Lund (Ref. 81). The displacement geometry diagram for this system, which makes use of this formulation is shown in Figure 3.29. The following analysis is general and applies to both liquid and gas bearings. The equations of motion are:

$$\begin{aligned} \alpha_{11} m \ddot{x}_1 + x_1 - \xi x_2 &= \alpha_{11} m a \omega^2 \sin \omega t \\ K_{xx}x_2 + K_{xy}y_2 + C_{xx}\dot{x}_2 + C_{xy}\dot{y}_2 &= \frac{\xi}{\alpha_{11}} [x_1 - \xi x_2] \\ \alpha_{11} m \ddot{y}_1 + y_1 - \xi y_2 &= \alpha_{11} m a \omega^2 \cos \omega t \\ K_{yx}x_2 + K_{yy}y_2 + C_{yx}\dot{x}_2 + C_{yy}\dot{y}_2 &= \frac{\xi}{\alpha_{11}} [y_1 - \xi y_2] \end{aligned} \quad (5.47)$$

In these equations the shaft influence coefficients are written:

$$\alpha_{ii} = \begin{cases} (\alpha_{aa} + \alpha_{ab}) & \text{1st mode} \\ (\alpha_{aa} - \alpha_{ab}) & \text{2nd mode} \end{cases} \quad (5.48)$$

where  $\alpha_{aa}$  is the deflection at a due to a unit force at a, for simple supports and  $\alpha_{ab}$  is the deflection at a due to a unit force at b, for simple supports. Also,

$$\xi = \begin{cases} 1 & \text{1st mode} \\ \xi & \text{2nd mode} \end{cases}$$

Let  $x_1$ ,  $x_2$ ,  $y_1$  and  $y_2$  be complex displacements. From the general solution to Equations 5.47(a) and 5.47(b):

$$\frac{x_1}{a} = \frac{\xi \left(\frac{x_2}{a}\right) - 1 \left(\frac{\omega}{\omega_c}\right)^2}{1 - \left(\frac{\omega}{\omega_c}\right)^2}$$

$$\frac{y_1}{a} = \frac{\xi \left(\frac{y_2}{a}\right) - 1 \left(\frac{\omega}{\omega_c}\right)^2}{1 - \left(\frac{\omega}{\omega_c}\right)^2} \quad (5.49)$$

where

$$\omega_c^2 = \frac{1}{a\alpha_{11}}$$

Substitute these expressions into Equations 5.47(b) and 5.47(d) to make  $X_2$  and  $Y_2$  the unknown variables. Make the resulting equations dimensionless by introducing the parameter groupings:

$$K_x = \frac{CK_{xx}}{W}$$

$$\bar{K}_x = \frac{CK_{xy}}{W}$$

$$\bar{K}_y = \frac{CK_{yx}}{W}$$

$$\omega C_x = \frac{C\omega C_{xx}}{W}$$

$$\bar{\omega C}_x = \frac{C\omega C_{xy}}{W}$$

$$\bar{\omega C}_y = \frac{C\omega C_{yx}}{W}$$

$$K_y = \frac{C_{xy}}{W} \quad \omega C_y = \frac{C_{yy}}{W} \quad (5.50)$$

$$\text{and} \quad \kappa = \frac{C_{xx}^2}{W C_{11}} \frac{\left(\frac{\omega}{\omega_c}\right)^2}{1 - \left(\frac{\omega}{\omega_c}\right)^2}$$

Thus:

$$\begin{pmatrix} \left[ K_x - \kappa + i \omega C_x \right] \left[ -\bar{K}_x + i \omega \bar{C}_x \right] \\ \left[ \bar{K}_y + i \omega \bar{C}_y \right] \left[ K_y - \kappa + i \omega C_y \right] \end{pmatrix} \begin{pmatrix} \xi_{\frac{x}{a}}^2 \\ \xi_{\frac{y}{a}}^2 \end{pmatrix} = \kappa \begin{pmatrix} -1 \\ 1 \end{pmatrix} \quad (5.51)$$

The solution  $e^{\nu t}$  corresponds to small harmonic motions of the rotor where  $\nu$  is the complex eigenvalue and  $\tau = \omega_c t$ ,  $\omega_c^2 = \frac{1}{W C_{11}}$ . Substituting and writing

$$\bar{\kappa} = \frac{C_{xx}^2}{W C_{11}} \frac{(s\gamma)^2}{1 + (s\gamma)^2} \quad (5.52)$$

where  $\gamma = (\nu/\omega)$  and  $s = (\omega/\omega_c)$  leads to the following stability determinant.

$$\begin{vmatrix} \left[ K_x + \bar{\kappa} + \gamma \omega C_x \right] & \left[ -\bar{K}_x + \gamma \omega \bar{C}_x \right] \\ \left[ \bar{K}_y + \gamma \omega \bar{C}_y \right] & \left[ K_y + \bar{\kappa} + \gamma \omega C_y \right] \end{vmatrix} = 0 \quad (5.53)$$

As in the case of the simple rotor, the motion is stable when the roots of the determinant are negative, and unstable for positive roots. The threshold of stability is defined where the roots,  $\nu$ , are purely imaginary. This leaves  $\bar{\kappa}$  real. For non-trivial solutions, equating both the real parts and the imaginary parts to zero yields

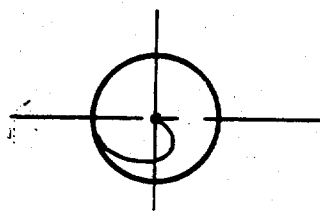
$$\bar{\kappa} = - \frac{\left[ K_x \omega C_y + K_y \omega C_x \right] - \left[ \bar{K}_x \omega \bar{C}_y + \bar{K}_y \omega \bar{C}_x \right]}{\omega C_x + \omega C_y} \quad (5.54)$$

$$\gamma^2 = - \frac{\begin{bmatrix} K_x + \bar{K} & 0 \\ 0 & K_y + \bar{K} \end{bmatrix} - \begin{bmatrix} \bar{K}_x & \bar{K}_y \\ \bar{K}_y & \bar{K}_x \end{bmatrix}}{\omega C_{\bar{x}} \omega C_{\bar{y}} - \omega \bar{C}_{\bar{x}} \omega \bar{C}_{\bar{y}}} \quad (5.55)$$

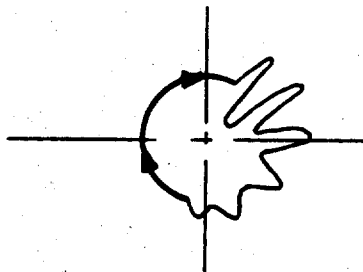
Substituting 5.54 into 5.55 gives  $\gamma$ , thus defining the eigenfrequency,  $\gamma$ , as a fraction of the rotor speed. Introducing  $\gamma$  and  $\bar{K}$  into Equation 5.52 then gives  $s$ , the rotor speed at the onset of stability, expressed as a fraction of the rigid body critical speed.

Warner and Thoman (Ref. 33) give a curve whereby the stability threshold may be determined from the operating eccentricity ratio, and the rotor stiffness parameter  $\left[ \frac{\omega C_{\bar{x}}}{C_{\bar{y}}} \right]$ , where  $\xi = 1$  (fundamental mode).

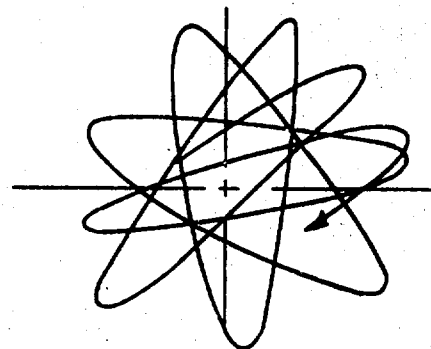
Lund (Ref. 75) has further extended the above analysis by investigating stability of an elastic rotor carried in damped, elastic, massive pedestals. The stability of a rotor in gas bearings has been examined in detail.



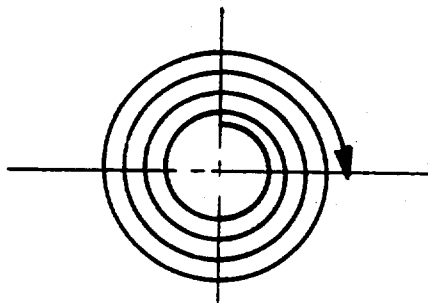
Highly stable unbalance whirl



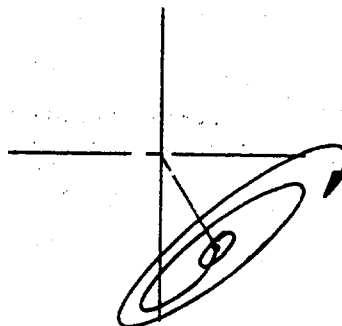
Stable with decaying transient arising from blow. Unbalance whirl or stable bearing.



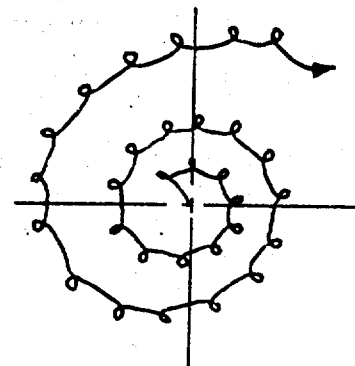
Rotation. Stable whirling with sustained transient. Gyroscopic whirl with friction.



Unstable whirl with growing radius. Coulomb friction whirl  $\omega > \omega_c$ .

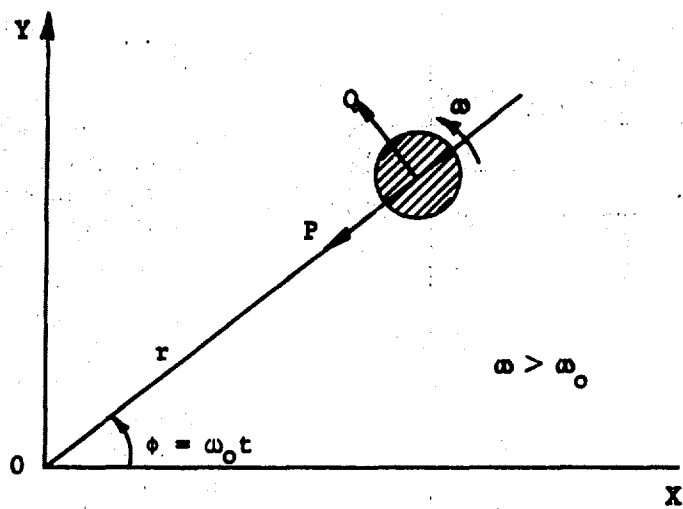


Stable orbit, small whirl radius. Unstable whirl, large radius. Horizontal journal bearing.

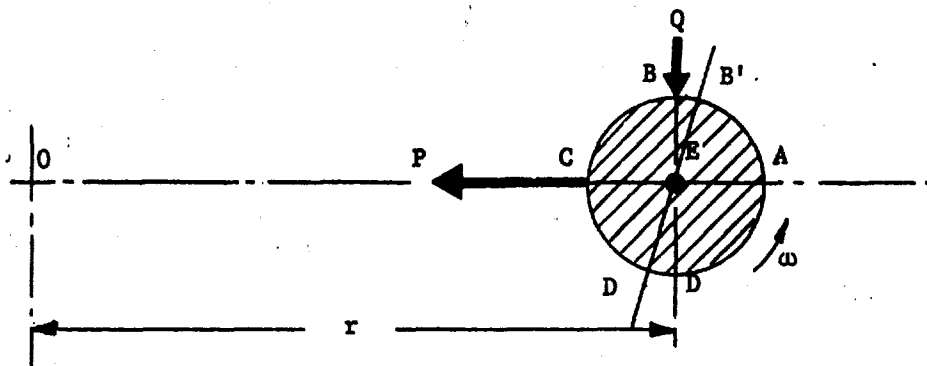


Unstable orbit with growing radius and steady backward whirl. Gyroscopic whirl with unbalance at  $\omega = \omega_c$ .

Fig. 5.01 Stable and Unstable Rotor Whirl Orbits

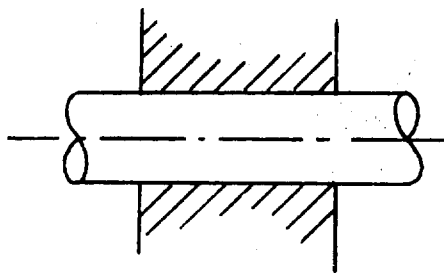


(a) Forces on a vertical rotor undergoing hysteretic whirl

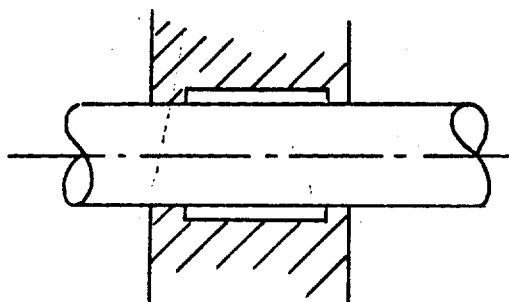


(b) Rotating shaft with tangential whirl-suppressing force

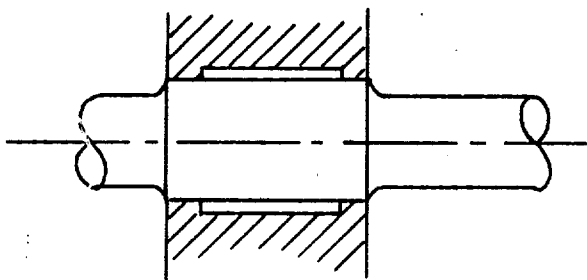
Figure 5.03



- (a) Non-uniform contact pressure along length of joint leads to slip at ends. Sharp rise in contact pressure at edge promotes fretting corrosion and fatigue cracking.

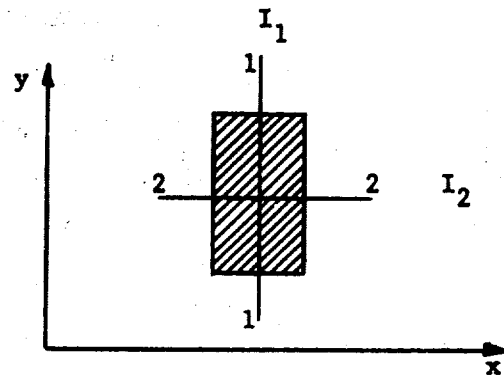


- (b) Short contact areas give uniform mounting pressure. Fretting corrosion and fatigue still significant; contact pressures may be higher than Case (a).

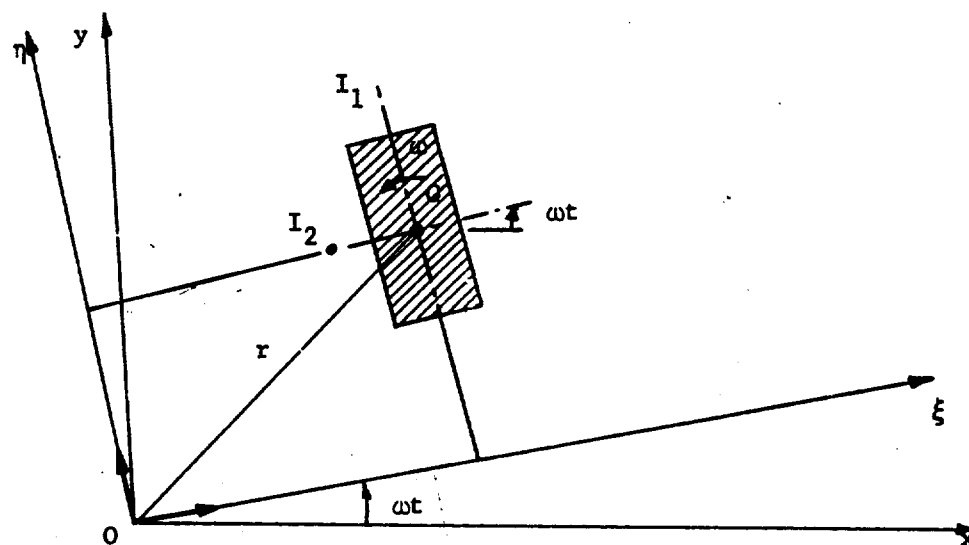


- (c) Short contact areas and decreased edge stress concentration. Minimum coulomb slippage and fatigue hazard.

Fig. 5.04 Methods of Mounting Rotor Components and Associated Problems

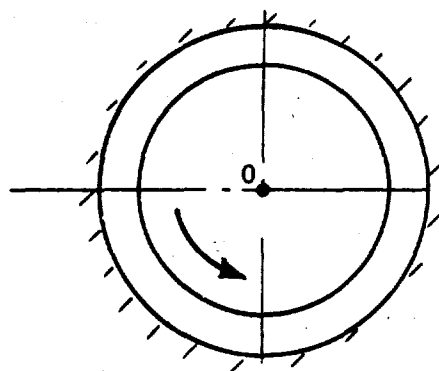


(a) Shaft Cross Section With Differing Principal Moments of Inertia

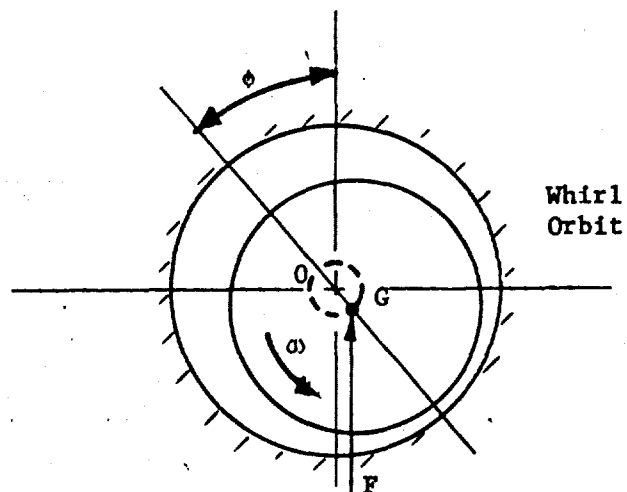


(b) Geometry of Shaft Displacement in  $\xi, \eta$  Rotating Axes

Fig. 5.05 Section of Rotor with Unsymmetrical Stiffness

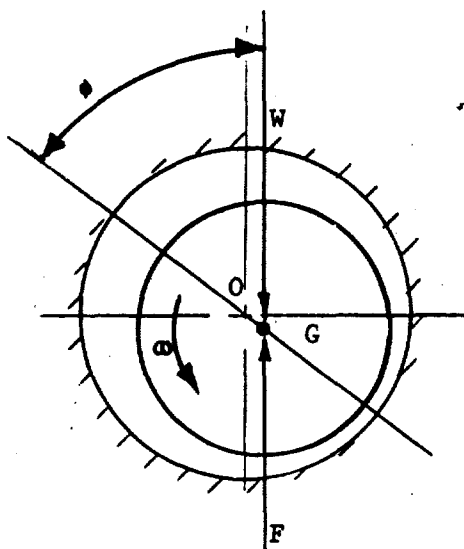


(a) Rotating unloaded vertical shaft in undisplaced position

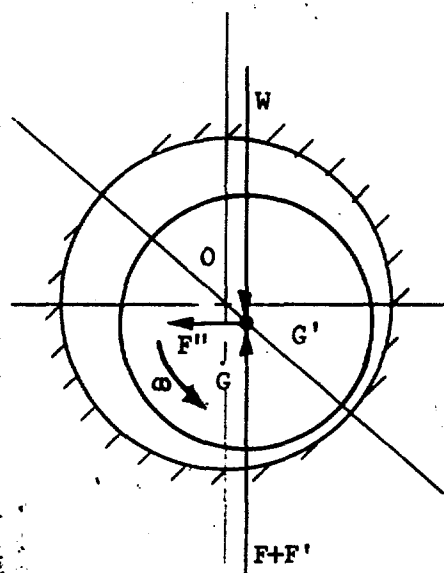


(b) Rotating unloaded vertical shaft in displaced position with whirl-inducing force

Fig. 5.06 Forces Acting on Vertical Rotor in Hydrodynamic Whirl



(a) Rotating loaded horizontal shaft. Equilibrium position.



(b) Rotating loaded horizontal shaft in displaced position with additional force components.

Fig. 5.07 Force on Horizontal Rotor in Hydrodynamic Whirl

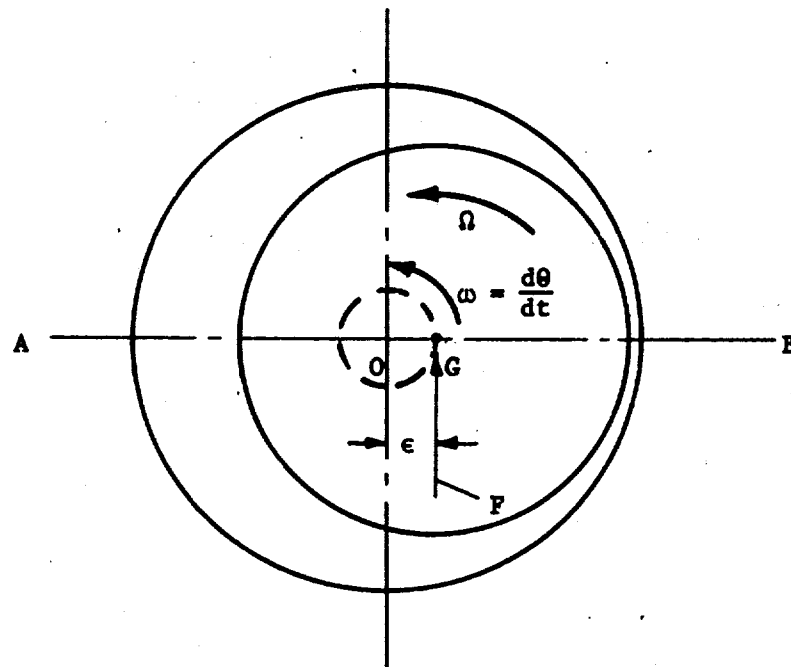
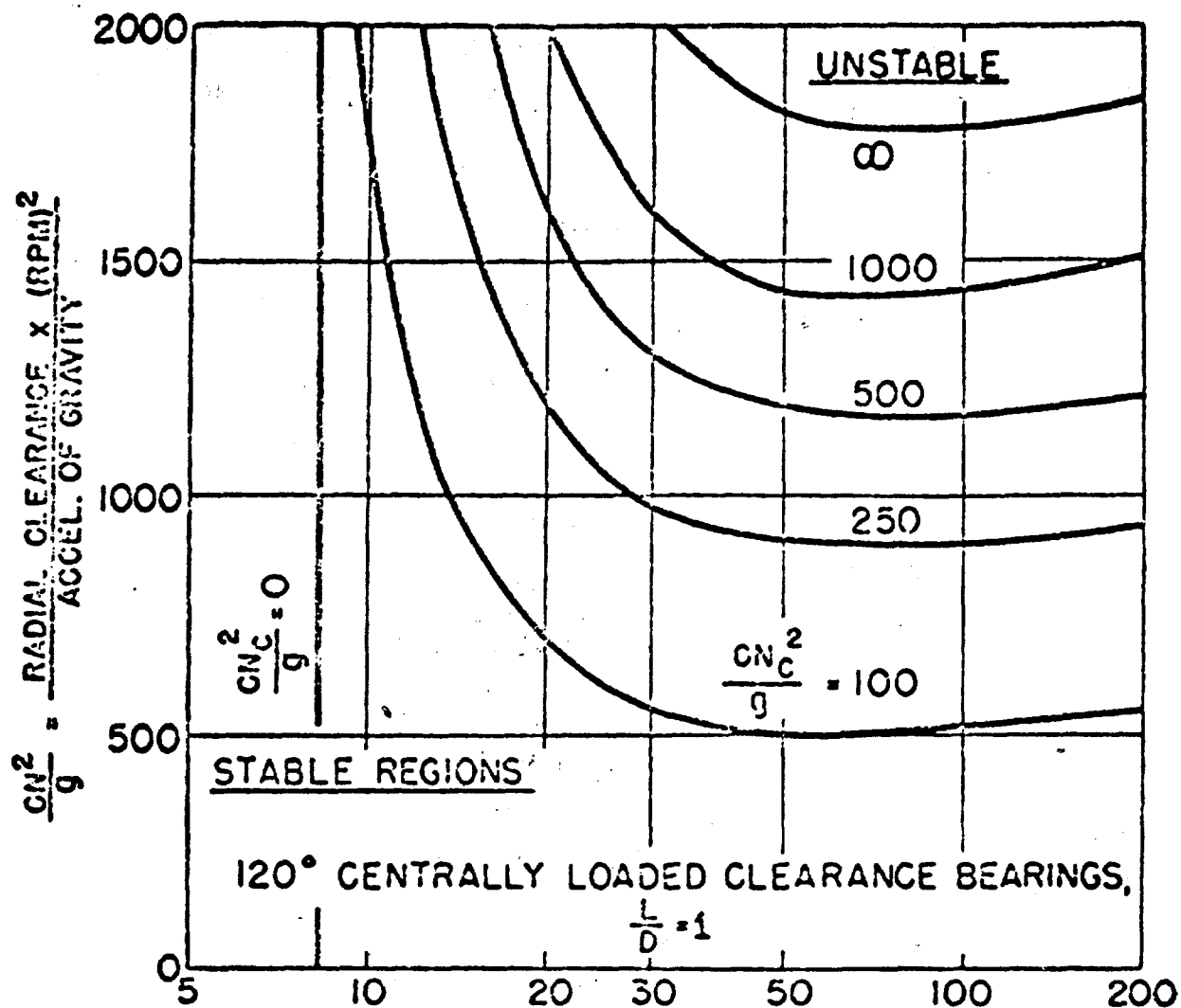


Fig. 5.08 Whirling Journal in Full Bearing Flow Continuity Condition



$$\left(\frac{R}{C}\right)^2 \frac{\mu N}{p} = \left(\frac{\text{JOUR. RADIUS}}{\text{RAD. CLEARANCE}}\right)^2 \frac{\text{VISCOSITY} \times (\text{RPM})}{\text{BRG. PRESSURE}}$$

DIMENSIONAL UNITS—INCH, POUND, SECOND

$\mu$  = CENTIPOISES  $\times 1.45 \times 10^{-7}$

$g$  = 386 INCHES/SEC.<sup>2</sup>

$N_c$  = ROTOR CRITICAL SPEED ON SIMPLE SUPPORTS, RPM

Fig. 5.09 Stability Chart. Flexible Rotor in Fluid-Film Bearing

Reprinted from OIL WIDTH OF FLEXIBLE ROTORS, Figure 1,  
by A.C. Haag and P.C. Warner for the ASME, Vol. 75,  
October 1953, pp. 1339-1344.

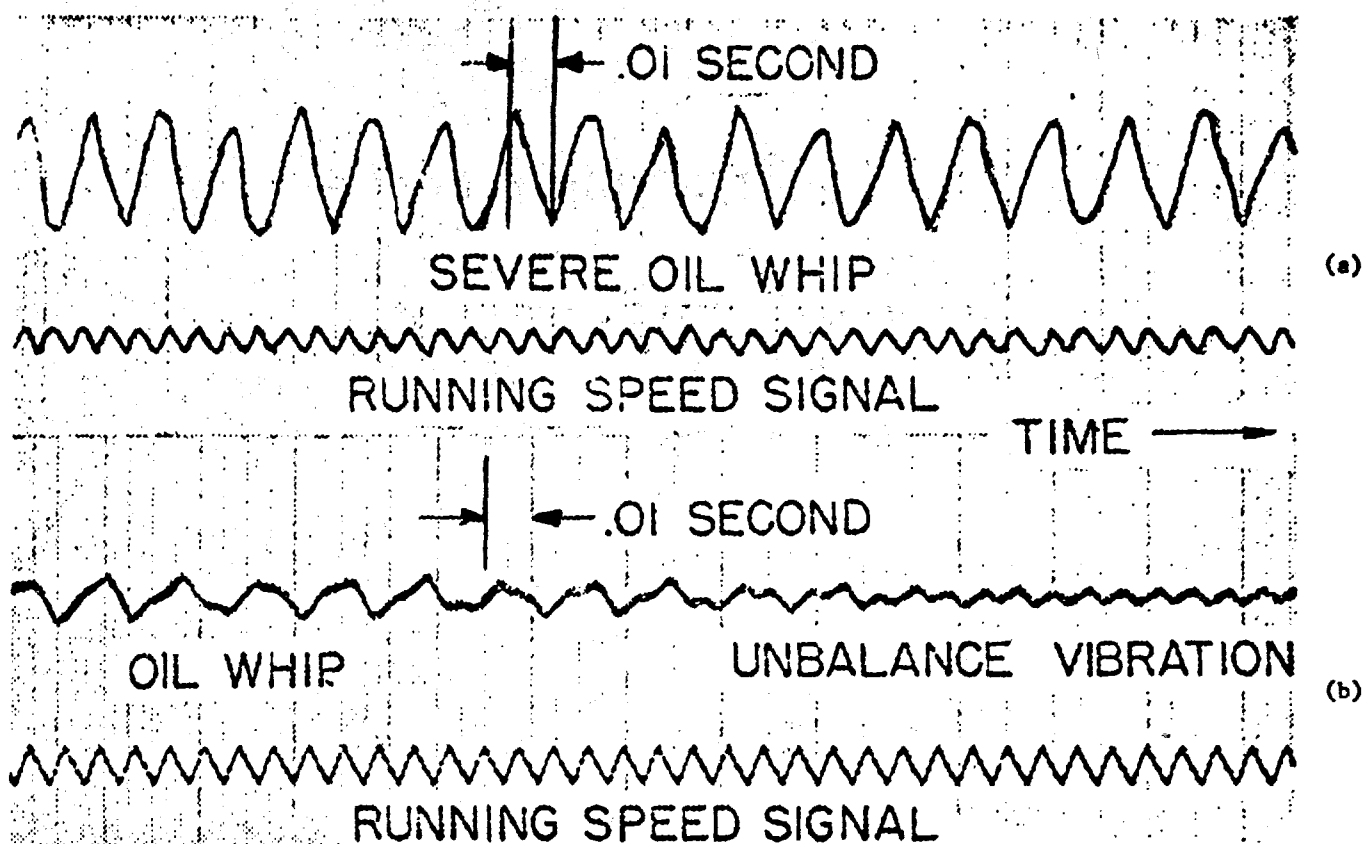


Fig. 5.10 Whirl Oscillogram Showing (a) Well-Developed Whirl and (b) Transition from Whirl to Stable Running with Decreasing Speed.

Reprinted from OIL WIDTH OF FLEXIBLE ROTORS, Figure 4, by A.C. Haag and P.C. Warner for the ASME, Vol. 75, October 1953, pp. 1339-1344.

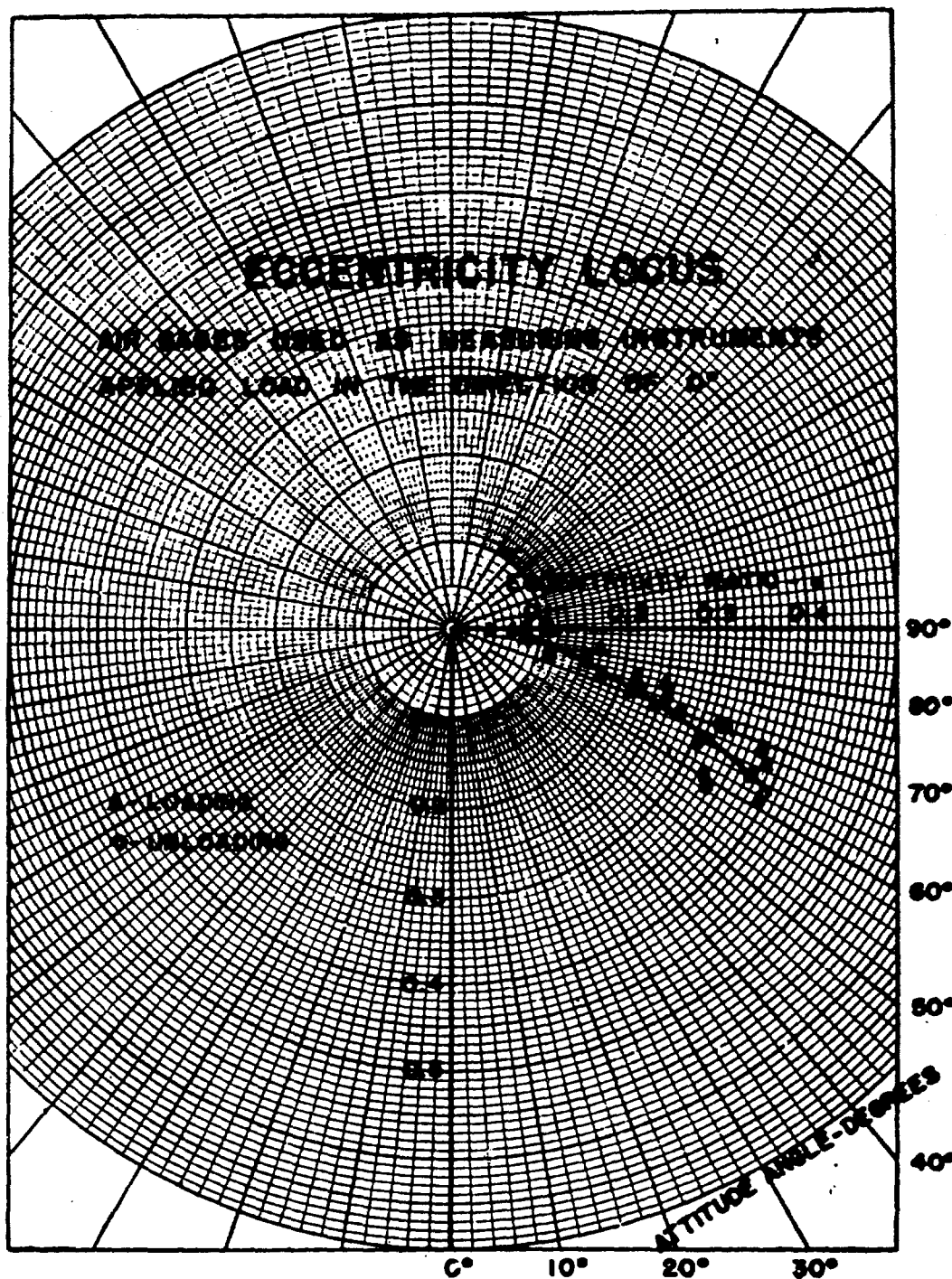


Fig. 5.11 Modified Bearing Force Eccentricity Curve

Reprinted from INVESTIGATION OF TRANSLATORY FLUID WHIRL  
IN VERTICAL MACHINES, Figure 12, by G.F. Boeker and  
B. Sternlicht for the ASME, Vol. 78, No. 1, January 1956.

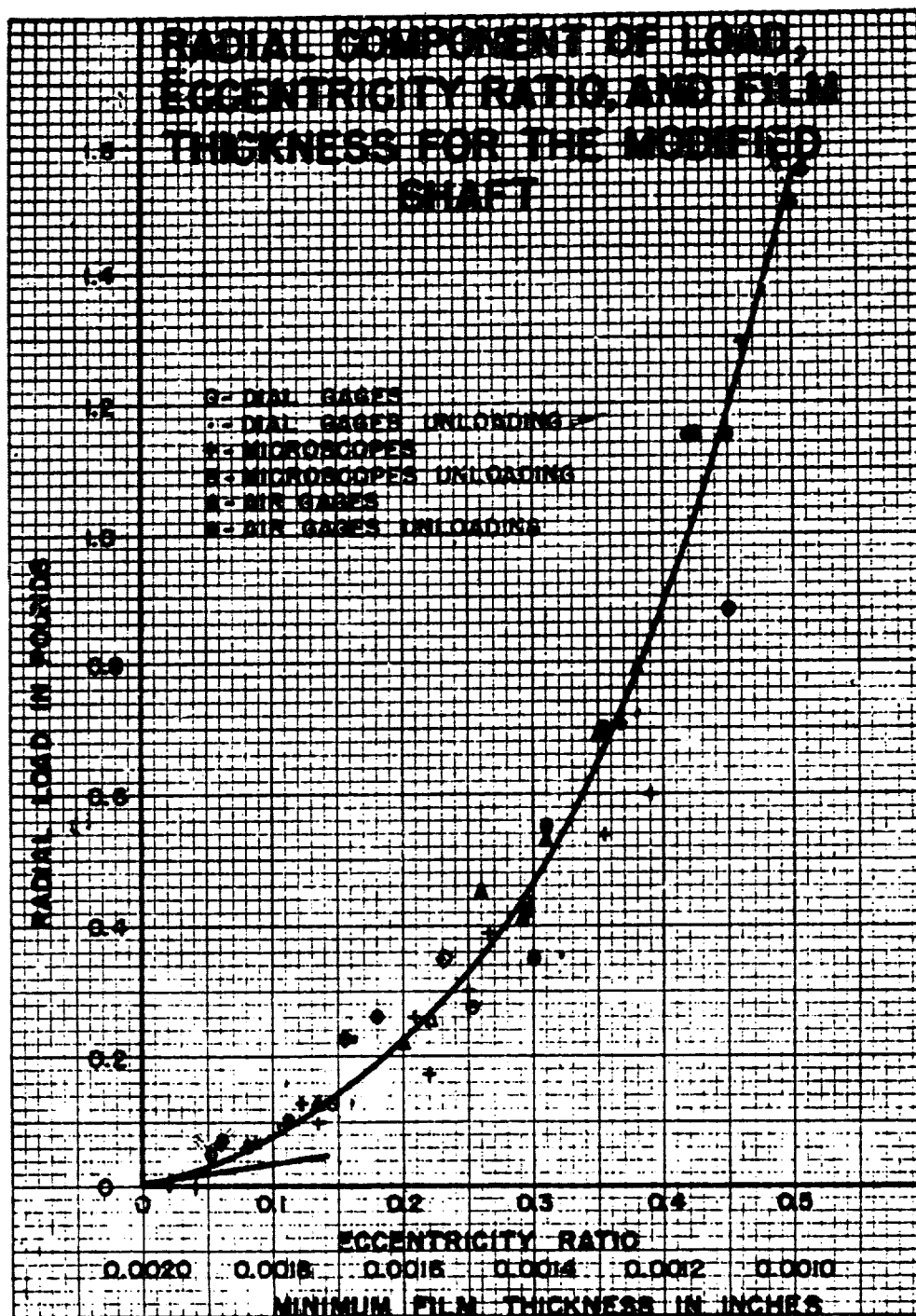
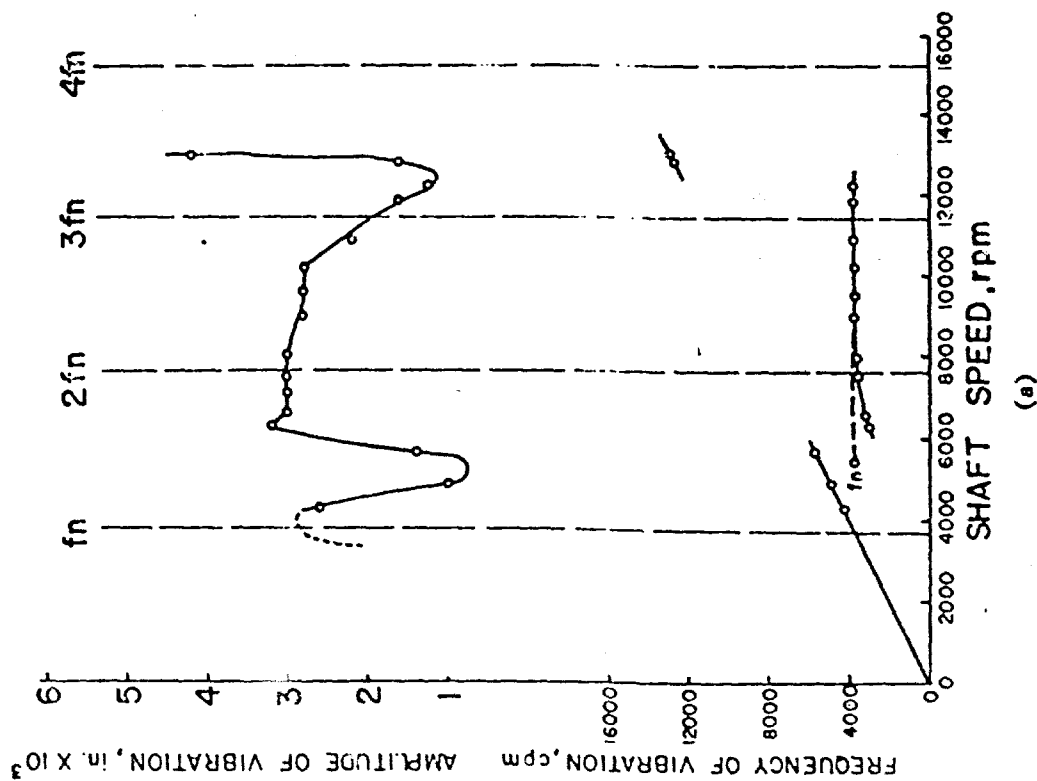
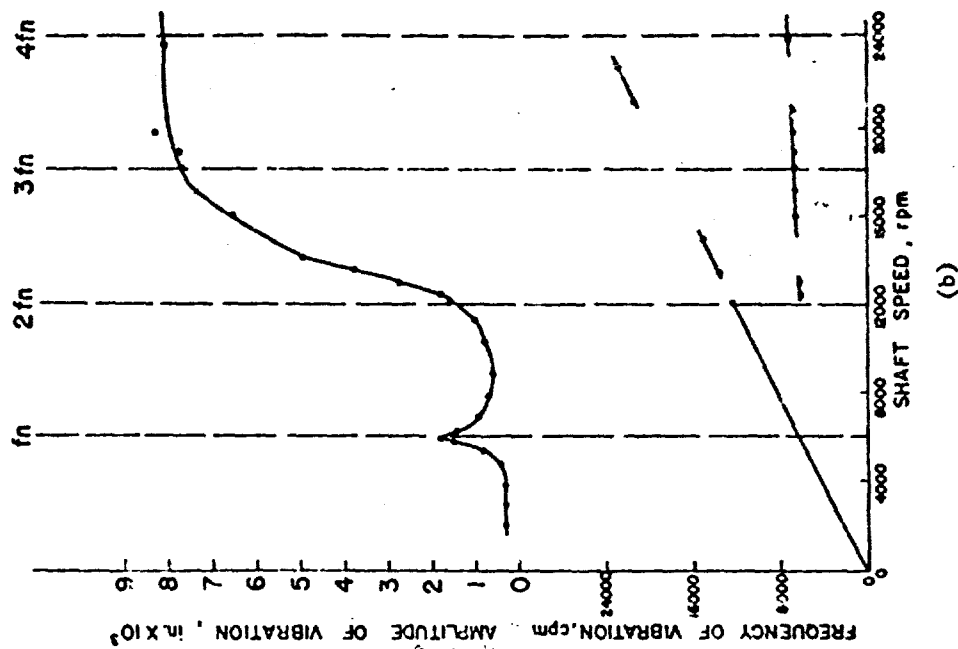


Fig. 5.12 Radial Component of Load vs. Eccentricity Ratio and Film Thickness for Modified Shaft

Reprinted from INVESTIGATION OF TRANSLATORY FLUID WHIRL IN VERTICAL MACHINES, Figure 14, by G.F. Boeker and B. Sternlicht for the ASME, Vol. 78, No. 1, January 1956.



(a)



(b)

Fig. 5.13 Typical Resonant Whip Curves for (a) 187 Pound Shaft and (b) 64 Pound Shaft

Reprinted from EXPERIMENTAL INVESTIGATION OF RESONANT WHIP, Figures 6 and 7, by Oscar Pinkus, ASME Transactions, July 1956.

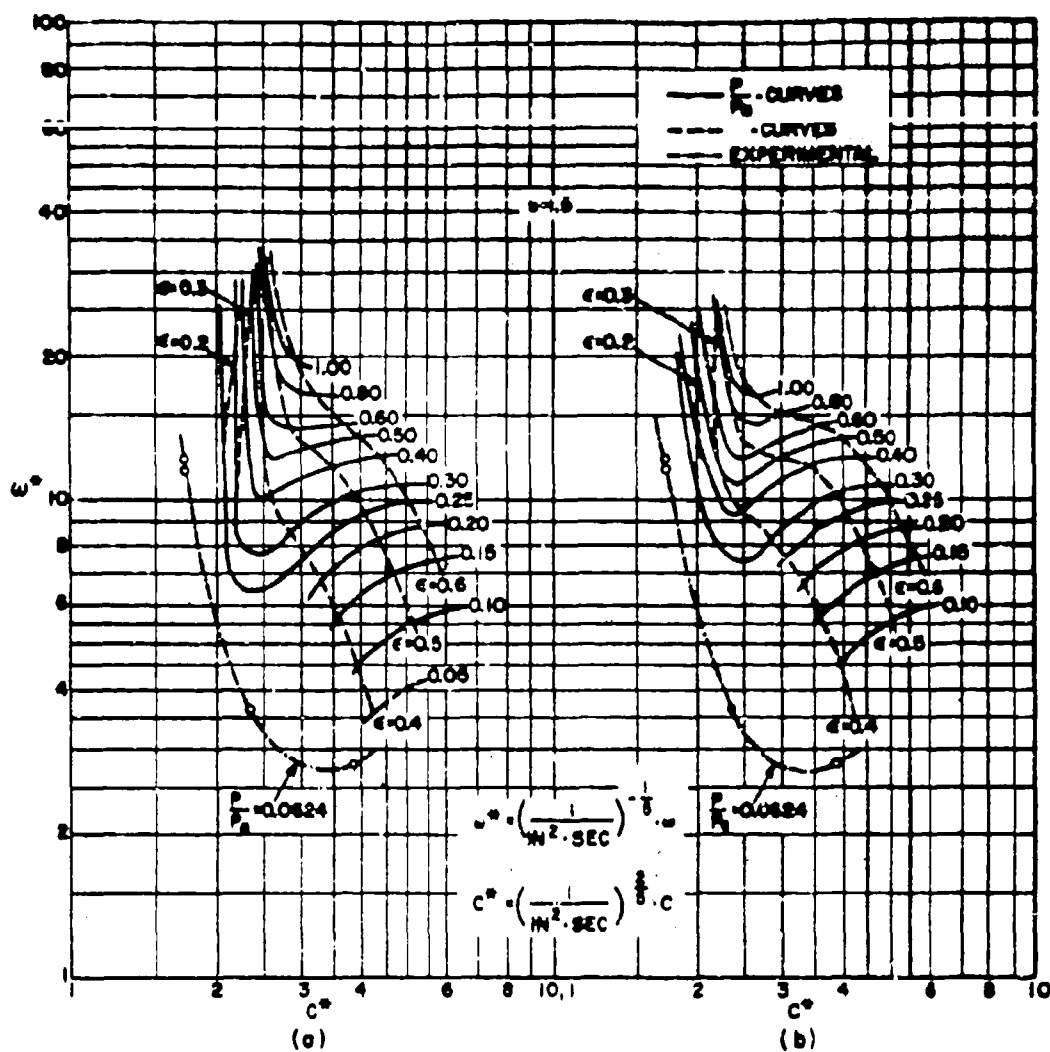


Fig. 5.14 Stability Curves,  $C^*$  vs.  $\omega^*$  for  $b = 1.5$

Reprinted from ON THE STABILITY OF ROTORS IN CYLINDRICAL JOURNAL BEARINGS, Figure 12, by G.M. Rantsepis and B. Sternlicht for the Journal of Basic Engineering, December 1962.

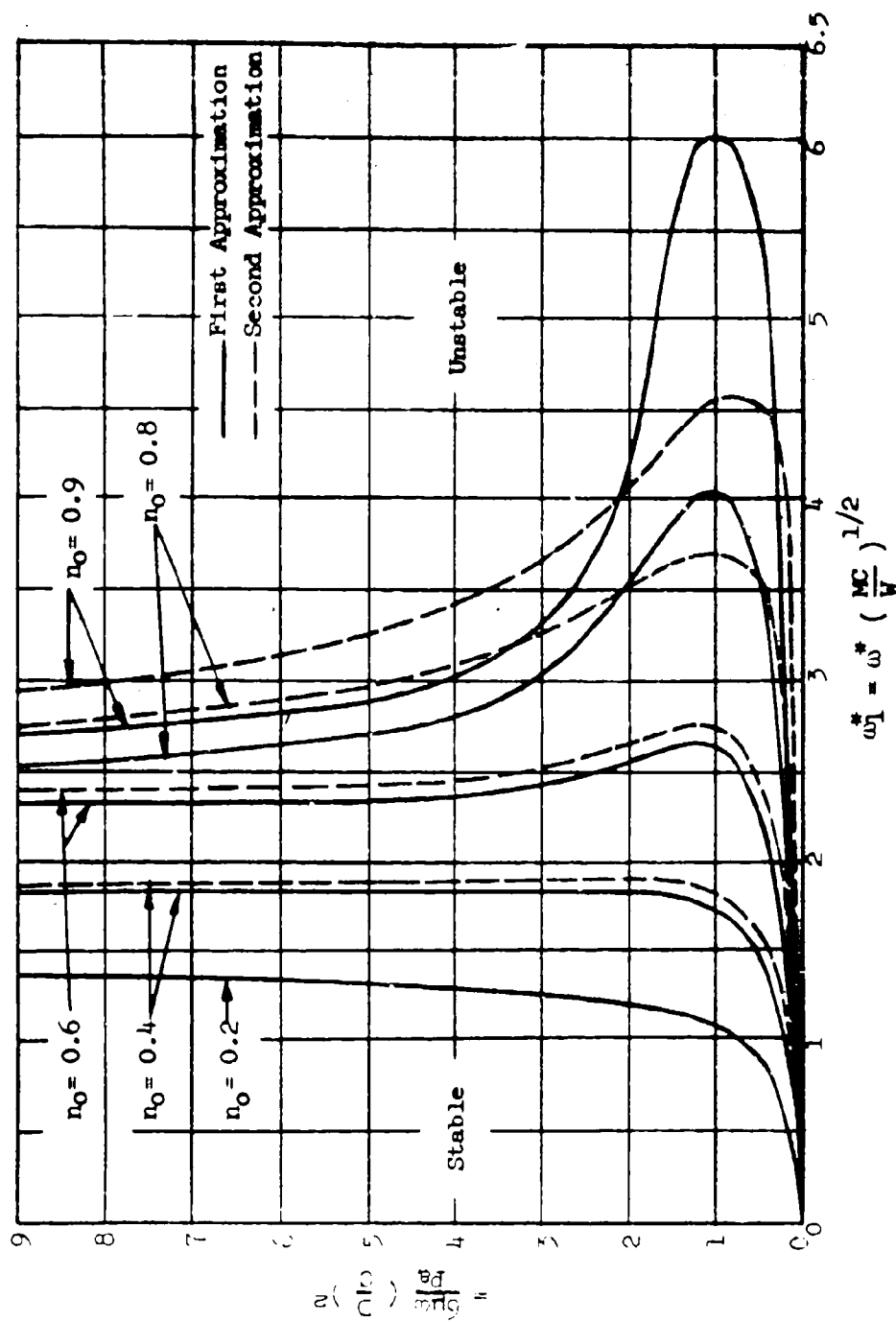


Fig. 5.15 Stability of an Infinitely-Long, Plain Cylindrical Gas Bearing

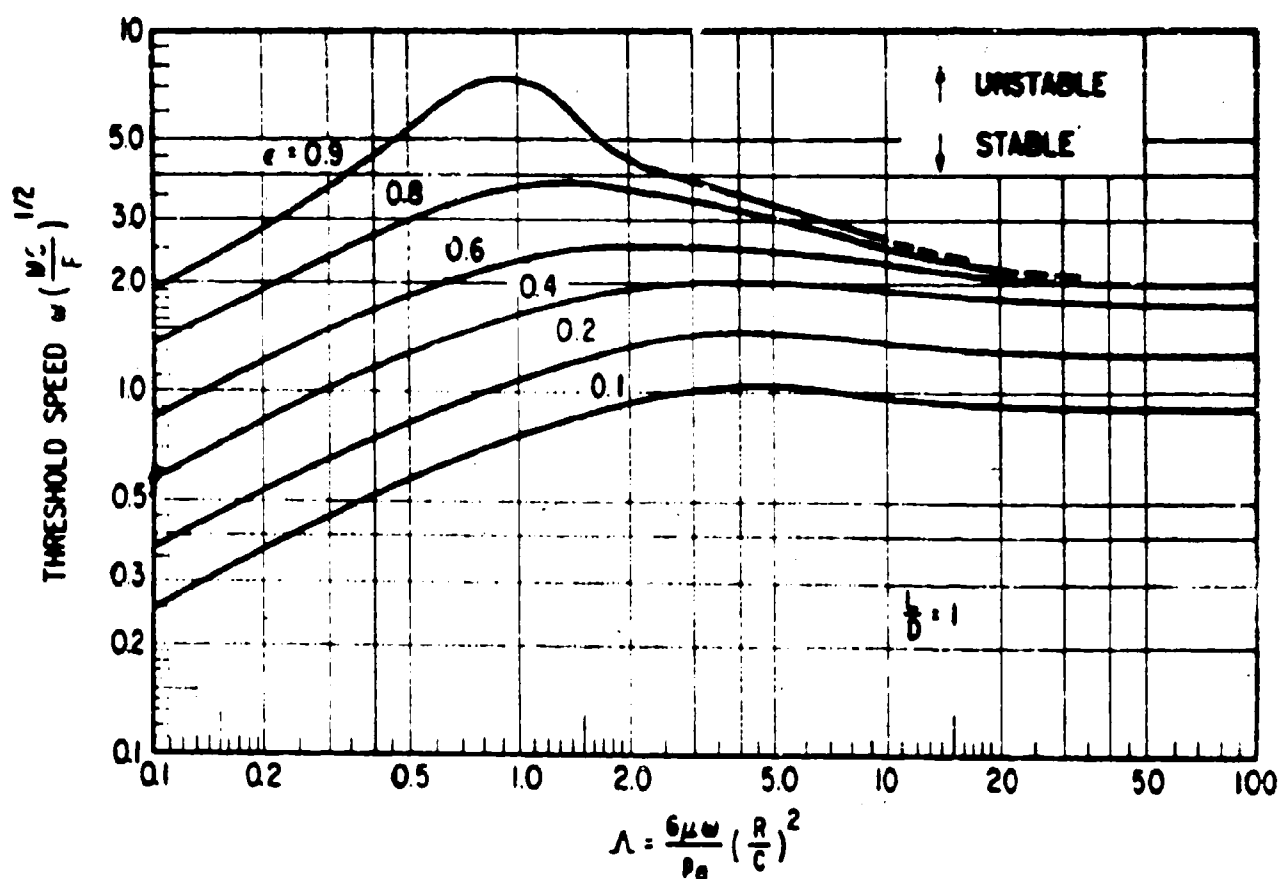


Fig. 5.16 Stability Chart for Finite Length ( $L/D = 1.0$ ) Cylindrical Gas Bearing

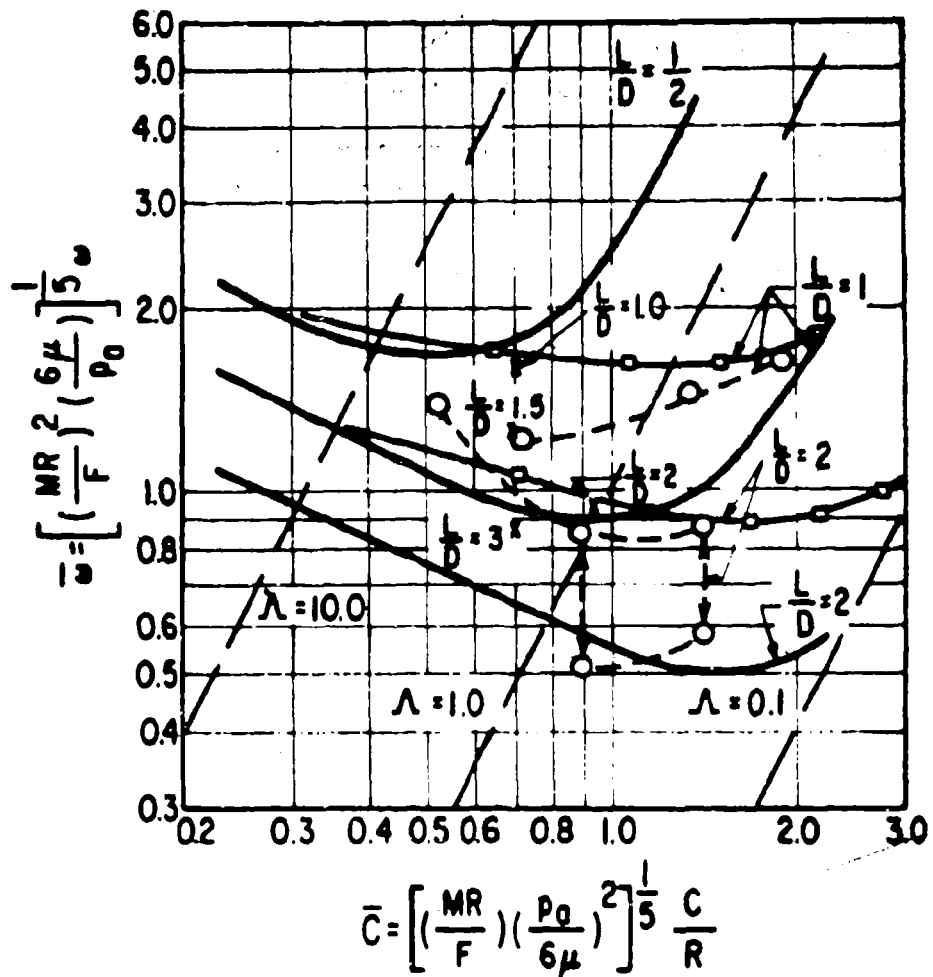
Reprinted from STABILITY ANALYSIS OF GAS-LUBRICATED, SELF-ACTING, PLAIN, CYLINDRICAL, JOURNAL BEARINGS OF FINITE LENGTH, USING GALERKIN'S METHOD, Figure 7, by H.S. Cheng and C.H.T. Pan, ASME Paper No. 64-LubS-5.

—○— NON-LINEAR GALERKIN  $\frac{F}{p_0 D^2} = 0.2$

— LINEARIZED PH-QUASI STATIC THEORY  $\frac{F}{p_0 D^2} = 0.2$

○ DATA AFTER STERNLICHT - WINN  $\frac{F}{p_0 D^2} = 0.1873$

⋈ DATA AFTER WHITLEY - BOWHILL - McEWAN  $\frac{F}{p_0 D^2} = 0.2$



LENGTH EFFECTS  $\frac{F}{p_0 D^2} = 0.2$

Fig. 5.17 Comparison Between Theoretical and Experimental Results. Finite Bearing.

Reprinted from STABILITY ANALYSIS OF GAS-LUBRICATED, SELF-ACTING, PLAIN, CYLINDRICAL, JOURNAL BEARINGS OF FINITE LENGTH, USING GALERKIN'S METHOD, Figure 12, by H.S. Cheng and C.H.T. Pan, ASME Paper No. 64-LubS-5.

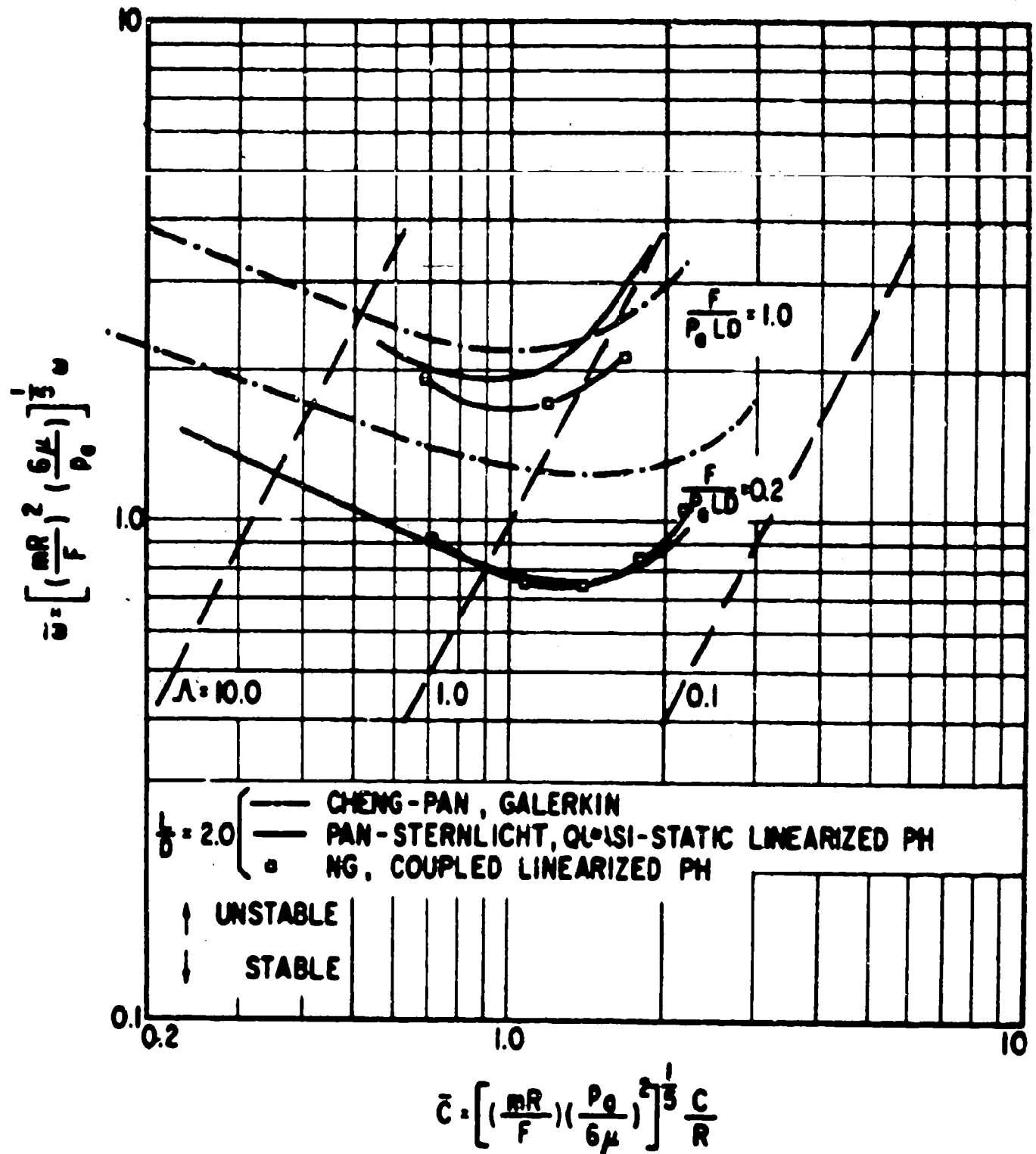


Fig. 5.18 Comparison of Linearized PH Results with Other Theories. Finite Bearing.

Reprinted from LINEARIZED PH STABILITY THEORY FOR FINITE LENGTH, SELF-ACTING, GAS-LUBRICATED, PLAIN JOURNAL BEARINGS, Figure 12, by Chung-Wah Ng, ASME Paper No. 64-LubS-28.

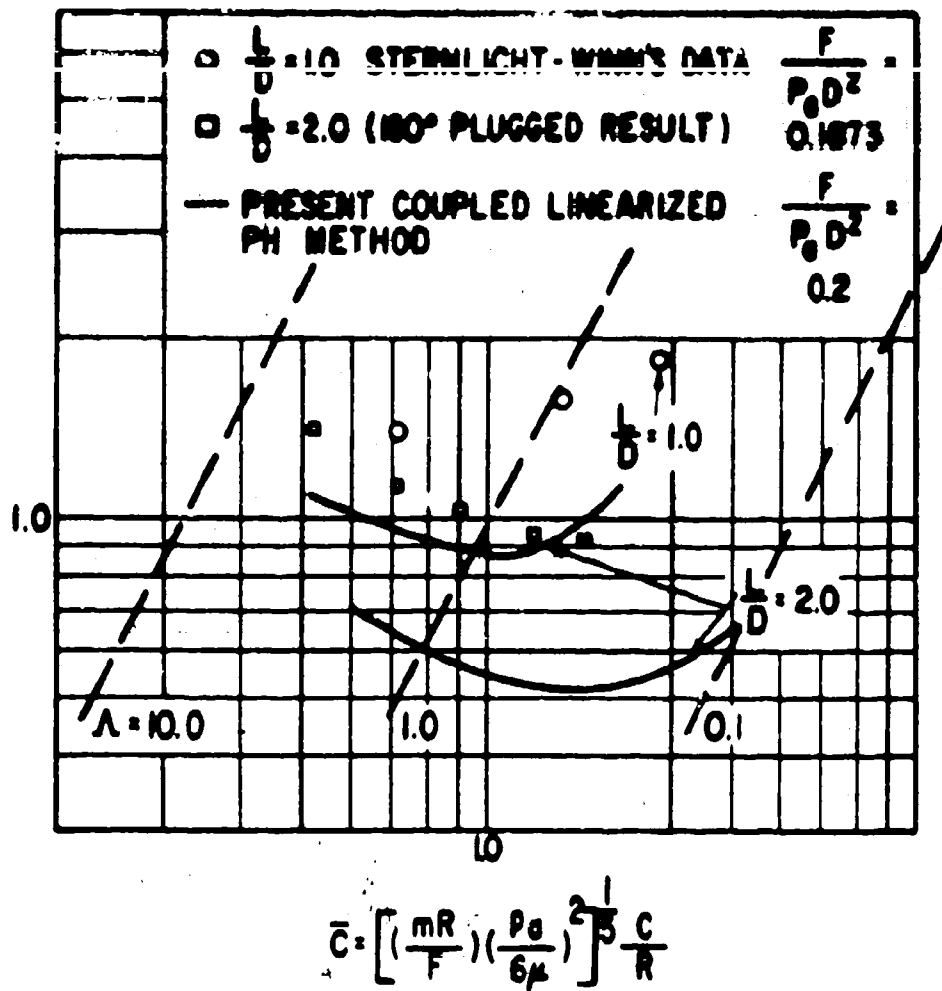


Fig. 5.19 Comparison of Linearized PH Results with Experimental Results

Reprinted from LINEARIZED PH STABILITY THEORY FOR FINITE LENGTH, SELF-ACTING, GAS-LUBRICATED, PLAIN JOURNAL BEARINGS, Figure 13, by Chung-Wah Ng, ASME Paper No. 64-LubS-28.

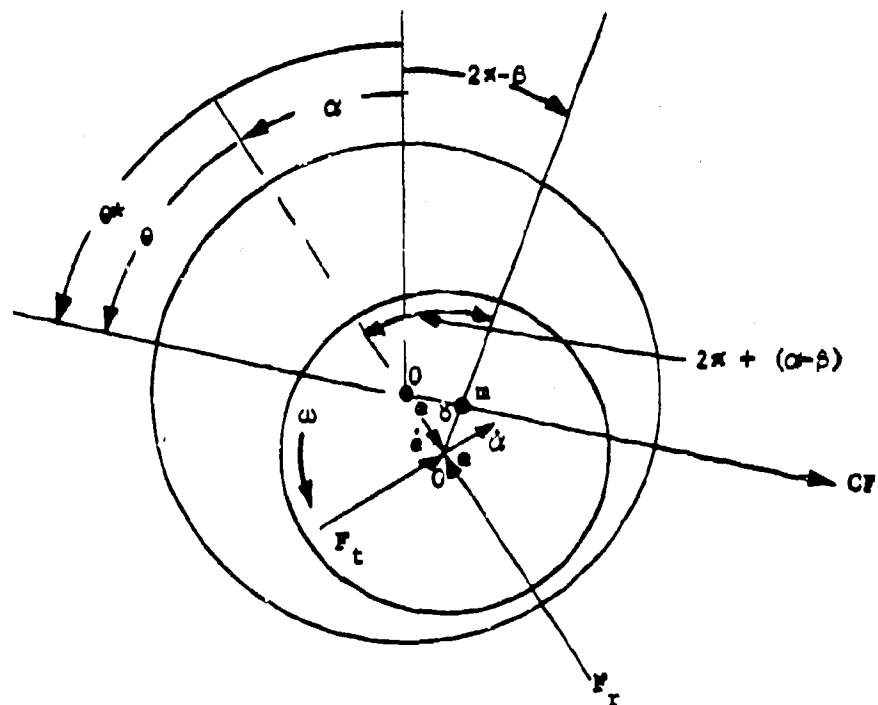


Fig. 5.20 Bearing Geometry for Synchronous Whirling of a Gas-Lubricated Bearing

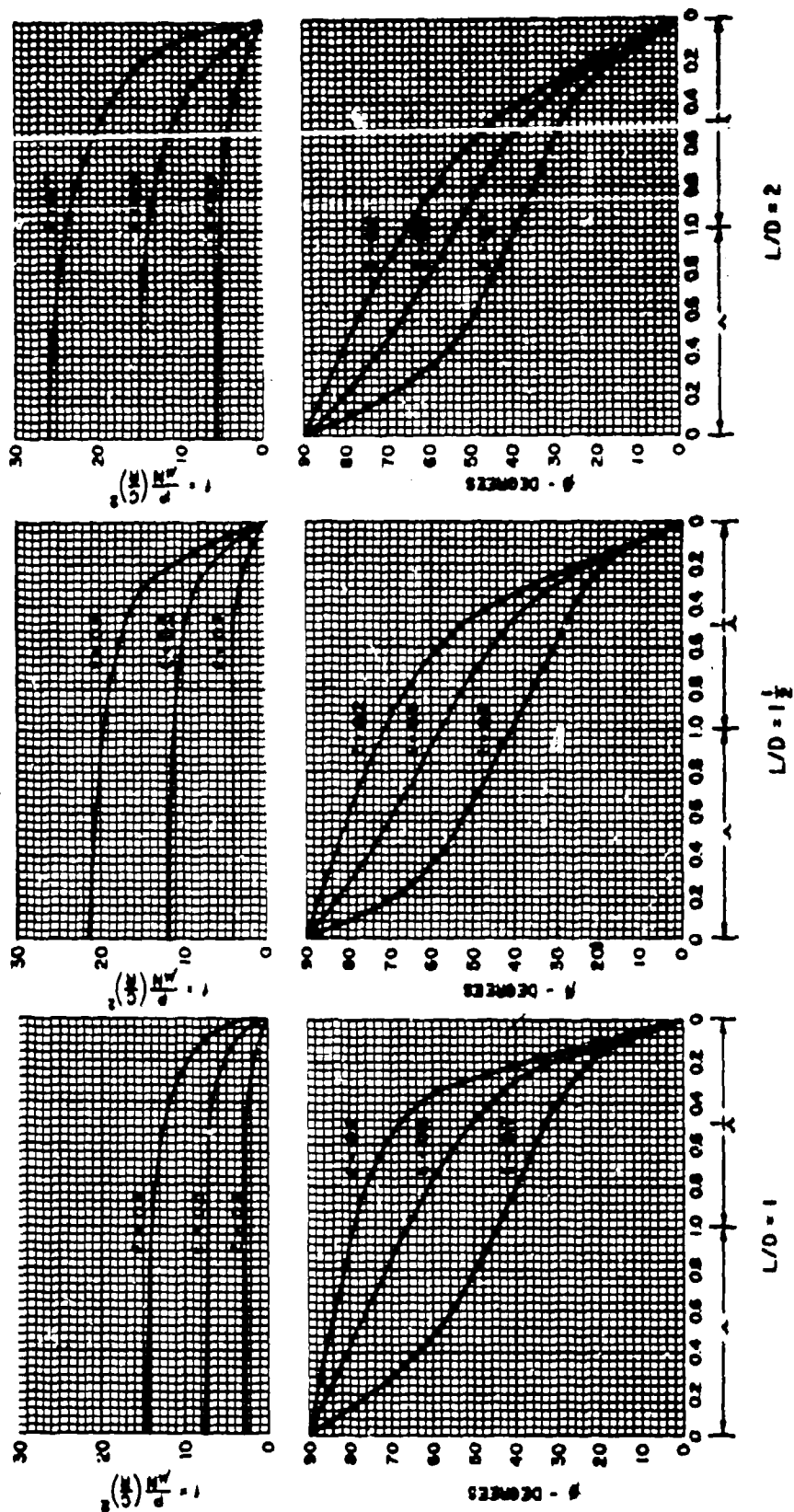


Fig. 5.21 Phase Angle and Nondimensional Force vs. Bearing Number for  $L/D = 1, 1.5, 2$

Reprinted from SYNCHRONOUS WHIRL IN PLAIN JOURNAL BEARINGS, Figure 2, by B. Stenlicht and R.C. Elwell, ASME Paper No. 62-LubS-19.

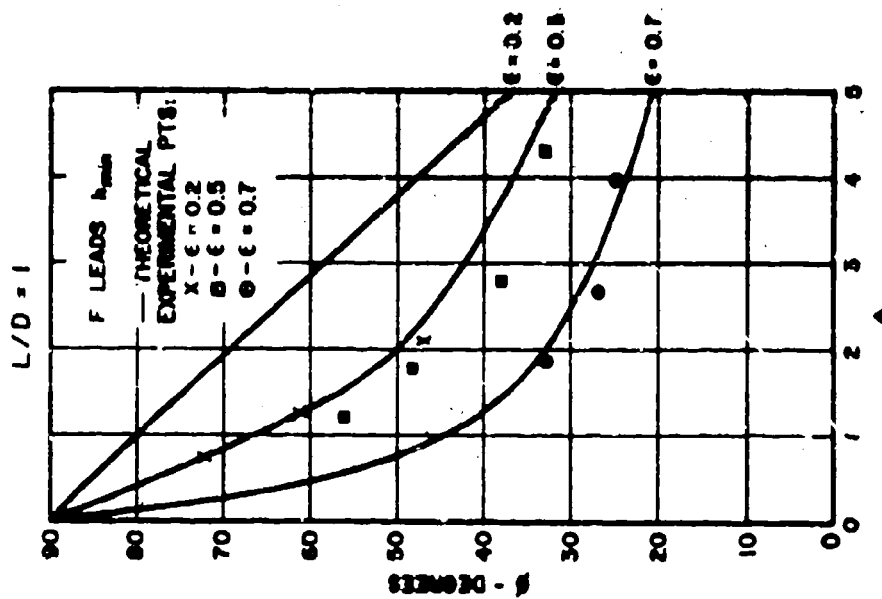
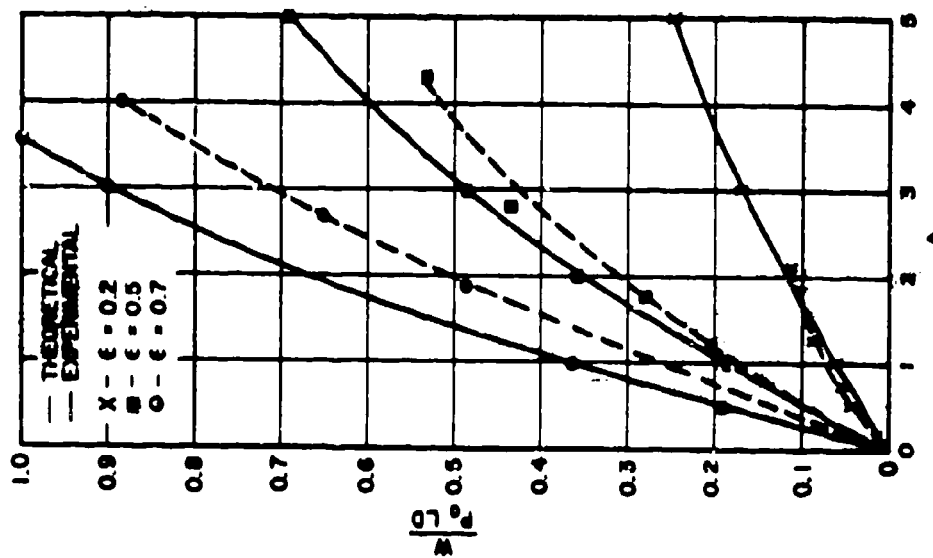


Fig. 5.22 Comparison of Theory and Experiment,  $L/D = 1$

Reprinted from *SPHERICAL BEARING IN PLAIN JOURNAL BEARINGS*,  
Figure 6a, by B. Stenlicht and R.C. Elwell, ASME Paper  
No. 62-LubS-19.

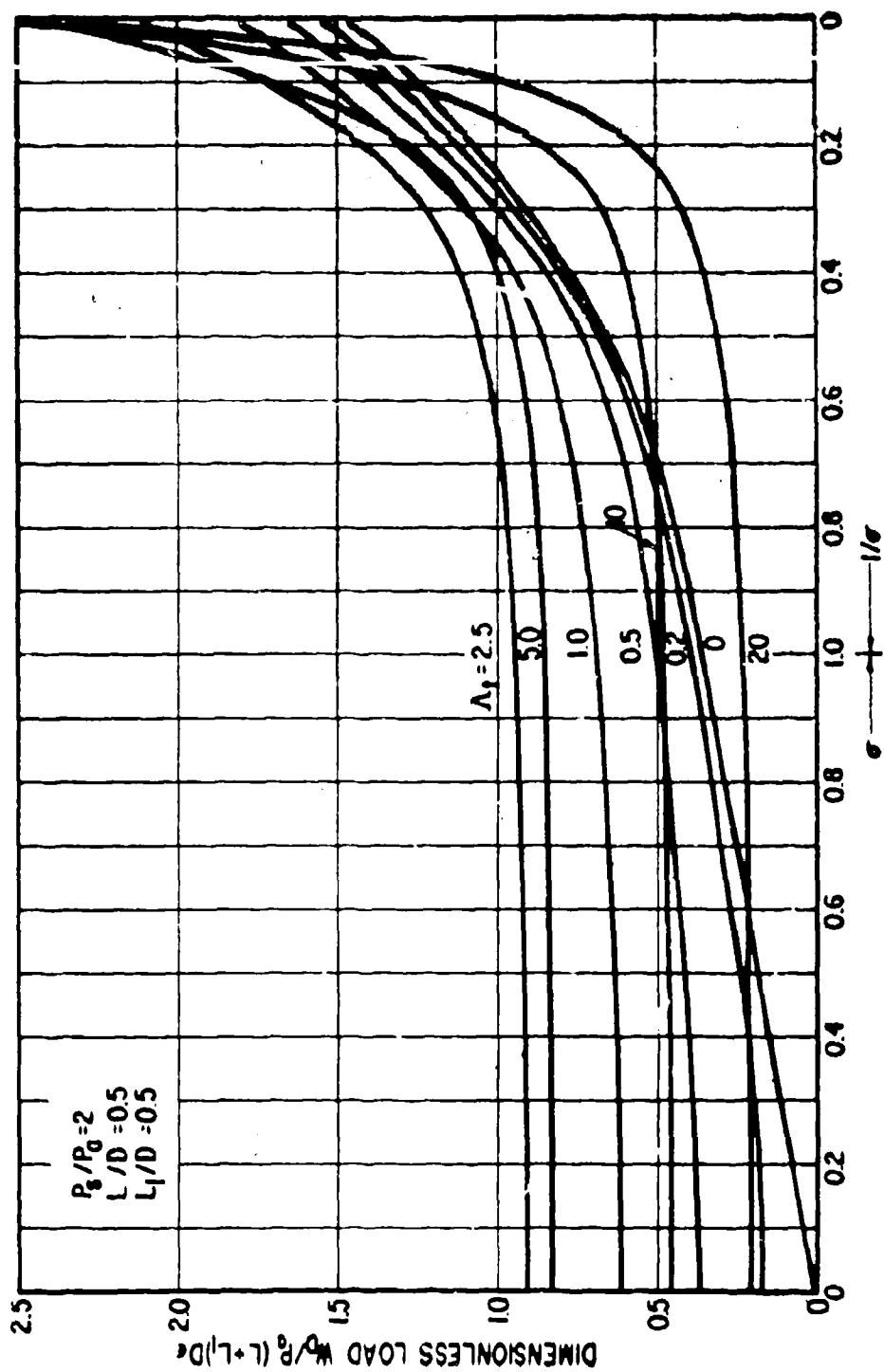


Fig. 5.23 Load vs. Vibration Frequency,  $P_0/P_0 = 2$ ,  $L/D = 0.5$ ,  $L_1/D = 0.5$

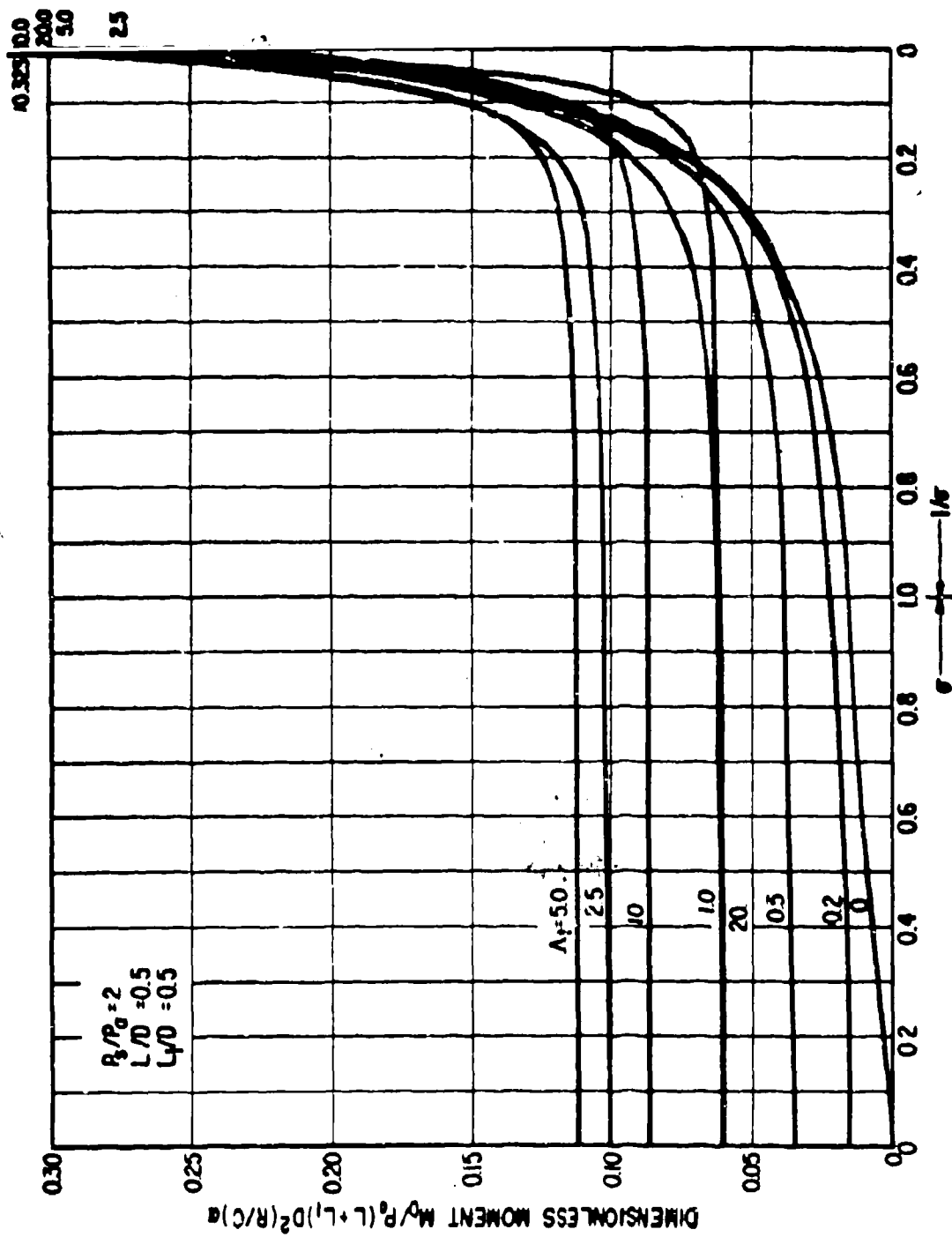


Fig. 5.24 Moment vs. Vibration Frequency,  $P_0/P_a = 2$ ,  $L/D = 0.5$ ,  $L_1/D = 0.5$

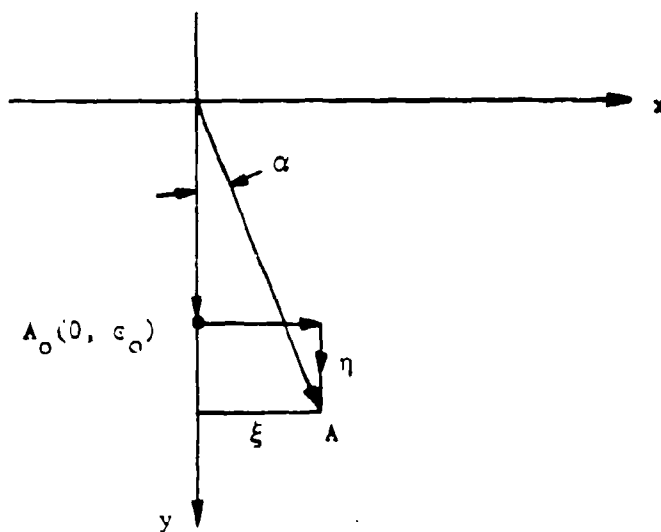


Fig. 5.25 Simple Rotor. Small Displacement from Equilibrium at  $A_0$

Table 3.01 Threshold of Instability for Symmetrical Rotor Supported in Plain Journal Bearings

L/D	$\epsilon$	A	$\nu/8$	s	$(\omega_c)_r/\omega_c$	$\omega/(\omega_c)_r$
0.5	0.2	0.1	0.3756	2.6096	0.9852	2.6488
	0.5	0.1	0.3538	2.8104	0.9974	2.8177
	0.8	0.1	0.2354	4.2438	0.9998	4.2446
0.5	0.2	100.0	0.3756	0.06678	0.02910	2.2948
	0.5	100.0	0.3538	0.2533	0.1315	1.9262
	0.8	100.0	0.2354	1.9267	0.7751	2.4857
1.0	0.2	0.1	0.37	2.6763	0.9948	2.6903
	0.3	0.1	0.37	2.7224	0.9971	2.7303
	0.7	0.1	0.29	3.4179	0.9998	3.4186
	0.8	0.1	0.22	4.5169	0.9999	4.5173
1.0	0.2	100.0	0.37	0.1951	0.0834	2.3420
	0.3	100.0	0.37	0.3198	0.1390	2.300
	0.7	100.0	0.29	1.6553	0.7000	2.3647
	0.8	100.0	0.22	3.1199	0.8998	3.4675

Notation:

$\epsilon$	Bearing eccentricity
A	Rotor parameter $(\pi k C^3 / 2 \mu L R^3 \omega_0)$
$\nu$	Whirl frequency
$\omega$	Whirl threshold speed
$\omega_0$	Rigid bearing critical speed $[k/m]^{1/2}$
$\omega_c$	Rotor-bearing critical speed
s	Resonant whip speed ratio, rigid bearings $\omega/\omega_0$

## TRANSITION OF A ROTOR THROUGH A CRITICAL SPEED

### Introduction

It is common for modern high-speed machines to operate beyond their fundamental flexural critical speed. Frequently, the operating speed range contains several critical speeds, each of which must be passed through on run-up and run-down. The increased rotor amplitude and transmitted bearing force associated with each critical speed raise the question: What are the conditions which make it safe for a rotor to pass through the critical speeds?

It has been shown in Section 3 that the motion which follows start-up in a simple rotor-bearing system consists of a steady-state, synchronous, unbalance whirl together with two transient whirls whose value depends on the initial conditions of the motion. In practical systems these transients are damped out by the rotor friction within relatively few cycles. In Section 3, the important features of the steady whirl motion are discussed. This chapter considers the state of motion which develops when the rotor speed is not constant, but is accelerating. In this condition, the transient whirls are sustained by the changing speed, and so form part of the solution which has practical interest. Of primary concern is how the rotor performance is influenced by the interaction between the accelerated motion, the sustained transient whirls, and the critical speed amplitude buildup.

### Flexible Undamped Rotor in Rigid Bearings

For simplicity, the simple, single-disk rotor without damping, mounted in rigid bearings, will be considered initially to determine the basic properties of the motion. The rotor whirl configuration is shown in Figure 6.01. The angle swept out by the rotor as its speed changes is given by

$$\phi = \omega_0 t \pm \alpha t^2 \quad (6.01)$$

where  $\omega_0$  is the initial angular velocity, and  $2\alpha$  is the angular acceleration, assumed constant. Differentiating gives the instantaneous angular velocity

$$\dot{\phi} = \omega_0 \pm 2\alpha t$$

Considering the motion of the disk, the coordinate equations for the c.g. are

$$\begin{aligned}x_G &= x + a \cos \phi = x + a \cos [\omega_0 t \pm \alpha t^2] \\y_G &= y + a \sin \phi = y + a \sin [\omega_0 t \pm \alpha t^2]\end{aligned}\quad (6.03)$$

The equations of motion for the accelerated system are therefore:

$$\begin{aligned}m\ddot{x}_G + kx_G &= k_a \cos [\omega_0 t \pm \alpha t^2] \\m\ddot{y}_G + ky_G &= k_a \sin [\omega_0 t \pm \alpha t^2] \\2\alpha I + ka [x \sin (\omega_0 t \pm \alpha t^2) - y \cos (\omega_0 t \pm \alpha t^2)] &= T\end{aligned}\quad (6.03)$$

The solution to these equations is influenced by the initial conditions which exist prior to the application of the accelerating torque. The first two equations may be solved separately as the rotational motion of the disk is specified, and the third equation gives the acceleration torque once the coordinate values are known..

For the case where the disk is whirling steadily at constant angular velocity,  $\omega$ , prior to the application of accelerating torque at time  $t = 0$ , the initial conditions are:

For  $t < 0$ ,

$$\begin{aligned}x_G &= \frac{a}{1 - \left(\frac{\omega}{\omega_0}\right)^2} \cos \omega t & y_G &= \frac{a}{1 - \left(\frac{\omega}{\omega_0}\right)^2} \sin \omega t \\ \dot{x}_G &= \frac{-\omega a}{1 - \left(\frac{\omega}{\omega_0}\right)^2} \sin \omega t & \dot{y}_G &= \frac{\omega a}{1 - \left(\frac{\omega}{\omega_0}\right)^2} \cos \omega t\end{aligned}$$

For  $t = 0$

$$\begin{aligned}x_G(0) &= \frac{a}{1 - \left(\frac{\omega}{\omega_0}\right)^2} & y_G(0) &= 0 \\ \dot{x}_G(0) &= 0 & \dot{y}_G(0) &= \frac{\omega a}{1 - \left(\frac{\omega}{\omega_0}\right)^2}\end{aligned}\quad (6.04)$$

With these initial conditions, the general solution to Equations (6.03) has the form

$$x_G = a\omega_0 \int_0^t \sin \omega_0 (t-\tau) \cos (\omega\tau \pm \alpha t^2) d\tau + \frac{a}{1 - \left(\frac{\omega}{\omega_0}\right)^2} \cos \omega_0 t \quad (6.05)$$

$$y_G = a\omega_0 \int_0^t \sin \omega_0 (t-\tau) \sin (\omega\tau \pm \alpha t^2) d\tau + \frac{a}{\omega_0} \frac{1}{1 - \left(\frac{\omega}{\omega_0}\right)^2} \sin \omega_0 t$$

Equations (6.05) may be integrated to give the amplitudes  $x_G$ ,  $y_G$  of the c.g. as the rotor responds to the accelerating torque,  $T$ . However, for stress calculations it is convenient to obtain the solution directly in terms of coordinates  $\xi_G$ ,  $\eta_G$  which rotate along with the shaft at speed  $\dot{\phi}$ . The transformation formulae are:

$$\begin{aligned} \xi_G &= x_G \cos \phi + y_G \sin \phi \\ \eta_G &= -x_G \sin \phi + y_G \cos \phi \end{aligned} \quad (6.06)$$

Substituting Equations (6.05) into (6.06) simplifying, and integrating gives the following expressions for  $\xi_G$ ,  $\eta_G$ , after considerable manipulation:

$$\begin{aligned} \xi_G &= a\omega_0 \left[ \frac{\pi}{8\alpha} \right]^{\frac{1}{2}} \left\{ \mp \sin z \left[ C(z) - C(z_0) \right] \pm \cos z \left[ S(z) - S(z_0) \right] \right. \\ &\quad \left. \pm \sin z^1 \left[ C(z^1) - C(z_0^1) \right] \mp \cos z^1 \left[ S(z^1) - S(z_0^1) \right] \right\} \\ &\quad + \frac{a}{1 - \left(\frac{\omega}{\omega_0}\right)^2} \left[ -\cos \omega_0 t \cdot \cos (\omega t \pm \alpha t^2) + \frac{\omega}{\omega_0} \sin \omega_0 t \cdot \sin (\omega t \pm \alpha t^2) \right] \\ \eta_G &= a\omega_0 \left[ \frac{\pi}{8\alpha} \right]^{\frac{1}{2}} \left\{ -\cos z \left[ C(z) - C(z_0) \right] - \sin z \left[ S(z) - S(z_0) \right] \right. \\ &\quad \left. + \cos z^1 \left[ C(z^1) - C(z_0^1) \right] + \sin z^1 \left[ S(z^1) - S(z_0^1) \right] \right\} \end{aligned}$$

$$+ \frac{a}{1 - \frac{\omega}{\omega_c}} 2 \left[ \cos \omega_0 t \cdot \sin (\alpha t \pm \alpha t^2) + \frac{\omega}{\omega_0} \sin \omega_0 t \cdot \cos (\alpha t \pm \alpha t^2) \right] \quad (6.07)$$

where

$$\begin{aligned} z &= \left[ \alpha t \pm \frac{\omega - \omega_0}{2 \alpha} \right]^2 & z_0 &= \left[ \frac{\omega - \omega_0}{2 \alpha} \right]^2 \\ \sigma &= \left[ \alpha t \pm \frac{\omega - \omega_0}{2 \alpha} \right]^2 & \sigma' &= \left[ \alpha t \pm \frac{\omega + \omega_0}{2 \alpha} \right]^2 \\ z' &= \left[ \alpha t \pm \frac{\omega + \omega_0}{2 \alpha} \right]^2 & z_0' &= \left[ \frac{\omega + \omega_0}{2 \alpha} \right]^2 \end{aligned} \quad (6.08)$$

and

$$\begin{aligned} C(z) - C(z_0) &= \int_0^z \frac{\cos \sigma d \sigma}{\sqrt{2 \pi \sigma}} - \int_0^{z_0} \frac{\cos \sigma d \sigma}{\sqrt{2 \pi \sigma}} = \int_{z_0}^z \frac{\cos \sigma d \sigma}{\sqrt{2 \pi \sigma}} \\ S(z) - S(z_0) &= \int_0^z \frac{\sin \sigma d \sigma}{\sqrt{2 \pi \sigma}} - \int_0^{z_0} \frac{\sin \sigma d \sigma}{\sqrt{2 \pi \sigma}} = \int_{z_0}^z \frac{\sin \sigma d \sigma}{\sqrt{2 \pi \sigma}} \end{aligned} \quad (6.09)$$

are the Fresnel integrals of the above variable groups which arise in the derivation of the expressions for  $\xi_G$  and  $\eta_G$ .

Equations (6.09) allow the deflections of single-disk rotor in rigid bearings to be calculated during any stage of its motion: with velocity below, at, or above the critical speed,  $\omega_c$ ; and either accelerating or decelerating. The  $\xi$  axis is in the plane of the unbalance; but even though the system is frictionless, the whirl radius is no longer a straight line due to the acceleration. Its maximum value may be found from the coordinates of G:

$$r_G = \left[ \xi_G^2 + \eta_G^2 \right]^{\frac{1}{2}} = \left[ x_G^2 + y_G^2 \right]^{\frac{1}{2}} \quad (6.10)$$

For a specified acceleration,  $\alpha$ , it is thus possible to examine the characteristics of the amplitude build-up, and to determine the value of the maximum amplitude,  $r_G$ , and the speed ratio,  $\frac{\omega}{\omega_c}$ , at which it occurs. A minimum  $\alpha$ , corresponding to a maximum permissible amplitude build-up and associated bending stress, may then be specified for rotor operation.

An example of this calculation is given in Figure 6.02. The rotor has a critical speed,  $\eta_c$ , of 1000 RPM, i.e.,  $\omega_c = 105$  rad/sec. The acceleration is 20 rad/sec.<sup>2</sup>, i.e.,  $\alpha = 10$  rad/sec.<sup>2</sup> and dissipative forces are absent from the motion.

### Influence of External Friction on Rotor Motion

When external friction forces act on the rotor during its accelerated motion, energy is dissipated and the amplitude build-up becomes less severe than for the frictionless rotor considered previously. In this case, the equations of motion for the c.g. of the single-disk rotor in rigid bearings are

$$\begin{aligned} m\ddot{x}_G + c\dot{x} + kx &= ka \cos [\omega t + \alpha t^2] \\ m\ddot{y}_G + c\dot{y} + ky &= ka \sin [\omega t + \alpha t^2] \\ 2\alpha x + ka [x \sin (\omega t + \alpha t^2) - y \cos (\omega t + \alpha t^2)] &= T \end{aligned} \quad (6.11)$$

Again, considering the case where the rotor is in a state of steady unbalance whirl prior to the application of  $T$  at  $t = 0$ , the general formulae for the  $x$ ,  $y$  displacement are

$$\begin{aligned} x &= a\omega_0 \int_0^t \exp \left[ -\frac{c}{2m}(t-\tau) \right] \sin \omega_0 (t-\tau) \cos (\omega\tau + \alpha\tau^2) d\tau + \frac{a}{1-(\frac{\omega}{\omega_0})^2} \cos \omega_0 t \\ y &= a\omega_0 \int_0^t \exp \left[ -\frac{c}{2m}(t-\tau) \right] \sin \omega_0 (t-\tau) \sin (\omega\tau + \alpha\tau^2) d\tau + \frac{\omega}{\omega_0} \frac{a}{1-(\frac{\omega}{\omega_0})^2} \sin \omega_0 t \end{aligned}$$

When these expressions are transformed into rotating coordinates,  $\xi$  and  $\eta$  and the expressions

$$\tau = \left[ \sqrt{\frac{\sigma}{\alpha}} - \frac{\omega - \omega_0}{2\alpha} \right] = \sqrt{\frac{\sigma'}{\alpha}} - \frac{\omega + \omega_0}{2\alpha} ; \quad t = \sqrt{\frac{z}{\alpha}} - \frac{\omega - \omega_0}{2\alpha} = \sqrt{\frac{z'}{\alpha}} - \frac{\omega + \omega_0}{2\alpha}$$

are substituted for the time-arguments, the expressions for the rotor displacements become

$$\xi = a\omega_0 \sqrt{\frac{\pi}{8\alpha}} \exp \left[ -\frac{c}{2m}t \right] \left\{ -\sin z \int_{z_0}^z \exp \frac{c}{2m} \left[ \sqrt{\frac{\sigma}{\alpha}} - \frac{\omega - \omega_0}{2\alpha} \right] \frac{\cos \sigma d\sigma}{\sqrt{2\pi\sigma}} \right.$$

$$\begin{aligned}
& + \cos z \int_{z_0}^z \exp \frac{c}{2m} \left[ \sqrt{\frac{\sigma}{\alpha}} - \frac{\omega - \omega_0}{2\alpha} \right] \frac{\sin \sigma d\sigma}{\sqrt{2\pi\sigma}} \\
& + \sin z' \int_{z_1}^{z'}, \exp \frac{c}{2m} \left[ \sqrt{\frac{\sigma}{\alpha}} - \frac{\omega + \omega_0}{2\alpha} \right] \frac{\cos \sigma' d\sigma'}{\sqrt{2\pi\sigma'}} \\
& - \cos z' \int_{z_1}^{z'}, \exp \frac{c}{2m} \left[ \sqrt{\frac{\sigma}{\alpha}} - \frac{\omega + \omega_0}{2\alpha} \right] \frac{\sin \sigma' d\sigma'}{\sqrt{2\pi\sigma'}} \Bigg\} + \\
& \frac{a}{1 - \left(\frac{\omega}{\omega_0}\right)^2} \left[ \cos \omega_0 t \cos (\omega t + \alpha t^2) + \frac{\omega}{\omega_0} \sin \omega_0 t \sin (\omega t + \alpha t^2) \right] \\
\eta = & a\omega \sqrt{\frac{\pi}{8\alpha}} \cdot \exp \left[ -\frac{c}{2m} t \right] \Bigg\{ - \cos z \int_{z_0}^z \exp \frac{c}{2m} \left[ \sqrt{\frac{\sigma}{\alpha}} - \frac{\omega - \omega_0}{2\alpha} \right] \frac{\cos \sigma d\sigma}{\sqrt{2\pi\sigma}} \\
& - \sin z \int_{z_0}^z \exp \frac{c}{2m} \left[ \sqrt{\frac{\sigma}{\alpha}} - \frac{\omega - \omega_0}{2\alpha} \right] \frac{\sin \sigma d\sigma}{\sqrt{2\pi\sigma}} + \\
& \cos z' \int_{z_0}^{z'}, \exp \frac{c}{2m} \left[ \sqrt{\frac{\sigma}{\alpha}} - \frac{\omega + \omega_0}{2\alpha} \right] \frac{\cos \sigma' d\sigma'}{\sqrt{2\pi\sigma'}} \\
& + \sin z' \int_{z_0}^{z'}, \exp \frac{c}{2m} \left[ \sqrt{\frac{\sigma}{\alpha}} - \frac{\omega + \omega_0}{2\alpha} \right] \frac{\sin \sigma' d\sigma'}{\sqrt{2\pi\sigma'}} \Bigg\} + \\
& \frac{a}{1 - \left(\frac{\omega}{\omega_0}\right)^2} \left[ - \cos \omega_0 t \sin (\omega t + \alpha t^2) + \frac{\omega}{\omega_0} \sin \omega_0 t \cdot \cos (\omega t + \alpha t^2) \right] \quad (6.12)
\end{aligned}$$

The integrals in the above expressions cannot be found directly from tables; but as the value of the exponential index is reasonably small, the integrals may be obtained approximately by a combination of known functions. In this case, a linear approximation may be used for the exponential index, and the equations may be solved for a number of separate time-periods. This has been done for the example given in the previous section considering that the friction coefficient  $(c/2m) = 1.00$ . The results are shown in Figure 6.03. Comparing Figures 6.02 and 6.03, the influence of external friction on the same rotor with the same rate of acceleration may be seen. Friction reduces the maximum amplitude build-up from 34.0 to 21.0. The transmitted bearing force is reduced in the same proportion. The speed at which this maximum amplitude occurs is virtually identical in both cases.

### Amplitude Buildup

A more extensive set of displacement-time curves has been obtained by Lewis (Ref. 78) for the case of a simple rotor in rigid bearings in both undamped and damped motion. Considering undamped rotor motions, the influence of several different rates of acceleration  $q$  on a rotor are shown in Figure 6.04. Curve B shows the individual cyclic oscillations, and the other curves show the envelopes of the amplitude maximum values. Low  $q$  values denote rapid acceleration; high values correspond to slower rates. The periodic force variation for  $q = 10$  is given in Curve A starting at  $t = 0$ . Allowing the rotor to start from a steady whirl condition as in the previous section, the resultant motion builds up as shown in Curve B, for  $q = 10$ , and in the remaining curves for the higher  $q$  values indicated. The full curves correspond to accelerations; whereas the dotted curves apply to decelerations. These results clearly indicate how any machine may be driven through its critical speed even where the rotor-bearing system has little friction damping. The maximum amplitude which develops is seen to be a function of the applied acceleration, and a finite time is required for the build-up of large amplitude whirl motions. The faster the acceleration rate, the later the maximum amplitude occurs after the critical speed. The amplitude build-up occurs in the same speed location for the deceleration characteristics, being slightly larger in each case. This indicates also the advantage of keeping those rotor critical speeds, which must occur within the speed range, well below the machine operating speed. A.C. torque characteristics depend on the amount of electrical slip present. As this is nearly zero at rated speed, the drive torque and, hence, acceleration are smaller than at lower speeds; hence, the time taken to pass through the critical speed is greater. This results in the build-up of larger amplitudes as indicated in Figure 6.04.

After the maximum amplitude has been passed, the undamped system continues to oscillate with an amplitude close to the maximum attained. This is little diminished by the higher exciting frequency which, though this superposes a further vibration with a stronger force, it does so at frequencies to which the system has less inherent susceptibility, and so the vibration is sustained.

The influence of friction on amplitude build-up is shown in Figure 6.05, for four values of dimensionless damping  $\gamma$ , with both accelerated and decelerated motion. The general nature of rotor response is the same as in the undamped case, with the difference that amplitudes are reduced by the presence of friction. This reduction is most significant in the cases of slower acceleration. The greater the value of  $\gamma$ , the greater is the overall amplitude reduction. This applies to both the steady-state motion, and to the transients in the motion which tend to die out more rapidly, as indicated by the smooth amplitude envelopes for higher  $\gamma$ .

When the damping is small, the envelope curves are oscillating in character when the maximum has been passed; but eventually they become asymptotic to the resonance curves for constant frequency.

#### Effect of Flexible Bearings on Transition Phenomena

Support flexibility may arise from either the bearing or the pedestal, or both, as discussed in Chapter 3. The inclusion of support flexibility greatly complicates the already lengthy analysis, and so this section contains but an indication of the procedure. Referring to Figure 6.06, the equations of motion for the undamped single-disk, flexible rotor shown are

$$m\ddot{x} + k(x - x_0) = ka \cos \phi$$

$$m\ddot{y} + k(y - y_0) = ka \sin \phi$$

$$2k_1 x_0 - k(x - x_0) = -ka \cos \phi$$

$$2k_2 y_0 - k(y - y_0) = -ka \sin \phi$$

$$2QI + ka(x - x_0) \sin \phi - ka(y - y_0) \cos \phi = T \quad (6.13)$$

where  $k$  is the shaft stiffness,  $k_1$  and  $k_2$  are the vertical and horizontal elastic stiffnesses of the supports respectively, and again

$$\phi = \left[ \omega t + \alpha t^2 \right]$$

On writing

$$K_1 = \frac{2kk_1}{2k_1+k}$$

$$K_2 = \frac{2kk_2}{2k_2+k}$$

The equations of motion become:

$$m\ddot{x} + k_1x = K_1a \cos [\omega t + \alpha t^2]$$

$$m\ddot{y} + k_2y = K_2a \sin [\omega t + \alpha t^2]$$

$$2\alpha I + aK_1 x \sin \phi - aK_2 y \cos \phi + a^2 \frac{c_2 - c_1}{2} \sin 2\phi = T \quad (6.14)$$

As in the case of a shaft on rigid supports, the coordinate displacements are obtained from

$$x = a\omega_x \int_0^t \sin \omega_x (t-\tau) \cos (\omega\tau + \alpha\tau^2) d\tau + \frac{a}{1 - (\frac{\omega}{\omega_0})^2} \cos \omega_x t$$

$$y = a\omega_y \int_0^t \sin \omega_y (t-\tau) \sin (\omega\tau + \alpha\tau^2) d\tau + \frac{a}{1 - (\frac{\omega}{\omega_0})^2} \sin \omega_y t$$

in which

$$\omega_x = \left[ \frac{K_1}{m} \right]^{\frac{1}{2}} \quad \omega_y = \left[ \frac{K_2}{m} \right]^{\frac{1}{2}}$$

After performing the above integrations, the displacement formulae resemble Equations (6.12) taking into account the differing stiffness effects. As an example, consider the case  $k_1 = 2K$ ,  $K_2 = 0.89 K$ ,  $[k/m]^{\frac{1}{2}} = 105 \text{ rad/sec.}$ , and  $\alpha = 10 \text{ rad/sec.}^2$ . The response curves are shown in Figure 6.07. These indicate the differing response in the coordinate directions. The whirl orbit is elliptical in the early stages of the motion, but the ellipse changes in size and proportion as the speed increases because the stiffness difference makes the dynamic response different in the x and y directions. The rotor response in rotating coordinates  $\xi$  and  $\eta$  is also given. These results show the same phase difference between maximum coordinate responses. Also, the transient motion is more strikingly depicted by allowing the coordinates to rotate, and so emphasizes transient translatory motions. In addition to the above effects,

it can be seen from the third of Equations (6.14) that a component with twice rotational frequency exists in the motion. This tends to create a sub-harmonic peak at approximately one-half the major response peaks shown in Figure 6.07.

#### Experimental Observation of Transition Phenomena

The simple flexible rotor discussed previously with  $\omega_c = 105 \text{ rad/sec.}^2$  was driven through its critical speed using a 3 KW, D.C. motor, over a speed range  $0 < \omega < 125 \text{ rad/sec.}$  Shaft stresses were recorded using resistance strain gages mounted near the disk. These stresses rotated with the shaft, and hence allowed the calculated stress and displacement values in the  $\xi, \eta$  direction to be checked for a shaft with friction. These results are shown in Figure 6.08. These coordinates show reasonably good qualitative agreement with the curves of Figure 6.02.

The shaft motions discussed in this chapter apply in all cases to a simple, single-disk, flexible-shaft rotor. This simplifies the resulting analysis and makes identification of the major rotor dynamic features more straightforward. The same features apply to the rotors of all machines which operate at speeds beyond their first system critical and, therefore, may be used as design guides.

It will be noted that no mention has been made of rotors which are mounted in fluid-film gas bearings. Where no fluid-film instabilities exist, the rotor performance would be similar to the flexible bearing case. No design information is at present available on the transition of a rotor through a critical speed when the rotor experiences a fluid-film whirl at a speed below its critical speed. Data is also lacking on the transition of rotors in gas bearings through critical speeds.



1  
2  
3  
4  
5  
6  
7

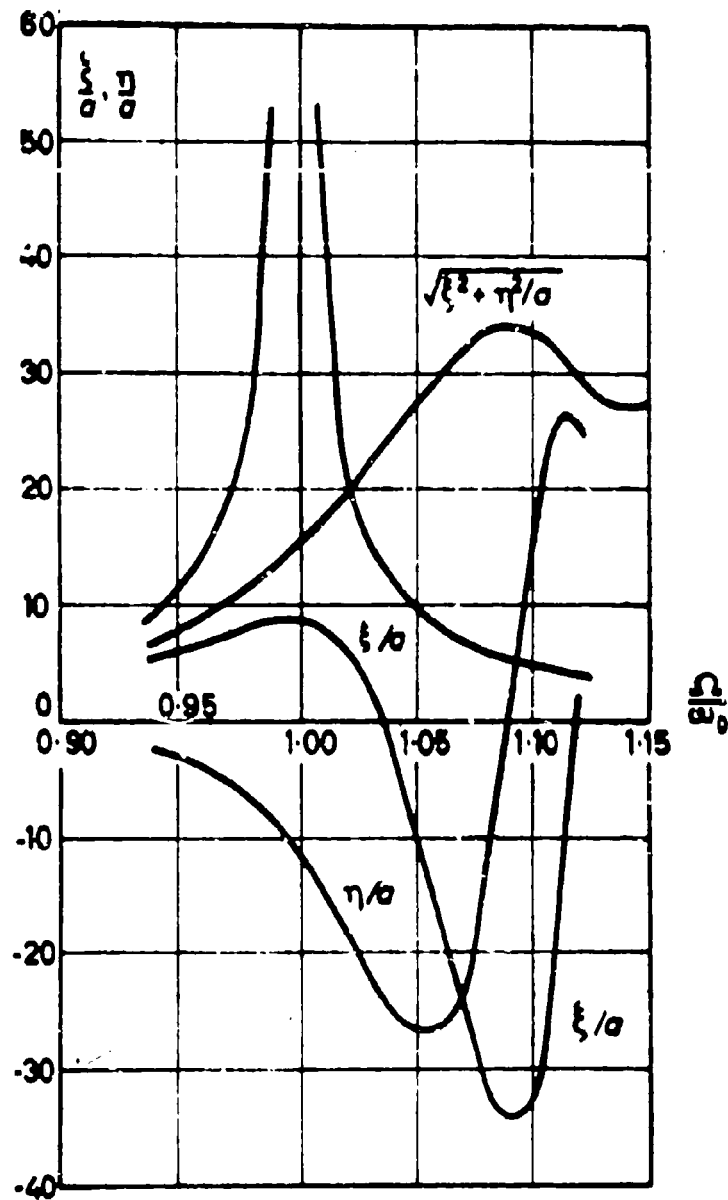


Fig. 6.02 Amplitude Response of Undamped Rotor

Reprinted from FLEXURAL VIBRATIONS OF ROTATING SHAFTS, Figure 19, by F. M. Dimentberg. 1961 Butterworth's London

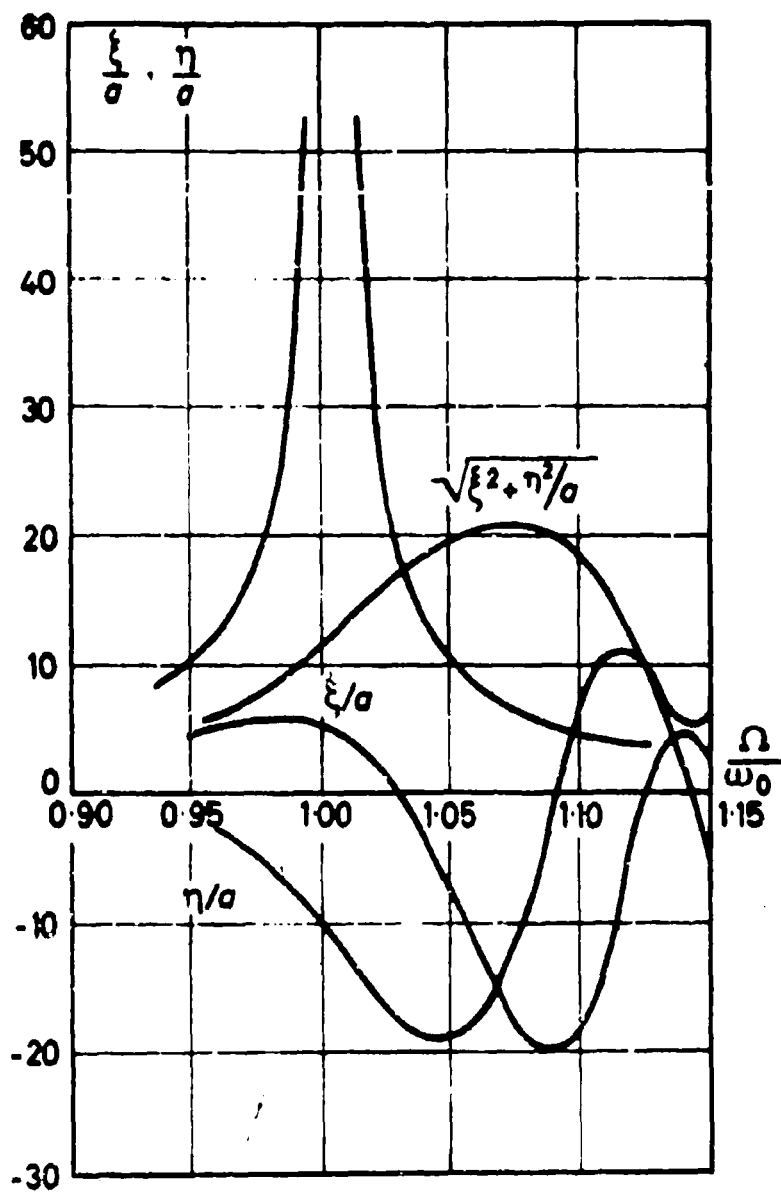


Fig. 6.03 Amplitude Response of Damped Rotor

Reprinted from FLEXURAL VIBRATIONS OF  
ROTATING SHAFTS, Figure 21, by F. M.  
Dimentberg. 1961 Butterworth's  
London

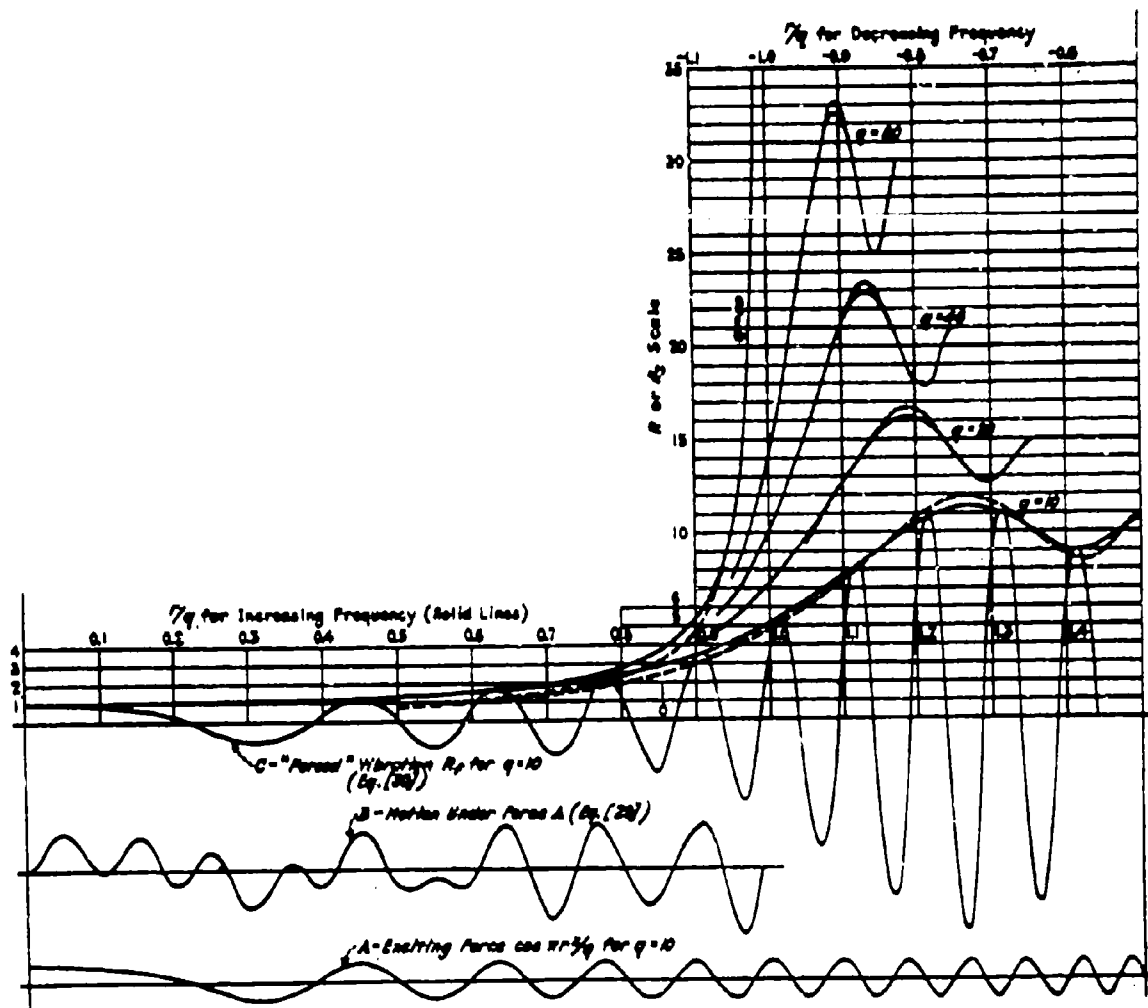


Fig. 6.04 Amplitude Buildup for Varying Acceleration Rates

Reprinted from VIBRATION DURING ACCELERATION THROUGH A CRITICAL SPEED, Figure 1, by Frank M. Lewis  
ASME Paper APM 54-24.

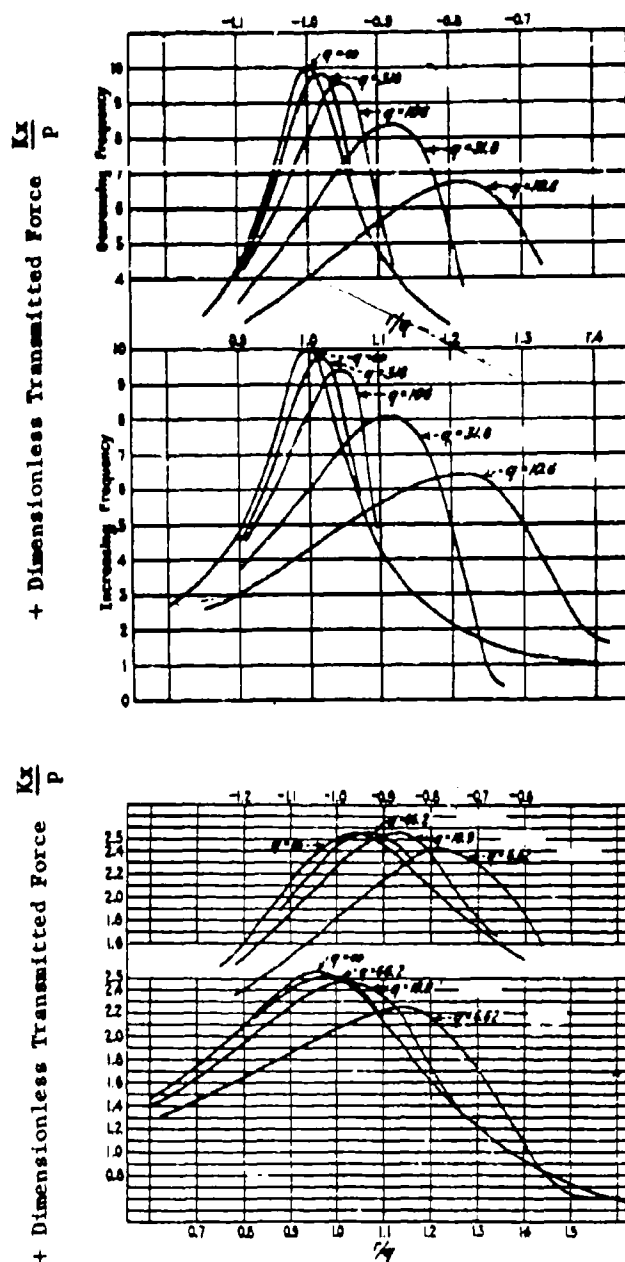


Fig. 6.05 Influence of Friction On Rate and Extent of Amplitude Buildup

Reprinted from VIBRATION DURING ACCELERATION THROUGH A CRITICAL SPEED, Figure 5, by Frank M. Lewis ASME Paper APM 54-24

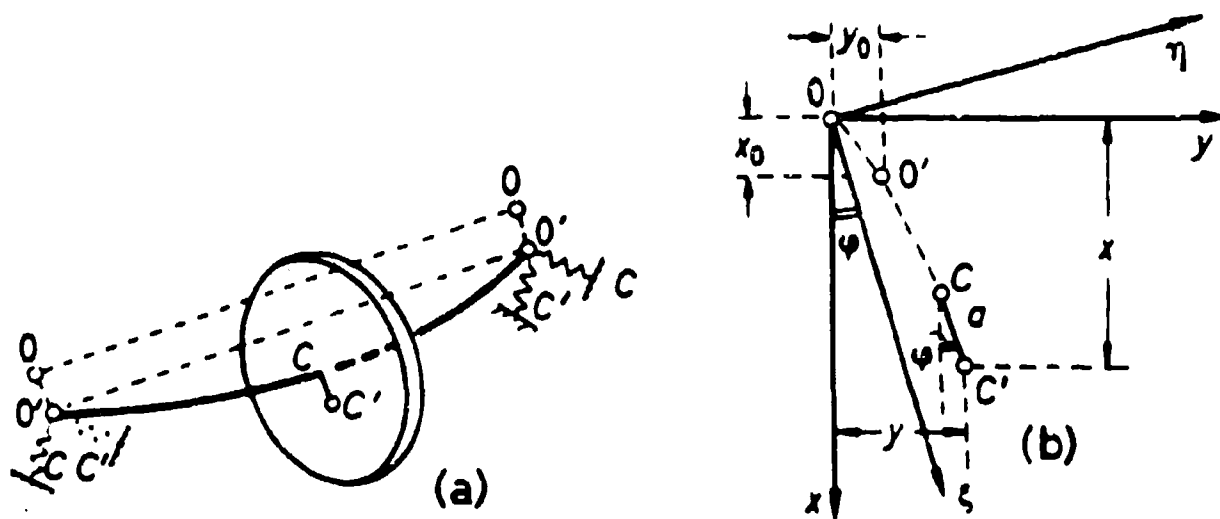


Fig. 6.06 Rotor Whirl Geometry for Flexible Rotor With Damping

Reprinted from FLEXURAL VIBRATIONS OF ROTATING SHAFTS,  
Figure 22, by F. M. Dimentberg. 1961 Butterworth's  
London

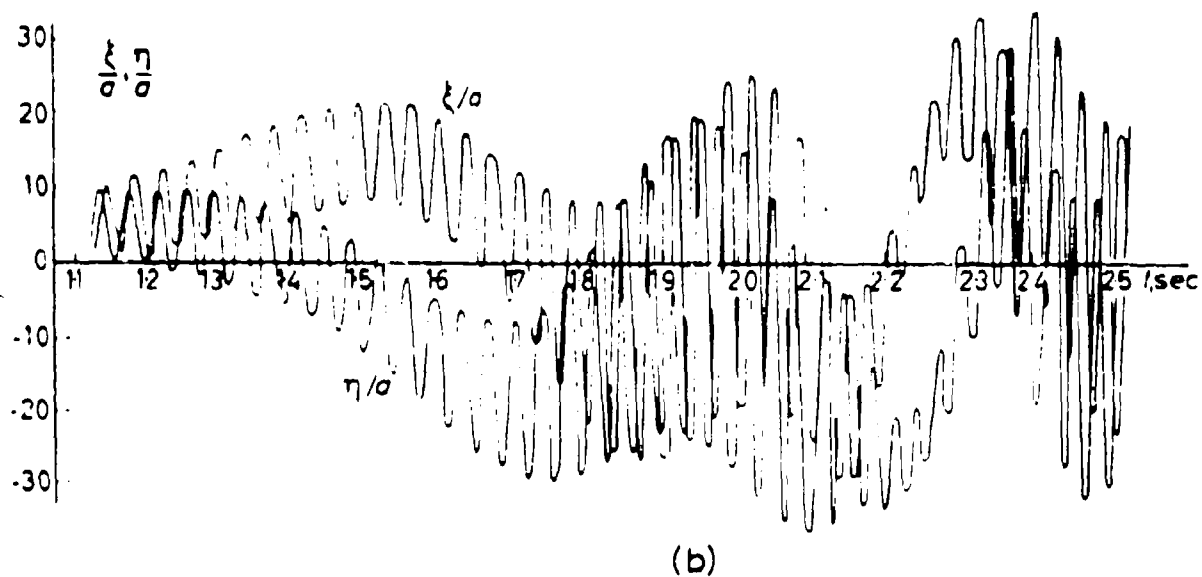
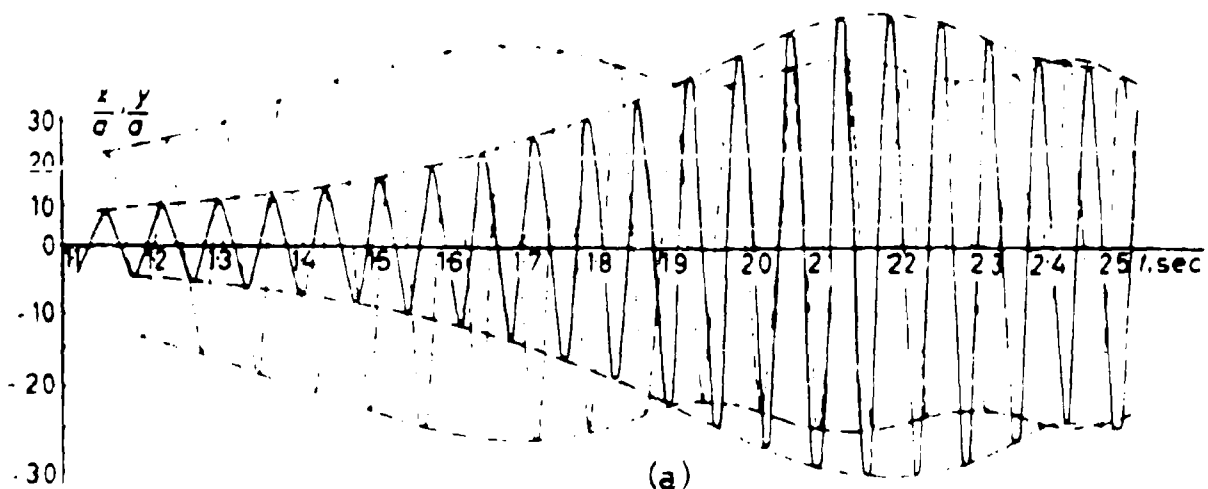


Fig. 6.07 Time-Response of Damped Flexible Rotor

Reprinted from FLEXURAL VIBRATIONS OF ROTATING SHAFTS,  
Figure 23a, b, by F. M. Dimentberg. 1961 Butterworth's  
London

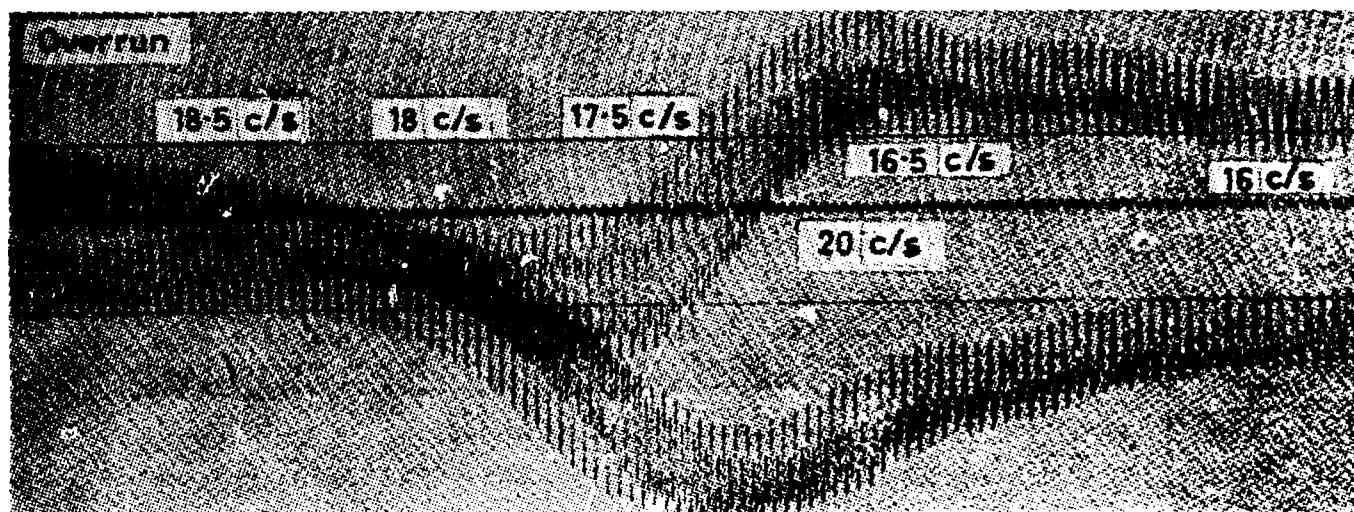
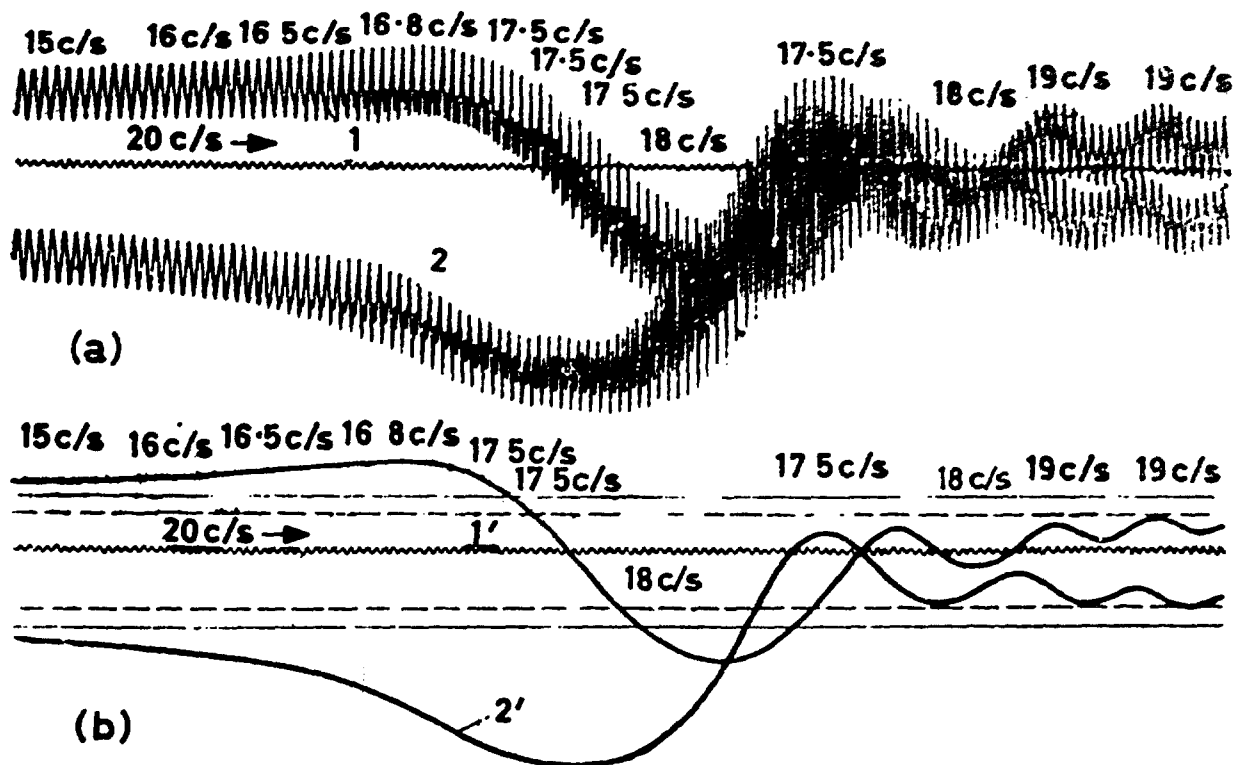


Fig. 6.08 Experimental Rotor Amplitude Response

Reprinted from FLEXURAL VIBRATIONS OF ROTATING SHAFTS, Figure 25, 26, by F. M. Dimentberg. 1961 Butterworth's London

## VII

### BALANCING OF ROTATING MACHINERY

#### Need for Balancing

No rotor is capable of smooth operation without adequate balance. The most sophisticated rotor and bearing design efforts cannot assure good balance, although the unbalance remaining after construction may be minimized by assigning meaningful working tolerances to each rotor component and by effective inspection procedures. All high-speed rotors must be machine balanced after manufacture, and the more refined the balancing technique, the less residual unbalance will ultimately remain. A well-balanced rotor will give rise to nominal transmitted forces, structural vibration, noise, and long-term rotordynamic problems. But, no amount of balancing can eliminate resonant whipping or half-frequency whirl, or dissimilar stiffness instability. These disturbances require adequate system design and damping to minimize their effects.

Rotor unbalance varies in magnitude, position and angle along the length of the rotor. During operation, the unbalance causes centrifugal forces and couples which bend the rotor causing it to whirl around its static equilibrium position. Excessive unbalance may endanger the safe operation of the machine. Rotor balancing consists of determining the magnitude and location of the residual unbalance followed by the insertion of correction weights in the selected balancing planes to nullify the unbalance effects. Actual rotors are never perfectly balanced since this would require a large number of measurements to determine the quite random distribution of unbalance along the rotor length, followed by the application of correction weights wherever needed. Both requirements are impractical, and so it becomes necessary to select a level of unbalance which, in a given application, will assure minimum whirl amplitudes throughout the operating speed-range.

### Concept of Unbalance

Rotor unbalance is usually specified in ounce-inches (oz.in) since unbalance is conceived as the product of the unbalance weight times its distance from the rotor geometric axis in the unbalance plane. The centrifugal force generated by the unbalance is then

$$\left[ \text{Centrifugal Force, lb} \right] = \left[ \text{Constant, } \frac{(2\pi)^2}{(16)(386.4)} \right] \cdot \left[ \text{Unbalance(oz.in)} \right] \cdot \left[ \text{Speed (r.p.s.)} \right]^2$$

Unbalance may also be designated by considering the rotor weight to be concentrated at its c.g., and eccentric from the geometric axis by a certain distance,  $a$  inches. The centrifugal force is then related to this distance by

$$\left[ \text{Centrifugal Force, lb.} \right] = \left[ \text{Constant, } \frac{(2\pi)^2}{(386.4)} \right] \left[ \text{Rotor weight, lb} \right] \cdot \left[ \text{Eccentricity of c.g., in.} \right] \cdot \left[ \text{Speed(rps)} \right]^2$$

These concepts of unbalance are valid in the case of rigid rotors such as a wheel mounted on a short shaft between rigid bearings or in a longer rotor at slow speeds. It fails, however, to describe the general unbalance condition of a flexible high-speed rotor.

### Rigid Rotor Balancing

It is well known that a rigid rotor may be brought into a state of balance by the appropriate addition of correction weights in any two normal planes along the rotor length. The complete rotor motion may be described through the displacement of the c.g. and by the rotor inclination. The rigid rotor is effectively a particle, and all forces and moments which determine its motion, including unbalance, may be concentrated into a single force and a single moment acting at the rotor c.g. It follows that by reducing the distributed unbalance to such an equivalent force and equivalent moment located at the c.g., it is possible to specify the total unbalance by two quantities known as static unbalance

and dynamic unbalance respectively. Static unbalance may be detected and corrected, without rotation, by placing the rotor on knife edges and allowing it to find its equilibrium position with the heavy side downwards (Figure 7.01). The rotor may then be statically balanced by the addition of a correction weight or weights, the total effect of which balances the resultant static unbalance of the rotor, without regard to the axial position of the weights. Dynamic balance, however, may only be detected by running the rotor, and in this case the axial distribution of the added correction weights is important, as the unbalance couple must also be balanced. It is clear from the above that the addition of a maximum of two correctly sized and positioned balance weights will completely compensate for the initial unbalance of a rigid rotor. Furthermore, the size, position and angular orientation of the two correction weights is completely optional as long as their equivalent force and moment cancels the rotor unbalance force and moment.

#### Flexible Rotor Balancing

The flexible rotor poses a more difficult problem because the distribution and variation of the unbalance causes the rotor to deflect in accordance with the resulting centrifugal force. This deflection profile may be a complicated shape. In any case, it is not possible to reproduce or annul the same shape by applying a single force and a single moment at the center of gravity as in the case of a rigid rotor. Hence, if a flexible rotor is balanced as if it were rigid, and correction weights have been added in two planes which cancel the unbalance static and dynamic effects, the rotor will nevertheless bend locally. When the speed is sufficiently high, the centrifugal forces resulting from these local deformations may generate large rotor amplitudes capable of making the original balance meaningless. In addition, when the rotor approaches one of its critical speeds, it tends to assume the mode shape of that critical speed in proportion to the residual unbalance. Rotor amplitudes may be minimized by an optimum selection of damping planes. At higher rotor speeds, more balancing planes are required to distribute the balance weights more uniformly throughout the rotor to attain the same minimum amplitude level. If the rotor is sufficiently flexible, and if the speed is sufficiently high, two balancing

planes alone are not enough. Theoretically it is necessary to have, as a minimum, as many balance planes as the number of the next bending critical speed beyond the operating speed range. Figure 7.02 shows the relationship between balancing planes and critical speed for a uniform rotor in rigid bearings. A flexible rotor in flexible bearings should be balanced as a rigid body for low-speed operation, selecting the balance planes and their disposition so that the low-speed balance is also effective at high speeds. Figure 7.03 illustrates this principle. This will be discussed in further detail later in this section.

### Practical Rotor Balancing

In practice, two basic approaches exist: (1) machine balancing in the shop following rotor assembly, and (2) field balancing following installation at the site. All conventional balancing machines operate through the addition of correction weights in two balancing planes. In view of the previous comments, it is clear that, strictly speaking, balancing machines are only of use with rotors which behave as if they were rigid throughout their operating speed range. Balancing machine speeds are low, and the rotor is supported in bearings and pedestals which are not the same as those in the actual machine arrangement. The machine rotor-bearing system is never machine-balanced. Since the rotor motion and the rotor amplitude are greatly influenced by the actual bearing stiffness and the actual pedestal stiffness, it is usually not possible to achieve a sufficiently fine level of balance using the balancing machine alone. The resonances governed by the pedestals and the bearings in the actual machine tend to amplify the effect of the rotor unbalance above the level achieved in the balancing machine. It is, therefore, almost always necessary to refine the rotor balance by further operation on the rotor in its own bearings and pedestals. Such an operation is known as field balancing.

### Field Balancing

Instrumentation is provided with which the whirl amplitude of the rotor may be measured to a high degree of accuracy, especially in high-speed applications. The measurement may normally be taken using distance-measuring probes such as capacitance probes, inductance probes, or photo-cells which are located within or just outside the bearing. It is common to provide such probes to monitor the

whirl orbit of the journal in any case. In this manner, the rotor amplitude is measured at the bearings and, if required, at other points along the length of the rotor. The rotor is brought up to speed, and as the amplitude grows, a speed is ultimately reached beyond which the amplitude is too large to safely permit any further increase in speed. At this point, it is necessary to determine what additional correction weights should be added in the balancing planes to restore the original balance. Known correction weights are added, one at a time, in known locations, and the individual effect on the rotor amplitude is measured. From these measurements, a calculation procedure is used to evaluate the effective unbalance of the rotor. This allows the required correction weight details to be established.

#### Balancing Machines

A number of balancing techniques are described by Stodola (Ref.18). Of these, the method due to Akimoff (Ref.146) is of importance since it forms the basis of modern balancing machines. Akimoff's machine is shown diagrammatically in Figure 7.04 . On this machine, the rotor may be balanced without changing the supports. The actual values and angular positions of the balance weights may be determined by trial and error, by graphical construction, or by using a balancing head, such as that due to Thearle, as described by Den Hartog (Ref. 17 ). Methods for doing this are described in the following sections. The machine consists of frame A, supported in bearings  $B_1$  and  $B_2$  which allow the machine to rock in the vertical plane. The rotor is supported in a rigid bearing  $D_1$  and in a bearing  $D_2$  which is guided to move vertically between the supporting springs, S. When bearing  $D_2$  is clamped and the rotor is driven through a flexible coupling, the effect of the moment of the rotor centrifugal unbalance force is neutralized by the fixed axis,  $B_1 B_2$ . The rotor may then be statically balanced by adding trial weights,  $G_{11}$ , in the balance plane, I, until the rocking motion about axis  $B_1 B_2$  has reached a minimum. Then frame A is clamped to the base, B, and bearing  $D_2$  is freed. During subsequent rotation, the resultant unbalance moment which arises from rotor unbalance and the added static balance weight,  $G_1$ , acts on the rotor. Dynamic balance is

then obtained by the addition of a second balance weight,  $G_2$ , in balance plane 1, adjusted in magnitude and position until the rotor vibration is minimized. Final balance is then obtained by applying  $G_2$  in the balance plane close to  $D_1$  (as shown dotted) with the same unbalance radius and size as  $G_2$  but 180 degrees out-of-phase with  $G_2$ . This gives an applied balancing couple,  $+G_2 -G_2$ , and allows the rotor to operate without the restraint previously provided by the rigid bearing  $D_1$ . The static balancing portion of this operation may be carried out on horizontal knife-edges if desired. Variants of the above machine exist in which the axis  $B_1, B_2$  is replaced by springs, and the rotor is supported in rigid bearings and pedestals on a rigid table. In this arrangement, the table is provided with frictionless pivots at  $P_1$  and  $P_2$ , which may be locked when necessary during balancing as shown in Figure 7.05. The balancing technique is the same as for the Akimoff machine.

#### Determination of Required Correction Weights

Although the angular position of the unbalance may be found directly by marking the run-out side of the rotor as it rotates, this method lacks the refinement necessary for sensitive balancing of high-speed rotors. Where a balancing machine or bearing is fitted with electrical displacement probes capable of detecting spring-supported rigid bearing displacements or journal displacements during field balancing, the required correction weights may be found by the following technique. The rotor is operated: (1) unbalanced; (2) with a trial balance weight in a selected position; (3) with the same balance weight placed diametrically opposite the position used in (2). With displacement readings from these three conditions, the required balance weight and its angular positions may be determined for both static and dynamic balance. The graphical construction for doing this is shown in Figure 7.06. The steps are:

1. Let  $\overline{OA}$  represent, to scale, the original unbalance of the rotor. Let  $\overline{OB}$  also represent, to a different scale, the vibrational amplitude observed as a result of this unbalance measured at the balancing speed during Test 1.
2. Let  $\overline{OB}$  be the unbalance vector of the rotor measured in Test 2, after the trial unbalance has been added in the first hole. By the laws of

vector addition

$$\overline{OB} = \overline{OA} + \overline{AB}$$

where  $\overline{AB}$  is the displacement due to the added trail unbalance

3. Similarly  $\overline{OC}$  represents the total unbalance displacement determined during Test 3. As in (2) above,  $\overline{OC} = \overline{OA} + \overline{AC}$  and as the unbalance in this case is 180 degrees out-of-phase with the unbalance position in Test 2, it follows that  $\overline{AC}$  is equal and opposite to  $\overline{AB}$  as shown in the figure.

The amplitude measurements provide information on the relative lengths of the unbalance forces OA, OB and OC; but their absolute magnitudes and phase relationships remain unknown. These facts may be obtained geometrically. Noting that OA is the median of the triangle OBC, of which the two relative lengths OB, OC are known, and the magnitude of BC (= 2: x unbalance) is double the length of OA to form OD. Then in the triangle ODC, the side DC is equal to OB. Thus, in ODC all three sides are known. Thus, the relative lengths of AB and OA are known, and since AB represents a known unbalance weight artificially introduced, the magnitude of the original unbalance OA may be deduced. In addition, through the construction the angular location ( $\alpha$ ), of the original unbalance OA with respect to the known angular location AB is determined.

However, an ambiguity exists with the above construction. In finding the original triangle, OCD, from the unbalance vectors, the triangle OC'D might have been obtained instead by construction. This would have led to obtaining the direction C'B' instead of direction CB for the unbalance weights. This ambiguity may be overcome by a fourth run.

This method assumes only that the displacement response of the rotor is proportional to the unbalance mass. This has been found to be a reliable premise in practice. The above steps may be repeated until the desired degree of balance is attained.

A method attributed to Ribary (Ref.147) and Hopkirk (Ref.148) makes use of an original unbalance test plus three trial unbalance measurements situated 120 degrees apart. A similar procedure to that described above is needed to determine the magnitude of the original rotor unbalance. A simple graphical construction for doing this has been proposed by Somerville (Ref.149). This method has been applied to checking the accuracy of balancing machines of the Akimoff type by McInante (Ref.150).

A balancing head is a device consisting of a well-balanced, disk-like container which is attached concentrically to the rotor and within which there are two weights on rotatable arms. The arms may be clamped or free, as required. A self-balancing type of diagram due to Thearle operates by replacing the arms with balls which are free to roll and to assume any preferred circumferential position when released. Initially, the balls are clamped 180 degrees apart, so that the balancing head is in perfect balance. The only unbalance in the rotor-head system is, therefore, that due to the machine. The rotor is then rotated above its critical speed and the balls are released. The balls then assume an angular position which tends to provide the optimum balance for the rotor due to the self-balancing action of an eccentric mass at speeds above the critical. All vibration then ceases. The balls are then clamped once more, in the optimum balance position. This principle, attributed to Leblanc, is discussed by Stodola (Ref.18) using mercury instead of two balls as the self-balancing medium. Den Hartog (Ref.17) has questioned the validity of this device. Two devices of this type situated in the balancing planes must be installed to obtain complete static and dynamic balance of a rigid rotor. A disadvantage is that the rotor must be run above its critical speed for this method to be used. Not all rotors are designed to operate at such speeds — which may cause overstressing or even bursting. As remarked earlier, two-plane balancing is inadequate for the delicate balance required in high-speed rotors operating beyond their fundamental critical speed and in these cases, the influence coefficient method described in the following section must be used.

### Influence Coefficient Method

This method is based on the assumption that the rotor-bearing system has a linear response in that the rotor whirl amplitude is directly proportional to rotor unbalance. In built-up rotors, frictional and hysteretic effects occur due to the deflected whirling shape of the rotor at a given speed. This introduces a degree of non-linearity into the system, but the effect is usually small, and the influence coefficient method is capable of providing a high degree of balance in practice. This method may be applied at any speed and is not dependent on the critical speeds of the rotor. The rotor may be balanced to any desired level, if an adequate number of planes are provided.

Assume that the rotor displacements are to be measured with a displacement probe at each bearing, and let rotor amplitudes at these probes be  $x_1$  and  $x_2$  respectively. Also, let there be four balancing planes in the rotor, and let the total rotor unbalance be represented by four discrete unbalances,  $u_1$ ,  $u_2$ ,  $u_3$ , and  $u_4$ , located at the balancing planes. Then at a particular speed, the rotor amplitudes may be expressed by the linear equations

$$x_1 = \alpha_{11} u_1 + \alpha_{12} u_2 + \alpha_{13} u_3 + \alpha_{14} u_4$$

$$x_2 = \alpha_{21} u_1 + \alpha_{22} u_2 + \alpha_{23} u_3 + \alpha_{24} u_4$$

The  $\alpha$ -terms are the influence coefficients, the numerical value of which depends on the speed of rotation. They are complex in nature, with components in the x- and y- directions, to account for both the magnitude of the displacement and the local phase angle. Similarly, both x and u are complex.

With four balancing planes and only two probes, it is necessary to perform ten separate tests at two different speeds. The procedure is as follows:

1. Select a suitable rotor speed at which the balancing may be performed.

2. Select an angular reference plane in the rotor from which the angular position of the unbalances may be measured. This reference plane defines the real axis for the complex unbalance.
3. Measure the magnitude of the two amplitudes and the phase angle with the uncorrected rotor running at the selected test speed and denote the resulting values  $x_{10}$  and  $x_{20}$ .
4. Insert a trial weight,  $T$ , on the reference line in balancing plane I, and again bring the rotor up to test speed.
5. Measure the two amplitudes as in (3). Denote these values  $x_{11}$  and  $x_{21}$ .
6. Calculate the values of the influence coefficients from

$$\alpha_{11} = \frac{x_{11} - x_{10}}{T}$$

$$\alpha_{21} = \frac{x_{21} - x_{20}}{T}$$

7. Proceed in this manner, inserting trial weights in the remaining three balance planes until the full set of eight influence coefficients is obtained.
8. Select a second balancing speed.
9. Repeat the above test sequence, steps (3) through (7), and obtain a second set of eight coefficients. The total number of coefficients is now 16.
10. Using the four amplitude measurements for the uncorrected rotor, obtain a set of four equations with the four unbalance components as follows:

$$x_{10} = \alpha_{11} u_1 + \alpha_{12} u_2 + \alpha_{13} u_3 + \alpha_{14} u_4$$

$$x_{20} = \alpha_{21} u_1 + \alpha_{22} u_2 + \alpha_{23} u_3 + \alpha_{24} u_4$$

$$x_{16} = \alpha_{31} u_1 + \alpha_{32} u_2 + \alpha_{33} u_3 + \alpha_{34} u_4$$

$$x_{26} = \alpha_{41} u_1 + \alpha_{42} u_2 + \alpha_{43} u_3 + \alpha_{44} u_4$$

The unbalances  $u_1$ ,  $u_2$ ,  $u_3$ , and  $u_4$  may be calculated from the above. These calculations are quite extensive, and are most conveniently performed on a computer.

A numerical example will illustrate the higher accuracy of the influence coefficient method over the rigid rotor methods. For this purpose, a gas-bearing-supported rotor is considered which is dynamically rigid on passing through its two lowest critical speeds. These criticals occur at 13,500 RPM and at 17,000 RPM. The third critical speed occurs at 85,000 RPM. The rotor has an overhung turbine wheel at one end and an overhung thrust collar at the other end. During machine operation, there is access to only two balance planes — one at each end. On the test stand, however, there is also access to two balance planes located between the bearings called the midplanes in contrast to the two endplanes.

The comparison between the two balancing methods is based strictly on computer calculations — no actual tests have been performed. First, the rotor is given a random distribution of unbalance and the corresponding rotor amplitude is shown by the curve labelled "Uncorrected Rotor" in Figure 7.07. This figure shows the amplitude at one bearing only, the amplitude at the other bearing is completely analogous. Note that only the second critical speed appears, whereas the other bearing shows only the first critical speed. This is due to the particular geometry of the system. Next, let the rotor be balanced as if it was rigid and insert the correction weights in either the two endplanes or in the two midplanes. The two corresponding amplitude curves show that although the rotor balance is improved, local deflections of the rotor prevent the balance from being perfect. Also, note that it is advantageous to apply the correction weights in the midplanes closer to the center of gravity than in the endplanes. Then, balance the rotor by the influence coefficient method. First, use only the two endplanes and balance at 40,000 RPM. The resulting amplitude curve shows improvement in the rotor balance; but overall the improvement is not quite as good as the results attained by the rigid rotor method. Secondly, use all four balance planes simultaneously and balance at

20,000 RPM and at 50,000 RPM. The rotor is now perfectly balanced for all practical purposes. It is evident that the higher the number of balance planes, the closer it is possible to match the residual unbalance in the rotor and the better the rotor balance will be. On the other hand, a large number of balance planes do require a large number of measurements and it does not seem too practical to go beyond 4 or 5 balance planes. However, since most rotors operate below their third critical speed 3 or 4 planes are completely adequate.

#### Acceptable Level of Unbalance

The degree of residual unbalance which will allow a machine to give safe, efficient, and trouble-free operation over a sustained period of time is difficult to specify because of the many factors and criteria involved. A machine may operate safely and yet its noise level may be irritating to human beings. Unbalance, which is feasible for a rotor at one speed, may be both unnecessary and beyond the range of capability of conventional balancing machinery at higher speeds. Two-plane, field balancing may be the only practical possibility due to constructional inconvenience; but multiplane balancing may be needed to attain the balance level required by government specification.

A number of unbalance force formulae are shown in Figure 7.08, together with the basic formulae. Formula 1,  $v = 5630(W/N^2)$  is effective up to around 3600 RPM, but beyond this, it is too severe and its requirements are beyond the capability of conventional balancing machines at high speeds. To overcome this, Formula 2,  $v = 5630(W/N^2) [1 + 65 \cdot 10^{-9} N^2]$ , was developed. Rotors may readily be balanced to this specification at all speeds. Both formulae are based on permitting a certain percentage of the rotor weight (one percent below 3600 RPM, to 7.5 percent at 10,000 RPM) to be the maximum transmitted force on a rigid bearing, simply-supported rotor. At speeds above 1000 RPM, Formula 2 approximates Formula 3,  $v = 4(W/N)$ , the simple criterion used by some turbine manufacturers. These formulae give safe transmitted force values by prescribing realistic residual unbalance levels.

Unfortunately, specification of a safe level of transmitted force does not also mean that the rotor whirl amplitude will be acceptable. Many experimenters such as Yates (Ref.151), Rathbone (Ref.152), and Reiher & Meister (Ref.153) have given results for various qualitative evaluations of the vibration from residual unbalance based on amplitude measurements. Figure 7.09 is a composite of several investigations covering a wide variety of machinery. Figure 7.10 is a chart of human perception of vibration level — again drawn from several investigators.

Table 7.01 is due to Federn (Ref.154) in which many types of rotating machinery have been classified into types. The eccentricity of the c.g. has been taken as the unbalance variable, as discussed previously under "Concept of Unbalance." Ranges of eccentricity which give safe operation and small rotor amplitude for each type of machine are specified. Feldman (Ref.155) has assigned the speed ranges listed for the machinery groups. These data agree quite well with the results given by the formulae listed previously, giving the overall vibration levels below the results obtained using Formula 1.

The above results were, in general, obtained using relatively small machinery much of which would have been dynamically rigid during operation. Although perfectly valid for these cases, the application of this data to large, flexible, high-speed machinery should be considered more in the making of a guide to suitable balance levels rather than as a specification in view of the differences between rigid and flexible rotors discussed previously.

Table 7.01 Guide to the Required Quality of Balancing (Federn)

Quality Group	Operating Speed RPM	Rotor Type	Displacement of c.g. $10^{-3}$ in
A	7000 - 40000	Small high speed de- vices. Gyros, grinders.	$\pm 0.008$ to $0.039$
B	7000 - 40000	Very high speed motors, small gas turbines, gas turbines, blowers, grinders.	$\pm 0.020$ to $0.073$
C	1000 - 7000	Rigid, small motor armatures, turbo- generators, superchargers	$\pm 0.078$ to $0.390$
D	1000 - 7000	Commercial electric motors, fans, gears, crankshafts.	$\pm 0.197$ to $0.985$
E	200 - 1000	Propeller shafts, reciprocating engines, slow speed rotating machinery.	$\pm 0.780$ to $3.900$

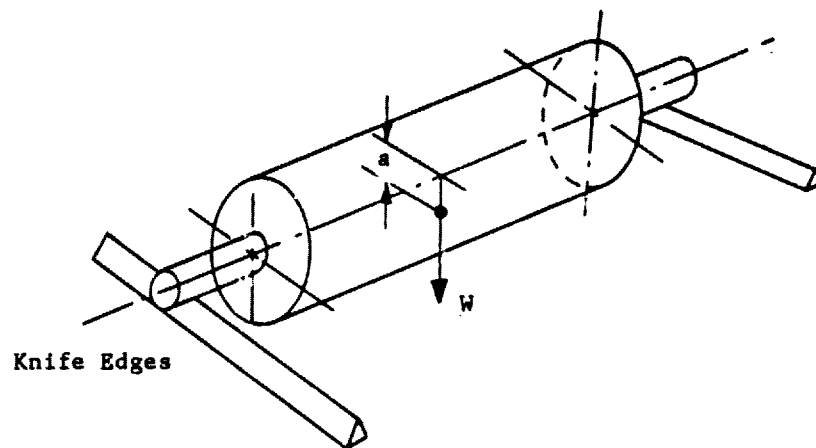
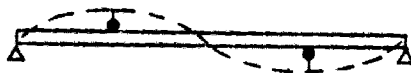


Fig. 7.01 Static Balance of a Rigid Rotor, on Knife Edges



First Critical



Second Critical



Third Critical

Fig. 7.02 Location of Balancing Planes Relative to Critical Modes

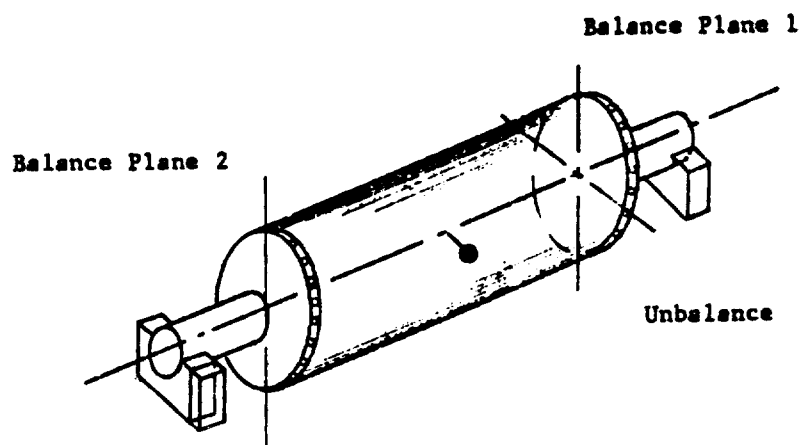


Fig. 7.03 Location of Balance Planes in Typical Rotor

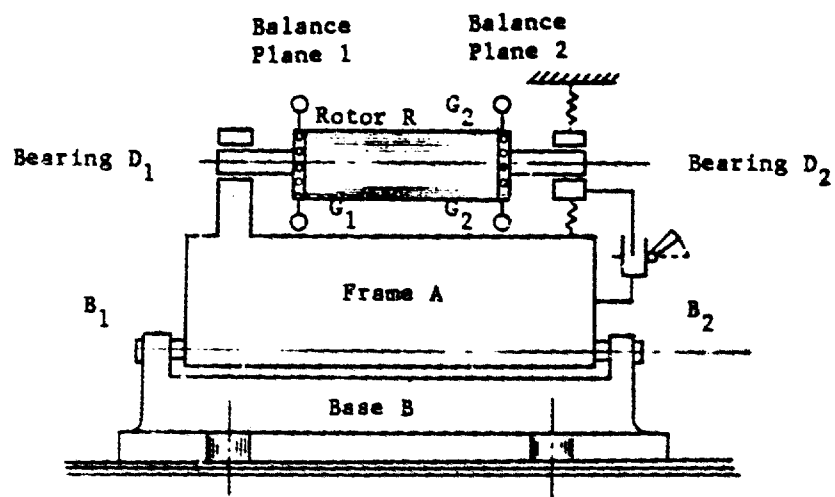


Fig. 7.04 Akimoff-Type Balancing Machine

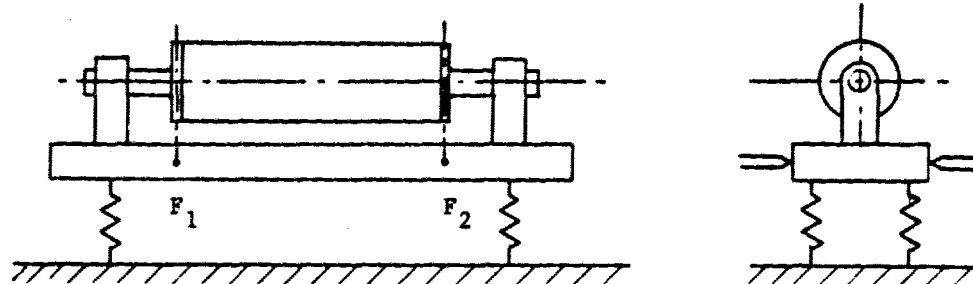


Fig. 7.05 Spring-Supported Balancing Machine

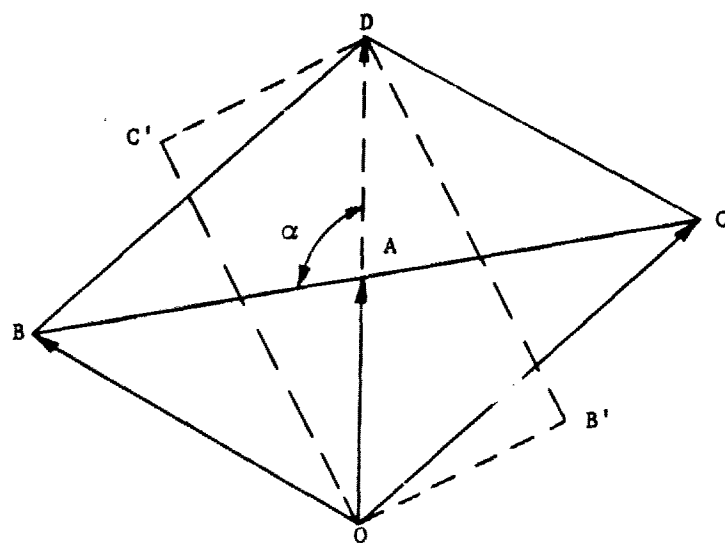


Fig. 7.06 Graphical Construction for Determining Angular Position of Required Balance Weight

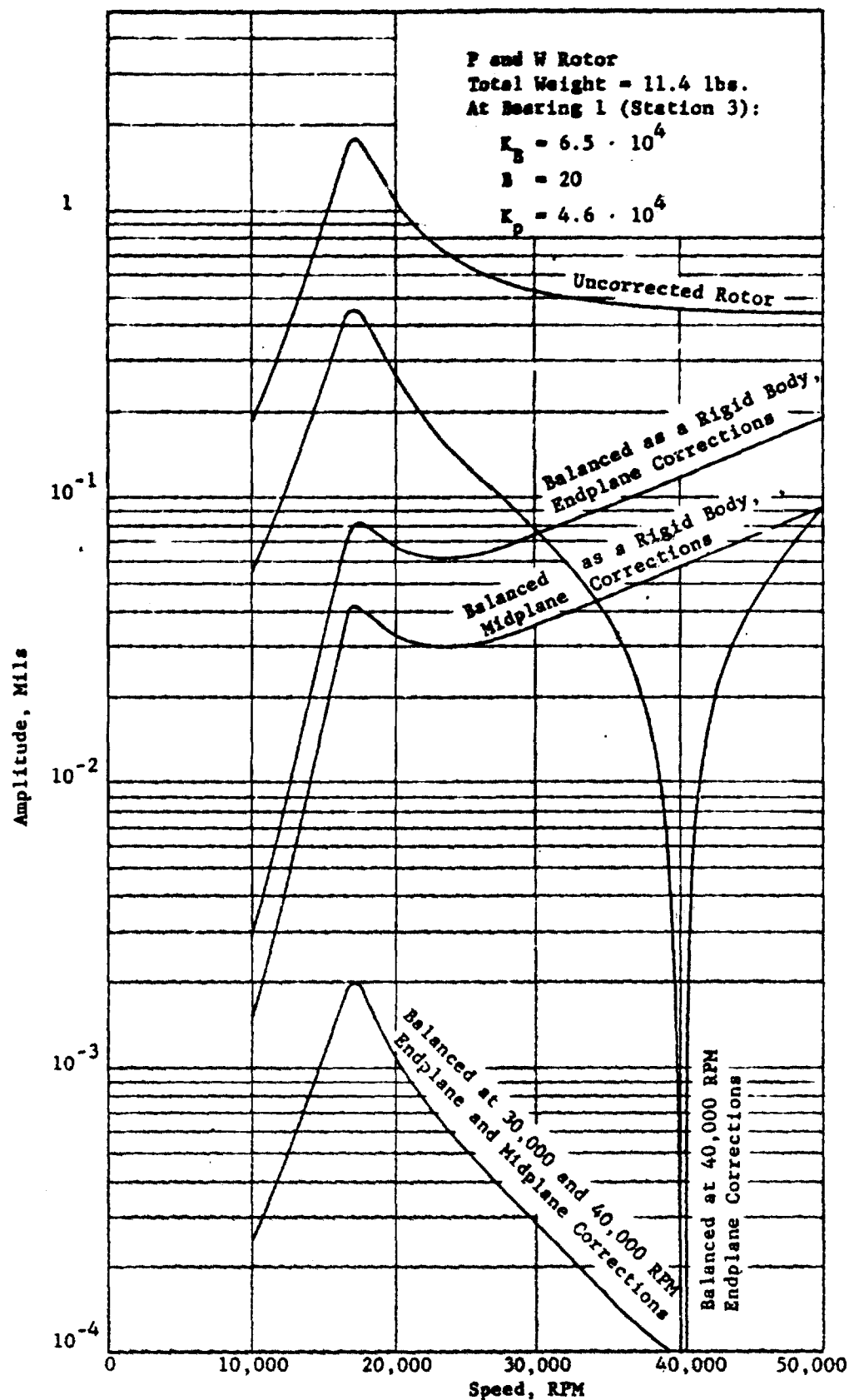


Fig. 7.07 Comparative Multiplane Balancing of a Simple Rotor in Flexible Bearings

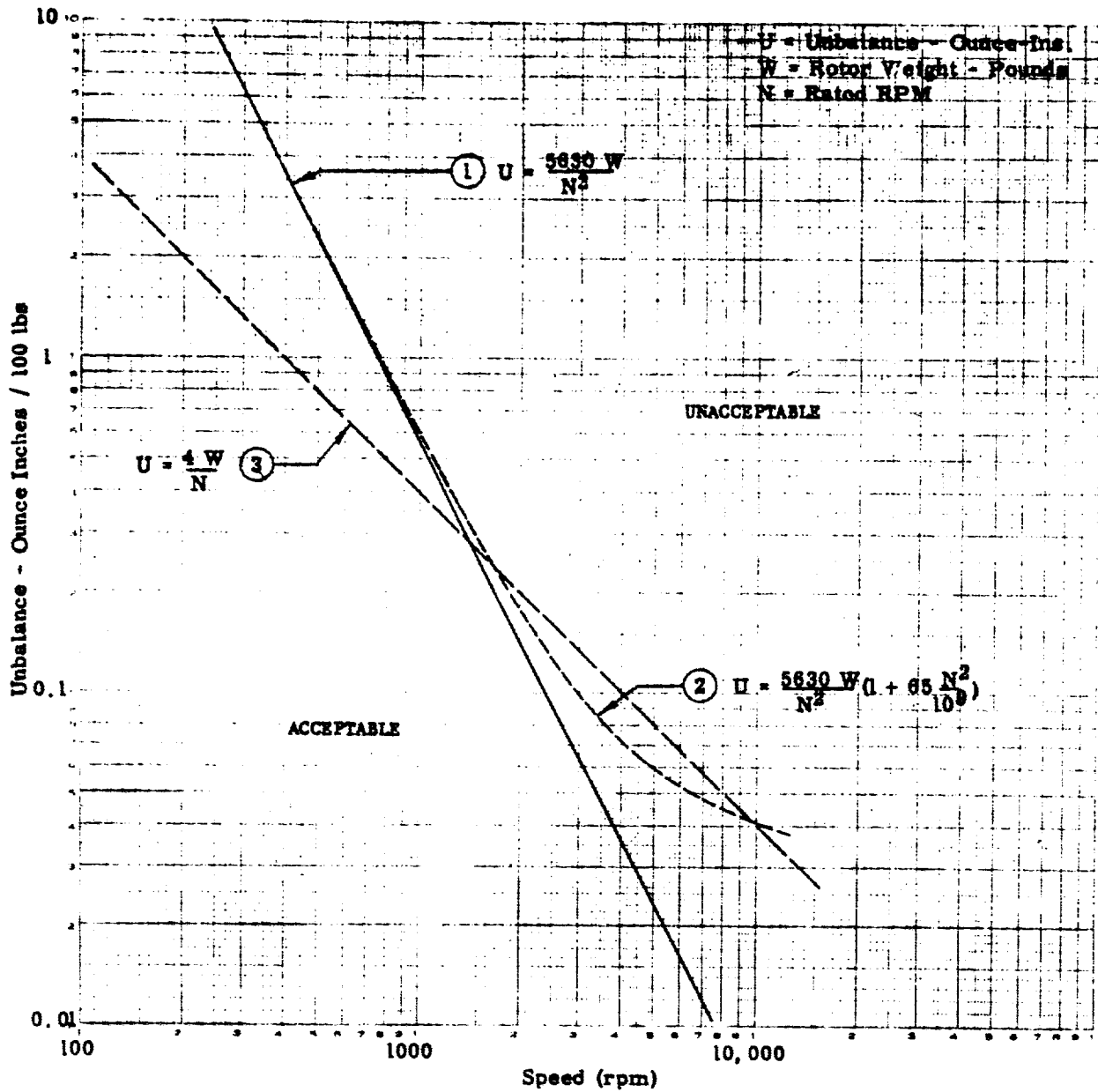


Fig. 7.08 Unbalance Tolerance Curves

Reprinted from General Electric Report No. 58GL122, "Proceedings - Balancing Seminar, Vol. IV: "Unbalance Tolerances and Criteria" by S. Feldman (BuShips, USN), April 17, 1958. Figure 1.

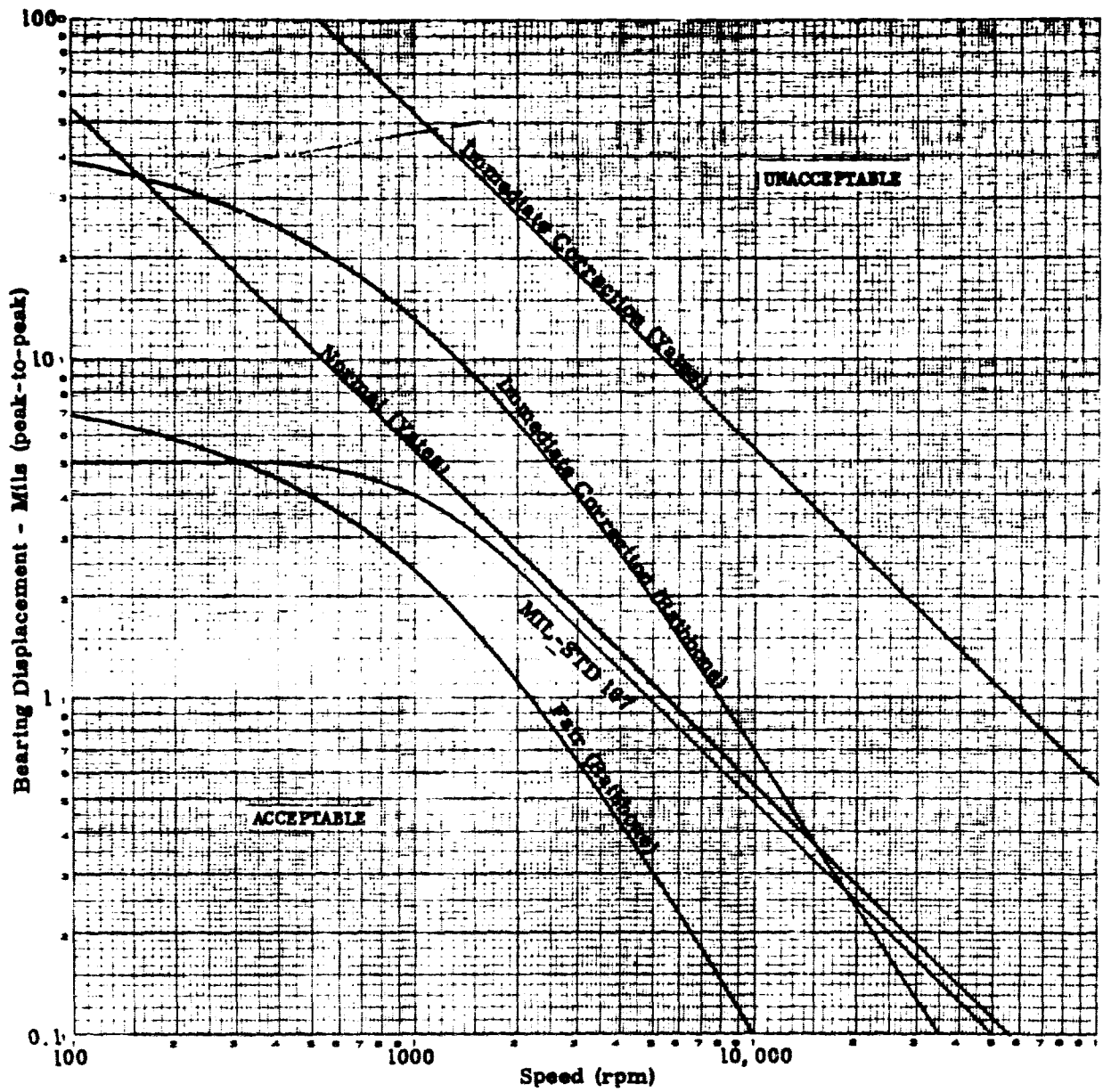


Fig. 7.09 Machinery Vibration Tolerance Curves

Reprinted from General Electric Report No. 58GL122, "Proceedings - Balancing Seminar, Vol. IV: "Unbalance Tolerances and Criteria" by S. Feldman (BuShips, USN), April 17, 1958, Figure 5.

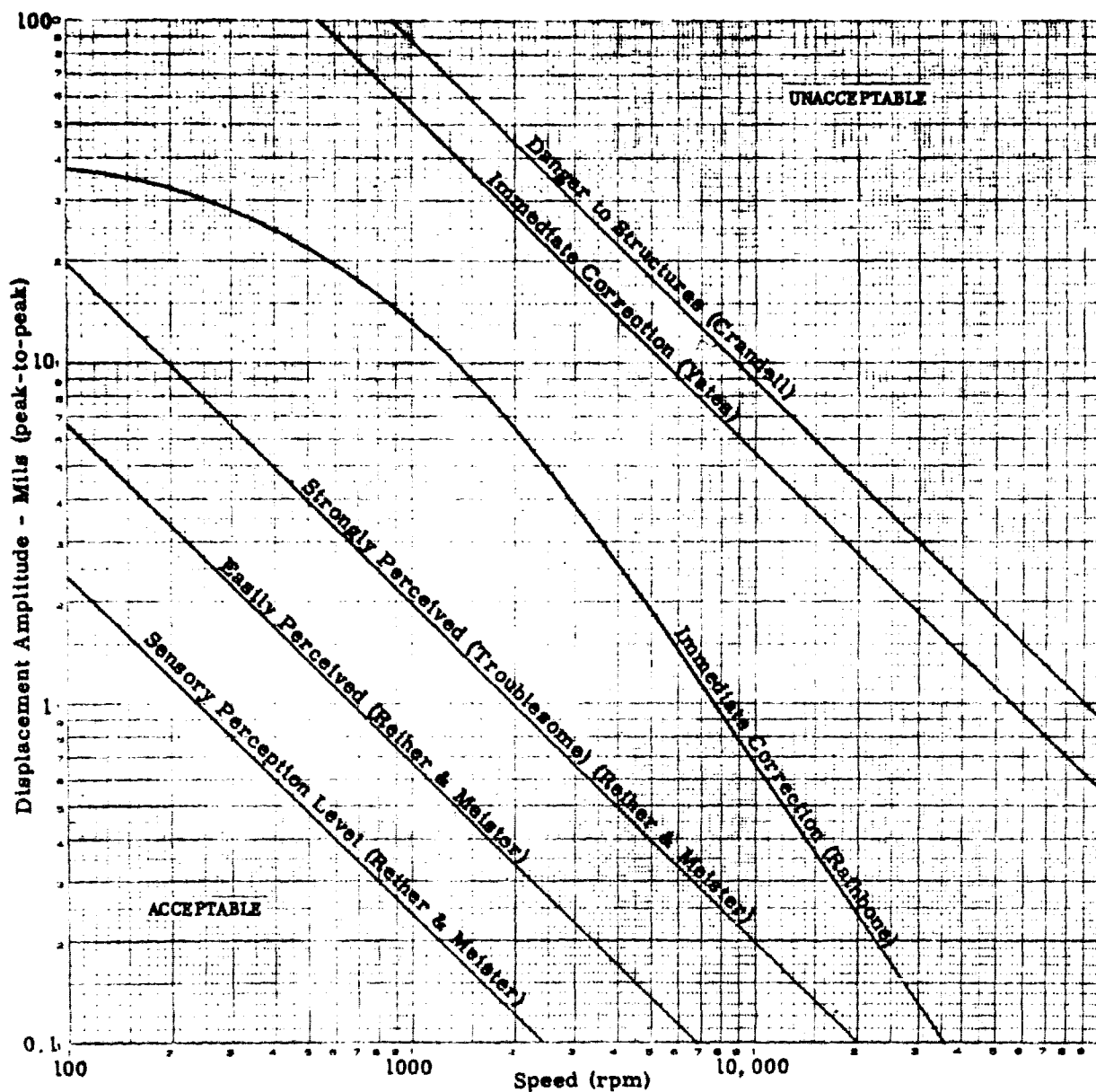


Fig. 7.10 Vibration Tolerance Chart - Physiological and Mechanical

Reprinted from General Electric Report No. 58GL122, "Proceedings - Balancing Seminar, Vol. IV: "Unbalance Tolerances and Criteria" by S. Feldman (BuShips, USN), April 17, 1958, Figure 4.

## VIII

### TORSIONAL AND AXIAL EFFECTS

#### Nature of Influence on System

In addition to the lateral rotor motions discussed previously, most rotors are subjected to both torsional and axial effects. These may take the form of a constant-valued applied torque or force which influences other motions without determining them, or they may be time-dependent, and capable of generating motions in their own plane of action. A combination of both types is also possible.

Drive torque will not influence the rotor motions unless it is a significant proportion of the rotor buckling torque or unless the rotor is very flexible and the working deflections are large. Axial thrust acting on the rotor from unbalanced gas or liquid pressure in a pump, compressor, or turbine affects the motions similarly. However, in any machine where either torque or force are applied during operation, the effects are rarely static even though the harmonic component may be very small in proportion. Thus the possibility exists for heavy vibrations to occur at the torsional and axial critical speeds of the machine, in addition to the bending-torsional-axial critical speed. This latter mode may therefore be excited by a cyclic component associated with any one of its steady-state components.

The present chapter discusses the sources of torsional and axial vibration, the calculations of torsional and axial systems, and methods used in practice to limit the motions within acceptable limits. The basic properties of bending-torsion-axial interaction are then presented, together with several results obtained. An important distinction to note is that bending effects excited by synchronous unbalance promote whirling of the deflected rotor shape about the static deflection line, whereas torsional and axial harmonic excitations promote vibrations of the rotor in those directions. Where these effects influence bending of the rotor, the result is again whirling, and not vibration.

### Sources of Torsional Excitation

Torsional vibrations arise directly from all sources listed in Table 8.01. These may be classified into primary sources such as internal combustion engines and propellers, and secondary sources such as machine misalignment, unbalance, impulsive loads and so on. Any machine which is driven by a reciprocating prime mover is a potential torsional vibration hazard. Power conversion from reciprocating motion to rotary motion introduces a range of harmonic components of which only the lowest orders can be balanced out with crankshaft weights, a flywheel, and by the number and arrangement of cylinders. Higher harmonics and the angular non-uniformity of the crank-effort diagram cause drive torque fluctuations in the most sophisticated engine output. Reciprocating pumps and compressors require similar attention to engine design. Propellers are a strong source of torsional excitation in propulsion systems. An aircraft propeller, or a turbine or compressor blade frequently vibrates while it is operating in a turbulent wake or slipstream of varying velocity. Ship propellers are influenced by cavitation. Both high- and low-frequency oscillations may occur in the power transmission system, which may be long and massive. This may give rise to system vibrations, and so to gearbox noise and wear. A combination of a reciprocating-engine driving a propeller or fan is a particularly dangerous arrangement.

Fans, pumps, and turbines are each capable of exciting troublesome moderate-to-high frequency oscillations in a system. In a fan or turbine, these may be associated with incorrect setting of the diffuser or vane angles. Pump system troubles may begin with cavitation in the vane passages, causing rotating unbalance and also drive speed fluctuations.

A non-constant drive resulting from eccentric meshing of the teeth of a gear pair may arise through radially-eccentric mounting of the gears, or by angular misalignment of the meshing. In both cases, this leads to a synchronous disturbance as the tooth contact point varies in radius throughout each cycle, giving rise to a small cyclic torque component in the drive. A similar condition may result from indexing errors in relative tooth uniformity,

caused during manufacture. Here, the frequency of the error depends upon the original gear-cutting machine, and on the number of teeth on the cut gear. Gear tooth contact effects can be minimized in high-speed gearboxes by providing helical teeth rather than spur, or spiral-bevel rather than straight bevel.

Rotating unbalance from a gear or shaft can give rise to torsional oscillations which are synchronous with operating speed by rocking a gear in and out of mesh once per revolution, in the manner described above, especially if the gear mesh is at the end of overhung shafts. Good shaft balancing, short spans, and rigid bearings can do much to minimize these oscillations. Couplings can give rise to a cyclic disturbance at some multiple of running speed if either the radial or angular misalignment is sufficiently in error. Misaligned universal joints create a twice-per-cycle disturbance. This problem has been overcome with the con-vel joint in which uniform torque is transmitted by the constant rolling action of a rolling element surface.

Electrical unbalance results from non-uniformities in the magnetic field of the machine, or due to worn bearings which allow a gravity deflection of the rotor.

Shock loads and starting transients give rise to vibrations which decay rapidly, but may be of such severity while they last that permanent damage is done to a gear mesh, a key way, or to a shaft. Abrupt accelerations and decelerations fall into this category. In systems operating with substantial torsional fatigue hazard, the shock loading may be sufficient to precipitate final component failure.

#### Critical Speeds of Torsional Systems

Torsional critical speeds depend on the inertia-stiffness properties of the machine system, and on its size. Commonly, at least one torsional critical speed will lie within the operating speed range. Torsional systems are usually readily represented by a number of inertias connected by flexible shafts,

Figure 8.01. The frequency equations for a number of standard discrete-mass cases are given in Table 8.02. In each case, the shaft is considered perfectly elastic, massless, and without damping. The speed change across the gear mesh results in a higher effective inertia on the high-speed side of the mesh. The frequency of the four-inertia system, case 8, is expressed in determinant form due to the growing size of the frequency equation, for convenience.

Practical systems frequently require 10 or 20 inertias to represent them with sufficient accuracy. The laboriousness of obtaining the roots of the frequency equation in these cases is readily apparent. Frequently the first or second torsional critical speeds alone are required. These results may be conveniently obtained using the Holzer tabular method, described in Den Hartog (Ref. 17), and Nestorides (Ref. 4), although any of the iterative methods for taking the roots of a matrix described in Chapter 4 would be as effective. The Holzer table is well suited to the digital computer, and this combination allows any machine to be accurately represented in terms of stiffness and inertia, and so calculated with excellent accuracy (Rieger, Ref. 156). In many applications, the only torsional damping available is shaft hysteretic damping and any residual Coulomb slippage. Both sources are very small, and so even the secondary sources of torsional excitation are capable of producing considerable vibration amplitudes in the vicinity of a system critical speed. This fact has been demonstrated in the failure of gears and shafts many times.

#### Methods of Suppressing Torsional Vibrations

In common with other motions, torsional vibrations are most effectively reduced by eliminating the source of torsional excitation. Without stimulus there can be no vibration. Table 8.01 indicates a number of remedies which have been shown to be effective in dealing with torsional vibrations. Effectiveness in each case arises from modifying the source of vibration in some manner. Where possible, the source is eliminated entirely, for example, by using

accurately-cut gears and by mounting them concentrically on shafts and in bearings which have sufficient radial stiffness. In other cases, considerable improvement can be made by reducing the size of the torsional excitation. In an internal combustion engine, this may be done by proper design of cylinder firing order, and by selection of suitable crank angles for the number of cylinders required. Furthermore, the design and fitting of the most effective balance weights to minimize or eliminate completely the primary and secondary unbalance forces and couples on the crankshaft makes a significant contribution to the smoothness of the crankshaft drive torque produced.

All rotating components in a power transmission system should be statically and dynamically balanced for flexural motions, as rotating unbalance frequently leads to the generation of torsional oscillations through the flexibility of the system, the gearing and the degree to which there is coupling between the bending and torsional deformations of the system.

In certain instances, it is possible to de-tune the system, using a vibration absorber as shown in Figure 8.02, which has its natural frequency tuned to the operating speed of the machine. Hence, during operation, the tuner vibrates heavily, leaving the machine substantially vibration-free. These devices are difficult to tune precisely, as the resonant peak of maximum effectiveness is very sharp and requires constant speed. Several detuners may be used together, or the detuner may be damped. Additional damping increases the range of effectiveness, but decreases the maximum effectiveness at resonance.

By far the most common vibration suppression device is the torsional vibration damper with which the troublesome oscillations are minimized by attenuation, and through dissipation of the vibrational energy. Many types of torsional vibration dampers are available commercially. The Coulomb friction damper (Figure 8.03), operates by dissipating energy at the friction interface through relative slippage between the inertia ring and the oscillating hub. Frequent adjustment of the interface contact pressure may be required due to wear. The viscous friction damper (Figure 8.04) consists of an inertia ring and an oscillating housing which are unattached mechanically. Between these

components is a thin fluid film, usually of a highly viscous material, such as a silicone oil. Slip between the components during operation shears the fluid film and dissipates the energy. Pumping chamber dampers (Figure 8.05) also use an inertia ring. Relative motions of the hub tend to pump the working fluid through small orifices and through confined spaces, to dissipate energy. Torsional dampers may be designed to give very effective vibration suppression over wide ranges of operating conditions. However, the design must be based on the dynamical characteristics of the entire system to achieve maximum effectiveness in operation.

#### Sources of Axial Vibration

Pressure fluctuations in process fluid machinery often contain a cyclic component generated by some rotating mechanical asymmetry. The forces involved can be quite large, and so operation in the vicinity of an axial critical speed has been known to give rise to sizeable vibrations in that direction. Other systems which drive propellers or fans are well-known to be susceptible to axial modes due to the aerodynamic forces involved in the motion. Vertical rotating machinery supported on a lightly-loaded thrust bearing may experience vertical vibrations of the rotor if the machine operating speed lies near the axial natural frequency of the rotor-thrust bearing combination. Motions of this type have been discussed by Den Hartog (Ref 17) with regard to self-excited oscillations in steam turbines, and in vertical Francis water turbines. These motions may occur with both rolling-element thrust bearings, and with fluid-film thrust bearings. Sizeable vibrations are less likely to occur with liquid-film thrust bearings because of the squeeze-film damping present; but with gas-bearing machinery, the hydrodynamic film stiffness and damping are considerably smaller, and the possibility of dangerous vibrations is much greater, particularly as the operating film thickness is smaller, and a touch at the high operating speed usually employed could be catastrophic. Where a hydrostatic thrust bearing is used, the film stiffness is larger, but damping is still small, and this leads to similar motions as in the case of hydrodynamic bearings, but at higher operational speeds. It is

important to note that the stiffness of fluid-film thrust bearings is highly non-linear with displacement, and so the calculated natural frequency based on a specified operating film thickness is only valid for small amplitude motions. An example of such a calculation is given in the following section. Alternatively, where the bearing is supported by a thin diaphragm as in certain totally enclosed process gas systems, axial vibrations of the bearing shell and rotor may occur due to the diaphragm flexibility as a plate. The vibrations in this case are linear up to quite large amplitudes.

The above comments apply to axial systems, in which the rotor moves as a rigid body against the flexibility of a bearing or pedestal. Where long connecting drive shafts are used, or with systems having heavy end masses and relatively small diameter connecting shafts, elastic axial vibrations of the rotor itself may occur. However, the relative stiffness in this direction generally causes these vibrations to occur at fairly high frequencies.

#### Critical Speeds of Axial Vibration

The speed at which an axial system becomes resonant is identical with its natural axial vibration frequency. The system may respond to any of the stimuli discussed above, either at rotational speed for a synchronous excitation, or to a higher or lower frequency, depending on the non-synchronous source; or it may experience self-excited oscillations at its natural frequency, at any speed including zero rpm. Natural frequencies of several simple axial systems are given in Table 8.03. The system flexibility may be the bearing, Cases 1 and 2; or the rotor shaft, Case 3 and 4, 6 and 7; or either shaft and bearing, or bearing and pedestal or diaphragm, Case 5. The mass in all cases consists of the rotor, the end disks, or the bearing shell, or a combination of these masses. Case 2 shows the damped natural frequency which may differ from the undamped natural frequency for cases where the bearing fluid-film damping is considerable.

### Suppression of Axial Vibrations

Axial vibrations cause trouble less frequently than either bending or torsional vibrations and so less specific information is available on their suppression. However, the established principles of vibration suppression may be applied as follows in any troublesome case:

1. Remove the axial natural frequency from the troublesome frequency range, preferably by stiffening the bearing, or by reducing the weight of the rotor. Both effects raise the critical speed. Where this is not effective, decrease the bearing stiffness by using a greater film thickness, or by using a floating ring bearing, and operate the machine beyond the axial critical, providing good bearing damping capacity to limit motions on passing through the critical speed.
2. Change the lubricant to increase the fluid-film damping available. Adequately designed squeeze-film damping is amongst the most effective damping available, and thrust bearings provide a conveniently available source.
3. Design a simple pendulum detuner for the rotor to absorb the critical vibrations.
4. Design a Coulomb damper to absorb the energy of the axial vibration, Figure 8.03.

### Axial Vibrations of a Hydrostatic Thrust Bearing

Thrust bearings are often the most flexible components in an axial system, and so the possibility of vibrations due to this source is considerable. With rolling element bearings the stiffness is usually fairly large, and so the axial natural frequency is likely to be high in, or beyond, the operating speed range. Liquid-lubricated bearings may have lower stiffnesses, particularly hydrodynamic thrust bearings but the damping due to squeeze-film action is high, and so failure by surface touching is uncommon in a bearing whose static load-carrying capacity is adequately designed. In a hydrostatic liquid thrust bearing, the stiffness is determined by the bearing inlet pressure and the

operating film thickness. Large squeeze-film damping is again available. Annular and spherical hydrostatic thrust bearings have been investigated by Sternlicht (Ref. 157), Raimondi (Ref. 158) and Rieger (Ref. 159).

The operating stiffness of a hydrodynamic thrust bearing is usually extremely low, and this combined with the small inherent damping makes this bearing type a potential hazard in most machines. However, the hydrostatic gas bearing combines practical load-carrying capacity with low friction, thus overcoming the above problem. Although the overall stiffness increase between the two bearing types may not be great (due to a considerable increase in the designed gas film thickness for the same applied thrust load), the amplitude-of-motion tolerance is much larger due to the thickened film, non-linear stiffening of the film accompanies the smaller thicknesses and the damping capacity is larger. These bearings are susceptible to a self-excited instability known as 'pneumatic hammer', as are all hydrostatic bearings, in which the large-amplitude oscillations which develop may cause bearing failure.

The bearing considered in this section is shown in Figure 8.06, and consists of two circular plates. The upper load-carrying plate has a circular recess, the depth of which can be varied. The pressurized gas enters through the restrictor in the lower plate, and flows through the recess radially out to atmosphere. The pressure distribution between the plates is shown in Figure 8.06, and is known to be in the form of a frustum of height  $(p_o - p_a)$ , where  $p_o$  is the recess pressure and  $p_a$  is the external pressure. The operating film thickness is  $H_o$ . Any small incremental change  $h$  in film thickness corresponds to a pressure increment  $p$ . Linear relationships are assumed to exist throughout, based on small deviations from equilibrium values. Changes in gas density  $\rho$  are due to pressure variations, and so the basic gas law  $\rho/p = RT$  may be used, where the symbols have their usual meanings.

The pressure at any point in the annulus, between radii  $R_r$  and  $R$  is given by

$$P_a = P_r - (P_r - P_a) \frac{r - R_r}{R - R_r} \quad (8-1)$$

In practice, good load capacity with low gas leakage is achieved with  $R_r = 1/3 R$ . Adopting these proportions, and writing the equation of motion for the system mass  $m$  gives:

$$\begin{aligned} m\ddot{h} &= 2\pi \left[ \int_{R_r}^R p r \, dr - \int_{R_r}^R p \frac{r - R_r}{R - R_r} \cdot dr \right] \\ &= \pi \left[ R^2 - \frac{2R^3 + R_r^3 - 3R^2 R_r}{3(R - R_r)} \right] \\ &= pA_e \end{aligned} \quad (8-2)$$

where

$$\begin{aligned} A_e &= \pi R_e^2 \\ R_e^2 &= \left[ R^2 - \frac{2R^3 + R_r^3 - 3R^2 R_r}{3(R - R_r)} \right] \end{aligned}$$

For a given supply pressure, gas flow into the bearing depends on recess pressure only, as this determines the orifice flow. Bearing outflow is a function of recess pressure and the film thickness in the annular clearance. For small deviations from the equilibrium point shown in Figure 8.07 ( $p$  and  $h$ ) there are corresponding variations in inflow and outflow which may be represented approximately by:

$$\begin{aligned} \text{Inflow } w_1 &= \left( \frac{dw_1}{dP} \right)_0 p = \alpha p \\ \text{Outflow } w_2 &= \left( \frac{\partial w_2}{\partial P} \right)_0 p + \left( \frac{\partial w_2}{\partial H} \right)_0 h = \beta p + \theta h \end{aligned} \quad (8-3)$$

The time rate of change of the bearing gas mass content is then:

$$\dot{w} = \dot{w}_1 - \dot{w}_2 = -(\alpha + \beta)\dot{p} - \theta\dot{h} \quad (8-4)$$

where  $\alpha$ ,  $\beta$ , and  $\theta$  are all positive coefficients. The bearing gas mass is then:

$$M = 2\pi \left( \int_0^R (\Delta + H)p_r r dr + \int_{R_r}^R H p_a r dr \right)$$

Using Equations 8.01 and 8.02 this reduces to:

$$M = \frac{1}{RT_0} \left[ H p_r A_e + \Delta p_r \pi R_r^2 + H p_a (\pi R^2 - A_e) \right] \quad (8-5)$$

The time rate of change of the bearing gas constant ( $R$ ) is equivalent to the difference between the inflow and the outflow ( $w$ ), and corresponds to the time-rates of small deviations from the equilibrium point ( $\dot{p}$  and  $\dot{h}$ ), i.e.,

$$\dot{w} = \dot{M} = \left( \frac{\partial M}{\partial p} \right)_0 \dot{p} + \left( \frac{\partial M}{\partial h} \right)_0 \dot{h} = q\dot{p} + s\dot{h} \quad (8-6)$$

where, by partial differentiation of Equation 8.05

$$q = \left( \frac{\partial M}{\partial p} \right)_0 = \frac{A_e H_0 + \Delta \pi R_r^2}{R T_0}$$

$$s = \left( \frac{\partial M}{\partial h} \right)_0 = \frac{A_e (p_0 - p_a) + \pi R^2 p_a}{R T_0}$$

Combining Equations 8.05 and 8.06 to eliminate  $w$  gives

$$q\dot{p} + s\dot{h} + (\alpha + \beta)p + \theta h = 0 \quad (8-7)$$

As  $p = (m/A_g) \ddot{h}$ , and  $\dot{p} = (m/A_g) \ddot{h}$ , substituting leads to the following basic differential equation of the system:

$$\ddot{h} + \left( \frac{\alpha + \beta}{q} \right) \dot{h} + \frac{SA_g}{mg} \ddot{h} + \frac{9A_g}{mq} h = 0 \quad (8-7)$$

The inherent stability of the system for axial motions may now be examined by applying the Routh criterion to this expression, which has the form:

$$\ddot{h} + c_2 \dot{h} + c_1 \ddot{h} + c_0 h = 0$$

where  $c_0$ ,  $c_1$ , and  $c_2$  are all positive coefficients.

The system is stable where the inequality  $c_1, c_2 > c_0$  is satisfied. In terms of the system parameters this requires

$$\frac{\alpha + \beta}{\theta} > \frac{q}{s} \quad (8-8)$$

for stable operations of the system. Considering Figure 8.07, large values of the ratio  $\frac{\alpha + \beta}{\theta}$  correspond to large values of recess pressure  $p_0$  and small values of annulus height  $H_0$ . The ratio  $\frac{\alpha}{\theta}$  is large where the maximum load is supported with the minimum possible  $H_0$ . However this also leads to small  $\frac{\beta}{\theta}$  values. The value  $\frac{q}{s}$  is proportional to the recess depth  $\Delta$ , the annulus height  $H_0$ , and inversely as the recess pressure  $p_0$ . Thus  $p_0$  and  $H_0$  have an opposite effect on the magnitudes of the ratios forming the two sides of the above inequality. It is also clear the  $\Delta$  should be minimum for stability. The value of  $\alpha$  is also influenced by the manner in which the pressurized gas is supplied to the bearing. Results indicate that a large diameter nozzle gives a larger  $\alpha$ -value than both a small diameter nozzle, and a capillary.

The above analysis indicates that where stability considerations are important in the design of pressurized gas thrust bearings, the gas storage capacity of the bearing should be minimized, requiring a small recess depth. A small pressure difference ( $p_g - p_r$ ) tends to promote stable operation, and this is

provided by having a large diameter inlet nozzle, rather than a small nozzle or a capillary. Choked flow or inherently-compensated bearings promote unstable operation. Good design requires that, where possible, the bearing annular clearance should become the flow restrictor, rather than the inlet nozzle. The above theoretical results have been substantiated by experiments conducted by Licht, Fuller and Sternlicht (Ref. 141) who, for a bearing with 3.00 in O.D. pressure,  $p_s = 73.5$  psig, nozzle diameter 0.032 - 0.078, and recess depth 0.003 - 0.500, found large amplitude self-excited oscillations in the range 25-30 cps. This work has been further extended by Licht (Ref. 142).

#### Effect of Axial Force and Drive Torque on Bending Motions

In many turbomachines, the operating conditions are such that the bending motions of the rotor are influenced by the drive torque, and by the axial thrust. These effects may alter the position of the bending critical speed in relation to the operating speed, and so affect the dynamic performance of the machine. The present section describes the extent of these effects on several common machine configurations.

The operation of turbomachines such as pumps, compressors, turbines, and expanders involves a pressure difference to promote flow. In many instances, this pressure difference is not inherently balanced in the machine layout, and the resulting axial thrust must then be accommodated with a large thrust bearing. This is a common feature of axial flow machinery, including steam turbines, unless a central inlet divided-flow design is used. Centrifugal pumps and blowers are sometimes designed with double-acting impellers to avoid large thrust loads. From a rotordynamic standpoint, the most undesirable condition occurs where a large thrust is generated near one end of a slender, high-speed rotor, and this thrust is absorbed by a thrust bearing located near the other end of the rotor. The rotor then acts as a slender column, and if the axial compressive load is a significant proportion of the buckling load, the bending critical speed may be reduced considerably. A similar condition occurs with long slender rotors which operate with high drive torque, either steady-state or during transient run-up. As the machine torque approaches the torsional buckling load of the rotor shaft, the bending critical speed is again depressed.

Both axial and torsional effects may be present together in a particular machine, and their overall effect on critical speed performance for that configuration must then be considered.

Several cases of single-disk rotors supported in rigid bearings have been studied in detail by Grammel (Ref.160). For a shaft having symmetrical lateral stiffness subjected to an end thrust  $P$ , the relationship between the simple natural frequency  $\omega_0$  and the thrust-load natural frequency  $\omega$  is given by:

$$\frac{\omega}{\omega_c} = 1 - k_1 \left( \frac{PL^2}{EI} \right) \quad (8-9)$$

where  $k_1$  is a numerical coefficient given in Table 8.04 by Ziegler (Ref. 20). The value of  $k_1$  is influenced by the type of bearings (system end constraints) used. Where the shaft is acted on by an applied torque,  $T$ , the effect on the natural frequency  $\omega$  of the system is given by:

$$\frac{\omega}{\omega_c} = 1 - k_2 \left( \frac{TL}{EI} \right)^2 \quad (8-10)$$

where  $k_2$  is a numerical coefficient, given in Table 8.04, for instances where the applied torque is only a small proportion of the buckling torque. The value of  $k_2$  is again influenced by the shaft end-support conditions. The drive torque may be applied in a number of ways, and over any shaft length. If the drive torque is applied semi-tangentially, as shown in Table 8.04, Wehrli (Ref.162) has shown that a critical interval exists

$$1 - k_3 \frac{TL}{EI} \leq \frac{\omega}{\omega_c} \leq 1 + k_3 \frac{TL}{EI} \quad (8-11)$$

above and below which the motion is stable. The numerical coefficient  $k_3$  is given in Table 8.04 and this result also applies for relatively small values of applied torque. In case 7,  $k_3$  depends on the angle  $\theta$  adopted by the universal joints with respect to one another, in the unloaded state. For  $\theta = 0$ , the limits of the critical interval are more accurately given by:

Case 7,  $\theta = 0$

$$\frac{\omega_{1,2}}{\omega_c} = 1 - \frac{1}{1920} \left[ 51 \pm 45(1 + 2\nu) \right] \left( \frac{TL}{EI} \right)^2 \quad (8-12)$$

where  $\nu$  is Poisson's ratio for the shaft material.

For a quasi-tangential couple acting on the disk, as in the case of a turbine having two diametrically-opposite sets of inlet blades, two critical angular velocities exist. For small values of  $T$  these are given by:

$$\frac{\omega}{\omega_c} = 1 \pm k_4 \frac{TL}{EI} \quad (8-13)$$

where  $k_4$  is a numerical coefficient given in Table 8.04. In cases 2 and 3 these two critical speed values coincide when  $T$  is small. For cases 6 and 8, the critical interval is again given by:

$$1 - k_3 \frac{TL}{EI} \leq \frac{\omega}{\omega_c} \leq 1 + k_3 \frac{TL}{EI} \quad (8-14)$$

in terms of the corresponding values in the Table.

Where axial thrust and drive torque are present simultaneously in a given system, the combined effect may be determined from the expression

$$\frac{\omega}{\omega_c} = 1 - k_1 \frac{PL^2}{EI} - k_5 \left( \frac{TL}{EI} \right)^2 \quad (8-15)$$

in which  $k_1$  and  $k_5$  are numerical coefficients, given in Table 8.04.

In the case of a uniform shaft which has its mass and elasticity uniformly distributed along its length, the basic differential equation of motion for free vibrations in the  $x, z$  plane including axial force effects is:

$$EI \frac{\partial^4 X}{\partial z^4} + P \frac{\partial^2 X}{\partial z^2} + \frac{wA}{g} \frac{\partial^2 X}{\partial t^2} = 0 \quad (8-16)$$

A similar expression exists for free vibrations in the y, z plane. For harmonic motions in a natural mode, the solution for transverse displacements of the rotor is:

$$X = x(z) \cos \omega t \quad (8-17)$$

where

$$x(z) = A \cos \alpha_1 z + B \sin \alpha_1 z + C \cosh \alpha_2 z + D \sinh \alpha_2 z$$

$$\alpha_1 = \left[ \frac{P}{2EI} + \sqrt{\left( \frac{P}{2EI} \right)^2 + \frac{wA \omega^2}{gEI}} \right]^{1/2}$$

$$\alpha_2 = \left[ -\frac{P}{2EI} + \sqrt{\left( \frac{P}{2EI} \right)^2 + \frac{wA \omega^2}{gEI}} \right]^{1/2} \quad (8-18)$$

In the case where the uniform shaft is supported at either end in rigid bearings which permit shaft angular deflection but no displacement, the frequency equation may be determined by substituting the end conditions of zero displacement and zero bending moment at  $z = 0$  and  $z = L$ , and rejecting trivial solutions to obtain:

$$\sin \alpha_1 L \sinh \alpha_2 L = 0$$

The frequency parameters  $\alpha_1$  and  $\alpha_2$  are always real, positive and  $\alpha_2 = n\alpha_1$ .

The frequency equation may be solved by writing

$$\sin \alpha_1 L \sinh n\alpha_1 L = 0$$

and substituting trial  $\alpha_1 L$  values. As  $n$  approaches 1.0,  $\alpha_1$  approaches  $\alpha_2$  and the condition is  $P = 0$ , i.e. a whirling uniform rotor, for which the lowest eigenvalue is  $\alpha_1 L = \alpha_2 L = \pi$ . As  $n$  varies, so the  $\alpha_1 L$  solution departs from  $\pi$ . Uniform rotors supported in other types of end conditions may also be analyzed by the above method.

In general, the effect of end thrust is to lower the eigenvalue and so to depress the critical speed below that of a simple rotor,  $\alpha L = \pi$ .

If the shaft in the above problem is subjected to applied torque the analysis becomes far more complicated, but the results are comparatively simple. Greenhill (Ref.39) has examined the influence of both axial torque and rotation on the buckling of a long uniform shaft. Formulae were obtained for maximum shaft-lengths consistent with stability against buckling, for relatively low-speed operation. Southwell and Gough (Ref.91) have considered the other aspect of the problem, i.e., where the speed is the major factor, and the influence of moderate applied torque and end thrust on the critical speed is required. The basic equations derived by Greenhill again apply. The applied torque gives rise to the following bending moments in the shaft:

$$- T \frac{dx}{dz} \quad \text{about the y-axis}$$

$$T \frac{dy}{dz} \quad \text{about the x-axis}$$

as shown in Figure 4.12. Considering motions in the x, z plane, the equation of motion is:

$$EI \frac{\partial^4 x}{\partial z^4} - T \frac{\partial^3 x}{\partial z^3} + P \frac{\partial^2 x}{\partial z^2} + \frac{wA}{g} \frac{\partial^2 x}{\partial t^2} = 0 \quad (8.19)$$

and in the y, z plane

$$EI \frac{\partial^4 y}{\partial z^4} + T \frac{\partial^3 y}{\partial z^3} + P \frac{\partial^2 y}{\partial z^2} + \frac{wA}{g} \frac{\partial^2 y}{\partial t^2} = 0 \quad (8.20)$$

Putting  $R = x + iY$  and combining gives

$$EI \frac{\partial^4 R}{\partial z^4} + iT \frac{\partial^3 R}{\partial z^3} + P \frac{\partial^2 R}{\partial z^2} + \frac{wA}{g} \frac{\partial^2 R}{\partial t^2} = 0 \quad (8.21)$$

The solution to this equation is:

$$R = r(z) \cos \omega t \quad (8.22)$$

where

$$r(z) = A_1 e^{i\lambda_1 z} + A_2 e^{i\lambda_2 z} + A_3 e^{i\lambda_3 z} + A_4 e^{i\lambda_4 z}$$

where  $\lambda_1, \lambda_2, \lambda_3$  and  $\lambda_4$  are the roots of

$$EI\lambda^4 + T\lambda^3 - P\lambda^2 - \frac{WAgD^2}{8} = 0 \quad (8-23)$$

For long end bearings, the boundary conditions are:

$$x = y = 0; \quad \text{at } z = 0 \text{ and } z = L$$

$$\frac{dx}{dz} = \frac{dy}{dz} = 0; \quad \text{at } z = 0 \text{ and } z = L \quad (8-24)$$

Substituting gives

$$A_1 + A_2 + A_3 + A_4 = 0$$

$$\lambda_1 A_1 + \lambda_2 A_2 + \lambda_3 A_3 + \lambda_4 A_4 = 0$$

$$a_1 A_1 + a_2 A_2 + a_3 A_3 + a_4 A_4 = 0$$

$$a_1 \lambda_1 A_1 + a_2 \lambda_2 A_2 + a_3 \lambda_3 A_3 + a_4 \lambda_4 A_4 = 0 \quad (8-25)$$

where  $a_i = e^{i\lambda_i z}$ . The critical speed condition is obtained from the condition where the determinant of the coefficients  $A_i$  equals zero. Expanding this leads to

$$\Sigma(a_1 a_3 + a_2 a_4)(\lambda_1 - \lambda_2)(\lambda_3 - \lambda_4) = 0$$

Dividing through by  $\sqrt{a_1 a_2 a_3 a_4}$  and noticing that

$$\sqrt{\frac{a_1 a_2}{a_3 a_4}} + \sqrt{\frac{a_3 a_4}{a_1 a_2}} = 2 \cos (\lambda_1 + \lambda_2 - \lambda_3 - \lambda_4) \frac{L}{2}$$

leads to the critical speed condition for fixed direction bearings:

$$\Sigma (\lambda_1^2 - \lambda_2^2)(\lambda_3^2 - \lambda_4^2) \cos (\lambda_1 + \lambda_2 - \lambda_3 - \lambda_4) \frac{L}{2} = 0 \quad (8.26)$$

Similarly, for short bearings, the boundary conditions are at both  $z = 0$  and  $z = L$

$$x = y = 0;$$

$$EI \frac{d^2 x}{dz^2} - T \frac{dx}{dz} = 0;$$

since moment and displacement both vanish at the ends

$$EI \frac{d^2 y}{dz^2} + T \frac{dy}{dz} = 0;$$

These expressions lead to the critical speed equation:

$$\Sigma (\lambda_1^2 - \lambda_2^2)(\lambda_3^2 - \lambda_4^2) \cos (\lambda_1 + \lambda_2 - \lambda_3 - \lambda_4) \frac{L}{2} = 0 \quad (8.27)$$

Southwell and Gough give two diagrams for the above bearing conditions which allow the value of the critical speed parameter  $C$  to be determined directly as a function of the torque and thrust parameters,  $A$  and  $B$ , where:

$$A = \frac{TL}{2EI} \quad B = \frac{PL^2}{4EI} \quad C = \frac{WAD^2 L}{16 EIg}$$

These diagrams are reproduced as Figures 8.08 and 8.09 in this report.

The effect of axial torque alone on bending critical speeds has recently been considered by Rosenberg(Ref.161), for a uniform rotor. Results up to the sixth bending mode are given.

Table 8.01 VIBRATION IN MECHANICAL SYSTEMS, SOURCES AND REMEDIES.

<u>Source of Vibration</u>	<u>Cause</u>	<u>Remedy</u>
1. Internal Combustion Engine	Gas pressure fluctuations. Inadequate engine component design.	Modify firing order, crank angles and timing (Gasoline). Maintain electrical system. Use larger flywheel. Re-select balance weights. Use fluid coupling.
2. Propellers. Fans, pumps, turbines	Pressure fluctuations during rotation. Vibration of blades.	Use ducted propeller. Increase ship-propeller clearance. Eliminate struts. Use higher internal damping material. Increase number of blades. Reduce cavitation effects. Modify guild vane inlet angle. Add flow straighteners on honeycomb.
3. Bevel and Spur Gearing Non-constant drive.	Eccentric mounting of gears. Oblique mounting of gears. Index error in teeth. Misaligned assembly. Excessive backlash.	Remount concentrically. Locate gears accurately on shaft. Recut teeth or replace gear. Re-align in bearings. Helical tooth required.
4. Rotating Unbalance	Shaft eccentricity. Shaft flexibility.  Shaft asymmetry	Reassemble concentrically or rebalance. Multiplane balance through speed range.  Balance or cut for symmetrical stiffness in both flexure planes.
5. Coupling	Improper alignment. Universal joint with large angle.	Realign. Increase coupling flexibility. Reduce angle. Use constant velocity joint. Use bevel gears.
6. Electrical Unbalance	Drive motor	Modify: magnetic design of poles; number, or edges. Increase number of poles.
7. Starting Transient, Shock Load.	Rapid start-up. Load application. Load reduction.	Gentler electrical starter. Gentler clutch, automatic operation. Fluid coupling. Magnetic coupling.

Table 8.02 Natural Frequency Formulas for Torsional Systems




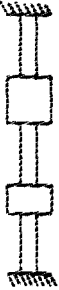


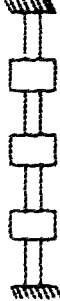






	1. $\omega^2 = \frac{1}{I} (q_1 + q_2)$
	2. $\omega^2 = q(\frac{1}{I_1} + \frac{1}{I_2})$
	3. $\omega = \frac{1}{2} \left[ \omega_1^2 + \omega_2^2 \pm \sqrt{(\omega_1^2 + \omega_2^2)^2 - 4\omega_1^2\omega_2^2} \right]$ $\omega_1^2 = q_1/I_1; \quad \omega_2^2 = q_2/I_2; \quad I = (I_1 + I_2)/2$
	4. $I_1 I_2 \omega^4 - [q_1 I_2 + q_2 (I_1 + I_2) + q_3 I_1] \omega^2 + (q_1 q_2 + q_2 q_3 + q_3 q_1) = 0$
	5. $I_1 I_2 I_3 \omega^6 - [q_1 (I_1 I_3 + I_2 I_3) + q_2 (I_1 I_2 + I_1 I_3)] \omega^4 + q_1 q_2 (I_1 + I_2 + I_3) \omega^2 = 0$
	6. $I_1 I_2 I_3 \omega^6 - [q_1 I_2 I_3 + q_2 (I_1 I_3 + I_2 I_3) + q_3 (I_1 I_2 + I_1 I_3)] \omega^4 + [I_1 q_2 q_3 + I_2 (q_1 q_3 + q_2 q_3) + I_3 (q_1 q_2 + q_2 q_3 + q_1 q_3)] \omega^2 - q_1 q_2 q_3 = 0$
	7. $I_1 I_2 I_3 \omega^6 - [q_1 I_2 I_3 + q_2 (I_1 I_3 + I_2 I_3) + q_3 (I_1 I_2 + I_1 I_3) + q_4 I_1 I_2] \omega^4 + [I_1 (q_2 q_3 + q_3 q_4 + q_4 q_2) + I_2 (q_1 q_3 + q_2 q_3 + q_2 q_4 + q_4 q_1) + I_3 (q_1 q_2 q_3 + q_3 q_4)] \omega^2 - [q_1 q_2 (q_3 + q_4) + q_3 q_4 (q_1 + q_2)] = 0$

Table 8.03 Natural Frequencies of Axial Vibration

	1. $\omega^2 = \frac{k}{m}$
	2. $\omega^2 = \omega_c^2 \left[ 1 - \zeta^2 \right]$ $\zeta = \frac{c}{c_c}$ $c_c = 2\sqrt{km}$
	3. $\omega^2 = k \left[ \frac{1}{m_1} + \frac{1}{m_2} \right]$
	4. $\omega^2 = \frac{Ak}{L} \left[ \frac{1}{m_a} + \frac{1}{m_b} \right]$ $m_a = m_1 + 1/3 m_0 \cdot \frac{m_2}{m_1 + m_2}$ $m_b = m_2 + 1/3 m_0 \cdot \frac{m_1}{m_1 + m_2}$
	5. $\omega = \frac{1}{2} \left[ \omega_1^2 + m\omega_2^2 \pm \sqrt{\omega_1^2 + \omega_2^2 m^2 - 4\omega_1^2 \omega_2^2} \right]$ $\omega_1^2 = k_1/m_2$ $\omega_2^2 = k_2/m_2$ $m = (m_1 + m_2/m_1)$
	6. $m_1 m_2 m_3 \omega^6 - \left[ k_1(m_1 m_3 + m_2 m_3) + k_2(m_1 m_2 + m_1 m_3) \right] \omega^4 + k_1 k_2 (m_1 + m_2 + m_3) \omega^2 = 0$

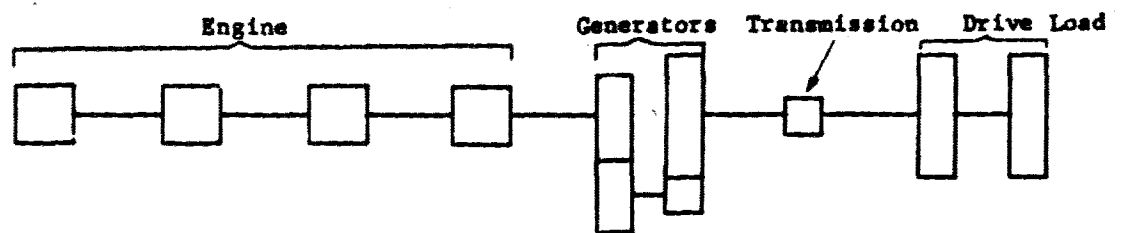


Fig. 8.01 Inertia-Stiffness Distribution for Torsional System

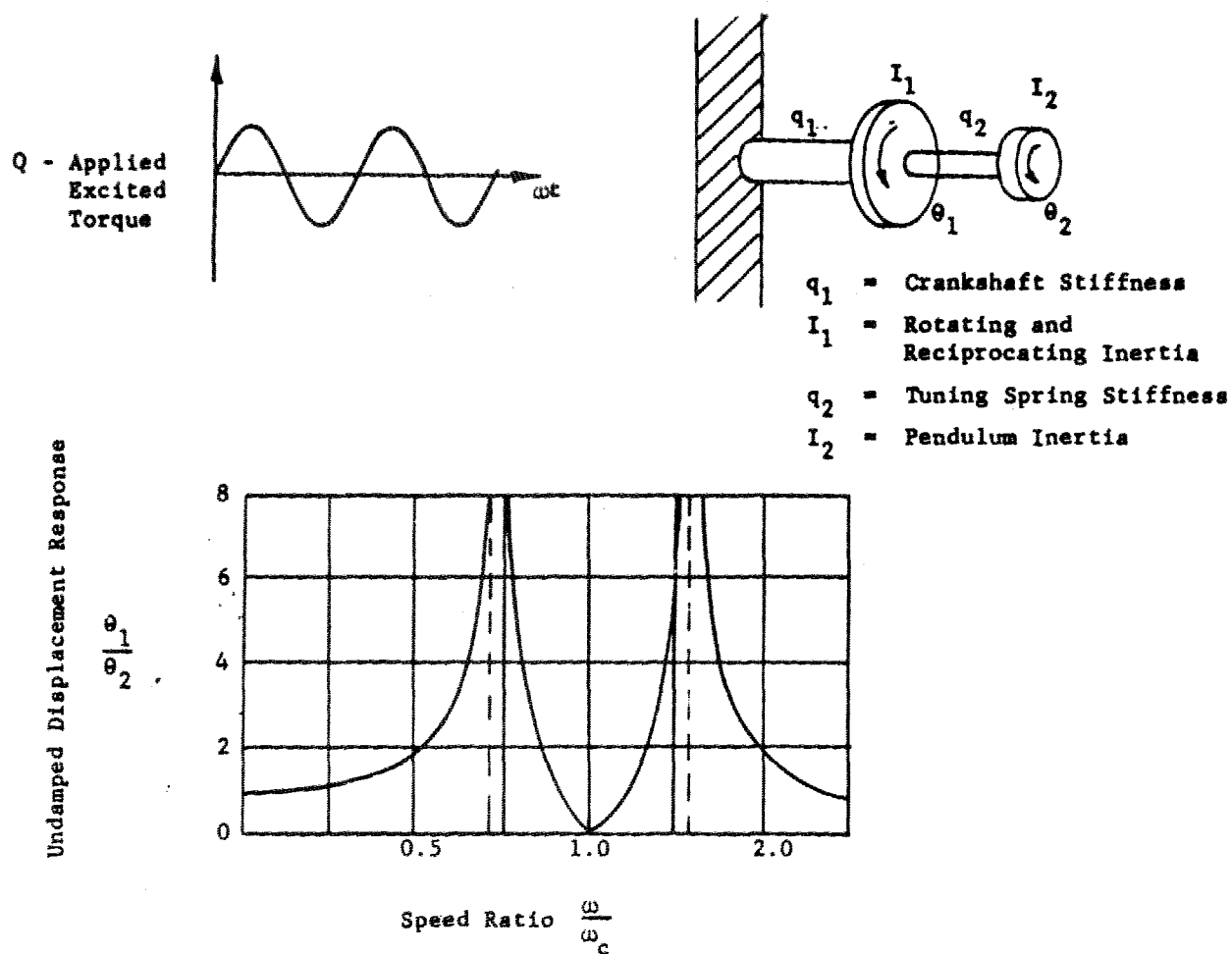
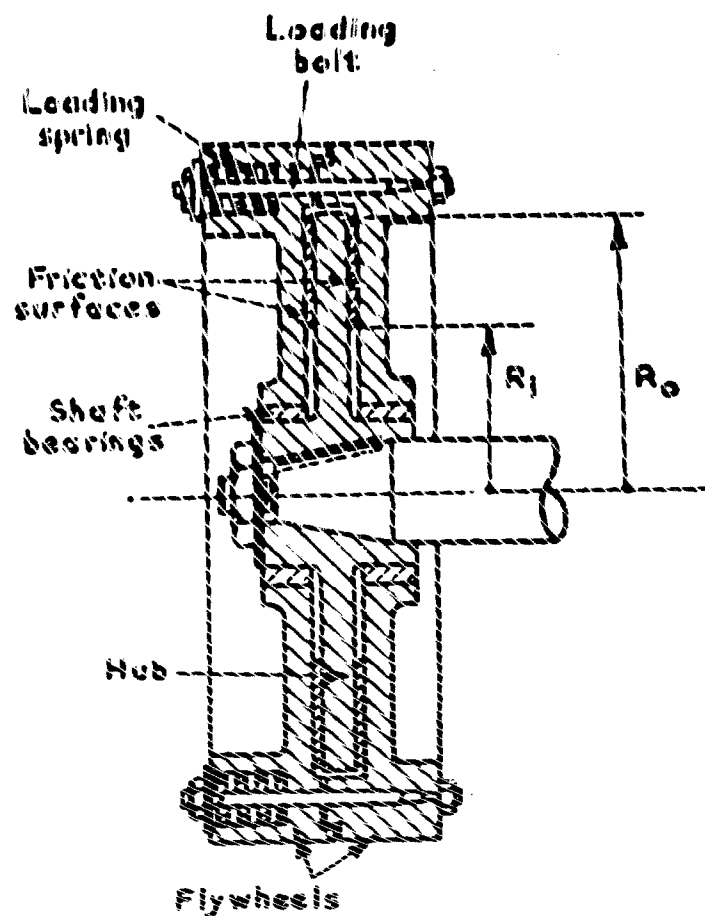


Fig. 8.02 Undamped Two-Degree-of-Freedom System Response at Main Mass,  $\theta_1$



### COULOMB FRICTION DAMPER

Fig. 8.03 Coulomb Friction Damper  
Courtesy of B.I.C.E.R.A. Torsional Vibration Handbook

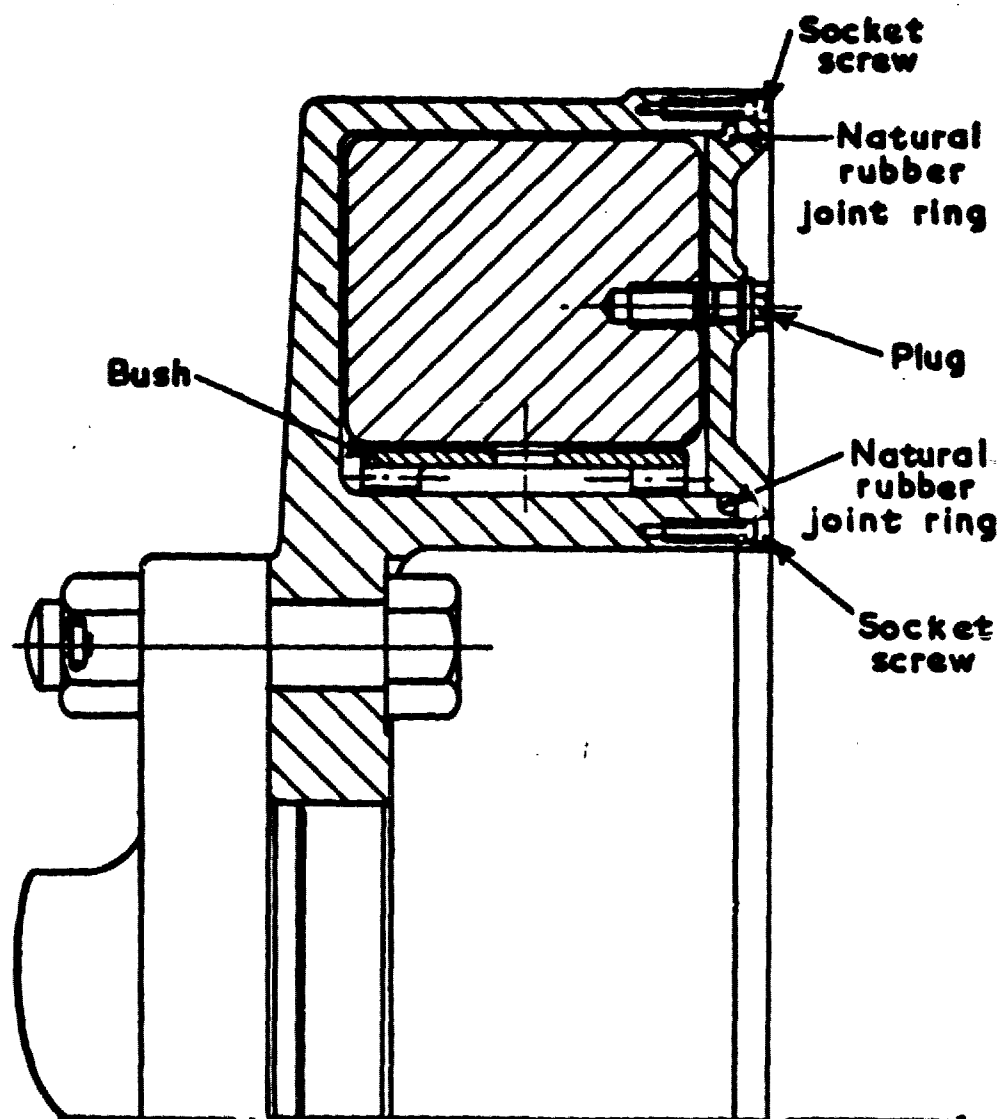


Fig. 8.04 Viscous Shear Damper  
Courtesy of B.I.C.E.R.A. Torsional Vibration Handbook

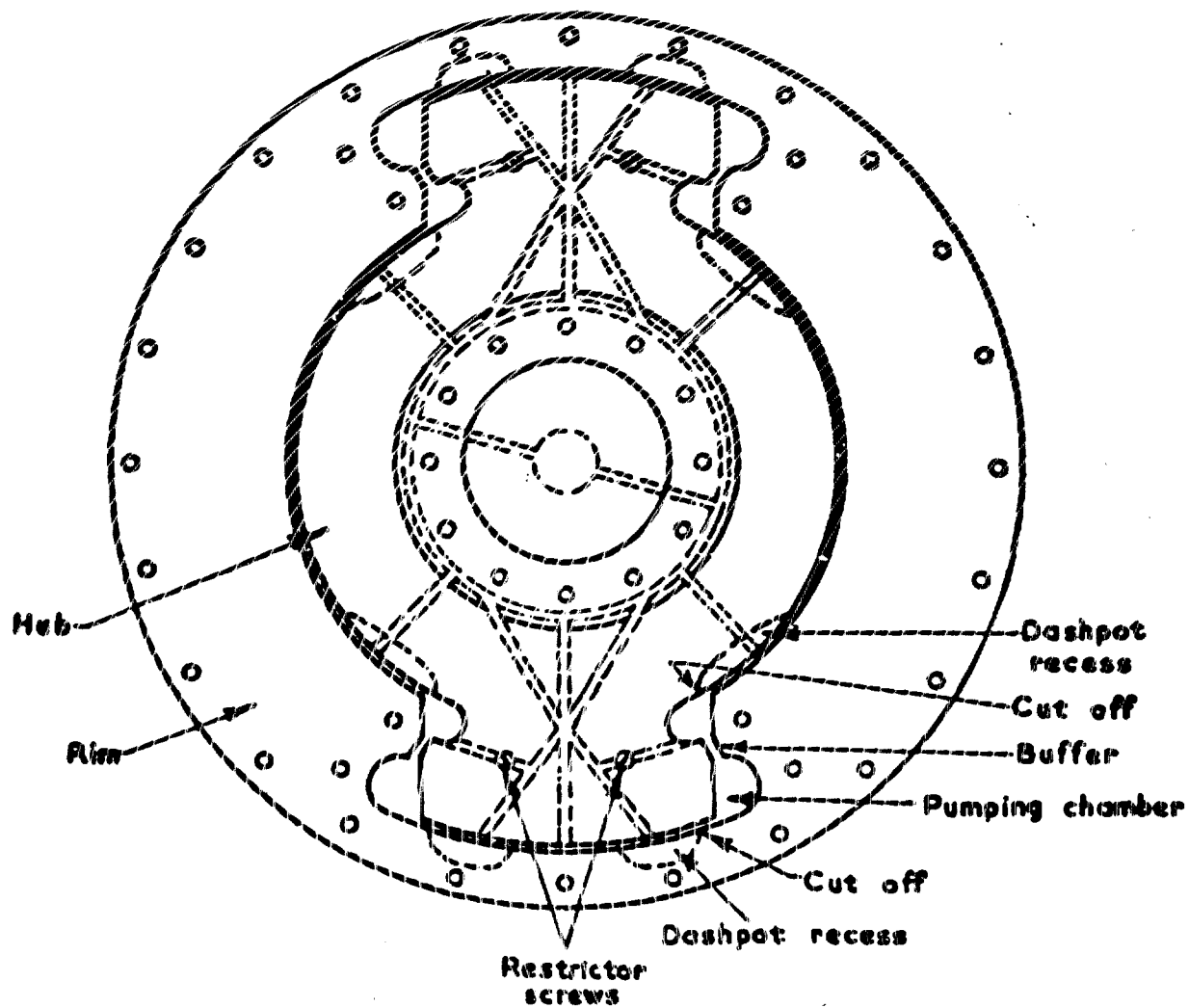


Fig. 8.05 Pumping Chamber Damper  
 Courtesy of B.I.C.E.R.A. Torsional Vibration Handbook

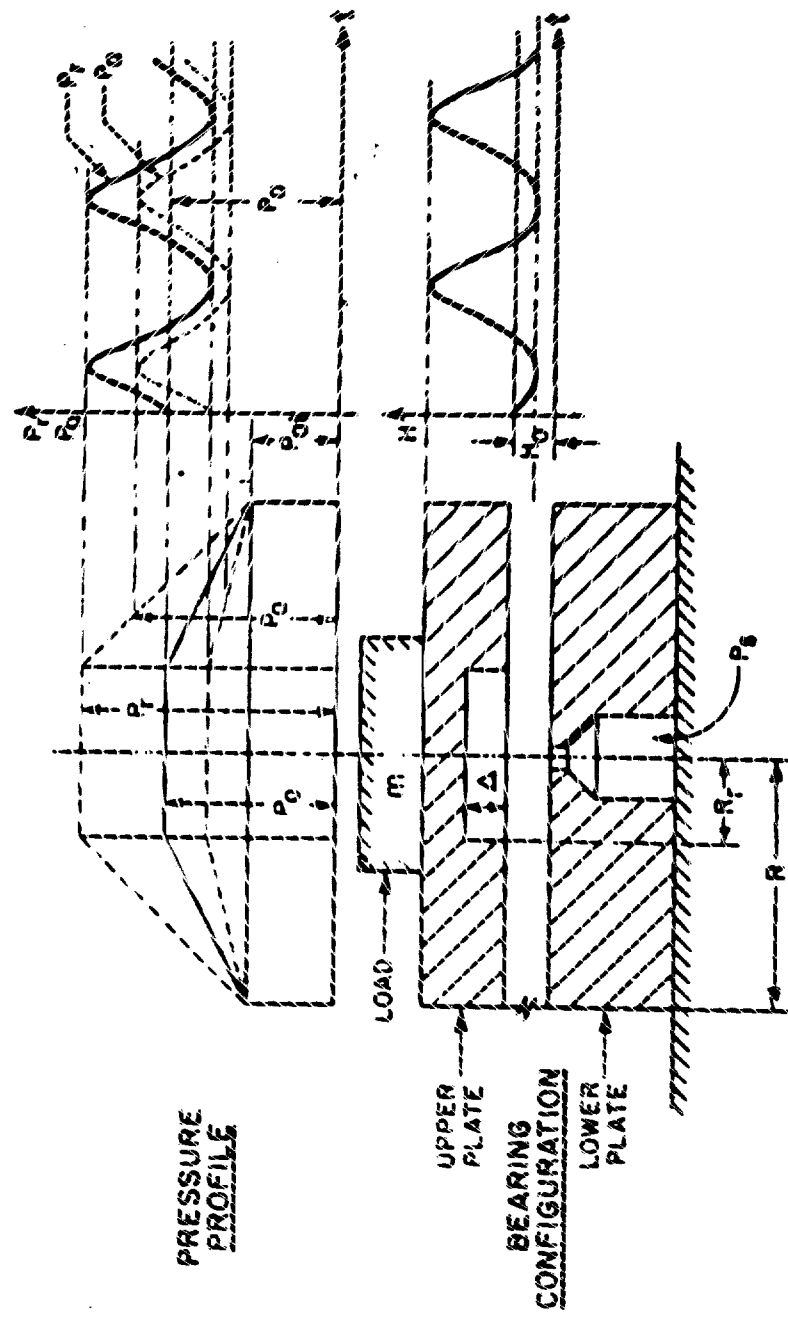


Fig. 8.06 Motion and Geometry of Hydrostatic Thrust Bearing

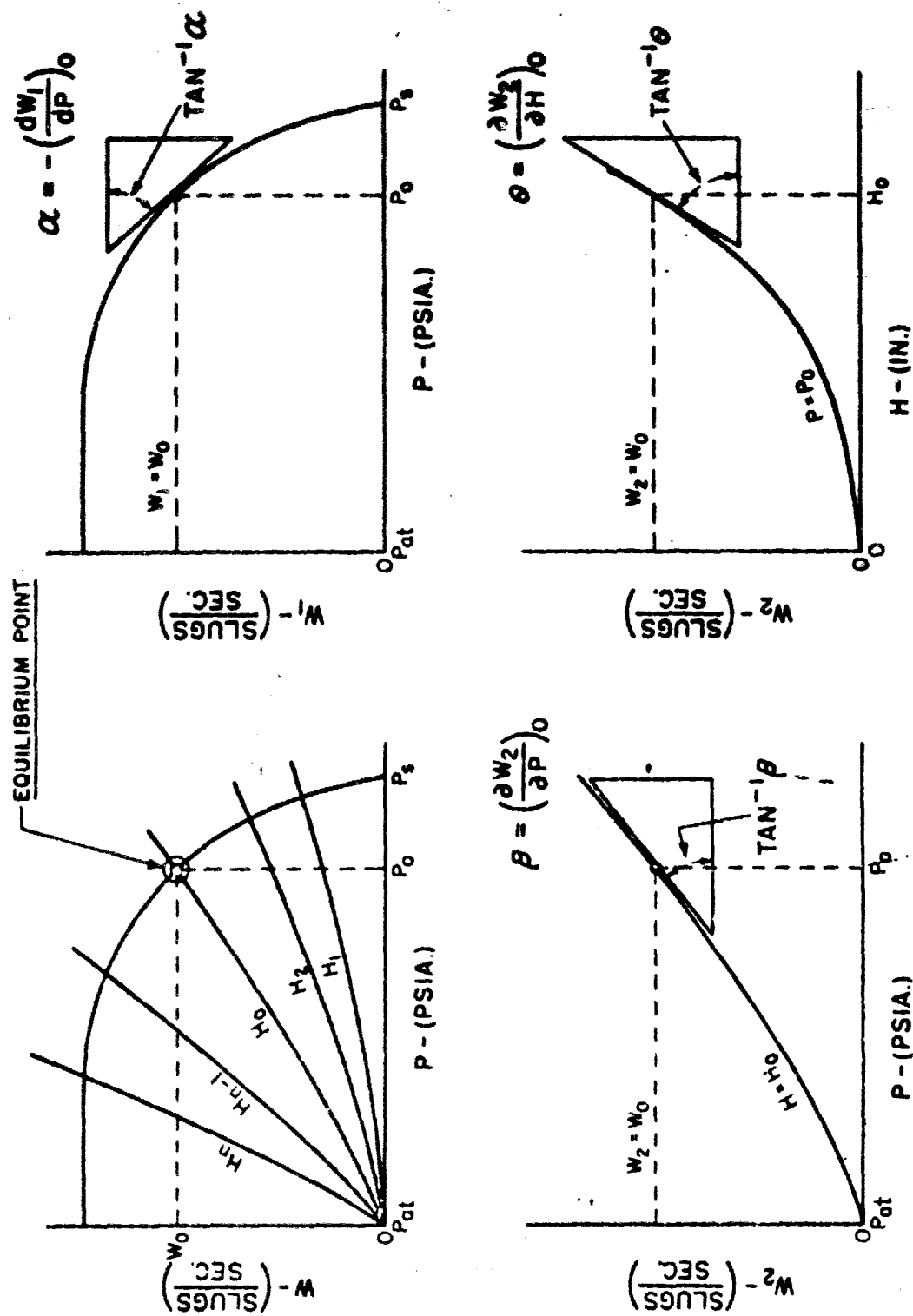


Fig. 8.07 Rates of Change of Mass Flow about Equilibrium Point

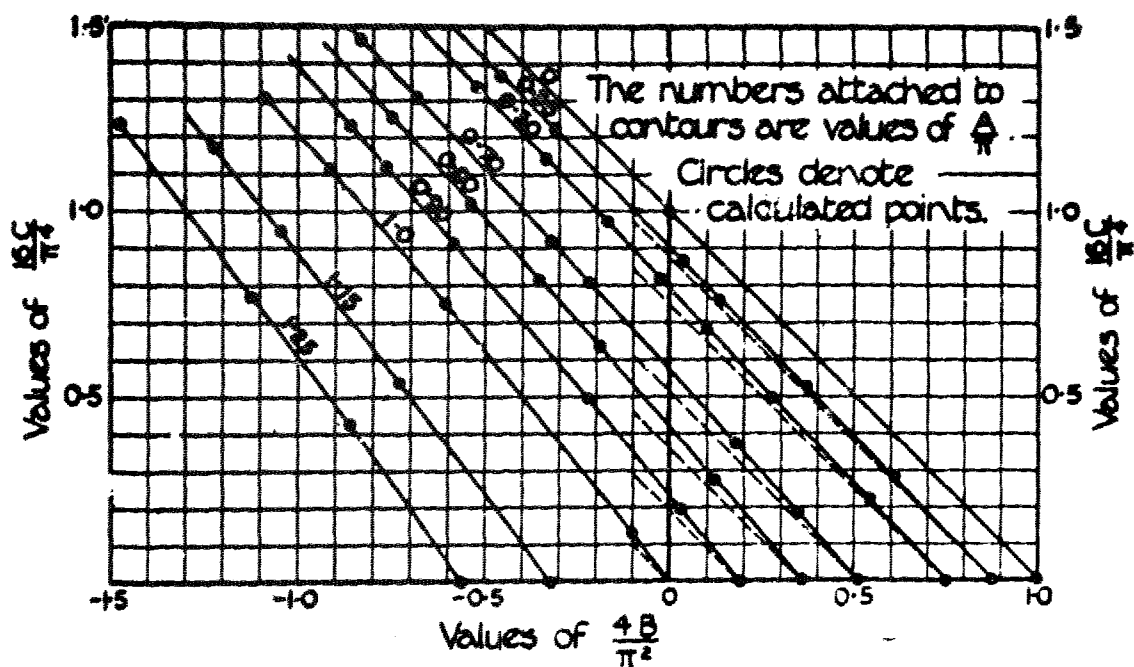


Fig. 8.08 Critical Speed Diagram for Simply Supported Shaft Subjected to End Thrust and Twist

Reprinted from British Association for the Advancement of Science. Report of the Eighty-Ninth Meeting. Figure 17, Edinburgh, 1921. 1922 John Murray, Albemarle Street

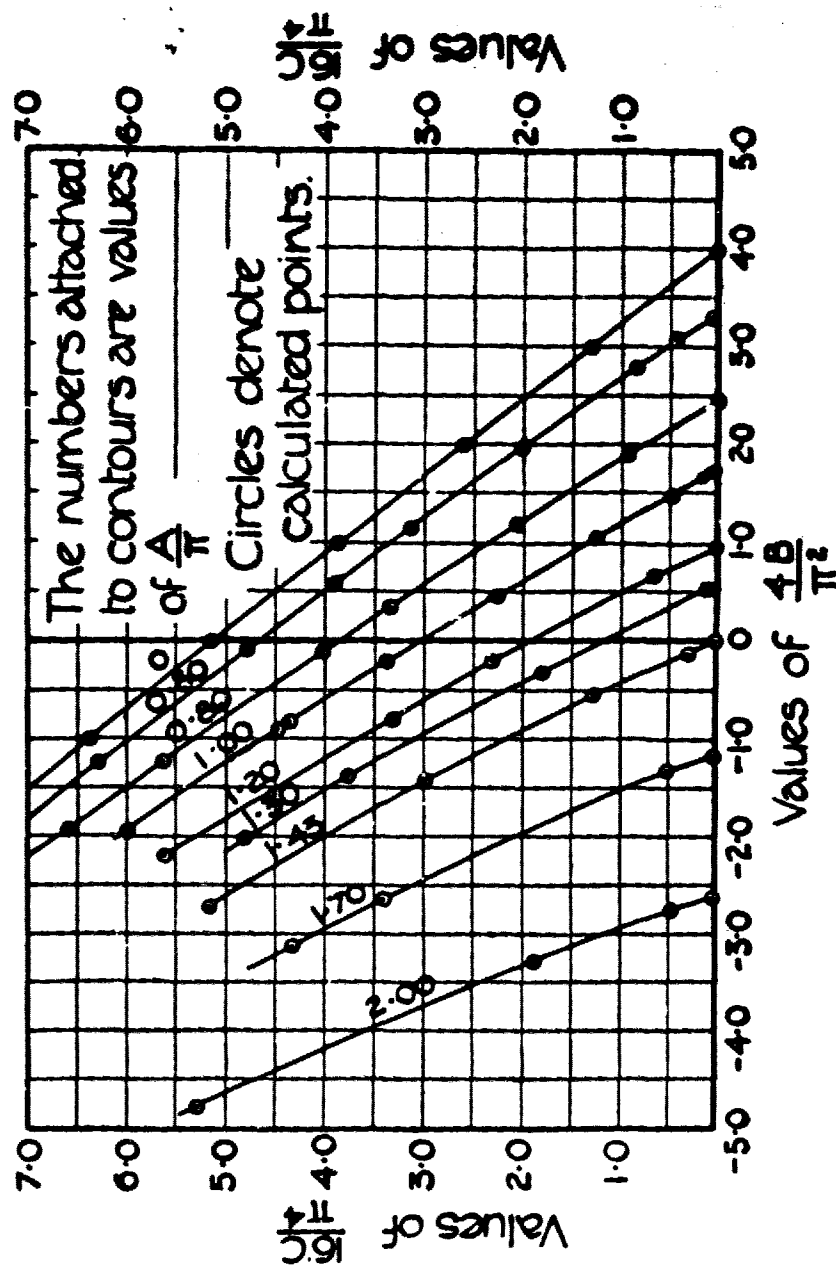


Fig. 8.09 Critical Speed Diagram for Simple Supported Shaft Subjected to End Thrust and Twist

Reprinted from British Association for the Advancement of Science. Report of the Eighty-Ninth Meeting. Figure 18, Edinburgh, 1921. 1922 John Murray, Albemarle Street

## APPENDIX A - FUNDAMENTALS OF HYDRODYNAMIC LUBRICATION THEORY

The theory of hydrodynamic lubrication is based on a particular formulation of the Navier-Stokes equations, known as Reynolds' equation. The underlying assumptions are:

1. The thickness of the fluid film  $y$  is very small compared with the length  $x$  and breadth  $z$ .
2. No variation of pressure occurs across the film thickness,  $\partial p / \partial y = 0$ .
3. The flow is laminar. No vortex flow and no turbulence exists within the film.
4. No external forces act on the fluid film. Thus,  $X = Y = Z = 0$ .
5. Fluid inertia is small compared with the viscous shear.
6. No slip occurs at the bearing surfaces.
7. Velocity gradients in the direction of film thickness are negligible.

With these assumptions, the generalized Reynolds' equation becomes:

$$\frac{\partial}{\partial x} \left( \frac{\rho h^3}{\mu} \frac{\partial p}{\partial x} \right) + \frac{\partial}{\partial z} \left( \frac{\rho h^3}{\mu} \frac{\partial p}{\partial z} \right) = 6 (U_1 - U_2) \frac{\partial(\rho h)}{\partial x} + 12\rho V + 12h \frac{\partial p}{\partial t} \quad (A-1)$$

This expression applies to both compressible and incompressible lubricants. The left-hand side describes the pressure distribution throughout the bearing. The first right-hand term is due to the bearing velocities along the oil film. The term  $12\rho V$  is due to the bearing surfaces in a direction normal to the oil film. The last term accounts for time-dependent pressure variations in the film. For a journal bearing, Figure A-1, the shaft alone rotates,  $U_2 = 0$ , and Reynolds' equation for a compressible lubricant becomes:

$$\frac{\partial}{\partial x} \left( \frac{\rho h^3}{\mu} \frac{\partial p}{\partial x} \right) + \frac{\partial}{\partial z} \left( \frac{\rho h^3}{\mu} \frac{\partial p}{\partial z} \right) = 6U \frac{\partial(\rho h)}{\partial x} + 12\rho V + 12h \frac{\partial p}{\partial t} \quad (A-2)$$

With a compressible lubricant  $\rho = \text{constant}$ , and for a journal bearing Reynolds' equation becomes:

$$\frac{\partial}{\partial x} \left( \frac{h^3}{\rho} \frac{\partial p}{\partial x} \right) + \frac{\partial}{\partial z} \left( \frac{h^3}{\rho} \frac{\partial p}{\partial z} \right) = 6U \frac{\partial h}{\partial x} + 12V \quad (\text{A-3})$$

These equations may contain viscosity, density, film thickness and time as parameters. These parameters both determine and depend on the temperature and pressure fields, and on the elastic behavior of the bearing surfaces under pressure and temperature. Thus, to obtain a complete and accurate representation of the hydrodynamics of the lubricating film, it may be necessary to consider simultaneously the Reynolds' equation, the energy equation, the elasticity equation and the equation of state. Both energy and elasticity considerations are discussed at length in the book by Pinkus and Sternlicht (Ref. 2). The equation of state applies to compressible lubricants, and is

$$p/\rho = RT$$

as given by the perfect gas law. In general, it is sufficiently accurate to ignore variations of  $\rho$  and  $\mu$  with  $T$ , and to substitute the equation of state into Reynolds' equation. Where this approximation is impossible, the equations must be solved simultaneously.

#### Incompressible Lubricants

For an incompressible fluid, the dynamic Reynolds' equation for journal bearings of finite length may be written

$$\frac{\partial}{\partial x} \left( \frac{h^3}{\mu} \frac{\partial p}{\partial x} \right) + \frac{\partial}{\partial z} \left( \frac{h^3}{\mu} \frac{\partial p}{\partial z} \right) = 6R\omega \left[ 1 - 2 \frac{a}{\omega} \right] \frac{\partial h}{\partial x} + 12 \dot{\rho} \cos \theta \quad (\text{A-4})$$

Introducing the dimensionless parameters

$$\bar{x} = x/D; \quad \bar{z} = z/L; \quad \bar{h} = h/2C; \quad \epsilon = \rho/C$$

$$\bar{p} = \left( \frac{2\pi}{\mu\omega} \right) \left( \frac{C}{R} \right)^3 p$$

and assuming constant viscosity, Reynolds' equation in dimensionless form becomes:

$$\frac{\partial}{\partial \bar{x}} \left( \bar{h}^3 \frac{\partial \bar{p}}{\partial \bar{x}} \right) + \left( \frac{D}{L} \right)^2 \frac{\partial}{\partial \bar{z}} \left( \bar{h}^3 \frac{\partial \bar{p}}{\partial \bar{z}} \right) = 6\pi \frac{\partial \bar{h}}{\partial \bar{x}} + 12\pi \frac{\left( \frac{\dot{\epsilon}}{\omega} \right)}{1 - 2 \left( \frac{\dot{\alpha}}{\omega} \right)} \cos \theta \quad (A-5)$$

where

$$\bar{h} = 1/2 (1 + \epsilon \cos \theta)$$

The resulting fluid-film forces in the radial and tangential directions acting on the rotor are

$$\begin{aligned} F_r &= -\lambda \omega \left( 1 - 2 \frac{\dot{\alpha}}{\omega} \right) \iint \bar{p} \cos \theta \, d\bar{x} \, d\bar{z} \\ &= \lambda \omega \left( 1 - 2 \frac{\dot{\alpha}}{\omega} \right) f_r \left[ \epsilon, \frac{\dot{\epsilon}/\omega}{1 - 2 \left( \frac{\dot{\alpha}}{\omega} \right)}, \frac{L}{D} \right] \\ F_t &= \lambda \omega \left( 1 - 2 \frac{\dot{\alpha}}{\omega} \right) \iint \bar{p} \sin \theta \, d\bar{x} \, d\bar{z} \\ &= \lambda \omega \left( 1 - 2 \frac{\dot{\alpha}}{\omega} \right) f_t \left[ \epsilon, \frac{\dot{\epsilon}/\omega}{1 - 2 \left( \frac{\dot{\alpha}}{\omega} \right)}, \frac{L}{D} \right] \end{aligned} \quad (A-6)$$

where

$$\lambda = \left( \frac{\mu R L}{\pi} \right) \left( \frac{R}{C} \right)^2$$

For rotor-bearing dynamic analysis, these forces are linearized with respect to displacement and velocity to give

$$dF = \lambda \omega \left( 1 - 2 \frac{\dot{\alpha}}{\omega} \right) \left[ \frac{\partial f}{\partial \epsilon} d\epsilon + \frac{\partial f}{\partial (\epsilon/\omega)} d \left( \frac{\epsilon}{\omega} \right) + \frac{\partial f}{\partial (\alpha/\omega)} d \left( \frac{\alpha}{\omega} \right) - \frac{2f}{1 - 2 \left( \frac{\dot{\alpha}}{\omega} \right)} d \left( \frac{\dot{\alpha}}{\omega} \right) \right]$$

Expanding the above expression in a Taylor series about the steady-state equilibrium position, it follows that  $\epsilon = \dot{\alpha} = 0$  and so  $\left[ \partial f / \partial \left( \frac{\dot{\alpha}}{\omega} \right) \right] = 0$

This gives

$$dF = \lambda \omega \left[ \frac{\partial f}{\partial \epsilon} d\epsilon + \frac{\partial f}{\partial (\dot{\epsilon}/\omega)} d\left(\frac{\dot{\epsilon}}{\omega}\right) - \frac{2f}{\epsilon} \frac{1}{\omega} \cdot \epsilon dx \right]$$

Changing from polar to rectangular coordinates as shown in Figure A-1

$$x = C\epsilon \cos \alpha \quad y = C\epsilon \sin \alpha$$

the force coordinates in the x and y directions are

$$\begin{aligned} dF_x = \frac{1}{C} \lambda \omega & \left\{ - \left[ \frac{\partial fr}{\partial \epsilon} \cos^2 \alpha + \frac{fr}{\epsilon} \sin^2 \alpha + \left( \frac{ft}{\epsilon} + \frac{\partial ft}{\partial \epsilon} \right) \cos \alpha \sin \alpha \right] dx \right. \\ & - \left[ \frac{\partial fr}{\partial (\dot{\epsilon}/\omega)} \cos^2 \alpha + \frac{2ft}{\epsilon} \sin^2 \alpha + \left( \frac{2fr}{\epsilon} + \frac{\partial ft}{\partial (\dot{\epsilon}/\omega)} \right) \cos \alpha \sin \alpha \right] \\ & \quad \left. \frac{1}{\omega} (dx) \right. \\ & + \left[ \frac{ft}{\epsilon} \cos^2 \alpha - \frac{\partial ft}{\partial \epsilon} \sin^2 \alpha + \left( \frac{fr}{\epsilon} - \frac{\partial fr}{\partial \epsilon} \right) \cos \alpha \sin \alpha \right] dy \\ & + \left. \left[ \frac{2fr}{\epsilon} \cos^2 \alpha - \frac{\partial ft}{\partial (\dot{\epsilon}/\omega)} \sin^2 \alpha + \left( \frac{2ft}{\epsilon} - \frac{\partial fr}{\partial (\dot{\epsilon}/\omega)} \right) \cos \alpha \sin \alpha \right] \frac{1}{\omega} (dy) \right\} \\ dF_y = \frac{1}{C} \lambda \omega & \left\{ \left[ \frac{\partial ft}{\partial \epsilon} \cos^2 \alpha + \frac{ft}{\epsilon} \sin^2 \alpha + \left( \frac{fr}{\epsilon} - \frac{\partial fr}{\partial \epsilon} \right) \cos \alpha \sin \alpha \right] dx \right. \\ & + \left[ \frac{\partial ft}{\partial (\dot{\epsilon}/\omega)} \cos^2 \alpha - \frac{2fr}{\epsilon} \sin^2 \alpha + \left( \frac{2ft}{\epsilon} - \frac{\partial fr}{\partial (\dot{\epsilon}/\omega)} \right) \cos \alpha \sin \alpha \right] \frac{1}{\omega} (dx) \\ & - \left[ \frac{fr}{\epsilon} \cos^2 \alpha + \frac{\partial fr}{\partial \epsilon} \sin^2 \alpha - \left( \frac{ft}{\epsilon} + \frac{\partial ft}{\partial \epsilon} \right) \cos \alpha \sin \alpha \right] dy \\ & - \left. \left[ \frac{2ft}{\epsilon} \cos^2 \alpha + \frac{\partial fr}{\partial (\dot{\epsilon}/\omega)} \sin^2 \alpha - \left( \frac{2fr}{\epsilon} + \frac{\partial ft}{\partial (\dot{\epsilon}/\omega)} \right) \cos \alpha \sin \alpha \right] \frac{1}{\omega} (dy) \right\} \quad (A-7) \end{aligned}$$

This is expressed in the form of displacement and velocity coefficients, commonly called spring and damping coefficients for rotor dynamic analysis as follows:

$$dF_x = E_{xx} dz + C_{xx} (dz) + E_{xy} dy + C_{xy} (dy)$$

$$dF_y = E_{yx} dz + C_{yx} (dz) + E_{yy} dy + C_{yy} (dy) \quad (A-8)$$

Numerical values of these spring and damping coefficients for incompressible bearings are given in Table A-1.

#### Compressible Lubricants

A number of techniques have been used to obtain solutions for the case of a finite-length gas bearing such as the perturbation method, Ausman (Ref. 113), the Galerkin method, Cheng (Ref. 126), the ph method Ausman (Ref. 128), and the linearized ph method, Ng (Ref. 127). Of these, the linearized ph method leads to an improved analytical solution which largely eliminates the defects of first-order perturbation. This method linearizes the compressible Reynolds' equation by setting the product ph of the pressure and film thickness as the dependent variable. The steady-state pressure distribution is given by

$$p = \left[ \frac{P_s}{1 + \epsilon \cos \theta} \right] \left[ 1 + \epsilon \frac{\Lambda}{1 + \Lambda^2} \left\{ g_1 \zeta \sin \theta + g_2 \zeta \cos \theta \right\} \right] \quad (A-9)$$

where

$$g_1 \zeta = 1 - A \sinh \alpha \zeta \sin \beta \zeta + B \cosh \alpha \zeta \cos \beta \zeta$$

$$g_2 \zeta = 1/\Lambda + A \cosh \alpha \zeta \cos \beta \zeta + B \sinh \alpha \zeta \sin \beta \zeta$$

$$A = \frac{\Lambda \cosh \alpha (L/D) \cos \beta (L/D) + \sinh \alpha (L/D) \sin \beta (L/D)}{\sinh^2 \alpha (L/D) + \cos^2 \beta (L/D)}$$

$$B = \frac{\Lambda \cosh \alpha (L/D) \sin \beta (L/D) - \sinh \alpha (L/D) \cos \beta (L/D)}{\sinh^2 \alpha (L/D) + \cos^2 \beta (L/D)}$$

$$\alpha^2 = 1/2 \left[ 1 + \sqrt{1 + \Lambda^2} \right]$$

$$\beta^2 = 1/2 \left[ -1 + \sqrt{1 + \Lambda^2} \right]$$

and

$$p = \frac{p^{(1)} + p_0 \epsilon \cos \theta}{1 + \epsilon \cos \theta}$$

where  $p^{(1)}$  is the first-order perturbation solution for pressure.

The radial and tangential components of load capacity are:

$$W_R = W_R^{(1)} \frac{2}{\epsilon^2} \left[ \frac{1 - \sqrt{1 - \epsilon^2}}{\sqrt{1 - \epsilon^2}} \right]$$

$$W_T = W_T^{(1)} \frac{2}{\epsilon^2} \left[ 1 - \sqrt{1 - \epsilon^2} \right]$$

where  $W_R^{(1)}$  and  $W_T^{(1)}$  are the first-order perturbation results. The total load capacity and attitude angle are given by

$$W = W^{(1)} \frac{2}{\epsilon^2} \cdot \frac{1 - \sqrt{1 - \epsilon^2}}{\sqrt{1 - \epsilon^2}} \cdot \sqrt{1 - \epsilon^2} \sin^2 \phi^{(1)}$$

$$\tan \phi = 1 - \epsilon^2 \tan \phi^{(1)}$$

where  $W^{(1)}$  and  $\phi^{(1)}$  are the first-order perturbation results. Figure A-2 shows  $W^{(1)}$  and  $\phi^{(1)}$  as function of the bearing number  $\Lambda$  for various (L/D) ratios.

The Reynolds' equation for dynamic loading with a compressible lubricant may be solved by a number of methods, including the finite-difference technique, Sternlicht (Ref. 118). The force derivations with respect to displacement and velocity are

$$\frac{\partial W_R}{\partial \epsilon'} = \left( \frac{2}{1 - 2\alpha'} \right) \left( \frac{\partial W_T}{\partial \epsilon} \right)_D = 2 \left( \frac{\partial W_T}{\partial \epsilon} \right)_S$$

$$\frac{\partial W_R}{\partial \epsilon'} = - \left( \frac{2}{1 - 2\alpha'} \right) \left( \frac{\partial W_R}{\partial \epsilon} \right)_D = -2 \left( \frac{\partial W_R}{\partial \epsilon} \right)_S \quad (A-10)$$

$$\text{where } \epsilon' = \frac{d\epsilon}{\omega dt} \text{ and } \alpha' = \frac{d\alpha}{\omega dt}$$

and subscripts D and S correspond to Dynamic and Static cases respectively. Figure A-2 shows dimensionless radial and tangential stiffnesses versus dynamic bearing number  $A^* = (1 - 2\epsilon^2)A$ , obtained from the first-order perturbation of  $\epsilon$  and  $\epsilon'$ . Where the rotor is not whirling,  $A^* = A$ . The velocity derivatives  $\frac{\partial k_r}{\partial \epsilon'}$  and  $\frac{\partial k_t}{\partial \epsilon'}$  may be obtained by differentiating the expressions for the displacement derivatives.

Using intrinsic time dependence and the linearized ph method, the Reynolds' equation can be solved for the stiffness and damping derivatives. These results have been obtained by Pan (Ref. 119) and are shown in Figure A-3.

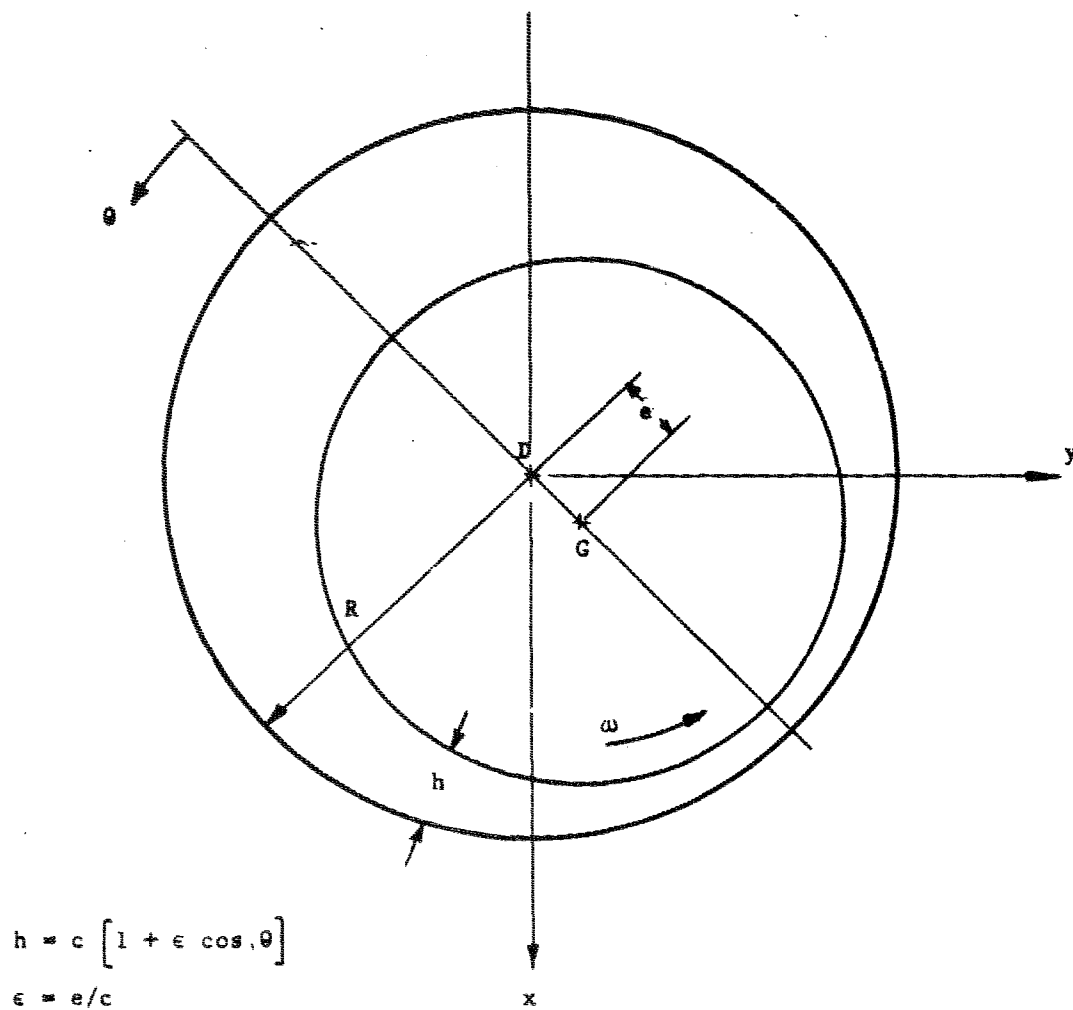


Figure A-1 Journal Bearing Geometry

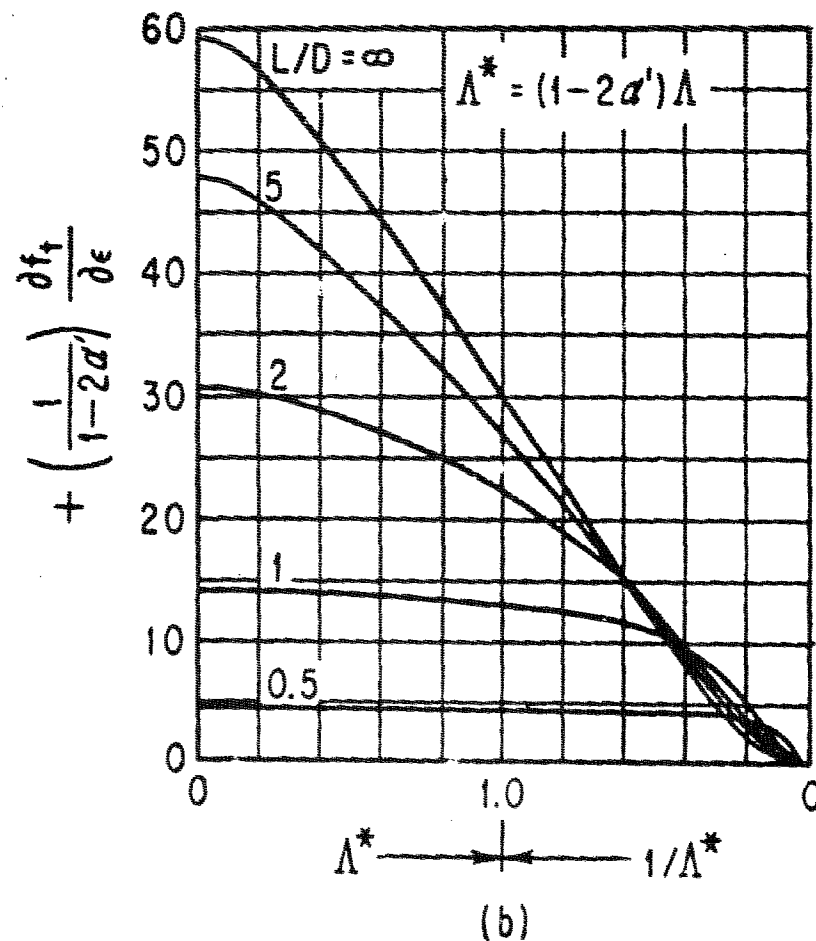
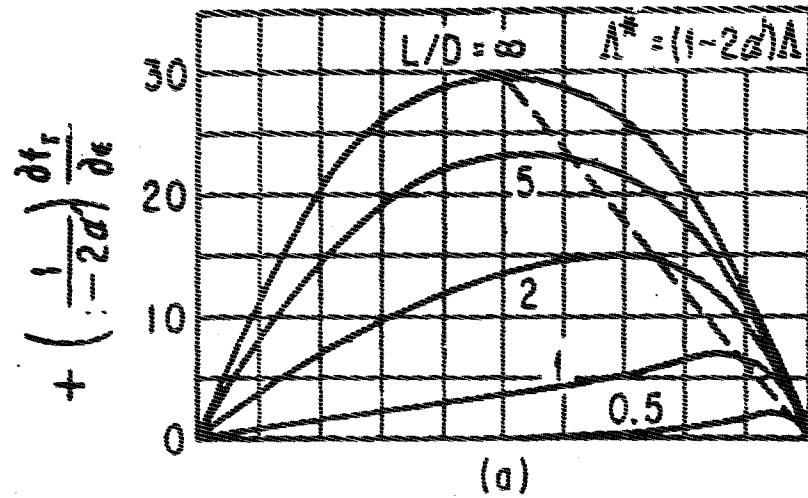


Fig. A-2a Dimensionless Radial Stiffness Versus Dynamic Compressibility Number (From Perturbation Solution)

Fig. A-2b Dimensionless Tangential Stiffness Versus Dynamic Compressibility Number (From Perturbation Solution)

Reprinted from MECHANICAL DESIGN AND SYSTEMS HANDBOOK, Figures 12.16a and 12.16b, Harold A. Rothbart, Editor, McGraw-Hill Book Company, 1964.

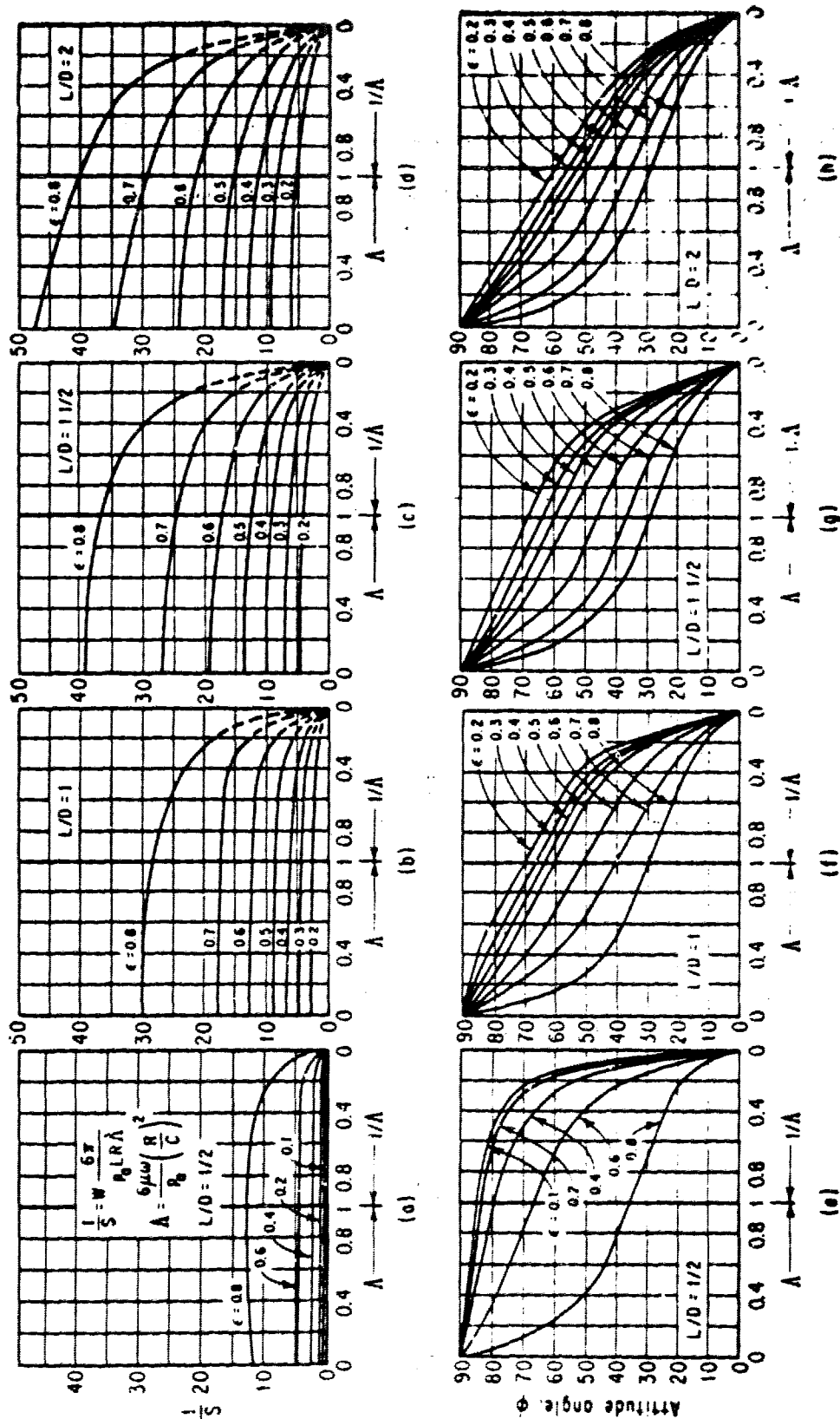
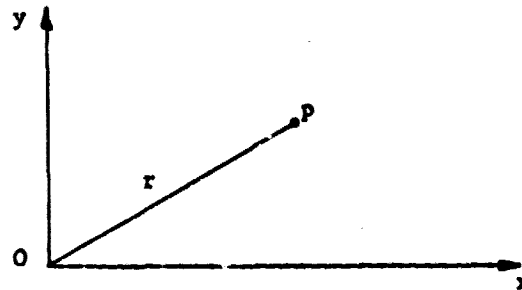


Fig. A-3 Solutions of Dimensionless Load and Attitude Angle for Several  $L/D$  Ratios. (a) Dimensionless Force vs. Bearing Number. (b) Dimensionless Force vs. Bearing Number. (c) Dimensionless Force vs. Bearing Number. (d) Dimensionless Force vs. Bearing Number. (e) Attitude Angle vs. Bearing Number. (f) Attitude Angle vs. Bearing Number. (g) Attitude Angle vs. Bearing Number. (h) Attitude Angle vs. Bearing Number.

Reprinted from MECHANICAL DESIGN AND SYSTEMS HANDBOOK, Figure 12.18, Harold A. Rothbart, Editor, McGraw-Hill Book Company, 1964

## APPENDIX B - TRANSFORMATION FORMULAE FOR STATIONARY AND ROTATING COORDINATES

The required transformations for cartesian coordinates to either stationary or rotating polar coordinates are obtained as follows:



Stationary:

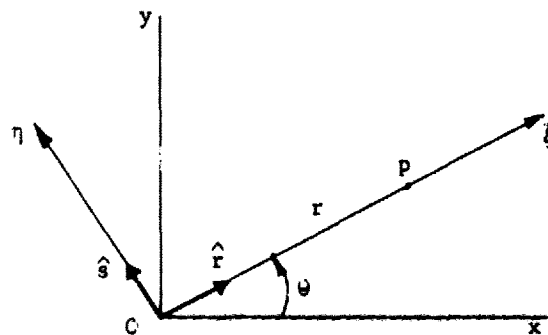
$$\begin{aligned} r &= x + iy \\ x &= r \cos \theta \\ y &= r \sin \theta \\ \ddot{x} &= (\ddot{r} - r\dot{\theta}^2) \cos \theta - (r\ddot{\theta} + 2\dot{r}\dot{\theta}) \sin \theta \\ \ddot{y} &= (\ddot{r} - r\dot{\theta}^2) \sin \theta + (r\ddot{\theta} + 2\dot{r}\dot{\theta}) \cos \theta \end{aligned}$$

Radial Acceleration:  $a_r = \ddot{x} \cos \theta + \ddot{y} \sin \theta$

$$= (\ddot{r} - r\dot{\theta}^2)$$

Tangential Acceleration:  $a_t = -\ddot{x} \sin \theta + \ddot{y} \cos \theta$

$$= (r\ddot{\theta} + 2\dot{r}\dot{\theta})$$



Let the rotating coordinates be  $\xi, \eta$  and let the corresponding unit vectors be  $\hat{i}, \hat{j}$ , as shown in Figure B-2. Let  $r$  be the modulus of  $OP = \vec{r}$  such that  $\vec{r} = \hat{i} r$ . The unit vectors vary in direction and so:

$$(d\hat{i}/dt) = \omega \hat{j} \quad (d\hat{j}/dt) = -\omega \hat{i}$$

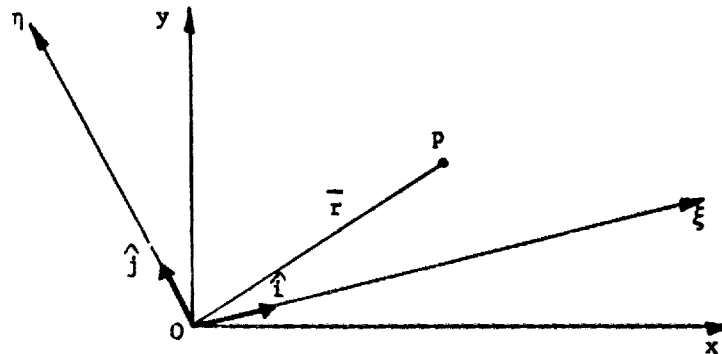
and so

$$\begin{aligned} \vec{v} &= (d\vec{r}/dt) = d/dt (\hat{i} r) \\ &= \hat{i} \dot{r} + \hat{j} r\omega \end{aligned}$$

Differentiating again gives

$$\begin{aligned} \vec{a} &= (d\vec{v}/dt) \\ &= \hat{i}(\ddot{r} - r\omega^2) + \hat{j}(r\ddot{\theta} + 2\dot{r}\omega) \end{aligned}$$

More generally, by not placing the rotating coordinate  $\xi$  along the radius  $OP$  the vector expression for the rotating radius is:



$$\vec{r} = \hat{i}\xi + \hat{j}\eta$$

where  $\hat{i}, \hat{j}$  are unit vectors in the  $\xi, \eta$  axes respectively, and

$$(d\hat{i}/dt) = \hat{j}\omega; \quad (d\hat{j}/dt) = -\hat{i}\omega \quad \text{as before.}$$

$$\begin{aligned} \vec{v} &= (d\vec{r}/dt) = \hat{i}\dot{\xi} + \hat{j}\dot{\eta} + \xi(d\hat{i}/dt) + \eta(d\hat{j}/dt) \\ &= \hat{i}(\dot{\xi} - \omega\eta) + \hat{j}(\dot{\eta} + \omega\xi) \\ \vec{a} &= \hat{i}(\ddot{\xi} - 2\omega\dot{\eta} - \omega^2\xi) + \hat{j}(\ddot{\eta} + 2\omega\dot{\xi} - \omega^2\eta) \end{aligned}$$

In addition, if the radius  $r$  relates to stationary  $x, y$  coordinates, and the radius  $z$  relates to the rotating coordinates  $\xi, \eta$ , the relationship between them is

$$r = ze^{i\omega t}$$

$$\dot{r} = (\dot{z} + i\omega z) e^{i\omega t}$$

$$\ddot{r} = (\ddot{z} + 2i\omega\dot{z} - \omega^2 z) e^{i\omega t}$$

To convert from rotating coordinates back to stationary coordinates, the transformation expressions are

$$z = re^{-i\omega t}$$

$$\dot{z} = (\dot{r} - i\omega r) e^{-i\omega t}$$

$$\ddot{z} = (\ddot{r} - 2i\omega\dot{r} - \omega^2 r) e^{-i\omega t}$$

#### APPENDIX C - REFERENCES

1. Dimantberg, F.M., "Flexural Vibrations of Rotating Shafts," Butterworth and Co., Ltd., London, (1961).
2. Pinkus, O., and Sternlicht, B., "Theory of Hydrodynamic Lubrication," McGraw-Hill Book Co., New York, 1961.
3. Johnson, D. C., "Modes and Frequencies of Shaft Coupled by Straight Spur Gears," Journal of Mechanical Engineering Sciences, Vol. 4, No. 3, Sept. 1962, pp 241-250.
4. Nestorides, E., "B.I.C.E.R.A. Handbook of Torsional Vibration," Cambridge University Press, England, 1958.
5. Wilson, W. Ker, "Practical Solution of Torsional Vibration Problems, Volumes 1 and 2," Third Edition, John Wiley and Sons, Inc., New York, 1963.
6. Linn, F. C., Prohl, M. A., "The Effect of Flexibility of Supports Upon the Critical Speeds of High-Speed Rotors," Soc. Naval Architects and Marine Engineers, No. 5, Annual Meeting, (1951).
7. Lund, J. W., "The Hydrostatic Gas Journal Bearing with Journal Rotation and Vibration," Trans. ASME, Jnl. of Basic Engineering, Series D, Paper No. 63-LUBS-4, 1963.
8. Taylor, G. I., "Stability of a Viscous Liquid Contained Between Two Rotating Cylinders," Series A, p. 223, 289, Phil. Trans. Roy. Soc. (1923).
9. Wilcock, D. F., "Turbulence in High-Speed Journal Bearings," Trans. ASME, Vol. 72 (1950).
10. Smith, M. I., Fuller, D. D., "Journal Bearing Operation at Super-Laminar Speeds," Trans. ASME, Vol. 78 (1956).
11. Constantinescu, V. N., "On Turbulent Lubrication," Proc. IME, Vol. 173, (1959).
12. Arwas, E. B., Sternlicht, B., Wernick, R. J., "Analysis of Plain Cylindrical Journal Bearings in Turbulent Regime," ASME Paper No. 63-LUB-11.
13. Ng, C. W., "Fluid Dynamic Foundation of Turbulent Lubrication Theory,"
14. Ng, C. W., Pan, C. H. T., "A Linearized Turbulent Lubrication Theory,"

15. Orcutt, F. K., Ng, C. W., Vohr, J. H., and Arvas, E. B., "Lubrication Analysis in Turbulent Regime," First Quarterly Report, NASA Contract NASw-1021, October, 1964, MTI Report 64TR57.
16. Orcutt, F. K., "Lubrication Analysis in Turbulent Regime," Second Quarterly Report, NASA Contract NASw-1021, January, 1965, MTI Report 65TR2.
17. Den Hartog, J. P., "Mechanical Vibrations," Fourth Edition, McGraw-Hill Book Company, New York, 1956.
18. Stodola, A., "Steam and Gas Turbines, Volumes 1 and 2," Translated by L. C. Loewenstein, McGraw-Hill Book Company, Inc., New York, 1927.
19. Geiger, J., Zeitschrift V.D.I. Vol. 66, Nr. 26, pp. 667-669 (1922).  
"Berechnung der Schwingungserscheinungen an Turbodynamos." Also,  
Zeitschrift V.D.I. Vol. 67, Nr. 12, pp 287-288 (1923).  
"Berechnung der Schwingungserscheinungen an Turbodynamos."
20. Ziegler, H., "On the Concept of Elastic Stability," Advances in Applied Mechanics, Volume 4, Academic Press Inc., New York, 1956.
21. Rowett, J., "Elastic Hysteresis of Steel," Proc. Roy. Soc., London, A. Vol. 89, p. 528, 1914.
22. Lazan, B. J. "Damping Constants and Stress Distribution in Resonance Response." Jl. App. Mech., Vol. 20, No. 2, June, 1940, p. 201.
23. Kimball, A. L., Lovell, J., Trans. ASME Vol. 48, P. 479 (1926), "Internal Friction as a Cause of Shaft Whirling."
24. Downham, E., "Some Preliminary Model Experiments on the Whirling of Shafts," A.R.C.R and M No. 2768, (1950).
25. Hull, E. H., "Shaft Whirling as Influenced by Stiffness Asymmetry," Jnl. Eng. Ind., Trans. ASME, V. 83, Series B, No. 2, pp. 219-226, (1961).
26. Kellenberger, W., "Forces, Double-Frequency, Flexural Vibrations in a Rotating, Horizontal, Cylindrical Shaft," The Brown Boveri Review, No. 3, Vol. 42, p. 79-85, (1955).
27. Soderberg, C. R., "On the Sub-Critical Speeds of the Rotating Shaft." Trans. ASME Vo. 54, p. APM p. 45-50. (1932).
28. Robertson, D., "Whirling of a Shaft with Skew Stiffness," The Engineer, Vol. 156, pp. 152-153, 179-181, 213-214, (1933).
29. Laffoon, C. M., Rose, B. A., "Special Problems of Two-Pole Generators," Trans. AIEE Vol. 59, pp 30-34, (1940).
30. Stoker, J. J., "Non-Linear Vibrations," Interscience Publishers, Inc. New York (1950).

31. McLaughlin,
32. Lund, J. W., Sternlicht, B., "Rotor-Bearing Dynamics with Emphasis on Attenuation," ASME Paper 61-WA-68 (1961).
33. Warner, P. C., Thoman, R. J., "Effect of the 150-Degree Partial Bearing on Rotor-Unbalance Vibration," ASME Paper 63-LUB-36 (1963).
34. Warner, P. C., "Static and Dynamic Properties of Partial Journal Bearings," ASME Paper 62-LUB 5-11 (1962).
35. Lund, J. W., Discussion of paper by P. C. Warner and R. J. Thoman, "Effect of 150-Degree Partial Bearing on Rotor-Unbalance Vibration," ASME Paper 63-LUB-36, (1963).
36. Rieger, N. F., "Unbalance Response of a Uniform Elastic Rotor, Supported in Damped Flexible Bearings," Westinghouse Electric Corporation Report on Attenuation of Bearing Transmitted Noise, Volume 2, Bureau of Ships Contract No. NObs 86914.
37. Rankine, W. J. McQ., "Centrifugal Whirling of Shafts," The Engineer, Vol. 27, p. 249, (1869).
38. Foppl, A., "Das Problem der Laval'schen Turbinenwelle," Der Civilingenieur, Vol. 41, p. 33-342, (1895).
39. Greenhill, Sir G., "On the Strength of Shafting When Exposed Both to Torsion and to End Thrust," Proc. I. Mech E. Vol. 36, pp. 182-225 (1883).
40. Dunkerley, S., "On the Whirling and Vibration of Shafts," Phil. Trans. Roy. Soc. London, Series A. Vol. 185, p. 279 (1895).
41. Chree, C., "The Whirling and Transverse Vibrations of Rotating Shafts," Phil. Mag., Vol. vii, p. 504 (1904).
42. Jeffcott, H. H., "The Lateral Vibrations of Loaded Shafts in the Neighborhood of a Whirling Speed: The Effect of Want of Balance," Phil. Mag., Vol. 37, pp. 304-314 (1919).
43. Morley, H., "The Calculation of Vibration and Whirling Speeds," Engrg. July 30, 1909, pp. 135, 205.
44. Kerr, W., "On the Whirling Speed of Loaded Shafts," Engrg, Feb. 18, pp. 150, 296, 386, 410, 420, (1916). With discussion by C. Chree, A. Morley, A. Stodola, H. Naylor, H. Jeffcott and J. Danus.
45. Rodgers, C., "On the Vibration and Critical Speeds of Rotors," Phil. Mag. Series 6, Vol. 44, pp. 122-156, (1922).

46. Howland, R. C. S., "The Vibrations of Revolving Shafts," Phil. Mag., 7th Series, Vol. 12, p. 297, (1931).
47. Robertson, D., "The Vibrations of Revolving Shafts," Phil. Mag. Series 7, Vol. 13, p. 862 (1932).
48. Robertson, D., "The Whirling of Shafts." The Engineer, Vol. 158, pp. 216-217, 228-231. (1934).
49. Robertson, D., "Hysteretic Influences on the Whirling of Rotors," Proc. 1 Mech. E. pp. 513-537, Vol. , (1935).
50. Robertson, D., "Transient Whirling of a Rotor," Phil. Mag., Series 7, Vol. 20, p. 793 (1935).
51. Robertson, D., "Subsidiary Whirling of Rotors Due to Speed Oscillation." Phil. Mag. Series 7, Vol. 21, pp. 474-501. (1936).
52. Robertson, D., "Whirling of a Journal in a Sleeve Bearing," Phil. Mag. Series 7, Vol. 15, p. 113-130 (1933).
53. Kimball, A. L., "Internal Friction Theory of Shaft Whipping," Phys. Rev., Vol. 21, p. 703 (1923). Abstract in Gen. Elec. Revue, Vol. 27, p. 244, (1924).
54. Newkirk, B. L., "Shaft Whipping," Gen. Elec. Rev., Vol. 27, p. 169-178, (1924).
55. Newkirk, B. L., Taylor, H. D., "Oil Film Whirl - An Investigation of Disturbances Due to Oil Films in Journal Bearings," Gen. Elec. Rev., (1925).
56. Newkirk, B. L., Grobel, L. P., "Oil Film Whirl - A Non-Whirling Bearing," Trans. Amer. Soc. Mech. Engrs., Vol. 56, No. 8, p. 607. (1934).
57. Newkirk, B. L., "Instability of Oil Films and More Stable Bearings," General Discussion on Lubrication and Lubricants. Inst. Mech. Engrs., London, (1937).
58. Newkirk, B. L., "Journal Bearing Instability," I Mech E. - ASME International Conference on Lubrication and Wear, London, October, 1957. Review paper Session 1, No. 2.
59. Swift, H. W., "Stability of Lubricating Films in Journal Bearings," Proc. Inst. Civ. Engrs. (London) Vol. 233, p. 267. (1932) also Engineering, Jan. 15, 1932.
60. Swift, H. W., "Fluctuating Loads in Sleeve Bearings," J. Inst. Civ. Engrs. Vol. 5, No. 4, p. 161 (1936-1937).

61. Burwell, J. T., "The Calculated Performance of Dynamically Loaded Sleeve Bearings," J. Appl. Mech. Trans. Amer. Soc. Mech. Engrs., Vol. 69, P. A231, (1947).
62. Burwell, J. T., "The Calculated Performance of Dynamically Loaded Sleeve Bearings - II," Journal of Applied Mechanics, Trans. ASME, Vol. 71, 1949, pp 358-360.
63. Burwell, J. T., "The Calculated Performance of Dynamically Loaded Bearings III," J. Appl. Mech. Trans. Amer. Soc. Mech. Engrs., Vol. 73, pp. 393, (1951).
64. Shawki, G. S. A., "Whirling of a Journal in a Sleeve Bearing. Experiments Under No-Load Conditions," London Engn., p. 243, Feb. 25, 1955.
65. Shawki, G. S. A., "Journal Bearing Performance for Combinations of Steady, Fundamental, and Low-Amplitude Harmonic Components of Load," Amer. Soc. Mech. Engrs. - Amer. Soc. Lubric. Engrs. Paper 55-LUB-15. (1955).
66. Shawki, G. S. A., Freeman, P., "Journal Bearing Performance Under Sinusoidally Alternating and Fluctuating Loads," Proc. I Mech. E., Vol. 169, p. 689 (1955).
67. Rayleigh, J. W. S., "The Theory of Sound," Dover Publications, New York American Edition, 1945.
68. Prohl, M. A., "A General Method for Calculating Critical Speeds of Flexible Rotors," J. Appl. Mech., Vol. 12, p. 142, (1945).
69. Myklestad, N. O., J. Aero Sci., Vol. 11, p. 153 (1944).
70. Lund, J. W., "IBM 704 Program Unbalance Response and Critical Speeds of a Rotor in Flexible Bearing Supports," MTI Report 62TR3 (1962).
71. Hagg, A. C., "The Influence of Oil-Film Journal Bearings on the Stability of Rotating Machines," Trans. ASME, Journal Appl. Mech., Vol. 68, p. 211, (1946).
72. Hagg, A. C., Warner, P. C., "Oil Whip of Flexible Rotors," Trans. ASME, Vol. 75, No. 7, pp. 1339-1344 (1953).
73. Hagg, A. C., Sankey, G. O., "Some Dynamic Properties of Oil-Film Journal Bearings with Reference to the Unbalance Vibration of Rotors," Trans. ASME Jnl. Appl. Mech., Vol. 78, p. 302-306, AMR Vol. 9, Revue 1665 (1956).
74. Sternlicht, B., "Elastic and Damping Properties of Cylindrical Journal Bearings," Trans. ASME, Series D., Vol. 81 (1959), p. 101-108.
75. Lund, J. W., "The Stability of an Elastic Rotor in Journal Bearings with Flexible, Damped Supports," Paper submitted to ASME Feb., 1965. See also "Attenuation of Rotor Unbalance Forces by Flexible Bearing Supports." Westinghouse Electric Corp. Report, Aug. 1964, Bureau of Ships Contract No. NOBS-86914, Vol. 2.
76. Taylor, H. D., "Critical Speed Behavior of Unsymmetrical Shafts." J. Appl. Mech. June A-71-A-79 (1940).

77. Foote, W. R., Poritsky, H., Slade, J. J., Jr., "Critical Speeds of a Rotor with Unequal Shaft Flexibilities Mounted in Bearings on Unequal Flexibility," J. Appl. Mech., A 77, A. 84 (1943).
78. Lewis, F., "Vibrations During Acceleration Through a Critical Speed," Trans. Amer. Soc., Mech. Engrs., Vol. 54, No. 23 (1932).
79. Palmgren, A., "Ball and Roller Bearing Engineering," Second Edition, 1945. SKF Industries Inc. Philadelphia, Pa.
80. Tondl, A., "The Stability of Motion of a Rotor with Unsymmetrical Shaft on an Elastically Supported Mass Foundations." Ing. - Arch. Vol. 29, No. 6, pp. 410-418 (1960). Also  
"Influence of Elastically Supported Frames on the Stability of Rotating Shafts with Consideration of the Internal and External Damping." Ost. Ing. - Arch., Vol. 14, No. 2, pp. 93-99 (1960).
81. Lund, J. W., "Spring and Damping Coefficients for the Tilting-Pad Journal Bearing," ASLE Transactions Vol. 7, pp. 342-352 (1964).
82. Duncan, J. P., Collar, A. R. "Elementary Matrices," Cambridge University Press, Cambridge, England (1938).
83. Bishop, R. E. D., "The Analysis of Vibrating Systems Which Embody Beams in Flexure, Proc. I Mech. E. Vol. 169, No. 51, (1955).
84. Gladwell, G. M. L., Bishop, R. E. D., "The Receptances of Uniform and Non-Uniform Rotating Shafts," J. Mech. Eng. Sci. Vol. 1, No. 1, pp. 78-91, (1959).
85. Temple, G. A., Bickley, W. G., "Rayleigh's Principle and its Application to Engineering Problems," Dover Publications Inc., New York (1949).
86. Rieger, N. F., "Critical Speeds of Stepped Shafts," Machine Design, Vol. 36, Sept. 1964.
87. Inglis, C. E., "The Determination of Critical Speeds, Natural Frequencies and Modes of Vibration by Means of Basic Functions," Trans. North East Coast Inst. of Engrs. and Ship Builders, Vol. 61, p. 111, 1943.
88. Borowicz, C., "Beitrage zur Berechnung krit. Geschwindigkeiten bei und mehrfach gelagerter Wellen," Munchen (1915). Method described by S. P. Timoshenki, "Vibration Problems in Engineering," Third Edition, p. 280.
89. Morley, A., "The Whirling Speed of Shafts Supported in Three Bearings," Engineering, Nov. 22, 1918, pp. 573, 601.
90. Southwell, R. V., "On the Free Transverse Vibrations of a Uniform Circular Disk Clamped at its Center," Proc. Roy. Soc. Series A, Vol. 101, p. 133, 1922.

91. Southwell, R. V., Gough, Barbara S., "On the Stability of a Rotating Shaft, Subjected Simultaneously to End Thrust and Twist." Report, British Assoc. Adv. of Sci. 1921, 89th Meeting, pp. 345, 355.
92. Jeffcott, H. H., "The Periods of Lateral Vibration of Loaded Shafts.— The Rational Derivation of Dunkerley's Empirical Rule for Determining Whirling Speeds," Proc. Roy. Soc. Vol. 95, No. A666, pp. 106 - 115, (1918).
93. Jeffcott, H. H., "The Whirling Speeds of a Loaded Shaft Supported in Three Bearings," Phil. Mag. Vol. 42, Ser. 6, No. 251, pp 635-668, (1921).
94. Foppl, L., "Kritische Drehzahlgebiete der Fliegend Angeordneten Scheibe," Stephen Timoshenko 60th Anniversary Volume, The Macmillan Company, New York, 1938, pp. 45-50.
95. Green, R. B., "Gyroscopic Effects on the Critical Speeds of Flexible Rotors," Trans. ASME Vol. Appl. Mech. p. 369 (1948).
96. Yamada, Y., "On the Critical Speeds of a Rotor System Having an Asymmetrical Disk," Proc. 4th, Jap. Nat. Congr. Appl. Mech. pp 381-384, (1954).
97. Foppl, A., "Stability of Equilibrium Beyond the Critical Speed" Communication A. Stodola, Cited in "Steam and Gas Turbines" Vol. 2, p. 1132. See Also Schweiz. Bauzeit. Vol. 69, p. 200, (1917) & Dingl. Pol Jnl. 1918, p.117.
98. Hummel, C., "Kritische Drehzahlen als Folge der Nachgiebigkeit des Schmiermittels im Lager." Forschungsh, Ver. dtsh. Ing. 287. (1936).
99. Cameron, A. "Oil Whirl in Bearings." Engineering, London, Vol. 179, p. 237, 1955.
100. Cameron, A., Solomon, P. J. B., "Vibrations in Journal Bearings: Preliminary Observations," (Instn Mech. Engrs. London). Proc. Conf. Lubrication and Wear, Paper 103, p. 191, (1957).
101. Parszewski, Z., Cameron, A., "Oil Whirl of Flexible Rotors," Proc. I. Mech. E. Vol. 176, No. 22, pp. 523-531. (1962).
102. Harrison, W. J., "The Hydrodynamical Theory of the Lubrication of a Cylindrical Bearing Under Variable Load, and of a Pivot Bearing," Trans. Edinburgh Philosophical Soc., Edinburgh, Scotland, Vol. 22, 1919, pp.373-388.
103. Boeker, G. F., Sternlicht, B., "Investigation of Translatory Fluid Whirl in Vertical Machines," Trans. ASME, Vol. 78, 1956, pp. 13-19.
104. Poritsky, H., "Contribution to the Theory of Oil Whip," Trans. ASME, Vol. 75, 1953, pp. 1153-1161.
105. Hagg, A. C., "Some Vibration Aspects of Lubrication," Lubrication Engrg. August 1948, pp. 166-169.
106. Hagg, A. C., Sankey, G. O., "Elastic and Damping Properties of Oil-Film Journal Bearings for Application to Unbalance Vibration Calculations," Jnl. Appl. Mech., March 1958, pp. 141-143, Design Data and Methods.

107. Huggins, N. J., "Non-Linear Modes of Vibration of a Rigid Rotor in Short Journal Bearings," Proc. I Mech E., Second Lubrication and Wear Convention, Proc., Eastbourne, May, 1964, Paper 18.
108. Newkirk, B. L., Lewis, J. F., "Oil-Film Whirl — An Investigation of Disturbances Due to Oil Films in Journal Bearings," Trans. ASME, Vol. 78, p. 21, 1956.
109. Newkirk, B. L., "Varieties of Shaft Disturbances Due to Fluid Films in Journal Bearings," Trans. ASME, Vol. 78, p. 985, 1956.
110. Pinkus, O., "Note on Oil Whip," Trans. ASME, Jnl. Appl. Mech. Vol. 20, p. 450, 1953.
111. Pinkus, O., "Experimental Investigation of Resonant Whip," Trans. ASME, Vol. 78, p. 975, 1956.
112. Lewis, J. F., Fulton, G. B., "Further Investigation of Disturbance Due to Oil Film in Journal Bearings," WADC Tech. Rep. 56-259, 1956.
113. Ausman, J. S., "The Fluid Dynamic Theory of Gas-Lubricated Bearings," ASME Paper No. 56 - LUB-6, presented at the Joint ASME-ASLE Conference, October, 1956.
114. Ausman, J. S., "Finite Gas-Lubricated Journal Bearing," Proc. I Mech E. Lubrication and Wear Conference, London, 1957. Proceedings, Paper 22, pp. 39-45.
115. Elrod, H. G., Bergdorfer, A., "Refinements of the Theory of the Infinitely-Long, Self-Acting Gas-Lubricated Journal Bearing," 1st International Symposium on Gas-Lubricated Bearings, ONR, Washington, D. C. Oct., 1959.
116. Reimondi, A. A., "A Numerical Solution for the Gas Lubricated Full Journal Bearing for Finite Length. Trans. ASLE, Vol. 4, No. 1, April 1961.
117. Sternlicht, B., "Gas-Lubricated Cylindrical Journal Bearings of the Finite Length, Part I - Static Loading," Trans. ASME, Jnl. Appl. Mech., Paper 61-APM-17 (1961).
118. Sternlicht, B., "Gas-Lubricated Cylindrical Journal Bearings of Finite Length, Part II - Dynamic Loading," General Electric Technical Report, ONR Contract No. Nonr 2844 (00), Task No. NR 097-348, September, 1960.
119. Pan, C. H. T., "On the Time Dependent Effects of Self-Acting Gas Dynamic Journal Bearings," Trans. ASME, Paper No. 62-LUB-10, 1963.
120. Sternlicht, B., Poritsky, H., Arwas, E. B., "Dynamic Stability Aspects of Cylindrical Journal Bearings Using Compressible and Incompressible Fluids," First International Symposium on Gas Lubricated Bearings, Washington, D.C. pp. 119-160, (1959).

121. Rentzepis, G. M., Sternlicht, B., "On the Stability of Rotors in Cylindrical Journal Bearings," Journal of Basic Engineering, Trans. ASME, Series D. Vol. 84, 1962, p. 521.
122. Sternlicht, B., Winn, L. W., "On the Load Capacity and Stability of Rotors in Self-Acting Gas Lubricated Plain Cylindrical Journal Bearings," Trans. ASME, Jnl. of Basic Engineering, Paper No. 62-LUB-8, 1963, p. 503.
123. Castelli, V., Elrod, H. G., "Solution of the Stability Problem for 360 Deg Self-Acting, Gas-Lubricated Bearings," Trans. ASME, Jnl. of Basic Engineering, Paper No. 64-LUBS-10, 1964.
124. Pan, C. H. T., Sternlicht, B., "Comparison Between Theories and Experiments for the Threshold of Instability of Rigid Rotor in Self-Acting, Plain-Cylindrical Journal Bearings, Trans. ASME, Jnl. of Basic Engineering, Paper No. 63-LUBS-3, 1964.
125. Cheng, H. S., Trumpler, P. R., "Stability of the High Speed Journal Bearing Under Steady Load," Journal of Engineering for Industry, Trans. ASME, Series B, Vol. 85, 1963, p. 274.
126. Cheng, H. S., Pan, C. H. T., "Stability Analysis of Gas-Lubricated, Self-Acting, Plain, Cylindrical, Journal Bearings of Finite Length, Using Galerkin's Method," Trans. ASME, Jnl. of Basic Engineering, Paper No. 64-LUBS-5, 1965.
127. Ng, C. W., "Linearized PH Stability Theory for Finite-Length Self-Acting Gas Lubricated, Plain Journal Bearings." Trans. ASME, Journal of Basic Engineering, Paper No. 64Lub28, 1965.
128. Ausman, S., "Linearized ph Stability Theory for Translatory Half-Speed, Whirl of Long Self-Acting Gas-Lubricated Journal Bearings," Trans. ASME, Jnl. of Basic Engineering, Series D., Vol. 85, 1963, pp. 611-619.
129. Sternlicht, B., Winn, L. W., "Geometry Effects on the Threshold of Half-Frequency Whirl in Self-Acting Gas Lubricated Journal Bearings," General Electric Technical Report, ONR, March 1962.
130. Fischer, G. K., Cherubim, J. L., Fuller, O. D., "Some Instabilities and Operating Characteristics of High-Speed Gas Lubricated Journal Bearings," ASME Paper No. 58-A-231, (1958).
131. Whitley, S., Betts, C., "Study of Gas-Lubricated, Hydrodynamic, Full Journal Bearings," British Journal of Applied Physics, Vol. 10, October, 1959, pp. 455-463. Also see Whitley, S., Bowhill, A. J., McEwan, Miss P. "Half-Speed Whirl and Load Capacity of Hydrodynamic Gas Journal Bearings," Proc. I Mech. E. Vol. 176, No. 22, 1962, pp. 554-565.
132. Bowman, R. M., Collingwood, L. C. Midgley, J. W., "Some Factors Affecting the Whirl Instability of a Journal Bearing Part 1," Paper No. 2, Lubrication and Wear Group Convention 1963.

133. Bowman, R. M., Collingwood, L. C., Midgley, J. W., "Some Factors Affecting the Whirl Instability of a Journal Bearing (Part 2), Paper No. 5, Lubrication and Wear Group Second Convention, Eastbourne, May 1964.
134. Sternlicht, B., Pan, C. H. T., "On The Translatory Whirl Motion of a Vertical Rotor in Plain Cylindrical Gas-Dynamic Journal Bearings," Trans. ASME, Jnl. of Basic Engineering, Series D, Vol. 84, 1962, p. 152.
135. Sternlicht, B., Elwell, R. C., "Synchronous Whirl in Plain Journal Bearings," Trans. ASME, Jnl. of Basic Engineering, Series D, Paper No. 62-LUBS-19, 1963.
136. Heinrich, G., "Theory of the Externally-Pressurized Bearing with Compressible Lubricant," Proc. First International Symposium on Gas-Lubricated Bearings, Washington, D. C., October, 1959. pp. 251-265.
137. Larson, R. H., Richardson, H. H., "A Preliminary Study of Whirl Instability for Pressurized Gas Bearings," Trans. ASME, Jnl. of Basic Engineering, Series D, December, 1962, P. 520.
138. Gross, W. A., "Investigation of Whirl in Externally Pressurized Air-Lubricated Journal Bearings," Trans. ASME, Jnl. of Basic Engineering, Paper No. 61-LUB-1, 1961.
139. Licht, L., Elrod, H., "Study of the Stability of Externally Pressurized Gas Bearings," Trans. ASME, Jnl. of Applied Mech., June 1960, pp. 250-258.
140. Roudebush, W. H., "An Analysis of the Effect of Several Parameters on the Stability of an Air-Lubricated, Hydrostatic Thrust Bearing," NACA TN 4095, October, 1957.
141. Licht, L., Fuller, D. D., Sternlicht, B., "Self-Excited Vibrations of an Air-Lubricated Thrust Bearing," Trans. ASME, Vol. 80, 1958, pp. 411-414.
142. Licht, L., "Air-Hammer Instability in Pressurized Journal-Gas Bearings," Paper No. 60-WA-10, presented at the ASME Winter Annual Meeting, New York, December, 1960.
143. Someya, T., "Stability of a Balanced Shaft Running in Cylindrical Journal Bearings," Inst. of Mech. Engrs., Second Lubrication and Wear Convention, Proceedings. Paper 21, 1964.
144. Jennings, U. D., Ocvirk, F. W., "The Simulation of Bearing Whirl on an Electronic-Analog Computer," Trans. ASME, Jnl. of Basic Engineering, Series D, 1962, pp 503-510.
145. Reddi, M. M., Trumpler, P. R., "Stability of the High-Speed Journal Bearing Under Steady Load," Trans. ASME, Jnl. of Engineering for Industry, Paper No. 61-WA-87, 1962.

146. Akimoff, B., "Balancing Apparatus," Trans. ASME, Vol. 39, 1918, p. 779. Described in Stodola "Steam and Gas Turbines," Vol. 1, p. 423.
147. Ribary, F., Brown Boveri Review, Vol. 23, 1936, p. 186.
148. Hopkirk, K. R., The Engineer, Vol. 170, 1940, p. 38.
149. Somervaille, I. J., "Balancing a Rotating Disc, Simple Graphical Construction." Engineering, February 19, 1954.
150. Macinante, J. A., "Calibrating Dynamic Balancing Machines. Graphical Method not Employing Previously Balanced Specimens." Engineering, August 10, 1956, Vol. 182, No. 4718.
151. Yates, H. G., "Vibration Diagnosis in Marine Geared Turbines." Trans. NE Coast. Inst., Engs. and Shipbuilders, Vol. 65, 1949, page 225.
152. Rathbone, T. C., "Vibration Tolerances." Power Plant Engineering, Vol. 43, November 1939, p. 721.
153. Reiher, H., Meister, E. J., "Die Empfindlichkeit des Menschen gen Erschütterungen." Forsch. gebiete Ingenieurw, Vol. 2, No. 11. November 1931, p. 381-386.
154. Federn, K., "Unwuchttoleranzen rotierender Körper". Werkstatt und Betrieb, Vol. 88, No. 5, May 1953, p. 243-250.
155. Feldman, S., "Dynamic Balancing for Noise Reduction." BuShips Report No. 371, Vol. 24, April 1955.
156. Rieger, N. F. "Vibration Analysis of Hydrofoil Gear Test Rig," MTI-64TR33, June 17, 1964.
157. Sternlicht, B., Elwell, R. C., "Theoretical and Experimental Analysis of Hydrostatic Thrust Bearings." Trends ASME Journal of Basic Engineering, September, 1960. Vol. 82, Series D.
158. Raimondi, A. A., "An Analysis of Orifice Compensated Hydrostatic Journal Bearings," ASME Paper 54-LUB-17, October, 1954.
159. Rieger, N. F., "Dynamical Analysis of High-Speed Centrifuge," MTI Report 63TR, September, 1963.
160. Grammel, R., Bienzeno, C. B., "Critical Speeds of Rotation." Chapter 3, Vol. 3, Technische Dynamik, Julius Springer, Berlin, (1953).
161. Rosenberg, H., "Influence of Axial Torques on the Critical Speeds of Uniform Shafts in Self-Aligning Bearings," University of Washington Press, Engineering Experiment Station, Department of Aeronautical Engr., Bulletin 118, pp. 88-94, 1951.
162. Wehrli, C. Doctoral Thesis. Eidg. Techn. Hochschule, Zurich, Switzerland. 1952 (to be published). Also see Ref. 20.

UNCLASSIFIED

Security Classification

DOCUMENT CONTROL DATA - R&D		
(Security classification of title, body of abstract and indexing annotation must be entered when the overall report is classified)		
1. ORIGINATING ACTIVITY (Corporate author) Mechanical Technology Incorporated 968 Albany-Shaker Road Latham, New York 12110		2a. REPORT SECURITY CLASSIFICATION UNCLASSIFIED
		2b. GROUP N/A
3. REPORT TITLE ROTOR-BEARING DYNAMICS DESIGN TECHNOLOGY Part I: State-Of-The-Art		
4. DESCRIPTIVE NOTES (Type of report and inclusive dates) Final Report for Period 1 April 1964-1 April 1965		
5. AUTHOR(S) (Last name, first name, initial) Rieger, Neville F.		
6. REPORT DATE May 1965	7a. TOTAL NO. OF PAGES 327	7b. NO. OF REFS 161
8a. CONTRACT OR GRANT NO. AF 33(615)-1895	9a. ORIGINATOR'S REPORT NUMBER(S)  MTI-65 TR 18	
8b. PROJECT NO. 3044  c. Task No. 304402  d.	9b. OTHER REPORT NO(S) (Any other numbers that may be assigned this report) AFAPL-TR-65-45, Part I	
10. AVAILABILITY/LIMITATION NOTICES Qualified requesters may obtain copies of this report from DDC. Foreign announcement and dissemination of this report by DDC is not authorized. Release to foreign nationals is not authorized. DDC release to the clearinghouse for Federal Scientific and Technical Information (formerly OTS) is not authorized.		
11. SUPPLEMENTARY NOTES	12. SPONSORING MILITARY ACTIVITY USAF RTD Air Force Aero Propulsion Laboratory Wright-Patterson AFB, Ohio 45433	
13. ABSTRACT The basic aspects of rotor-bearing dynamics have been collated and are here presented in systematic fashion. The rotor-bearing system and its forces are first discussed. The properties of rotor whirl, critical speed and system stability are discussed in detail. Effects arising from running a rotor through its critical speed are reviewed. Balancing of rigid and flexible rotors is considered with regard to balancing machines, computed calculation of unbalance, and acceptable levels of unbalance. Axial and torsional effects on machine systems are included. Throughout, the important literature relating to each topic is specified, discussed and set in perspective.		

DD FORM 1473  
1 JAN 64

UNCLASSIFIED

Security Classification

UNCLASSIFIED

Security Classification

14. KEY WORDS	LINK A		LINK B		LINK C	
	ROLE	WT	ROLE	WT	ROLE	WT
Bearings Lubrication Fluid Film Hydrodynamic Hydrostatic Rotor-Bearing Dynamics Stability Critical Speed Laminar Film Turbulent Film						

**INSTRUCTIONS**

1. **ORIGINATING ACTIVITY:** Enter the name and address of the contractor, subcontractor, grantee, Department of Defense activity or other organization (corporate author) issuing the report.

2a. **REPORT SECURITY CLASSIFICATION:** Enter the overall security classification of the report. Indicate whether "Restricted Data" is included. Marking is to be in accordance with appropriate security regulations.

2b. **GROUP:** Automatic downgrading is specified in DoD Directive 5200.10 and Armed Forces Industrial Manual. Enter the group number. Also, when applicable, show that optional markings have been used for Group 3 and Group 4 as authorized.

3. **REPORT TITLE:** Enter the complete report title in all capital letters. Titles in all cases should be unclassified. If a meaningful title cannot be selected without classification, show title classification in all capitals in parentheses immediately following the title.

4. **DESCRIPTIVE NOTES:** If appropriate, enter the type of report, e.g., interim, progress, summary, annual, or final. Give the inclusive dates when a specific reporting period is covered.

5. **AUTHOR(S):** Enter the name(s) of author(s) as shown on or in the report. Enter last name, first name, middle initial. If military, show rank and branch of service. The name of the principal author is an absolute minimum requirement.

6. **REPORT DATE:** Enter the date of the report as day, month, year, or month, year. If more than one date appears on the report, use date of publication.

7a. **TOTAL NUMBER OF PAGES:** The total page count should follow normal pagination procedures, i.e., enter the number of pages containing information.

7b. **NUMBER OF REFERENCES:** Enter the total number of references cited in the report.

8a. **CONTRACT OR GRANT NUMBER:** If appropriate, enter the applicable number of the contract or grant under which the report was written.

8b, 8c, & 8d. **PROJECT NUMBER:** Enter the appropriate military department identification, such as project number, subproject number, system numbers, task number, etc.

9a. **ORIGINATOR'S REPORT NUMBER(S):** Enter the official report number by which the document will be identified and controlled by the originating activity. This number must be unique to this report.

9b. **OTHER REPORT NUMBER(S):** If the report has been assigned any other report numbers (either by the originator or by the sponsor), also enter this number(s).

10. **AVAILABILITY/LIMITATION NOTICES:** Enter any limitations on further dissemination of the report, other than those imposed by security classification, using standard statements such as:

- (1) "Qualified requesters may obtain copies of this report from DDC."
- (2) "Foreign announcement and dissemination of this report by DDC is not authorized."
- (3) "U. S. Government agencies may obtain copies of this report directly from DDC. Other qualified DDC users shall request through \_\_\_\_\_."
- (4) "U. S. military agencies may obtain copies of this report directly from DDC. Other qualified users shall request through \_\_\_\_\_."
- (5) "All distribution of this report is controlled. Qualified DDC users shall request through \_\_\_\_\_."

If the report has been furnished to the Office of Technical Services, Department of Commerce, for sale to the public, indicate this fact and enter the price, if known.

11. **SUPPLEMENTARY NOTES:** Use for additional explanatory notes.

12. **SPONSORING MILITARY ACTIVITY:** Enter the name of the departmental project office or laboratory sponsoring (paying for) the research and development. Include address.

13. **ABSTRACT:** Enter an abstract giving a brief and factual summary of the document indicative of the report, even though it may also appear elsewhere in the body of the technical report. If additional space is required, a continuation sheet shall be attached.

It is highly desirable that the abstract of classified reports be unclassified. Each paragraph of the abstract shall end with an indication of the military security classification of the information in the paragraph, represented as (TS), (S), (C), or (U).

There is no limitation on the length of the abstract. However, the suggested length is from 150 to 225 words.

14. **KEY WORDS:** Key words are technically meaningful terms or short phrases that characterize a report and may be used as index entries for cataloging the report. Key words must be selected so that no security classification is required. Identifiers, such as equipment model designation, trade name, military project code name, geographic location, may be used as key words but will be followed by an indication of technical context. The assignment of links, rules, and weights is optional.

UNCLASSIFIED

Security Classification